

การพัฒนาถังปฏิบัติการแบบฟองอากาศรูปแบบใหม่ สำหรับกำจัดเหล็กปนเปื้อนในน้ำบาดาล

นายชาเล็ท บุน



จุฬาลงกรณ์มหาวิทยาลัย
CHULALONGKORN UNIVERSITY

บทคัดย่อและแฟ้มข้อมูลฉบับเต็มของวิทยานิพนธ์ตั้งแต่ปีการศึกษา 2554 ที่ให้บริการในคลังปัญญาจุฬาฯ (CUIR)

เป็นแฟ้มข้อมูลของนิสิตเจ้าของวิทยานิพนธ์ ที่ส่งผ่านทางบัณฑิตวิทยาลัย

วิทยานิพนธ์นี้เป็นส่วนหนึ่งของการศึกษาตามหลักสูตรปริญญาวิทยาศาสตรมหาบัณฑิต

The abstract and full text of theses from the academic year 2011 in Chulalongkorn University Intellectual Repository (CUIR) are the thesis authors' files submitted through the University Graduate School.

สาขาวิชาวิศวกรรมสิ่งแวดล้อม ภาควิชาวิศวกรรมสิ่งแวดล้อม

คณะวิศวกรรมศาสตร์ จุฬาลงกรณ์มหาวิทยาลัย

ปีการศึกษา 2558

ลิขสิทธิ์ของจุฬาลงกรณ์มหาวิทยาลัย

Development of Novel Bubble Column Reactor (BCR)
for Iron Removal in Groundwater

Mr. Saret Bun



A Thesis Submitted in Partial Fulfillment of the Requirements
for the Degree of Master of Engineering Program in Environmental Engineering

Department of Environmental Engineering

Faculty of Engineering

Chulalongkorn University

Academic Year 2015

Copyright of Chulalongkorn University

Thesis Title	Development of Novel Bubble Column Reactor (BCR) for Iron Removal in Groundwater
By	Mr. Saret Bun
Field of Study	Environmental Engineering
Thesis Advisor	Associate Professor Pisut Painmanakul, Ph.D.
Thesis Co-Advisor	Assistant Professor Jenyuk Lohwacharin, Ph.D.

Accepted by the Faculty of Engineering, Chulalongkorn University in Partial Fulfillment of the Requirements for the Master's Degree

.....Dean of the Faculty of Engineering
(Associate Professor Supot Teachavorasinskun, D.Eng.)

THESIS COMMITTEE

.....Chairman
(Associate Professor Chavalit Ratanatamskul, Ph.D.)

.....Thesis Advisor
(Associate Professor Pisut Painmanakul, Ph.D.)

.....Thesis Co-Advisor
(Assistant Professor Jenyuk Lohwacharin, Ph.D.)

.....Examiner
(Associate Professor Patiparn Punyapalakul, Ph.D.)

.....Examiner
(Assistant Professor On-anong Larpparisudthi, Ph.D.)

.....External Examiner
(Marupatch Jamnongwong, Ph.D.)

ชาเล็ท บุน : การพัฒนาถังปฏิกรณ์แบบฟองอากาศรูปแบบใหม่ สำหรับกำจัดเหล็กปนเปื้อนในน้ำบาดาล (Development of Novel Bubble Column Reactor (BCR) for Iron Removal in Groundwater) อ.ที่ปรึกษาวิทยานิพนธ์หลัก: รศ. ดร. พิสุทธิ เพียรมนกุล, อ.ที่ปรึกษาวิทยานิพนธ์ร่วม: ผศ. ดร. เจนยุกต์ โล่ห์วัชรินทร์, 195 หน้า.

เหล็กในรูปเฟอร์รัส (Ferrous) ในน้ำบาดาลที่ความเข้มข้นสูงเป็นปัญหาหนึ่งของการผลิตประปา การบำบัดน้ำบาดาลปนเปื้อนเหล็กนั้นสามารถทำได้โดยการเติมอากาศเข้าไปในระบบเพื่อทำให้เฟอร์รัสเกิดปฏิกิริยาออกซิเดชันและตกตะกอนแยกออกจากน้ำ โดยกระบวนการนี้สามารถทำได้อย่างมีประสิทธิภาพในคอลัมน์แบบฟองอากาศ (Bubble Column Reactor) หรือคอลัมน์แบบอากาศยก (Airlift Reactor) แต่อย่างไรก็ตามความสามารถในการบำบัดของอุปกรณ์ทั้งสองยังสามารถพัฒนาเพิ่มเติมจากเทคโนโลยีปัจจุบัน ดังนั้นงานวิจัยนี้จึงได้มีจุดมุ่งหมายในการพัฒนาอุปกรณ์เติมอากาศรูปแบบใหม่ (Novel Reactor) ต่อยอดจากคอลัมน์แบบเป่าฟองและแบบอากาศยก เพื่อใช้ในการบำบัดเหล็กปนเปื้อนในน้ำบาดาลโดยอุปกรณ์เติมอากาศรูปแบบใหม่นี้มีขนาดพื้นที่ หน้าตัด 0.4×0.5 เมตร ที่ความจุ 140 ลิตร พร้อมทั้งมีแผ่นกั้น ในแนวตั้งเพื่อทำให้เกิดการไหลแบบอากาศยกในลักษณะเดียวกันกับคอลัมน์แบบอากาศยก โดยอุปกรณ์รูปแบบนี้ได้เพิ่มแผ่นกั้นแนวนอนโดยมุ่งหมายให้เป็นตัวบังคับฟองอากาศให้ไหลอยู่ในอุปกรณ์นานยิ่งขึ้น และเพิ่มประสิทธิภาพการถ่ายเทมวลสารให้กับระบบ จากการศึกษาพลศาสตร์ของไหลและการถ่ายเท มวลสารพบว่า การติดตั้งแผ่นกั้นแนวนอนสามารถเพิ่มสัมประสิทธิ์การถ่ายเทมวลสาร ($K_L a$) ให้มากขึ้น เมื่อเทียบกับคอลัมน์แบบเป่าฟองและคอลัมน์แบบอากาศยก โดยแผ่นกั้นแนวนอนที่เหมาะสมสำหรับการเติม อากาศนั้นจะต้องทำมุม 50 องศา กับแนวนอน โดยมีแผ่นกั้นทั้งหมด 3 แผ่น ขนาดแผ่นละ 90 ตารางเซนติเมตร โดยจะต้องมีพื้นที่การไหลวนกลับ (recirculation area) เป็นระยะห่างจากขอบของอุปกรณ์ 10 เซนติเมตร ทั้งนี้อุปกรณ์แบบใหม่นี้สามารถเพิ่มความสัมประสิทธิ์การถ่ายเทมวลสารได้ร้อยละ 50-97 เมื่อเทียบกับคอลัมน์แบบฟองอากาศและร้อยละ 6-28 เมื่อเทียบกับคอลัมน์แบบอากาศยกขึ้นกับอัตราการไหล นอกจากนี้ในการบำบัดเหล็กในรูปเฟอร์รัสที่ความเข้มข้นเริ่มต้น 5 ถึง 50 มิลลิกรัมต่อลิตร ที่อัตราการไหลของแก๊ส 2 ถึง 10 ลิตรต่ออนาทินั้น อุปกรณ์รูปแบบใหม่นี้สามารถบำบัดเหล็ก ได้รวดเร็วกว่าคอลัมน์แบบฟองอากาศมาก โดยเฉพาะอย่างยิ่งที่ความเข้มข้นของธาตุเหล็กต่ำ โดยสรุปแล้ว การเพิ่มแผ่นกั้นแนวนอนในอุปกรณ์แบบใหม่นี้สามารถเพิ่มความสามารถในการถ่ายเทมวลสารได้ อีกทั้งยังสามารถนำไปประยุกต์ใช้ในการเติมอากาศและการบำบัดเหล็กในน้ำบาดาลได้เป็นอย่างดี

ภาควิชา วิศวกรรมสิ่งแวดล้อม

ลายมือชื่อนิสิต

สาขาวิชา วิศวกรรมสิ่งแวดล้อม

ลายมือชื่อ อ.ที่ปรึกษาหลัก

ปีการศึกษา 2558

ลายมือชื่อ อ.ที่ปรึกษาร่วม

5770534321 : MAJOR ENVIRONMENTAL ENGINEERING

KEYWORDS: BUBBLE COLUMN REACTOR, AIRLIFT REACTOR, OXYGEN MASS TRANSFER, DESIGN OF EXPERIMENT, OVERALL MASS TRANSFER COEFFICIENT, FERROUS IRON OXIDATION, GROUNDWATER

SARET BUN: Development of Novel Bubble Column Reactor (BCR) for Iron Removal in Groundwater. ADVISOR: ASSOC. PROF. PISUT PAINMANAKUL, Ph.D., CO-ADVISOR: ASST. PROF. JENYUK LOHWACHARIN, Ph.D., 195 pp.

Iron in groundwater mostly in ferrous form with the high concentration is likely the most common water problem. Bubble Column Reactor (BCR) or Airlift Reactor (ALR) is one of the best multiphase contactors that provides many advantages in aeration and oxidation. However, several inadequate points are still required to refine for improving its efficiency. This work aimed to optimize the novel reactor for improving the aeration process and ferrous iron oxidation. Novel Bubble Column Reactor (Novel BCR) that has a cross sectional dimension of 0.4m×0.5m (140L capacity), was developed by inserting the vertical baffle to create a liquid recirculation from a riser to downcomer compartment, and installing horizontal baffles in a riser to increase the bubble retention time and improve the air bubble distribution. Bubble hydrodynamic parameter was studied for well understand the internal mechanism in the reactor. The optimum level of Novel BCR was obtained from the condition that provided overall maximum liquid mass transfer coefficient ($K_L a$) after variation of various parameters. Main influenced factors of Novel BCR performance are the position of recirculation area (Y_r), amount of baffle (N_b), settling area on baffle (A_s), and baffle angle (α) with respective value: 10cm, 3 baffles, 90cm², and 50° at 0.45 of optimum downcomer-to-riser ratio. Novel BCR improved the oxygen transfer in terms of $K_L a$ coefficient from 50% to 97% compared to conventional BCR and 6% to 28% compared to ALR in the ranges of gas flow rate of 4 - 16 LPM. Moreover, the study of ferrous iron oxidation in this novel reactor was conducted by varying initial concentrations of ferrous iron (5 to 50 mg/L) and gas flow rates (2 to 10 LPM) as a semi-batch reactor. The oxidation is faster at lower initial concentration of ferrous iron and the operation in Novel BCR exhibited greater ferrous oxidation than conventional BCR. In the studied gas flow rates, increasing gas flow rate improved conversion yield of ferrous iron.

Department: Environmental Engineering Student's Signature

Field of Study: Environmental Engineering Advisor's Signature

Academic Year: 2015 Co-Advisor's Signature

ACKNOWLEDGEMENTS

I would like to express my gratitude to my thesis advisor, Assoc. Prof. Dr. Pisut Painmanakul for his support, motivation, enthusiasm and immense for critical thinking and knowledge. I also would like to thank my thesis co-advisor, Asst. Prof. Dr. Jenyuk Lohwacharin for his lighting up ideas, suggestions and providing additional resources. I also thank the thesis committee: Assoc. Prof. Dr. Chavalit Ratanatamskul, Assoc. Prof. Dr. Patiparn Punyapalakul, Asst. Prof. Dr. On-anong Larpparisudthi and Dr. Marupatch Jamnongwong for the useful suggestions and feedbacks.

This work was funded the financial support by Collaborative Research Program (CR) under ASEAN University Network Southeast Asia Engineering Education Development Network Program (AUN/SEED-Net) of Japan International Cooperation Agency (JICA).

Additionally, I would like to express my special appreciation and thank all lecturers, laboratory assistants and the staffs in Department of Environmental Engineering, Faculty of Engineering, Chulalongkorn University for sacrificing the precious knowledge and their help during my study, especially Asst. Prof. Dr. Chaiyaporn Puprasert and Assoc. Prof. Dr. Wiboonluk Pungrasmi.

Last but not least, I would like to thank the teamwork under the supervision of Dr. Pisut Painmanakul, namely Dr. Nattawin Chawaloesphonsiya, Mr. Kritchart Wongwailikhit, Mr. Rachagarn Pantavisit, Mr. Phaly Ham and all my laboratory colleagues who involved in this study for their assistance and good advices.

At the end as the most importantly, with the great support of my family, I would like to thank for their encouragement and compassion.

CONTENTS

	Page
THAI ABSTRACT	iv
ENGLISH ABSTRACT	v
ACKNOWLEDGEMENTS	vi
CONTENTS	vii
LIST OF FIGURE.....	xii
LIST OF TABLE	xvii
CHAPTER 1 INTRODUCTION	1
1.1 General Context	1
1.2 Problem Statement.....	4
1.3 Hypotheses	5
1.4 Objectives.....	6
1.5 Scope of Study.....	6
CHAPTER 2 THEORY AND LITERATURE REVIEW.....	8
2.1 Iron in Groundwater	8
2.1.1 Source of Iron.....	8
2.1.2 Iron Occurrence	9
2.1.3 Chemical Properties.....	9
2.1.4 Iron Measurement.....	11
2.2 Iron Treatment Method.....	11
2.2.1 Oxidation Process	12
2.2.2 Ion Exchange Process	17
2.2.3 Membrane Process.....	18

	Page
2.2.4 Stabilization Process	18
2.2.5 Lime Treatment Process	19
2.3 Aeration Process.....	19
2.3.1 Dissolved Oxygen (DO)	19
2.3.2 Theory of Gas Transfer	20
2.3.3 Oxygen Transfer in Clean Water.....	23
2.3.4 Bubble Aeration and Diffuser Device	25
2.4 Bubble Column	27
2.4.1 Design and Scale-up	28
2.4.2 Fluid Dynamics and Regime Analysis	29
2.4.3 Gas Holdup	30
2.4.4 Bubble Characteristics	31
2.4.5 Mass and Heat Transfer Coefficient	31
2.5 Airlift Reactor	32
2.5.1 General Concepts.....	32
2.5.2 Reactor Classification	33
2.5.3 Gas Holdup	34
2.5.4 Liquid Recirculation.....	34
2.6 Sequencing Batch Reactor and Settling Process	35
2.6.1 Sequencing Batch Reactor.....	35
2.6.2 Settling Process.....	37
2.7 Design of Experiment (DOE).....	40
2.7.1 Classical DOE One Factor at a Time.....	40

	Page
2.7.2 Statistical DOE	41
2.7.3 Factorial Designs	42
2.7.4 The 2^k Factorial Design.....	47
2.7.5 Response Surface Methodology - Central Composite Design.....	51
2.8 Literature Review	53
2.8.1 Reactor Development	53
2.8.2 Iron Removal by BCR or ALR.....	56
2.9 Summary and Research Focuses.....	57
CHAPTER 3 METHODOLOGY	62
3.1 Study Overview	62
3.2 Experimental Set-up.....	64
3.3 Materials and Chemicals	65
3.3.1 Novel Bubble Column Reactor.....	65
3.3.2 Reactor Comprised Devices.....	67
3.3.3 Analysis Equipment.....	69
3.3.4 Chemical Reagents.....	70
3.4 Design of Experiment (DOE).....	71
3.5 Analytical Parameters	72
3.5.1 Oxygen Concentration.....	72
3.5.2 Mass Transfer Parameters.....	72
3.5.3 Power Consumption	73
3.5.4 Aeration Performance (OTR, OTE, AE).....	74
3.5.5 Bubble Hydrodynamic Parameters	74

	Page
3.5.6 Ferrous and Total Iron Concentration.....	76
3.5.7 Removal Efficiency (%R).....	76
3.6 Experimental Procedures	76
3.6.1 Design and Installation	77
3.6.2 Optimization of Novel BCR.....	81
3.6.3 Deoxygenation Process	86
3.6.4 Aeration Process	87
3.6.5 Oxidation of Ferrous Iron	88
3.6.6 Ferric Iron Separation Process.....	89
CHAPTER 4 RESULTS AND DISCUSSIONS.....	93
4.1 Development of Novel BCR.....	94
4.1.1 Downcomer-to-Riser Ratio.....	95
4.1.2 Reactor Development Stage I.....	96
4.1.3 Reactor Development Stage II.....	112
4.1.4 Final Optimization and Prediction Equation.....	124
4.2 Comparison of Reactor Performance	130
4.2.1 Overall Mass Transfer Coefficient.....	130
4.2.2 Oxygen Transfer Rate.....	133
4.2.3 Oxygen Transfer Efficiency.....	134
4.2.4 Power Consumption	135
4.2.5 Aeration Efficiency.....	137
4.2.6 Summary Reactor Performance.....	138
4.3 Study Bubble Hydrodynamic Parameters.....	139

	Page
4.3.1 Bubble Size Distribution.....	139
4.3.2 Terminal Rising Bubble Velocity.....	146
4.3.3 Specific Interfacial Area.....	147
4.3.4 Liquid Film Mass Transfer Coefficient (K_L).....	149
4.3.5 Gas Holdup.....	151
4.4 Ferrous Iron Oxidation.....	151
4.4.1 Effect of Initial Concentration of Ferrous.....	152
4.4.2 Effect of Gas Flow Rate.....	153
4.4.3 Study Simple Kinetic Rate.....	154
4.4.4 Proposed Separation Process for Ferric Iron.....	155
Figure 4.58. Summary the separation process for ferric iron in this work.....	160
CHAPTER 5 CONCLUSION AND RECOMMENDATION.....	161
5.1 Conclusion.....	161
5.2 Recommendation.....	163
REFERENCES.....	164
APPENDIX.....	171
VITA.....	195

LIST OF FIGURE

	Page
Figure 1.1. The 15 nations with largest estimated annual groundwater extraction .2	
Figure 1.2. Two commonly types for aeration (a) natural draft coke tray aerator (b) common bubble column diffused aerator.....3	3
Figure 2.1. Iron forms in water as functions of E_H vs. pH (Crittenden et al., 2012).10	10
Figure 2.2. Ferrous iron oxidation rate by oxygen (Crittenden et al., 2012).....13	13
Figure 2.3. Effect of temperature on ferrous oxidation kinetics (Crittenden et al., 2012)14	14
Figure 2.4. Water quality and DO content in ppm at 20°C (Thomson, 2007).....20	20
Figure 2.5. Equilibrium condition schema in air-water of component A.....21	21
Figure 2.6. Mass transfer for (a) stripping and (b) absorption by using two-film theory (Crittenden et al., 2012).....23	23
Figure 2.7. The typically air diffuser system, aeration process (Crittenden et al., 2012)25	25
Figure 2.8. Types of Bubble Column Reactor (a) single stage, (b) multiple stage, (c) loop reactor, (d) downflow bubble column, and (e) three phase fluidized bed reactor/slurry reactor (Ranade, 2001).....28	28
Figure 2.9. Possible flow regimes schematic in bubble columns.....30	30
Figure 2.10. Different types of gas-liquid contactor: simple BCR, internal-loop split ALR, internal-loop draft tube ALR, and external-loop ALR (left to right).....33	33
Figure 2.11. Typical operation cycles in SBR.....35	35
Figure 2.12. Relation of type of settling, concentration, morphology of particle (Crittenden et al., 2012).....38	38
Figure 2.13. Accelerator® solids contact clarifier (Hartung, 1951)39	39
Figure 2.14. Two one-haft fractions of 2^3 design (Montgomery, 2008).....51	51

Figure 2.15. A contour plot of a response surface	52
Figure 2.16. Simplex design (left) and central composite design (right) for $k = 3$...	53
Figure 2.17. Airlift contactor (ALC) development with perforated plate in riser	54
Figure 2.18. Airlift reactor (ALR) development with mesh baffle-plates	54
Figure 2.19. Airlift reactor (ALR) development with sieve plate in riser	55
Figure 3.1. Overview of the framework	62
Figure 3.2. Experimental set-up of Novel BCR	64
Figure 3.3. Three gas-liquid contactors: (a) BCR, (b) Internal ALR, (c) Novel BCR	65
Figure 3.4. Fitted vertical baffle in the reactor top view (a) and vertical baffle flat (b) for changing from BCR to ALR	66
Figure 3.5. Horizontal baffles with free area for settleable particle	66
Figure 3.6. Baffle connecting: (a) L-supporter in different angles, and (b) baffles installation	67
Figure 3.7. Rigid stone diffuser for air distribution	68
Figure 3.8. An interface of an application Minitab 17	72
Figure 3.9. Experimental procedure	77
Figure 3.10. The reactor development concept	77
Figure 3.11. The variation of downcomer and riser compartment	78
Figure 3.12. Installation of modified baffles (angle) in the riser compartment	79
Figure 3.13. Modified baffles length installed in the riser compartment	79
Figure 3.14. Design of the bottom recirculation area (a) and its position (b)	80
Figure 3.15. Designed baffle flat for installing the riser compartment	80
Figure 3.16. Novel BCR after comprised all baffles	81
Figure 3.17. The development processes to obtain best reactor	82
Figure 3.18. The effective plot between factor levels and response values	83
Figure 3.19. Factor screening process by 2^k factorial design	83
Figure 3.20. Experimental process of optimization part and prediction equation	85

Figure 3.21. Process of oxygenation and K_La coefficient obtaining	87
Figure 3.22. Experimental process of ferrous iron oxidation	88
Figure 3.23. Serried processes for separation of ferric iron after oxidation	90
Figure 3.24. Flow diagram for studying ferric iron separation process	90
Figure 4.1. Reactor development process involve design, perform, and analysis..	94
Figure 4.2. Variation of average K_La coefficient value with different A_d/A_r ratio.....	96
Figure 4.3. Experimental results, K_La coefficient of first factors screening	99
Figure 4.4. Normal probability plot for 1 st factors screening.....	99
Figure 4.5. The versus order plot for 1 st factors screening.....	100
Figure 4.6. The versus fits plot for 1 st factors screening.....	100
Figure 4.7. Pareto chart of standardized effect by single and interaction terms.	101
Figure 4.8. Main effective plot for single interaction (linear response)	102
Figure 4.9. Interaction plot for two-way interaction.....	103
Figure 4.10. Experimental results, K_La coefficient of first factors optimization	106
Figure 4.11. Residual plot of experimental result including (a) normal probability plot, (b) versus fits, and (c) versus order.....	107
Figure 4.12. Main effects plot of the fitted mean value of K_La coefficient.....	108
Figure 4.13. Interaction effects plot of fitted mean value of K_La coefficient.....	110
Figure 4.14. Surface plot of two factors a time for first factor optimization.....	111
Figure 4.15. Contour plot of two factors a time for first factor optimization	111
Figure 4.16. Main effective plot for 2 nd factors screening	115
Figure 4.17. Interaction plot for 2 nd factors screening.....	115
Figure 4.18. Experimental results, K_La coefficient of second factors optimization	119
Figure 4.19. Residual plot for model adequacy checking of experimental results	119
Figure 4.20. Main effects plot of the fitted mean value of K_La coefficient.....	121

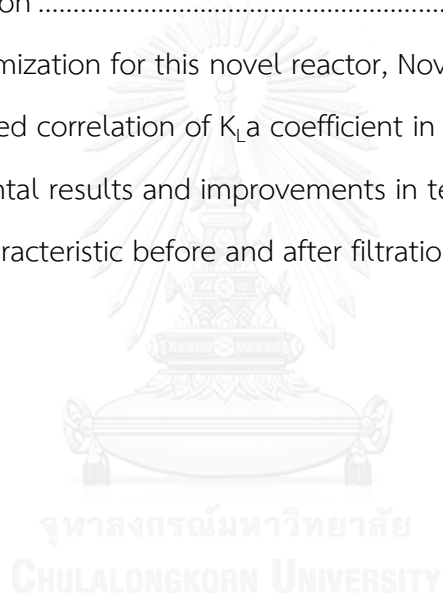
Figure 4.21. Interaction effects plot of the fitted mean value of K_La coefficient	122
Figure 4.22. Surface plot of two factors a time for second factor optimization ..	123
Figure 4.23. Contour plot of two factors a time for second factor optimization.	123
Figure 4.24. Optimum level for all investigated parameters of Novel BCR.....	125
Figure 4.25. Scatter plot between prediction equation and experimental result	126
Figure 4.26. Output change (%) vs. input change (%) of gas flow rate factor	128
Figure 4.27. Output change (%) vs. input change (%) of baffle angle factor	129
Figure 4.28. Output change (%) vs. input change (%) of amount of baffle factor	129
Figure 4.29. Comparison of three various gas-liquid contactors (BCR, ALR, Novel BCR) in terms of K_La coefficient	132
Figure 4.30. The K_La coefficient conversation from 27°C to a standard temperature (20°C) of Novel BCR performance.....	132
Figure 4.31. Experimental result vs. calculated result in terms of K_La coefficient	133
Figure 4.32. The SOTR vs. gas flow rate in BCR, ALR, and Novel BCR	134
Figure 4.33. The SOTE vs. gas flow rate in BCR, ALR, and Novel BCR.....	135
Figure 4.34. The pressure drop vs. gas flow rate	136
Figure 4.35. Unit volume power consumption (P/V) vs. K_La in different reactors	136
Figure 4.36. Aeration efficiency (at 20°C) vs. gas flow rate in BCR, ALR, and Novel BCR.....	137
Figure 4.37. Bubble size distribution in BCR with different gas flow rates.....	139
Figure 4.38. All-in-one bubble size distribution in BCR.....	140
Figure 4.39. Bubble size in BCR from mean value and d_{32} calculation value	140
Figure 4.40. Bubble size distribution in ALR with different gas flow rates.....	141
Figure 4.41. All-in-one bubble size distribution in ALR.....	142
Figure 4.42. Bubble size in ALR from mean value and d_{32} calculation value	142
Figure 4.43. Bubble size distribution in Novel BCR with different gas flow rate ..	143

Figure 4.44. All-in-one bubble size distribution in Novel BCR.....	144
Figure 4.45. Bubble size in Novel BCR from mean value and d_{32} calculation value	144
Figure 4.46. The bubble size (d_{23}) in different reactors	145
Figure 4.47. Terminal rising bubble velocity in different reactors	146
Figure 4.48. Specific interfacial area vs. gas flow rate in different reactors.....	148
Figure 4.49. K_L coefficient at 20°C vs. gas flow rate in different reactors	149
Figure 4.50. Comparison of experimental K_L values in Novel BCR with values obtained by Higbie's model	150
Figure 4.51. Semi-logarithmic scale plot of ferrous reduction ratio with different $[Fe^{2+}]_0$ in BCR and Novel BCR ($Q_g = 10$ LPM)	152
Figure 4.52. Ferrous concentration along aeration time with different gas flow rate (Q_g) in Novel BCR ($[Fe^{2+}]_0 = 15$ mg/L).....	153
Figure 4.53. Scatter plot for the rate constant in zero, first, and second-order...	154
Figure 4.54. Ferrous concentration obtained from experiment and calculation of proposed kinetic rate	155
Figure 4.55. Sampling ports for batch settling test.....	156
Figure 4.56. Settling result of fraction removal vs. overflow in Novel BCR.....	157
Figure 4.57. Residual turbidity after jar test from different alum concentrations	158
Figure 4.58. Summary the separation process for ferric iron in this work	160

LIST OF TABLE

	Page
Table 2.1. Iron oxidation reactions	10
Table 2.2. Effect of ionic strength on ferrous oxygenation rate constant	14
Table 2.3. Oxygen transfer efficiency from different airflow rate and diffusers	26
Table 2.4. Experimental conditions of classical design with 3 factors with 2 levels	41
Table 2.5. Experimental conditions of statistical design	42
Table 2.6. DOE application (Živorad, 2004).....	43
Table 2.7. General experimental design for two-factor factorial design.....	44
Table 2.8. Analysis of variation for two-factor factorial, fixed effects model	46
Table 2.9. Analysis of variance for 2^k factorial design.....	49
Table 2.10. Summary of exited works for iron removal technology	58
Table 2.11. BCR applications in air-water study and investigated parameter.....	59
Table 3.1. Variables with factor levels for primary factor screening.....	84
Table 3.2. The parameter measurement for factor screening experimental process	84
Table 3.3. Parameter measurement for optimization process	86
Table 3.4. Parameter measurement for ferrous iron oxidation	89
Table 3.5. Parameter measurement for ferric iron separation.....	91
Table 4.1. Experimental condition for study downcomer-to-riser ratio.....	95
Table 4.2. Experimental design by 2^{k-1} factorial for 1^{st} factors screening.....	97
Table 4.3. Experimental result designed by 2^{k-1} factorial for 1^{st} factors screening.....	98
Table 4.4. Single response of effective value, T-value, and P-value.....	103
Table 4.5. Variables with factor levels for CCD-RSD.....	104
Table 4.6. Experimental condition designed by CCD for 1^{st} factors optimization.....	105
Table 4.7. Experimental result for first factor optimization.....	106

Table 4.8. Experimental result statistical analysis of first factor optimization	109
Table 4.9. Variables with factor levels for 2^{k-1} factorial design.....	112
Table 4.10. Experimental design and results for second factor screening	114
Table 4.11. Variables with factor levels for CCD-RSD	116
Table 4.12. Experimental condition designed by CCD for 1 st factors optimization	118
Table 4.13. Experimental result statistical analysis of second factor optimization	120
Table 4.14. Final optimization for this novel reactor, Novel BCR	124
Table 4.15. Constructed correlation of K_La coefficient in Novel BCR.....	127
Table 4.16. Experimental results and improvements in terms of K_La coefficient	131
Table 4.17. Water characteristic before and after filtration test.....	159



CHAPTER 1

INTRODUCTION

1.1 General Context

Water is counted as the renewable resource that cannot run or use out. However it still has the problems of the distribution in both time and space such as too less water, too much water, too polluted water, etc. Day-to-day, people try to find out the solution in order to manage these water problems to accommodate the requirement for many main sectors including irrigation and drainage, flood protection, sanitation, hydropower plan, and especially for water supply. The water supply is very important for surviving all of the life as exactly that the people, animals, and plants need for drinking and living activities. Water supply refers to the water pump out by both private and public water supply and distribution to the customer. Demand of the water supply has continued to increase as the world's population and economic activities have risen as well.

As normally known that about three-quarters of the earth's surface is covered by water but freshwater still be limited its amount while about 97% of the earth water is oceans and salt water. There is only 1% of earth water is available as freshwater for daily water supply during other 2% is in glaciers, ice caps, and snowy mountain ranges. The freshwater which was mentioned store in lake or river or streams, called surface water and store in the soil or bedrock, called groundwater. Groundwater is one of the great value items which is provided by subsurface layer onto both productivity and human living region. Groundwater is estimated about 982 km³ annually extracted as the most extracted raw material in the world (Margat *et al.*, 2013) for providing to many different sectors including Agriculture (approximate 60%), and the rest for Domestic and Industrial sector (Vrba *et al.*, 2004). However other report (NGA, 2013) showed that more than half of the groundwater withdraw is used as domestic water supplies and it provides range about 25 to 40% of the world drinking water. In terms of groundwater use, irrigated land about 38% is supplied by it (Siebert *et al.*, 2010).

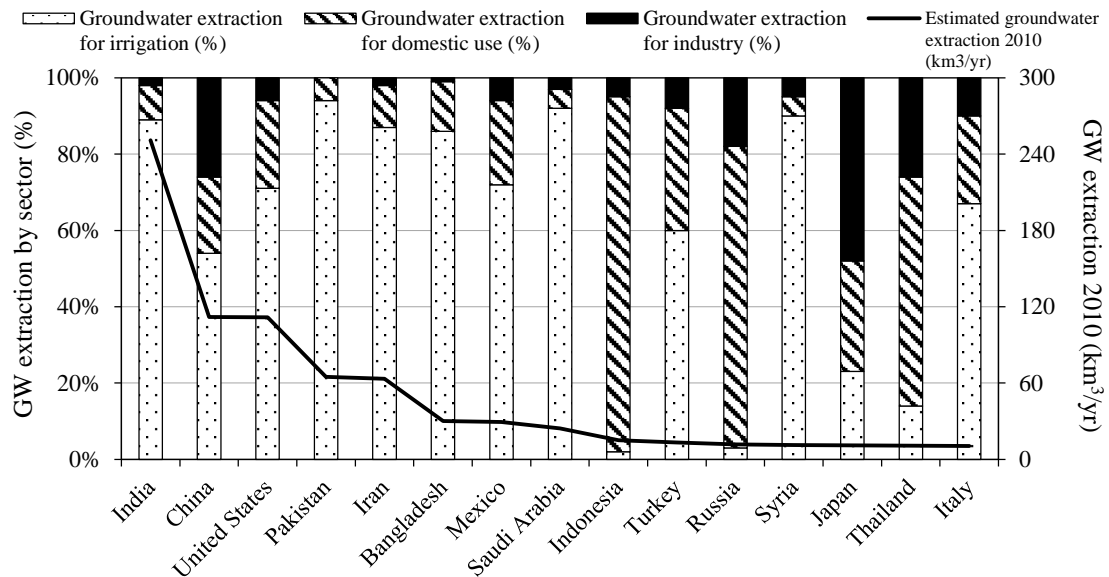


Figure 1.1. The 15 nations with largest estimated annual groundwater extraction

In Thailand, surface water and groundwater serve as main water supply source. Specifically, there are four types of domestic water supply source to all of the people in Thailand during 1990 to 1996 such as tap water, public well, private well, and other (canal, river, rain). Thailand is counted as fourteenth largest country that extracted much groundwater, about 10.74 km³ annually less than the largest user of groundwater in the world, India, approximately 251 km³ as present in Figure 1.1 (Margat *et al.*, 2013). Groundwater source in Thailand acts one fifth of 220 nation towns/cities and for half of 700 sanitary districts, residential water uses up 75% from groundwater sources with support for some 35 million people in villages and in urban areas. Both government and private sector worked more than 200 000 groundwater well projects, about 7.55 million cubic meter per day (2700 million cubic meter per year) (Facon, 2001). Most of the groundwater usage in Thailand is for domestic water supply, approximate 60% while other 26% is used for industrial requirement, and the rest is for irrigation (2010).

Due to aforementioned benefits of groundwater and the problem challenging, groundwater quality and quantity must be primarily concerned for sustainable usage. Because of the natural filtration, groundwater appears clear and clean. However some

chemicals from natural and human-induced sources can be found, for instance, high amount of dissolved Iron and/or Arsenic metals. Some activities of agricultural activity, industrial discharge, urban activity, waste disposal, and groundwater pump can reduce the groundwater quality. If we take a look onto iron in groundwater, it presents in groundwater mostly in the form of ferrous ion (Fe^{2+}) and have the varied concentration from 0 to 50 mg/L (Lenntech, 2015), which higher than WHO recommended value of 0.3 mg/L for drinking water source. Therefore, the presence of iron is likely the most common water problem faced by consumers and water treatment operators (Sarin *et al.*, 2004).

Aeration is the commonly process for oxidizing ferrous iron in water with high concentration, higher than 5 mg/L (Michalakos *et al.*, 1997), as well as to avoid the chemicals requirement. In the frequently technology application of an aeration process, the water can be saturated of oxygen by operating different methods such as conventional tray aerator, gas-liquid contactor (bubble column reactor), etc., as show in Figure 1.2.

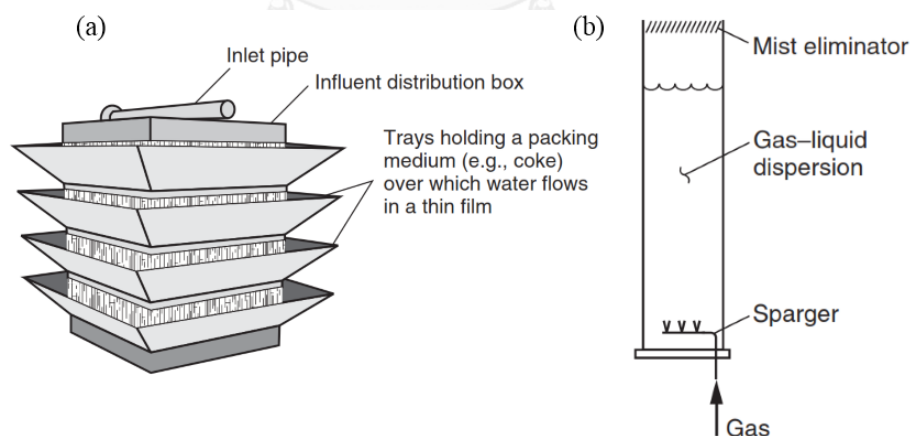


Figure 1.2. Two commonly types for aeration (a) natural draft coke tray aerator (b) common bubble column diffused aerator

One of the best multiphase contactors, Airlift Reactor (ALR) is considered as the promising type of gas-liquid reactor that provides many advantages including well mixing performance, low shear rate, low energy consumption, low reaction time, and

high gas-liquid mass transfer (Bekassy-Molnar *et al.*, 1997). Airlift Reactor is a special modification from bubble column or conventional bubble column reactor (BCR). This reactor class have been studied to apply for oxidize ferrous iron for drinking water purpose as well (El Azher *et al.*, 2008).

1.2 Problem Statement

U.S. EPA (1991) and World Health Organization (WHO) recommend that 0.3 mg/L is the limitation of iron in drinking water for taste and aesthetic reasons. Then one requires only 1 to 2 mg in daily of having iron in the water as the nutrition. However, 7 to 35 mg of iron in daily life is taken by most human (Crittenden *et al.*, 2012), thus, there is a daily iron consumption that accumulate in human body. Iron overload leads to a hemochromatosis that can effect to all body organs and also result with liver problem, diabetes. Other illness that can be leaded from hemochromatosis are diabetes, arthritis, cirrhosis, impotence and certain types of heart ailments or cancer.

Moreover, other disadvantages of the present of iron in the water supply system that usually face are taste/odor problem, stain laundry/household fixture, clog pipes, etc. Iron may react with tannins in tea, coffee, and some alcoholic beverage, that will affect both taste and appearance. As aforementioned, the presence of iron becomes the most common water problem faced by many consumers and water treatment operators (Sarin *et al.*, 2004).

Even though ALR has been receiving much attention from many researchers and industrial investments (Bekassy-Molnar *et al.*, 1997; Couvert *et al.*, 2004) due to its advantages as aforesaid, ***the development of the reactor for improving the oxygen transfer efficiency is still required*** in order to refine the inadequate points of airlift reactor. The reactor is more efficient after the bubble retention time in the reactor was extended. In detail of this relation, increasing the bubble retention time is significant improving the gas holdup parameter, which is the main actor for enhance the oxygen transfer. Then it is very useful for acquire the efficient way to extend the

bubble retention time in the system. Moreover, there are no blades or any baffles in simple airlift reactor for bubbles breaker after generated from the air sparger(s) that it causes the bubble integration as well as increasing the bubble size during the smaller bubble size is beneficial to improving the oxygen transfer. It is, therefore, valuable to seek efficient way to reduce or maintain the bubble size in the reactor. To intensify the oxygen transfer efficiency in airlift reactor, some works have focused on the designing efficient airlift structures (Bando *et al.*, 1992; Choi *et al.*, 1995; Kilonzo *et al.*, 2007; Lu *et al.*, 2000) and some works paid attention on the providing the internals into the reactor including sieve plates or perforated plates, baffles, packing, and static mixers (Chen *et al.*, 1997; Krichnavaruk *et al.*, 2002; X. Wu *et al.*, 2003; Zhang *et al.*, 2005). The reactor development for improving oxygen transfer from air bubble to liquid has been studied and reported by many investigators (Bekassy-Molnar *et al.*, 1997); however, development for the most efficiency is still the main challenge.

1.3 Hypotheses

- Ferrous iron in groundwater could be effectively oxidized by air-water contactor such as bubble column reactor (BCR) or airlift reactor (ALR).
- Adding the vertical baffle and installing horizontal baffles in a riser compartment for Novel Bubble Column Reactor (Novel BCR) or Modified Airlift Reactor (MALR) could provide better oxygen transfer efficiency.
- Better oxygen transfer efficiency could oxidize better ferrous iron.

1.4 Objectives

There are two main objectives of this work including:

- To evaluate the oxygen transfer of the new designed and modified rectangular airlift internal-loop reactor, called as Novel Bubble Column Reactor (Novel BCR) or Modified Airlift Reactor (MALR) in terms of overall volumetric oxygen transfer coefficient (K_La) and energy consumption. Novel BCR comprised the vertical baffle to create a liquid recirculation from a riser to downcomer compartment, and installing horizontal baffles in a riser compartment to extend the bubble retention time and improve the air bubble distribution.
- To study the removal of ferrous iron with high level concentration such as in groundwater, oxidized by using Novel BCR. The optimal Novel BCR configuration and operation condition was analyzed and applied for this ferrous iron removal part.

1.5 Scope of Study

In this study, several scopes will be covered as the following points:

Part I: Study of Reactor Development

- Study the aeration in new design BCR in different conditions in order to evaluate and compare each performance base on K_La coefficient by using tap water as liquid phase and oxygen from the air bubble generation as the gas phase.
- Design experimental condition by using Design of Experiment (DOE) method for different steps including apply in screening main influent factors, study the optimization of the main factors.
- Investigate all influencing factors for DOE in terms of geometry modification and important aeration parameters including downcomer-to-riser ratio (A_d/A_r),

baffle angle (α), baffle length (L_b), baffle quantity (N_b), recirculation area (A_r), the position of recirculation area (Y_r), baffle settling area (A_s), gas diffuser quantity (N_d), and gas flow rate (Q_g). In this study, terminology of baffle is referred to horizontal baffle.

- Analysis the experimental results including screening main influent factors part, optimizing the main factors part, and construct the prediction equation by DOE method of computer software, Minitab 17.
- Select the optimal design and operating condition of this Novel BCR for studying oxidation of ferrous iron in Part II.
- Study the Bubble Hydrodynamics Parameters in the investigated reactor, Novel BCR.

Part II: Study of Ferrous Iron Oxidation

- Study the oxidation of ferrous iron in the optimum condition of Novel BCR by using a single ferrous iron pollutant dissolved in de-aerated tap water as the synthetic groundwater. It was conducted as a Sequencing Batch Reactor (SBR).
- Investigate the experimental parameters including Gas Flow Rate (Q_g) and Initial Ferrous Iron Concentration ($[Fe(II)]_0$) based on actual amount and type of the real life.
- Sampling and analyst the samples along time by using Phenanthroline method.
- Construct the simple kinetic rate for this oxidation process of ferrous iron.
- Propose the appropriate techniques for separation process of ferric iron.
- All experiments were help in the laboratory of Department of Environmental Engineering, Faculty of Engineering, Chulalongkorn University.

CHAPTER 2

THEORY AND LITERATURE REVIEW

2.1 Iron in Groundwater

Iron is a common metallic element that usually occurs as natural in deeper wells with little or no oxygen present. It presents as a fourth most abundant element in the earth surface up to 5.6% of mass (McMurry *et al.*, 2004). Ferric oxides and hydroxide ($\text{Fe}(\text{OH})_3$, Fe_2O_3) are the common mineral sources. Red and yellowish color which present on/in the rocks and soils are the effect from ferric hydroxide. Iron (II) reduction can make iron dissolved in groundwater but it's not cause any problems. Iron (II) oxidized to be iron (III) after contact to oxygen in air or bacteria activity. Iron (III) is insoluble hydroxides in water and cause color and staining or/and blockage facilities.

2.1.1 Source of Iron

Amount of iron in groundwater are often higher than that in surface water. Amphibole, iron sulfide and iron rich clay minerals are the weathering iron-bearing minerals of the natural source of iron. Iron will dissolve in groundwater as well after it flows through organic rich soil. It is not only the natural sources, but manmade also such as industrial effluents, landfill leakages and acid mine drainage. Also some facilities which are going to contribute iron to groundwater: storage tank, piping, pump parts, and casing (NSE, 2008). Base on the natural condition of variation of pH and lack of oxygen, iron atoms reduced from iron (III) to iron (II). It will present in the form of soluble iron, iron (II) under condition of pH 5 to 8. But after groundwater is pumped to the surface which will contact with air (oxygen), oxidation process will be occurred. The pH values increase due to iron (II) precipitate to insoluble iron (III) after releases carbon dioxide (CO_2) to atmosphere.

2.1.2 Iron Occurrence

Iron is quite soluble during there is low oxygen containing as a reduced environment or water, for example, a groundwater or surface water contain a low oxygen. It usually found in a ferrous form such as ferrous sulfate, ferrous bicarbonate, and hydroxide forms. Total iron in groundwater is up to 10 mg/L during a low alkalinity (less than 50 mg/L as CaCO_3) (Crittenden *et al.*, 2012). In opposite, it is quit insoluble in an oxidizing environment or water which contain enough dissolved oxygen. There are three physical forms of iron based on an above water quality such as a soluble form (reduction), small colloid particles (oxidation), and large particles (oxidation). For the smaller particles that can pass through with the filter pore size 0.45 μm , it is classified as a soluble form. In an oxygenated surface water, total iron concentration ranges from 0.05 to 0.2 mg/L (pH 5 to 8) with the iron species consist in solids, should be a small colloid particles or large particles of ferric hydroxide ($\text{Fe}(\text{OH})_3$), sorb to a suspended solid (clay particles or organic colloids) and precipitates (Crittenden *et al.*, 2012).

2.1.3 Chemical Properties

The relationships between physical and chemical is important in order to explain what will occur and require in the water treatment system while the iron oxidizing chemistry is so complicated and not well understood. There are several parameters that will effect iron oxidation and reaction rate: temperature of the water, water pH, dissolved oxygen (DO), bicarbonate, natural organic matter (NOM), sulfate, dissolved silica, and a particles. Table 2.1 presents the ferrous ion oxidation in stoichiometric expressions with a requirement of oxygen, alkalinity, and sludge production.

Iron equilibrium form in different species that expect with conditions at any specific E_H -pH combination of the boundary by E_H -pH limit of water (Figure 2.1). A (s) presents the solid forms of iron. The solubility of iron is low and tends to precipitate while it is under reduced conditions ($E_H < 0$) and over pH in a wide range. Iron tends to precipitate to $\text{Fe}(\text{OH})_3$ while it's under oxidized condition ($E_H > 0$) and pH > 5.0. In the free space

in these two condition, iron (II) is relatively soluble and it is a condition of groundwater which E_H range from 0.20 to - 0.10V and pH range from 5 to 9 (Crittenden *et al.*, 2012).

Table 2.1. Iron oxidation reactions

Oxidant	Reaction	Oxidant Needed, mg/mg-Fe ²⁺	Alkalinity Consumed, mg/mg-Fe ²⁺	Sludge Produced, ^a kg/kg-Fe ²⁺
Oxygen	$4\text{Fe}(\text{HCO}_3)_2 + \text{O}_2 + 2\text{H}_2\text{O} \rightarrow 4\text{Fe}(\text{OH})_3 + 8\text{CO}_2$	0.14	1.80	1.90
Chlorine	$2\text{Fe}(\text{HCO}_3)_2 + \text{Ca}(\text{HCO}_3)_2 + \text{Cl}_2 \rightarrow 2\text{Fe}(\text{OH})_3 + \text{CaCl}_2 + 6\text{CO}_2$	0.64	2.70	1.90
Chlorine dioxide	$\text{Fe}(\text{HCO}_3)_2 + \text{NaHCO}_3 + \text{ClO}_2 \rightarrow \text{Fe}(\text{OH})_3 + \text{NaClO}_2 + 3\text{CO}_2$	1.21	2.70	1.90
Potassium permanganate	$3\text{Fe}(\text{HCO}_3)_2 + \text{KMnO}_4 + 2\text{H}_2\text{O} \rightarrow 3\text{Fe}(\text{OH})_3 + \text{MnO}_2 + \text{KHCO}_3 + 5\text{CO}_2$	0.94	1.50	2.43

^a Weight base on Fe(OH)₃ as the precipitate that portion of sludge contain FeCO₃ due to the adaptation from ASCE/AWWA, 1990

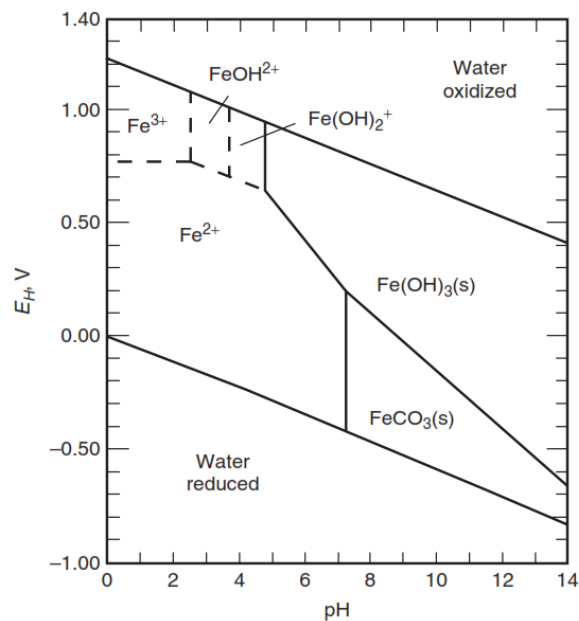


Figure 2.1. Iron forms in water as functions of E_H vs. pH (Crittenden *et al.*, 2012)

Figure 2.1, the E_H -pH diagram for iron species in water adapted from Langmuir (1997) which constructed with total iron activity 10^{-7} M (or 5.6 $\mu\text{g/L}$), SO_4^- 96 mg/L, species of CO_2 at 1000 mg- HCO_3^- /L, temperature at 25°C, and 1 atm pressure.

2.1.4 Iron Measurement

Iron (III) quite precipitates and colors reddish brown to the water. It will settle out. Organic iron is bound to organics (tannin or lignin) and makes the water colorless which difficult to remove. To estimate the present of organically-bound iron by sampling to run the water pass through filter 0.45 μm of syringe, the water is still colorless. As there was mentioned at the upward, iron (II) is a commonly found in deep wells where lacking of oxygen which usually called clear water iron that makes the water colorless as well (Marianne, 2007).

Application of the bench top analysis or colorimetric test is used for iron analysis in order to determine an accurate level or should obtain to the lab for certified analysis. Iron bacteria is also require to measure which use iron as food source with a present of slimy reddish brown as a good indication, usually found in the back of a toilet tank. Biological activity reaction test, a good way to confirm a present of iron bacteria, can be used for iron bacteria, called BART test (Marianne, 2007). It will never require a lab, microscope or incubator.

2.2 Iron Treatment Method

Iron and Manganese are often occur together in water during the general concepts to remove these soluble species are similar. There are several different treatment methods to remove iron and manganese such as (i) oxidation (oxygen called aeration, ozone, potassium permanganate, chlorine, chlorine dioxide followed by sedimentation and filtration to remove precipitant), (ii) ion exchange, (iii) membrane, (iv) stabilization, and (v) lime treatment process. There will be detailed of each method in the following points.

2.2.1 Oxidation Process

In order to precipitate iron to insoluble products, there is required oxidation process. Oxidation process is the transferring electrons from iron to oxidizing agent which are applying. Oxidation process will oxidize ferrous to ferric ion which form as insoluble hydroxide ($\text{Fe}(\text{OH})_3$).

- Iron oxidation kinetics

Base on exited work (Stumm *et al.*, 1961), the ferrous iron oxygenation rate will be a first order respect to ferrous and oxygen, and second order respect to hydroxide ion during iron is not present complex with NOM and pH is higher than 5.5. From the observation in the experiment, there is a proposed expression as following equation 2.1 and 2.2.

$$-\frac{d[\text{Fe}^{2+}]}{dt} = k[\text{Fe}^{2+}][\text{OH}^-]^2 P_{\text{O}_2} = k_r[\text{Fe}^{2+}] \quad \text{Eq. 2.1}$$

Or

$$k[\text{OH}^-]^2 P_{\text{O}_2} = -\frac{d[\text{Fe}^{2+}]}{[\text{Fe}^{2+}]dt} = -\frac{d \ln[\text{Fe}^{2+}]}{dt} \quad \text{Eq. 2.2}$$

Where $[\text{Fe}^{2+}]$ is the concentration of aqueous-phase ferrous iron [mol/L]; k is rate constant, $8.0 (\pm 2.5) \times 10^{13} \text{ L}^2/\text{mol}^2 \cdot \text{min} \cdot \text{atm}$ at 20°C (Stumm *et al.*, 1961); $[\text{OH}^-]$ is the concentration aqueous-phase hydroxide ion [mol/L]; P_{O_2} is partial pressure of oxygen [atm]; $k_r = k [\text{OH}^-]^2 P_{\text{O}_2}$, pseudo-first-order constant [min^{-1}]. Ferrous iron oxygenation rate is dependent on pH as presented in the Figure 2.2. Then equation 2.1 can be rearranged as equation 2.2. Partial pressure of oxygen is assumed as a constant, equation 2.3 is written. Base on (Snoeyink *et al.*, 1980), the ferrous iron oxygenation rate can be rewritten in logarithms form as equation 2.4 where $k'' = k'K_w^2$, constant.

$$-\frac{d \ln[\text{Fe}^{2+}]}{dt} = k'[\text{OH}^-]^2 \quad \text{Eq. 2.3}$$

$$\log(\text{rate}) = \log(k'') + 2\text{pH} \quad \text{Eq. 2.4}$$

- **Effect of pH**

As mentioned previously, pH higher than 5.5, ferrous iron oxygenation rate can be written as equation 2.1 by increase 100-fold per unit of pH. In opposite, it is independent of pH after pH less than 3.5 as shown in Figure 2.2. (Crittenden *et al.*, 2012). Figure 2.2 was conducted at 0.2 atm of P_{O_2} and 25°C of temperature.

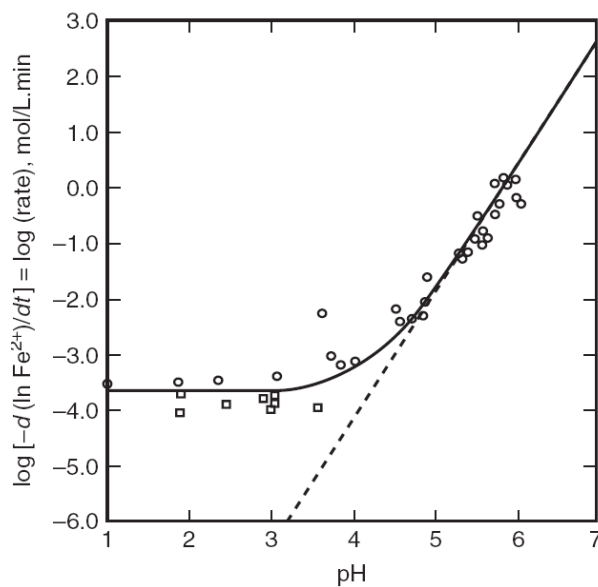


Figure 2.2. Ferrous iron oxidation rate by oxygen (Crittenden *et al.*, 2012)

- **Effect of temperature on ferrous ion oxygenation**

Ferrous iron oxygenation rate will be affected by temperature during the condition presented in Figure 2.3. The temperature was ranged from 5 to 30°C by plotting in first-order. From the result, the effect of temperature to ferrous oxygenation rate appears to be large, but the rate will vary slightly with temperature while the data are normalized with respect to changes in K_w and O_2 solubility. Figure 2.3 presents in the experimental condition of 0.11M ionic strength adjusted with $NaClO_4$, 9 mM as $NaHCO_3$ of alkalinity, 0.2 atm of P_{O_2} , pH value equal 6.82, and initial ferrous concentration as 34.7 μM (Sung *et al.*, 1980).

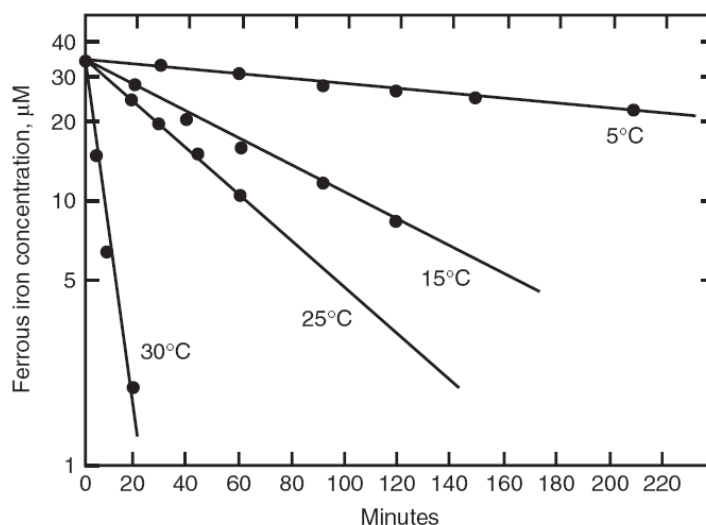


Figure 2.3. Effect of temperature on ferrous oxidation kinetics (Crittenden et al., 2012)

▪ Effect of ionic strength on ferrous ion oxygenation

From the exited work (Faust *et al.*, 1998), the effect of ionic strength to a ferrous iron oxygenation rate is presented in Table 2.2. The ionic strength was increased from 0.009 to 0.11 M and the rate constant decreases from 4.0×10^{13} to $1.2 \times 10^{13} \text{ M}^{-2} \cdot \text{atm}^{-1} \cdot \text{min}^{-1}$. Experiment was practiced in a condition 25°C temperature, $9 \times 10^{-3} \text{ M-HCO}_3^-$ of alkalinity, 0.20 atm of Po_2 , pH equal 6.84, and initial ferrous concentration equal $34.7 \mu\text{M}$.

Table 2.2. Effect of ionic strength on ferrous oxygenation rate constant

Ionic Strength mol/L	k $\times 10^{13} (\text{mol/L})^{-2} \cdot \text{atm}^{-1} \cdot \text{min}^{-1}$
0.009	4.0 ± 0.6
0.012	3.1 ± 0.7
0.020	2.9 ± 0.6
0.040	2.2 ± 0.5
0.060	1.8 ± 0.3
0.110	1.2 ± 0.2

Source (Crittenden *et al.*, 2012)

- **Effect of complexing agents**

Not only pH, temperature, and ionic strength that can affect the ferrous oxygenation rate, but a complexing agents also. For example, the oxidation kinetic will be slow down after a humic and tannic acids or other NOM bind or complex iron. The presence of humic acid with a low pH (less than 5) shows that soluble ferrous is not complex formation. Increasing pH value (greater than 8), the soluble ferrous presents in complex formation (Crittenden *et al.*, 2012). Furthermore, organically bound ferrous cannot be oxidized by aeration process effectiveness (Kawamura, 2000).

As mentioned, there are several common oxidants used to oxidize iron including: oxygen (O₂), ozone (O₃), chlorine (Cl₂), chlorine dioxide (ClO₂), potassium permanganate (KMnO₄), etc. Briefly description of each oxidant is presented as following.

- **Oxidation with air**

Dissolve oxygen was provided into water to convert from iron (II) to Fe(OH)₃. From stoichiometric equation, 1 mg of oxygen can oxidize soluble ferrous 7 mg or oxidation require oxygen 0.14 mg for 1 mg of ferrous (Table 2.1). Iron can be completely oxidized in about 15 minutes during pH approximate 7.5 to 8.0 with non-complex NOM.

Aeration devices of air-water contact system are classified into four different types as mention in *aeration and air stripping* point: diffusion or bubble aerator, mechanical aerator, droplet or thin-film contactor, and aspirator aerator. Diffused aeration is a process which installed an air diffuser device at the bottom of the reactor. The ratio of air and water in volumetric base is about 0.75 to 1.00 with oxygen transfer efficiency is about 5 to 10%. For coke tray aerator, a series of three to five trays with allow the water flow down provides oxygen to water. The water loading rate is about 600 to 800 L/m².min. About 15 to 30 min addition time for baffled basin is used to follow aeration device (Crittenden *et al.*, 2012). Base on (Kawamura, 2000), amount of iron is higher than 5 mg/L, alum addition after aeration should be required.

- **Oxidation with ozone**

Ozone oxidant can be apply to oxidize ferrous but it is not commonly used due to more costly spend. However, ozonation application is successful to remove ferrous by conventional treatment method with preozonation in Europe. From stoichiometric equation, a requirement ozone for oxidation ferrous 1 mg is 0.43 mg. Removal ferrous which complexed with NOM will not effected by ozonation of conventional processes. Base on practical, overdosing ozone will provide a various form of permanganate in pink color (Crittenden *et al.*, 2012).

- **Oxidation with chlorine**

In traditional practice, only chlorine or apply with potassium permanganate were used to control iron in pH condition follow by coagulation, sedimentation, and filtration. To oxidize soluble ferrous ion effectiveness, about 5 mg/L of free chlorine is used. However, high doses of chlorine is not prefer due to the disinfection by-product (DBP).

From stoichiometric equation, to oxidize ferrous ion 1 mg require 0.64 mg of chlorine (Table 2.1). A pH typically around 8.0 to 8.5 is required in order to archive an oxidation time about 15 to 30 mins. The oxidation rate will be reduce due to the present of ammonia because it will consume any chlorine and form chloramines. A commonly used method of iron and manganese removal are series of prechlorination, alum coagulation, sedimentation, and filtration. Permanganate is used to form manganese oxide on media surface of filtration (Crittenden *et al.*, 2012).

- **Oxidation with chlorine dioxide**

Chlorine dioxide oxidant is stronger than chlorine oxidant and provide better oxidation with soluble ferrous ion. Oxidation of ferrous by chlorine dioxide shows that five electrons transfer and result to Cl^- . From stoichiometry equation, to oxidize ferrous ion 1 mg require ClO_2 oxidant 1.21 mg (Table 2.1). Reaction rate of ferrous with chlorine dioxide is little bit fast. At pH value of 5.5, the time requirement for oxidize soluble

ferrous with chlorine dioxide is 5 seconds and be faster at higher pH value (Crittenden *et al.*, 2012). Moreover, it will be difficult to oxidize during the present of ferrous complex with NOM. If there is a ferrous complex with NOM, recommended to remove NOM first such coagulation or activated carbon (AC) processes.

- Oxidation with potassium permanganate

Soluble ferrous ion can be oxidized by using potassium permanganate with similar rate, but it is not commonly used due to much higher cost compare to chlorine. In the application that content both Fe^{2+} and Mn^{2+} , usually oxidize ferrous ion by chlorine first and follow potassium permanganate to oxidize Mn^{2+} . Requirement more than 1 hour for contact time and more oxidant dosages to oxidize ferrous complex with NOM. Usually, if there is a ferrous complex with NOM, KMnO_4 is not the common one. But apply KMnO_4 as a solution is a typical process. The type of filtration is used in iron and manganese removal is pressure filtration. Depth of greensand filter is applied as the conventional filtration with effective of less than 0.3 mm size. Pick color is easy to occur after KMnO_4 dose is not well controlled. So to identify a requirement of dose rate, bench and pilot scale experimental is very necessary.

2.2.2 Ion Exchange Process

Low concentration of Fe^{2+} and Mn^{2+} (less than 0.5 mg/L) could be removed by using ion exchange process. The application for Fe^{2+} and Mn^{2+} removal by ion exchange are generally applied for treatment industrial water with limited treatment and treatment groundwater usage in individual family (Crittenden *et al.*, 2012). A strong acid cation (SAC) is usually used as an exchange resin in sodium form. Even though SAC resin cannot remove a ferrous form with complexed NOM, strong base anion (SBA) resin can remove up to 95% base on (Clifford, 1999).

The exited work at Santa Monica city in California, iron in groundwater was remove by aeration and filtration of ion exchange media 0.762 m. The ion exchange media can remove iron about 1.0 mg/L of 30 000 m^3/day by soft the water in filtration process.

In that research, some important parameters include aeration process, contact basin process, and filtration process. Contact time 10 mins with air-to-water ration 0.75 are used in aeration process and 60 mins contact time is allowed for unbaffled contact basin. Filtration rate of 9.8 m/h with effective size of 0.4 mm of the resin bed. Resin life is around 12 years effectiveness (Crittenden *et al.*, 2012).

2.2.3 Membrane Process

Reverse osmosis (RO) is a one of the membrane treatment process that is used to separate dissolved solutes from water. Remove dissolved iron, reverse osmosis membrane can be used very effective (Crittenden *et al.*, 2012). Pretreatment system is always required to remove oxidized iron which can reduce the treatment efficiency, even it is small amount. Base on a research in Netherlands of (Duranceau, 2001), both Fe^{2+} and Mn^{2+} can be removed effectively after put a water under anaerobic conditions. This study operates with ferrous concentration from 11 to 25 mg/L.

2.2.4 Stabilization Process

SHMP-Sodium hexametaphosphate ($(\text{NaPO}_3)_6$) or polyphosphate or polysilicate is one of the chemical which is used to stabilize Fe^{2+} and Mn^{2+} in water treatment. There are three different form of this chemical include crystal, granular, and liquid form with highly soluble. A chemical should add before oxidation process, mean it is in soluble state.

SHMP can promote a growing of biological because it contents high phosphate, about 66% P_2O_5 with a formation of phosphate result as a by-product of reaction (Crittenden *et al.*, 2012). In a storage basin of treated water, SHMP need to be used carefully, otherwise, algal blooms and slimes might grow. In stabilization process, Fe^{2+} and Mn^{2+} will not be removed directly but will be held in aesthetically acceptable condition that will degrade by time. Analytical test can be determined a feed rates of SHMP which typically less than 2 mg/L. Range of 0.3 to 1.0 mg/L of ferrous iron and 0.05 to 0.1 mg/L of Mn^{2+} , stabilization process can be considered (Crittenden *et al.*, 2012).

2.2.5 Lime Treatment Process

Both Fe^{2+} and Mn^{2+} can be removed effectively by lime treatment process. Some conditions can improve the removal efficiency include it is a pre-aerated water, pH during process is higher than 9.8, alkalinity is higher than 20 mg/L as CaCO_3 (Crittenden *et al.*, 2012). Softening is one of the process with high cost.

2.3 Aeration Process

Aeration is the process to generate an air into the water in order to increase an amount of dissolved oxygen content in water by several different practices such as diffuser; stacked trays; or surface turbine and wheels. There are several main points that will be study in aeration process. Theory of gas transfer, bubble aeration, and fine pore diffuser which are the important theories for this work will be presented as follows.

2.3.1 Dissolved Oxygen (DO)

Dissolved oxygen is the amount of gaseous oxygen (level of free or non-compound oxygen) dissolved in any liquid or water which usually presents in the unit of mg/L or parts per million (ppm). DO is very important for all animals that are in the fresh water and oceans, especially, the life underwater. Its level is sufficient to support biological activity. Figure 2.4 presents about DO indicator on water quality as water contaminated at a temperature 20°C. There are three main factors affecting to the solubility of DO, include temperature, pressure (Henry's law), and mineral content of water, will be presented in theory of gas transfer of the next point. A saturate dissolved oxygen in water as a function of temperature and barometric pressure is presented in an Appendix 1.

The importance of DO are (i) to limit a biological reactions (aerobic bacteria or/and anaerobic bacteria, (ii) to monitor the process to ensure that there is enough dissolved oxygen for aerobic bacteria metabolism in wastewater treatment, septic condition, and to control DO level in activated sludge of aeration tank, (iii) to indicate the water

pollution in river as present, and (iv) to determine the level of BOD in water. The standard methods for dissolved oxygen are included membrane electrode method (DO meter), azide modification (chemical method), and copper sulfate-sulfamic acid flocculation modification.

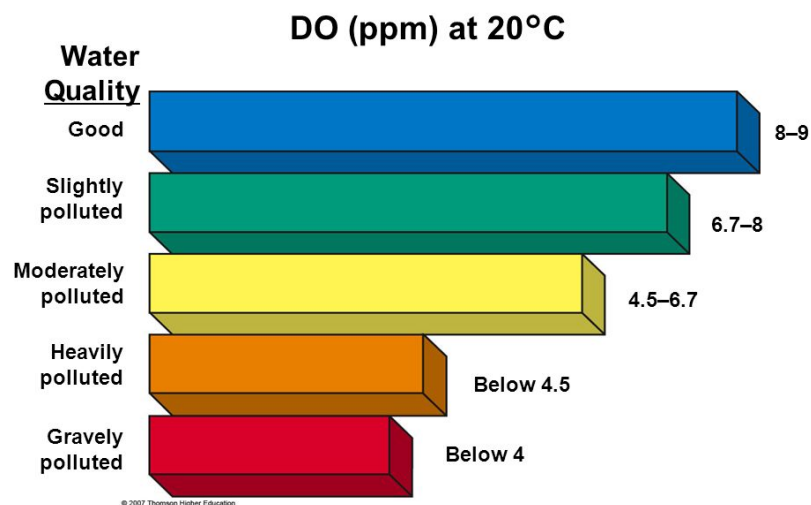


Figure 2.4. Water quality and DO content in ppm at 20°C (Thomson, 2007)

2.3.2 Theory of Gas Transfer

In order to processes an aeration and air stripping in both design and operation, understanding about the theory of gas transfer in terms of chemicals between water and air equilibrium partitioning, and the rate of mass transfer across air-water interface are very necessary. Base on (Edzwald, 2011), equilibrium is defined as a last state for the system to move towards. The system displacement from equilibrium determined the amount of the fluid (air) that needed for aeration as the driving force to governs mass transfer. For example, the rate of chemicals to change the phase is used to determine and required basin size for aeration or air stripping. Both of equilibrium and mass transfer will be used to construct mass balance equation as well as governing equations.

- Equilibrium

Henry's law can be used to describe the equilibrium partitioning between air and water in the application of aeration or air stripping in water treatment processes. It will consider in a closed system as present in Figure 2.5. The equilibrium can be expressed as the equation 2.5 during component A is in equilibrium with both phases at constant temperature. The equation is reduced to yield equation 2.6 after applied 1 atm of pressure where K_{eq} is equilibrium constant, a_{air} is component A activity in gas phase, a_{aq} is component A activity in aqueous phase.

$$K_{eq} = \frac{a_{air}}{a_{aq}} \quad \text{Eq. 2.5}$$

$$H = K_{eq} = \frac{P_A}{\gamma_A A} \quad \text{Eq. 2.6}$$

H is Henry's law constant of component A [atm-L/mol], P_A is pressure A in gas phase [atm], γ_A is an activity coefficient of component A in aqueous phase, A is an molar concentration in aqueous-phase of component A [mol/L] (Edzwald, 2011).

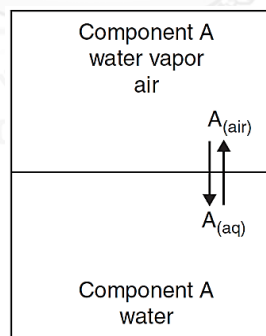


Figure 2.5. Equilibrium condition schema in air-water of component A

▪ Estimation of Henry's Constant

The Henry's constant can be estimated if that component's vapor pressure and aqueous solubility are provided or known. In order to estimate Henry's constant of component A, there are two different possible situations (Edzwald, 2011). One of them,

it is in a condition that component A is perfectly miscible in an aqueous phase and other one, it is immiscible in an aqueous phase.

$$H = P_{v,A} \quad \text{Eq. 2.7}$$

$$H = \frac{P_{v,A}}{C_{s,A}} \quad \text{Eq. 2.8}$$

For the first condition that component A is perfectly miscible in an aqueous phase, the exerted pressure and the vapor pressure will be the same at the desire temperature and component A mole fraction is 1 (x_{H_2O}). So the following expression is written as equation 2.7 where $P_{v,A}$ is the vapor pressure of component A at desire temperature [atm]. For other condition that it is immiscible in the aqueous phase. Another phase, called third phase of component A will form with aqueous phase and the component A solubility will increase. H will not be able to identify by vapor pressure and solubility if that third phase contains water because of the unknown of the third phase partitioning. In opposite during the third phase contain only the component A, the following expression is written as equation 2.8 (Edzwald, 2011). Where $C_{s,A}$ is solubility of component A aqueous [mg/L]. In both conditions, applying an H values from ± 50 to 100% of the values from experimental.

▪ Effects of temperature and solution property

Several factors that will affect the equilibrium partitioning of air and water include pressure, temperature, pH, surfactant and ionic strength. The effect of pressure on H is usually negligible due to the operation of aeration or air stripping in the atmosphere pressure. Increasing temperature tends to increase H value because of the decreasing of aqueous solubility after the vapor pressure increase. A pH will not affect the Henry's constant but the distribution of species of ionized and unionized forms. Surfactant is another factor that affect to the compounds volatility. During the less concentration of surfactant in nature, they do not affect the aeration or air stripping. VOCs or gases in water supply usually have high volatility that will result in decrease the solubility of

volatile component and increase a component A activity coefficient (γ_A in aqueous solution). A γ_A will increase with ionic strength increase too (Edzwald, 2011).

- Mass transfer

Some water treatment processes are also applied the transfer concept to change a material phase from liquid to gas or liquid to solid. The processes including aeration and air stripping, adsorption, ion exchange, and reverse osmosis are counted as an application of mass transfer. The displacement from the equilibrium is the force for mass transfer of one phase to other phase. Figure 2.6 presents about two different mass transfer situations of air and water at steady state. Usually, two-film model is applied in order to representative the rate of mass transfer for air stripping of VOCs, and other gas include H_2S ; and adsorption of the gas include O_2 , CO_2 , N_2 , O_3 (Crittenden *et al.*, 2012).

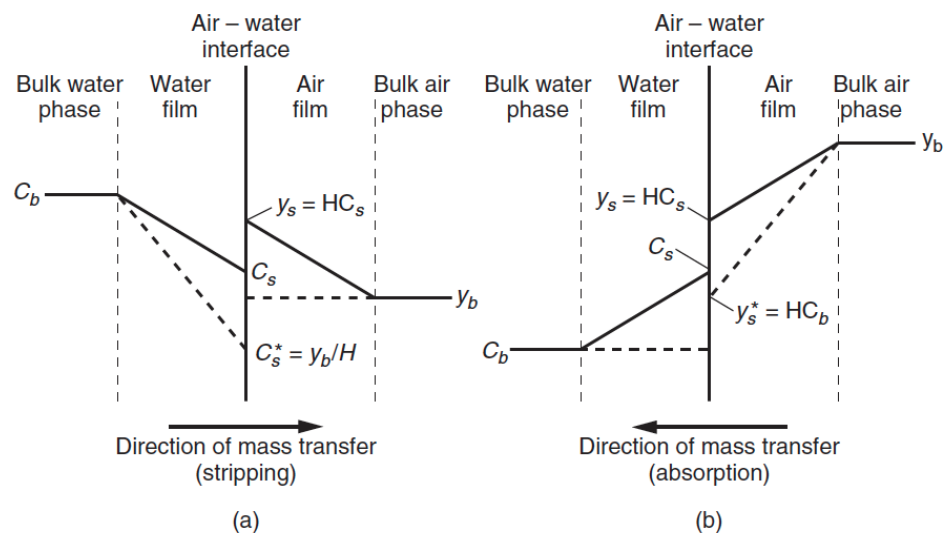


Figure 2.6. Mass transfer for (a) stripping and (b) absorption by using two-film theory (Crittenden *et al.*, 2012)

2.3.3 Oxygen Transfer in Clean Water

Given volume of water will be aerated, aeration devices are estimated based on an amount of oxygen transfer per unit of air applied to the water until reaching an

equilibrium condition. The evaluation of the oxygen transfer coefficient in clean water will be considered in the following paragraphs.

The method of the overall oxygen transfer coefficient in clean water, as detailed in (ASCE, 1992), will be briefly shown in this section. The process of this test starts from an initial dissolved oxygen removal from the water by using a sodium sulfite before reoxygenation to the saturated point. The dissolved oxygen in the water is monitored during the aeration period and measuring its concentrations. The data analysis obtained from a test is specified by equation 2.9, then, modify in a linear form as equation 2.10:

$$\frac{C_S - C_t}{C_S - C_0} = e^{-(K_L a)t} \quad \text{Eq. 2.9}$$

$$\log(C_S - C_t) = \log(C_S - C_0) - \frac{K_L a}{2.303} t \quad \text{Eq. 2.10}$$

where $K_L a$ is an overall liquid film coefficient, C_t is a concentration in liquid bulk phase at time t [mg/L], C_S is an equilibrium concentration with gas, given by Henry's law [mg/L], and C_0 is an initial concentration [mg/L]. This equation is used to estimate volumetric mass transfer coefficient $K_L a$ and equilibrium concentration C_x^* , which substitute a term C_S (ASCE, 1992).

- Effect of temperature on oxygen transfer

The same as an establishment of BOD rate coefficient, the temperature effects are treated by applying a van't Hoff-Arrhenius expression. Equation 2.11 was constructed for this conversion.

$$K_L a_{(T)} = K_L a_{(20^\circ C)} \theta^{T-20} \quad \text{Eq. 2.11}$$

Where $K_L a_{(T)}$ in an oxygen mass transfer coefficient at T temperature [s^{-1}], and $K_L a_{(20^\circ C)}$ is an oxygen mass transfer coefficient at $20^\circ C$ [s^{-1}]. θ value varies base on the test

condition and typical range from 1.015 to 1.040. Both diffuser and mechanical aeration devices typically used θ equal 1.024 (Metcalf, 2003).

2.3.4 Bubble Aeration and Diffuser Device

Bubble aeration process is a process of contacting gas bubbles with water in order to transfer gas such as oxygen, ozone, carbon dioxide to the water. Usually, diffuser system is installed near the bottom of the tank in the purpose to maximize gas-to-water contact as show in Figure 2.7. A diffuser device was classified into fine bubble size and coarse bubble size. Fine bubble size provides more oxygen transfer efficiency. Oxygen transfer efficiency depends on several factors such as diffuser characteristic including type, size, and shape; airflow rate; submerged depth; diffuser location; and water characteristic (quality). The oxygen transfer efficiency in clean water obtained from different gas flow rate and various types of diffuser device is presented in Table 2.3 with 4.5 m of the submerged depth (Metcalf, 2003).

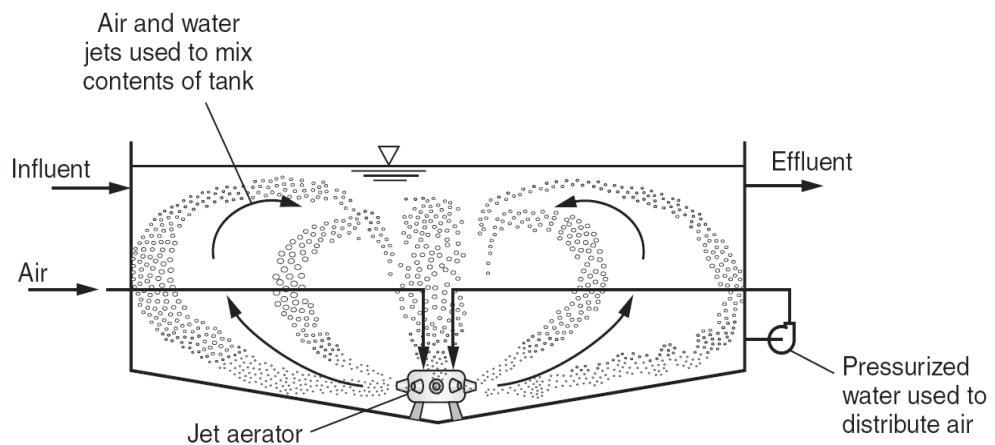


Figure 2.7. The typically air diffuser system, aeration process (Crittenden et al., 2012)

Table 2.3. Oxygen transfer efficiency from different airflow rate and diffusers

Diffuser type and placement	Air flow rate/diffuser [ft ³ /min]	SOTE (%) at 4.5 m submergence ^a
Ceramic disks-grid	0.4-3.4	25-35
Ceramic domes-grid	0.5-2.5	27-37
Ceramic plates-grid	2.0-5.0 ^b	26-33
Rigid porous plastic tubes		
Grid	2.4-4.0	28-32
Dual spiral roll	3.0-11.0	17-28
Single spiral roll	2.0-120	13-25
Non-rigid porous plastic tubes		
Grid	1.0-7.0	26-36
Single spiral roll	2.0-7.0	19-37
Perforated membrane tubes		
Grid	1.0-4.0	22-29
Quarter points	2.0-6.0	19-24
Single spiral roll	2.0-6.0	15-19
Perforated membrane panels	N/A	38-43 ^c
Jet aeration		
Side header	54-300	15-24
Nonporous diffuser		
Dual spiral roll	3.3-10	12-13
Mid-width	4.2-45	10-13
Single spiral roll	10-35	9-12

^a SOTE – Standard Oxygen Transfer Efficiency at a standard condition of tap water 20°C, 101.3 kN/m², and DO_{initial} = 0 mg/L N/A: not applicable

^b Units are ft³/ft² of diffuser.min ^c Personal communication, Parkson Corporation

Source (Metcalf, 2003)

- **Fine pore diffuser**

Usually, the definitions of fine and coarse bubble size are never provided well. Based on (EPA, 1989), a bubble size produced from coarse bubble diffusers is approximate 6-10 mm in clean water, however the initial bubble size from orifice should be bigger than this value due to a bubbles produced tend to shear and be broken down into a smaller. Diameter of a fine bubble is about 2-5 mm from fine pore devices, which effected by airflow and will be bigger after increase an airflow rate. Nowadays, fine pore media can be classified into three types such as ceramics, porous plastics, and perforated membranes with four types of diffuser base on its shape include plates, tubes, dome, and discs.

2.4 Bubble Column

Bubble column reactor (BCR) is counted in one type of the multiphase reactors with a gas distributors at the bottom. BCR is usually used as multiphase contactor in chemical, petrochemical, biochemical and metallurgical industries (Degaleesan *et al.*, 2001). In chemical processes, BCR is involved for some reactions include oxidation, chlorination, alkylation, polymerization, and hydrogenation. It provides more advantages than the other reactor such as the excellent heat and mass transfer characteristics, less maintenance and low operation costs (Kantarci *et al.*, 2005). Several types of BCR are commonly used for a development a research and real application shown in Figure 2.8.

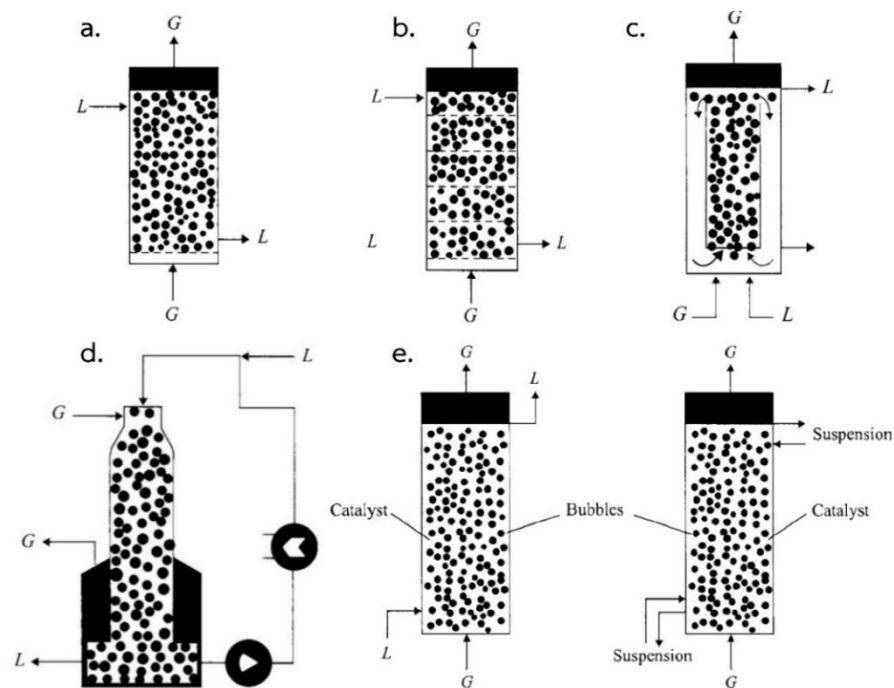


Figure 2.8. Types of Bubble Column Reactor (a) single stage, (b) multiple stage, (c) loop reactor, (d) downflow bubble column, and (e) three phase fluidized bed reactor/slurry reactor (Ranade, 2001)

2.4.1 Design and Scale-up

In recent years, the design and scale-up of BCR is more concerned because of the complex hydrodynamic and its transport characteristics. It still requires to understand well about the multiphase fluid dynamics and its effect on the design or scale-up, even though it is a simple design and scale-up. Industrial BCR is usually constructed with a ratio of length-to-diameter at least 5 and it will be varied from 2 to 5 for the application in biochemical (Degaleesan *et al.*, 2001).

The mode operation of BCR is generally classified into two types, namely semi-batch and continuous modes. In semi-batch mode operation, the suspension is stationary, there is no liquid throughputs and gas bubble upward to the column. In the continuous mode operation, both suspension and gas bubble flow upward to the column and suspension is continued to the feed tank. The gas superficial velocity should be

maintained higher than liquid superficial velocity at least an order of magnitude (Pino *et al.*, 1992).

There are three main phenomena for design and scale-up of BCR as following:

- Heat and mass transfer characteristics,
- Mixing characteristics, and
- Chemical reaction kinetics of the system.

Moreover, the following hydrodynamic parameter for designing a BCR are included:

- Interfacial area of the specific gas–liquid,
- Axial dispersion coefficients of solids,
- Mean bubble diameter,
- Axial dispersion coefficients of gas/liquid,
- Overall heat transfer coefficient between slurry and immersed,
- All species mass transfer coefficients,
- Gas holdups, and
- Liquid medium physicochemical properties.

2.4.2 Fluid Dynamics and Regime Analysis

The effect of fluid dynamic characterization will be resulted as significant to the operation and the performance of BCR. Flow regimes in bubble column are mainly dependent on the superficial gas velocity in the column. Three different types of flow regimes are usually found in the bubble column, homogeneous (bubbly blow), heterogeneous (churn-turbulent), and slug flow regime (Hyndman *et al.*, 1997). Homogeneous or bubbly flow regime is observed at low superficial gas velocities, about less than 5 cm/s in semi-batch column operation. In this operation, there is no bubble coalescence or break-up and generated bubbles are almost dictated by sparger design or diffuser and its property (Thorat *et al.*, 2004). Gas holdup in this flow regime is increasing in linear form to the gas velocity, based on the exited research study (Kawagoe *et al.*, 1976).

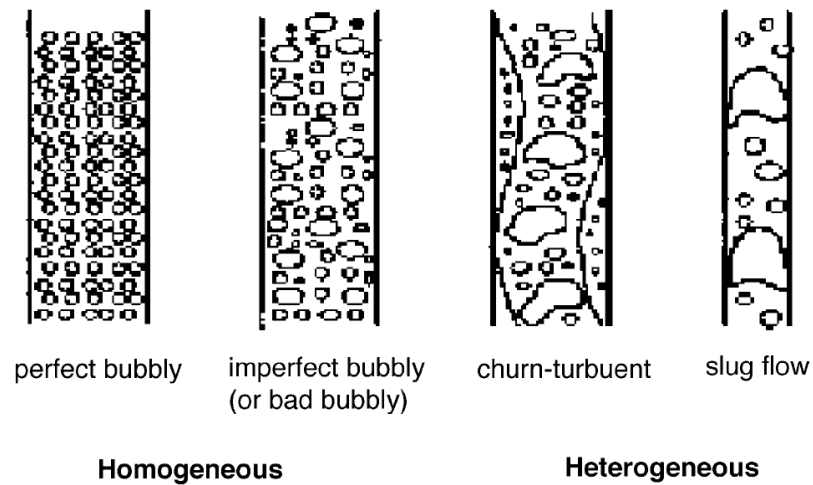


Figure 2.9. Possible flow regimes schematic in bubble columns

Heterogeneous or churn-turbulent flow regime occur after operation in at higher superficial gas velocities, (> 5 cm/s in batch columns). It is characterized by enhanced turbulent motion of the gas bubble and liquid recirculation. Heterogeneous flow is usually found in an industrial-size with large diameter columns (Hyndman *et al.*, 1997). Slug flow regime is usually found in a small diameter laboratory columns with high gas flow rate operation. It's in the form of bubble slugs after larger bubbles are stabilized by the column wall and the column diameter up to 15 cm as shown in Figure 2.9 (Kawagoe *et al.*, 1976). The large bubbles was clogged in the reactor (not float upward).

2.4.3 Gas Holdup

Gas holdup is a main parameter (dimensionless) for design and characterizing the transport phenomena in bubble columns which is defined from a volume fraction of gas phase occupied by gas bubbles. It is very important parameter that most of works related to gas-liquid contactor, were studied for design and analysis bubble columns.

Gas holdup is another important factor that affects to a pressure variation and liquid recirculation. Liquid recirculation is important for mixing, heat, and mass transfer. The gas holdup parameter depends on superficial gas velocity, column diameter, and physical properties in the operation condition (Y. Wu *et al.*, 2001).

2.4.4 Bubble Characteristics

Bubble quantity and characteristic such as population and rise velocities are a significant impact to the hydrodynamic parameters and also heat/mass transfer coefficients in bubble columns. That's why the bubble property is very important and required for future study. Dynamic gas disengagement (DGD) technique is a common method for studying bubble groups, bubble holdup structure, and rising velocity.

Gas velocity, liquid properties, gas distribution, operating pressure, and column diameter are the factors that affect the study of an average bubble size in bubble columns.

2.4.5 Mass and Heat Transfer Coefficient

Mass transfer coefficient ($K_L a$) is governed from the overall mass transfer rate per volume unit. Since the bubble shape is assumed as a sphere, the specific gas-liquid interfacial area is much related to gas holdup (ϵ_g) and bubble diameter (d_b) by equation 2.12.

$$a_s = (6 \times \epsilon_g) / (d_b) \quad \text{Eq. 2.12}$$

Volumetric mass transfer coefficient is a main parameter for design both industrial stirred and non-stirred gas-liquid reactors. It's the product from the liquid mass transfer coefficient (K_L) and interfacial area (a) (Kantarci *et al.*, 2005).

Bubble columns is generally found in many industrial productions and operated with the high heat transfer rates (Wolf-Dieter Deckwer *et al.*, 1992). It is up to 100 times of the heat transfer rate in gas-liquid bubble column greater than the operation in single phase flow (W-D Deckwer, 1980). Heat source and measurement of surface and bed temperature are the two requirements in general to measure the heat transfer coefficients. The heat transfer coefficient can be estimated by equation 2.13:

$$h = Q / \Delta t \quad \text{Eq. 2.13}$$

where h is the local instantaneous heat transfer coefficient [$W/m^2\text{ }^\circ C$], Δt is the different temperature between a surface of probe and bulk [$^\circ C$], and Q is the corresponding heat transfer flux [W/m^2] (Kantarci *et al.*, 2005).

2.5 Airlift Reactor

2.5.1 General Concepts

Airlift reactor (ALR) is a special design or modification from bubble column reactor (BCR). Airlift reactor is contained a liquid vessels divided into two zones which only one zone is sparged by the gas phase, called aerated compartment or riser. It improves liquid recirculation, gas transfer, and equalizes shear forces in the reactor. The different gas hold-up in the aerated and unaerated compartment results in different bulk densities of the fluid in these regions which causes fluid recirculation in the reactor as an airlift action. The major patterns of liquid circulation are determined by the design of the reactor, which has a channel for gas-liquid up flow and another channel for down flow. All the type of the airlift reactors are included four different sections with different flow characteristics as the followed description.

- Riser: riser is referred to the aerated compartment which the gas is supplied at the bottom of column. The gas and liquid flow is predominantly upward.
- Downcomer: it is an unaerated compartment which is parallel to the riser column. It is connected to the riser at the top and at the bottom, called top recirculation area and bottom recirculation area, respectively. The flow of gas and liquid is predominantly downward. The driving force for recirculation is the density difference between the downcomer and the riser.
- Base: base in airlift reactor is referred to the bottom recirculation which connect from the downcomer to the rise at the bottom. Bottom recirculation design is very simple and usually believed that the base does not significantly

affect the overall behavior of the reactor, but the design of this section can influence gas hold-up, liquid velocity, and solid phase flow.

- Gas separator: it is the top recirculation that connects the riser to downcomer. It is usually used for facilitating liquid recirculation and gas disengagement.

2.5.2 Reactor Classification

Airlift reactors can be classified into two different classes based on the loop of the downcomer including (i) the internal-loop (or baffled) vessels where what would otherwise be a simple bubble column has been split into a riser and a downcomer by the vertical baffle or draft tube, and (ii) the external-loop or (outer-loop) vessel where the riser and the downcomer are two quite separate tubes connected by horizontal recirculation at the bottom and the top, called base and gas separator as previously mentioned. The designs of both structures can be modified further, leading to variations in the fluid dynamics, in the extent of bubble disengagement from the fluid, and in the flow rates of the various phases. The different types of airlift reactor are shown in Figure 2.10.

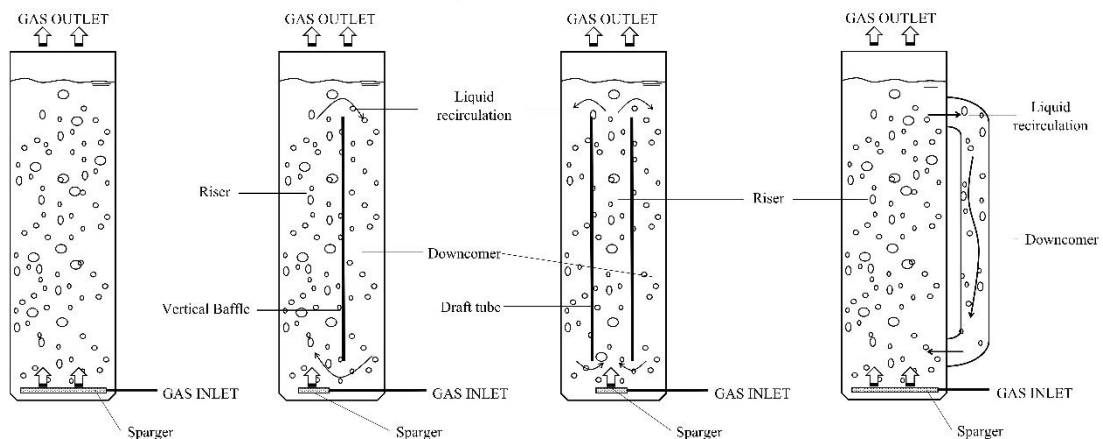


Figure 2.10. Different types of gas-liquid contactor: simple BCR, internal-loop split ALR, internal-loop draft tube ALR, and external-loop ALR (left to right)

2.5.3 Gas Holdup

Gas holdup (ϵ) is the volumetric fraction of the gas to the total volume of a gas-liquid dispersion. The overall gas holdup in the reactor is defined by equation 2.14, where the V_G is gas volume in the reactor, and $V_G + V_L$ is the mixed volume of both phases after supplied the gas. In airlift reactors, the individual riser gas holdup (ϵ_r) and downcomer (ϵ_d) are related to the overall gas holdup as presented in equation 2.15. This equation is exact for internal-loop airlifts and can be to use for external loops when the dispersion height in the riser is much close to the height in downcomer.

$$\epsilon = \frac{V_G}{V_L + V_G} \quad \text{Eq. 2.14}$$

$$\epsilon = \frac{A_r \epsilon_r + A_d \epsilon_d}{A_r + A_d} \quad \text{Eq. 2.15}$$

2.5.4 Liquid Recirculation

In airlift reactor, the liquid recirculates along a well path which are the up flow in riser and down flow in downcomer. It depends on difference of gas holdup between the riser and downcomer zones of an airlift reactor. A mean recirculation velocity (U_{Lc}) is defined by Blenke (1979), which can be calculated using the following equation 2.16 where x_c is the recirculation path length and t_c is the average time for one complete recirculation.

$$U_{Lc} = \frac{x_c}{t_c} \quad \text{Eq. 2.16}$$

Base on the mass balance, the superficial velocity in the downcomer (U_{Ld}) and the superficial velocity in the riser (U_{Lr}) are related as equation 2.17 where A_r and A_d are the cross sectional area of riser and downcomer respectively.

$$U_{Lr} A_r = U_{Ld} A_d \quad \text{Eq. 2.17}$$

The superficial velocity must be distinguished from the true linear liquid velocity, also known as the interstitial velocity (V_L). The interstitial velocity is related to the superficial velocity as shown in equation 2.18 and 2.19.

$$V_{Ld} = \frac{U_{Ld}}{1 - \epsilon_d} \quad \text{Eq. 2.18}$$

$$V_{Lr} = \frac{U_{Lr}}{1 - \epsilon_r} \quad \text{Eq. 2.19}$$

2.6 Sequencing Batch Reactor and Settling Process

2.6.1 Sequencing Batch Reactor

Sequencing batch reactor (SBR) has been used since the 1920s with successful operation for both municipal and industrial wastewater treatment, especially for practical in low or vary flow patterns areas (NEIW, 2005). The basic treatment process is based on a fill-and-draw that has five steps include fill, react, settle decant, and idle as shown in Figure 2.11.

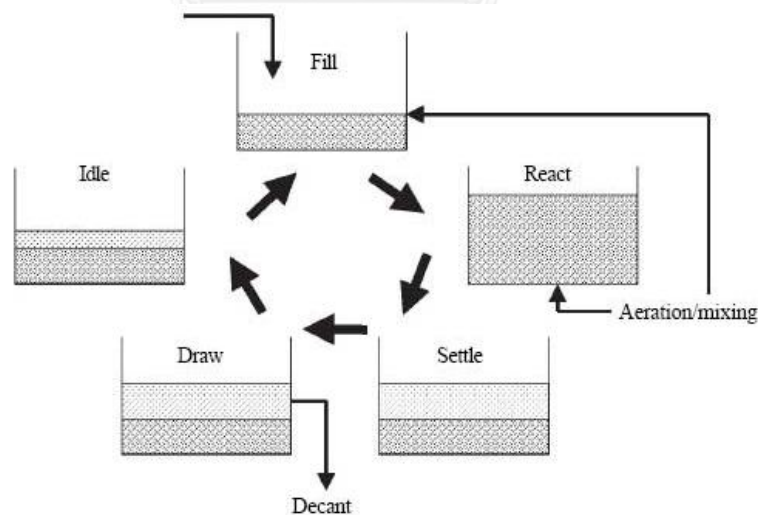


Figure 2.11. Typical operation cycles in SBR

- **Step 1: Filling Process**

In fill phase step, the reactor is filled with influent wastewater or contaminated water. It contains food for microbes in activated sludge, to make a biochemical reaction environment. Mixing and aeration can be supplied in this fill phase to make in three different scenarios.

- Static fill: in this scenario, there is not required a mixing or aeration during influent wastewater come into the reactor. Static fill is used while the initial startup phase of the facility. There is not required nitrify or denitrify at a plant with an application a low flow periods to save power.
- Mixed fill: the mechanical mixer are started in this scenario but still not yet operate the aeration. A uniform blend of the wastewater and biomass will be made after applying a mixing. There will be a presented an anoxic while the aeration is still not yet started and denitrification will be promoted. In this anaerobic conditions, the biomass undergoes to release phosphorous.
- Aerated fill: in this scenario, both mechanical mixing and aeration process are operated. There is a conversion from anaerobic to aerobic zone. The oxygen is required to turn off in order to promote anoxic condition for a denitrification. And the dissolved oxygen should be monitored for this phase to make sure that it's does not go over 0.2 mg/L to ensure that anoxic condition will occur at idle phase.

- **Step 2: Reacting Process**

In this part, the mechanical mixing and aeration process are still going on. Most of the carbonaceous BOD removal is react in this step. The nitrification occurs due the continuous of the mixing and aeration. Phosphorus released in the mixing fill is taken up in this step after it plus some additional of phosphorus.

- **Step 3: Settling Process**

In this step, the practical or activated sludge settle down under the quiescent condition, there is no flow enter, mechanical mixing, and no aeration process. The sludge tends to settle down due to its flocculent mass. The sludge mass is usually called the sludge blanket. This step is a critical step of the cycle because some sludge can be drawn off during subsequent decant phase, if the solids do not settle rapidly. Then, there is degrade effluent quality.

- **Step 4: Decanting Process**

In decant step or phase, the clear supernatant effluent will be collected. There are floating decanter and fixed-arm decanter. The inlet orifice slightly below the water surface will be maintained by floating decanter to minimize the removal of solids in this step. Operator of floating decanter should be flexibility to vary the fill and draw the water. Fixed-am decanter is used for the operator to lower or raise the level of decanter. It is important to make sure that is no surface foam or scum go to the clear water. It should be designed a maximum height to avoid disturbing the settled biomass.

- **Step 5: Idle Process**

The variation of the time is based on the flow rate and treatment strategy. In this step, small amount of sludge at the bottom of SBR needs to be pumped out, it is called as a wasting step.

2.6.2 Settling Process

The main objective of settling process is to remove a particles away from the water process by using gravity separation concept. Particles will settle down since the particle density is higher than that of water. In this process, particles are classified into four different types based on concentration and morphology (Figure 2.12) (Crittenden *et al.*, 2012). Type I is discrete particle settling, particles settling without influencing other particles. Type II is flocculant settling, differential flow path. Type III is hindered or zone

settling, large number of particles forming blanket that overtake other particles. Type IV is compression settling, water displaced from pores as particles settle and compress. Type III is hindered or zone settling, water displaced from pores as particles settle and compress. Type II is flocculant settling, differential flow paths. Type I is discrete particle settling, particles settling without influencing other particles.

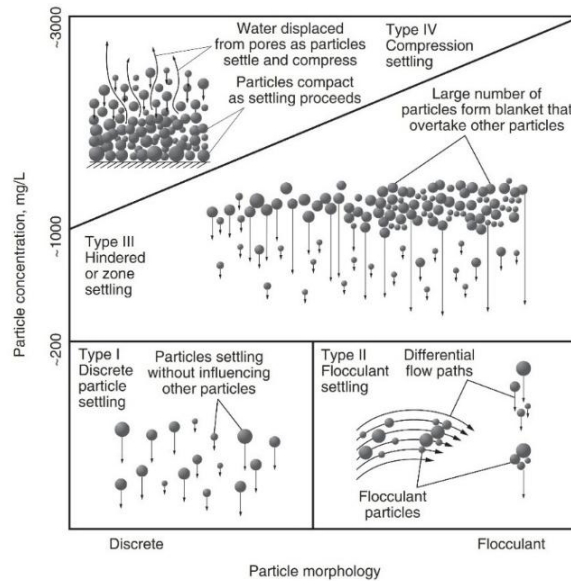


Figure 2.12. Relation of type of settling, concentration, morphology of particle
(Crittenden et al., 2012)

- Classification

According to (Hazen, 1904), understanding about surface loading rate and overflow rate (OR) conception for getting well known about the sedimentation process is surface loading rate or overflow rate (OR). In general, the sedimentation processes are classified into several classes as mention below:

- *Conventional horizontal flow:* The traditional process with a simple gravity settling (no any equipment to accelerate the settling) in a basin. Even though it is very simple to operate this process, larger area is required compared to the other type.

- *High-rate gravity settling*: Additional process that provides a device in order to increase the effective surface area. Multiple-trays sedimentation basin was applied to maximize the flow lengths but it is not popular in the present time.
- *Solids contact clarifier*: Integrated process between flocculation and sedimentation in the same basin with different zone as present in the Figure 2.13. To increase an opportunity of particles contacting therefor increasing the particles size and settling rates, there is a recycle of solids in order to make sure there is high solids in the reaction zone.
- *Floc blanket clarifiers*: Clarifiers that in flow at the bottom and out flow at the surface. It provides a submerged weir over and removed by blow down process. Blow down rate is focused in this process after different blow down provide different result.
- *Ballasted flocculation*: Polymer is used in this process to increase accelerates settling and density by fine sand, called micro-sand with floc particle. The collection at the bottom after a solid settled down and then pump into a hydro-cyclone (separate sand and attached floc) for sand recycle back to the system.

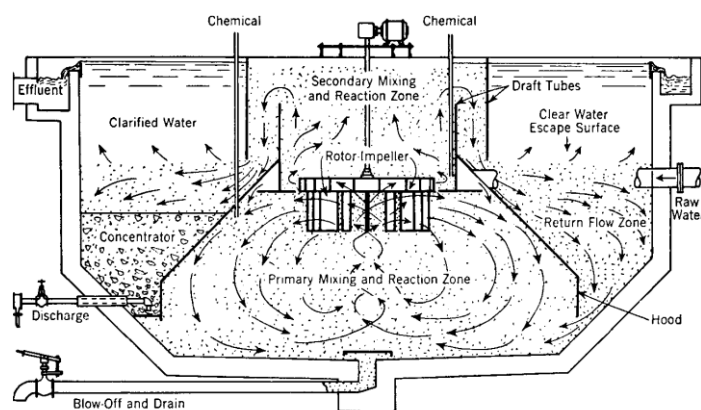


Figure 2.13. Accelerator® solids contact clarifier (Hartung, 1951)

2.7 Design of Experiment (DOE)

The experiment roles as a central place in science, especially, to dial the problem faced in the people living. To increase this research efficiency, the application of this new thing into the classical experimental research was applied. One of them is the applicant with statistical mathematical methods or with design of experiment (DOE). DOE is a mathematical approach to determine the relationship between causes (i.e. factors affecting a process) and effect (output of that process) in the system.

The essential of DOE are (a) to minimize or reduce amount of trial experiments, (b) to vary all factors in simultaneousness of an experimental activities, and (c) to choice the suitable strategy for an experiments. Design of experiment applies with the new approach in a research that is different from the traditional method or classical method of empirical research. Classical method requires more material, more time consumes, one factor at a time while other are in constant. For example, five factors for testing in which every factor varies in five levels, and then the full experimental is 5^5 equal 3125 different experiments. After apply DOE, it is possible to design the experiment with 32 trials only with the second order of rotatable design (Živorad, 2004). Two large groups of all empirical research methodologies are classical or passive group, and statistical designed or active group.

2.7.1 Classical DOE One Factor at a Time

The experiments are varied by one factor at a time while other independent factors are constant. As an example of the research that k is affected factors, which will affect the p level. The total experiments to trial is presented by equation 2.20.

$$N = k(p - 1) + 1 \quad \text{Eq. 2.20}$$

It is assumed that the experimental (y) is affected by three factors including temperature (x_1), pressure (x_2), and reaction time (x_3). The levels of the varied factor

are 2 ($p=2$), so the trialed experiment is 4 ($N=4$). The trial condition of the experiments is shown in Table 2.4.

From the experiment, the effect of each factor will be determined such as:

- The temperature effect (x_1): N° 1 and 2
- The pressure effect (x_2): N° 1 and 3
- The reaction time effect (x_3): N° 1 and 4

Usually, this classical method is applied to estimate the factors whether it affects to the experiment or not, it is not prefer to applied to estimate how much it influence the experimental response because all the factors are considered as independent factors.

Table 2.4. Experimental conditions of classical design with 3 factors with 2 levels

Number of trials	Factor level			y	
	x_1	x_2	x_3		
1	p_1	p_1	p_1	y_1	reference
2	p_2	p_1	p_1	y_2	
3	p_1	p_2	p_1	y_3	
4	p_1	p_1	p_2	y_4	

Modified from (Živorad, 2004)

2.7.2 Statistical DOE

Statistical design is used instead of classical design. With the same example in classical design, double amount of the experiments need to be obtained. It is usually called as “full factorial design”. Experiments of the using statistical DOE is shown in Table 2.5. Basic statistical design for all kinds of qualitative and categorical/qualitative factors is presented in the Table 2.6.

Table 2.5. Experimental conditions of statistical design

Number of trials	Factor level			y
	x ₁	x ₂	x ₃	
1	p ₁	p ₁	p ₁	y ₁
2	p ₂	p ₁	p ₁	y ₂
3	p ₁	p ₂	p ₁	y ₃
4	p ₁	p ₁	p ₂	y ₄
5	p ₂	p ₂	p ₁	y ₅
6	p ₂	p ₁	p ₂	y ₆
7	p ₁	p ₂	p ₂	y ₇
8	p ₂	p ₂	p ₂	y ₈

Modified from (Živorad, 2004)

2.7.3 Factorial Designs

In general, factorial designs are most effective for the study of the effects of two or more factors. All possible combinations of the levels of the factors are investigated for this design. Two factors, for example, a levels of factor A and b levels for factor B . It is usually said to be crossed (combination) after arrange for factorial design. Changing level of the factor can affect or change the response, it is called as a main effect. But in some cases, the difference in response of factor levels is not the same for all levels of other factors, it is called interaction of the factors. The regression model representation of two factor factorial experiment is shown in the equation 2.21. Whereas y is the response, β is determined parameter, x is the variable of factor, and ϵ is the random error (Montgomery, 2008).

$$y = \beta_0 + \beta_1 x_1 + \beta_2 x_2 + \beta_{12} x_{12} + \epsilon \quad \text{Eq. 2.21}$$

Table 2.6. DOE application (Živorad, 2004)

Experimental design	Factors	Application
Simple comparative design	Categorical/qualitative and quantitative	Check of method, testing of single factor effect
Random blocks and Latin squares	Difference between batches, treatment, samples	Calculation of effects with elimination of inequality of experimental conditions
Fractional replicate design	Categorical/qualitative and quantitative	Screening of factors
Random balance design	Categorical/qualitative and quantitative	Screening of factors
Full factorial design	Categorical/qualitative, quantitative and combined	Choice of factors, calculation of main effects and interactions
Central composite rotatable design	Quantitative	Regression models of second order
Central composite orthogonal design	Quantitative	Regression models of second order
Simplex lattice design	Quantitative	Mixture problems, regression models of second and higher order
Extreme vertex design	Quantitative with constraints	Mixture problems, regression models of second and higher order
Harley's, Kono's, Kifer's, D-Optimal	Quantitative	Regression models
Higher-order designs	Quantitative	Regression models of higher order

- Two-factor factorial design

This factorial design is investigated only two factors including factor A (a levels) and factor B (b levels) with n replicate(s). For two-factor factorial design, y_{ijk} is the response when factor A presents i^{th} level ($i=1, 2, \dots, a$) and factor B presents j^{th} level ($j=1, 2, \dots, b$) with k^{th} replicate(s) ($k=1, 2, \dots, n$). Two-factor factorial experiment can be designed as Table 2.7, presented in completely randomized design.

There are different concepts to write the model for factorial experiment, the effect model is written as the equation 2.22. Whereas μ is overall mean effect, τ_i is effect of factor A - i^{th} level, β_j is the effect of factor B - j^{th} level, $(\tau\beta)_{ij}$ is effect of interaction between τ_i and β_j , and ϵ_{ijk} is random error item.

$$y_{ijk} = \mu + \tau_i + \beta_j + (\tau\beta)_{ij} + \epsilon_{ijk} \quad \begin{cases} i = 1, 2, \dots, a \\ j = 1, 2, \dots, b \\ k = 1, 2, \dots, n \end{cases} \quad \text{Eq. 2.22}$$

Factor A , B , and interaction effects are fixed and treatment effects are overall mean deviations, then, $\sum_{i=1}^a \tau_i = \sum_{j=1}^b \beta_j = \sum_{i=1}^a (\tau\beta)_{ij} = \sum_{j=1}^b (\tau\beta)_{ij} = 0$. There are n replicates, abn are the total observation.

Table 2.7. General experimental design for two-factor factorial design

		Factor B			
		1	2	...	b
Factor A	1	$y_{111}, y_{112}, \dots, y_{11n}$	$y_{121}, y_{122}, \dots, y_{12n}$		$y_{1b1}, y_{1b2}, \dots, y_{1bn}$
	2	$y_{211}, y_{212}, \dots, y_{21n}$	$y_{221}, y_{222}, \dots, y_{22n}$		$y_{2b1}, y_{2b2}, \dots, y_{2bn}$
	⋮				
	a	$y_{a11}, y_{a12}, \dots, y_{a1n}$	$y_{a21}, y_{a22}, \dots, y_{a2n}$		$y_{ab1}, y_{ab2}, \dots, y_{abn}$

Therefore, the possible model of the factorial experiment in the mean models is presented in the equation 2.23 where the mean of ij^{th} cell is written as the equation 2.24 (Montgomery, 2008).

$$y_{ijk} = \mu_{ij} + \epsilon_{ijk} \begin{cases} i = 1, 2, \dots, a \\ j = 1, 2, \dots, b \\ k = 1, 2, \dots, n \end{cases} \quad \text{Eq. 2.23}$$

$$\mu_{ij} = \mu + \tau_i + \beta_j + (\tau\beta)_{ij} \quad \text{Eq. 2.24}$$

- Statistical analysis of fixed effects model

Before express the statistical analysis in mathematics, some assumptions is required. The $y_{i..}$, $y_{.j}$, $y_{ij.}$, and $y_{...}$ are presented the total of all observations in i^{th} level of factor A, j^{th} level of factor B, ij^{th} cell, and grand total of all observations, respectively. It can be written as the expression 2.25 and its total corrected sum of squares can be written as the expression 2.26.

$$\begin{aligned} y_{i..} &= \sum_{j=1}^b \sum_{k=1}^n y_{ijk} & \bar{y}_{i..} &= \frac{y_{i..}}{bn} & i &= 1, 2, \dots, a \\ y_{.j} &= \sum_{i=1}^a \sum_{k=1}^n y_{ijk} & \bar{y}_{.j} &= \frac{y_{.j}}{an} & j &= 1, 2, \dots, b \\ y_{ij.} &= \sum_{k=1}^n y_{ijk} & \bar{y}_{ij.} &= \frac{y_{ij.}}{n} & i &= 1, 2, \dots, a \\ & & & & j &= 1, 2, \dots, b \\ y_{...} &= \sum_{i=1}^a \sum_{j=1}^b \sum_{k=1}^n y_{ijk} & \bar{y}_{...} &= \frac{y_{...}}{abn} \end{aligned} \quad \text{Eq. 2.25}$$

$$\begin{aligned} \sum_{i=1}^a \sum_{j=1}^b \sum_{k=1}^n (y_{ijk} - \bar{y}_{...})^2 &= \sum_{i=1}^a \sum_{j=1}^b \sum_{k=1}^n [(\bar{y}_{i..} - \bar{y}_{...}) + (\bar{y}_{.j} - \bar{y}_{...}) \\ &\quad + (\bar{y}_{ij.} - \bar{y}_{i..} - \bar{y}_{.j} + \bar{y}_{...}) + (y_{ijk} - \bar{y}_{ij.})]^2 \\ &= bn \sum_{i=1}^a (\bar{y}_{i..} - \bar{y}_{...})^2 + an \sum_{j=1}^b (\bar{y}_{.j} - \bar{y}_{...})^2 \\ &\quad + n \sum_{i=1}^a \sum_{j=1}^b (\bar{y}_{ij.} - \bar{y}_{i..} - \bar{y}_{.j} + \bar{y}_{...})^2 \\ &\quad + \sum_{i=1}^a \sum_{j=1}^b \sum_{k=1}^n (y_{ijk} - \bar{y}_{ij.})^2 \end{aligned} \quad \text{Eq. 2.26}$$

While sum of squares of factor A (SS_A), factor B (SS_B), interaction of A and B (SS_{AB}), and sum of squares due to error (SS_E), the expression 2.26 can rewrite as equation 2.27 in fundamental ANOVA for two-factor factorial with at least two replicates ($n \geq 2$) (Montgomery, 2008). Moreover, number of freedom degrees is shown in Table 2.8.

Table 2.8. Analysis of variation for two-factor factorial, fixed effects model

Variation source	Sum of squares	Degree of freedom	Mean square	F_0
A treatments	SS_A	$a - 1$	$MS_A = SS_A / (a - 1)$	MS_A / MS_E
B treatments	SS_B	$b - 1$	$MS_B = SS_B / (b - 1)$	MS_B / MS_E
AB interaction	SS_{AB}	$(a - 1)(b - 1)$	$MS_{AB} = SS_{AB} / ((a - 1)(b - 1))$	MS_{AB} / MS_E
Error	SS_E	$ab(n - 1)$	$MS_E = SS_E / (ab(n - 1))$	
Total	SS_T	$abn - 1$		

$$SS_T = SS_A + SS_B + SS_{AB} + SS_E \quad \text{Eq. 2.27}$$

Whereas sums of squares of SS_A , SS_B , SS_{AB} , and SS_E are determined by equation 2.28, 2.29, 2.30, and 2.32, respectively. But SS_{AB} is required to estimate sum of squares between ab cell total, called subtotals ($SS_{Subtotals}$) present by equation 2.31.

$$SS_A = \frac{1}{bn} \sum_{i=1}^a y_{i..}^2 - \frac{y_{...}^2}{abn} \quad \text{Eq. 2.28}$$

$$SS_B = \frac{1}{an} \sum_{j=1}^b y_{.j.}^2 - \frac{y_{...}^2}{abn} \quad \text{Eq. 2.29}$$

$$SS_{AB} = SS_{Subtotals} - SS_A - SS_B \quad \text{Eq. 2.30}$$

$$SS_{Subtotals} = \frac{1}{n} \sum_{i=1}^a \sum_{j=1}^b y_{ij.}^2 - \frac{y_{...}^2}{abn} \quad \text{Eq. 2.31}$$

$$SS_E = SS_T - SS_{AB} - SS_A - SS_B = SS_T - \quad \text{Eq. 2.32}$$

Mean square is produced from the dividing of sum squares to degree of freedom. If null hypotheses don't effect by row, column, and interaction, then mean square of factor A (MS_A), B (MS_B), interaction (MS_{AB}), and error (MS_E) can estimate by σ^2 . In opposite, if it is effected by row or column or interaction, its corresponding mean squares will be larger than MS_E . Apply equation 2.32, all ratio of mean squares MS_A/MS_E , MS_B/MS_E , and MS_{AB}/MS_E , is distributed as F with numerator degree of freedom $a - 1$, $b - 1$, and $(a - 1)(b - 1)$, respectively. Table 2.8 is shown the test procedure of analysis of variance table (Montgomery, 2008).

- Model adequacy checking

After get the analysis result from ANOVA, model adequacy checking is required which its primary diagnostic tool is residual analysis. Residuals analysis for two-factor factorial with interaction is expressed by the equation 2.33 and it is modified to be the equation 2.34 while the fitted values equal average of the observations in ij^{th} cell ($\hat{y}_{ijk} = \bar{y}_{ijk}$) (Montgomery, 2008).

$$e_{ijk} = y_{ijk} - \hat{y}_{ijk} \quad \text{Eq. 2.33}$$

$$e_{ijk} = y_{ijk} - \bar{y}_{ijk} \quad \text{Eq. 2.34}$$

2.7.4 The 2^k Factorial Design

Factorial design is usually applied in the experiments investigate many factors and it was preferred to study the effect of each factor on the response. The k factors is the most important in factorial design with only two levels which can be two values of temperature, pressure, or time (called quantitative); or two machines, two operation with high level (HL) or low level (LL) of factor (called qualitative). Complete replication as a design require $2 \times 2 \times \dots \times 2 = 2^k$, called **2^k factorial design**. The 2^k design is commonly important for applying in an early part of experimental work after many factors are preferred to be investigated. It can reduce the amount of the running experiment. It is usually used in **factor screening experiments** (Montgomery, 2008).

- **General 2^k design**

The 2^k design content k main effects, $(k | 2)$ two-factor interactions, $(k | 3)$ three-factor interaction, and one k -factor interaction. The complete model contains $2^k - 1$ effects 2^k design. Usually, the design is written in the form of standard order. For example, the standard order for 2^4 design of A-B-C-D factors is (1), a, b, ab, c, ac, bc, abc, d, ad, bd, abd, cd, acd, bcd, and abcd. The general process for 2^k design statistical analysis (Montgomery, 2008) is:

- Step 1 - Estimate factor effects: this section is to estimate factor effects and determine the signs/magnitudes. This step can provide preliminary information.
- Step 2 - Form an initial model
 - If the design is replicated, fit the full model
 - If there is no replication, form the model using a normal probability plot of the effects
 - The full model is usually chosen, all main effects and interactions provide at least one point for replication.
- Step 3 - Perform statistical testing: analysis of variance is used for testing a significance of the main effects and interaction. Table 2.9 is presented the analysis of variance in a general form for 2^k factorial design n replicates.
- Step 4 - Refine model: this section, non-significant variables are removed from the full model.
- Step 5 - Analyze residuals: to check model adequacy and assumptions, residual analysis is used. It may have model refinement after residual analysis found inadequate or badly violated.

- Step 6 - Interpret results: this last step is just only a plot of the analysis graphic with main effect or interaction plots, or response surface and contour plots.

Some computer software packages (including Minitab, Design Expert, etc.) are usually examined this process of analysis.

Table 2.9. Analysis of variance for 2^k factorial design

Source of Variation	Sum of Square	Degrees of Freedom
k main effects		
A	SS_A	1
B	SS_B	1
:	:	:
K	SS_K	1
$(k 2)$ two-factor interactions		
AB	SS_{AB}	1
AC	SS_{AC}	1
:	:	:
JK	SS_{JK}	1
$(k 3)$ three-factor interactions		
ABC	SS_{ABC}	1
ABD	SS_{ABD}	1
:	:	:
IJK	SS_{IJK}	1
:	:	:
(k / k) k -factor interactions		
ABC...K	$SS_{ABC...K}$	1
Error	SS_E	$2^k (n-1)$
Total	SS_T	$n2^k - 1$

In general, the contrast for effect AB ... K can be determined by equation 2.35. Then estimate effects and compute the sums of squares can be done follow by equation 2.36 and 2.37 where n is replicated number.

$$\text{Contrast}_{AB\dots K} = (a \pm 1)(b \pm 1) \dots (k \pm 1) \quad \text{Eq. 2.35}$$

$$AB\dots K = \frac{2}{n2^k} (\text{Contrast}_{AB\dots K}) \quad \text{Eq. 2.36}$$

And
$$SS_{AB\dots K} = \frac{2}{n2^k} (\text{Contrast}_{AB\dots K})^2 \quad \text{Eq. 2.37}$$

- Single replicate of 2^k factorial design

The total number of combination experiments is usually high in 2^k factorial design. For example, 2^5 design has 32 combination experiments while 2^6 design has 64 experiments, and so on. The number of the replicates is very important and require to strictly study due to the limited of the resources. In general, the available resources is only for a single replicate of experimental run. Single-replicate strategy is commonly selected for applying in screening experiments during many factors were investigated. Single replicate of 2^k factorial design can be called unreplicated factorial (Montgomery, 2008). For this case application, the data analyzing is real high-order interaction occur in sometime and inappropriate to use error mean square by pooling high-order interactions. To solve this problem, Daniel recommends to examine a normal probability plot for the estimate of the effect (Daniel, 1959).

- One-half fraction of 2^k design

In the situation of three factors with two levels was considered, but the experiments cannot conduct for all run of $2^3 = 8$ combination experiments. In this case, four run experiments can be used. It's called one-half fraction of 2^3 design or 2^{3-1} design due to the design provide $2^{3-1} = 4$ combination experiments. Suppose that four combination experiments of a, b, c, and abc is selected as one-half fraction, the principal and alternate fraction are shown in Figure 2.14.

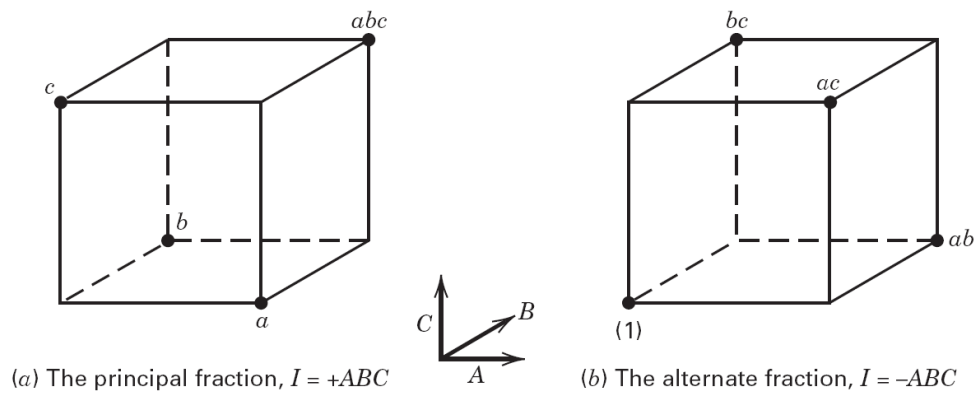


Figure 2.14. Two one-half fractions of 2^3 design (Montgomery, 2008)

2.7.5 Response Surface Methodology - Central Composite Design

Response surface methodology (RSM) is the mathematical and statistical techniques which is very important for modeling and analysis the problem which influenced by several variables and it was tried to optimize the response (Montgomery, 2008). For example, the environmental engineer wants to determine the level of temperature (x_1) and pressure (x_2) that can provide the maximum yield (y) of the process. The process yield (y) can be written in function of factors' level of temperature and pressure by equation 2.38 where ϵ is an error in response y . If $E(y)$ is expected response and η is the response surface, then the surface represented by equation 2.39.

$$y = f(x_1, x_2) + \epsilon \quad \text{Eq. 2.38}$$

$$\eta = f(x_1, x_2) \quad \text{Eq. 2.39}$$

It is usually presents the response surface graphically, as Figure 2.15 with the contours plot for better visualize of the response surface shape. Because of the unknown relationship between the variations and the response in RSM, determination of low-order polynomial is first examined and if it is well in linear function, first-order model is constructed as equation 2.40.

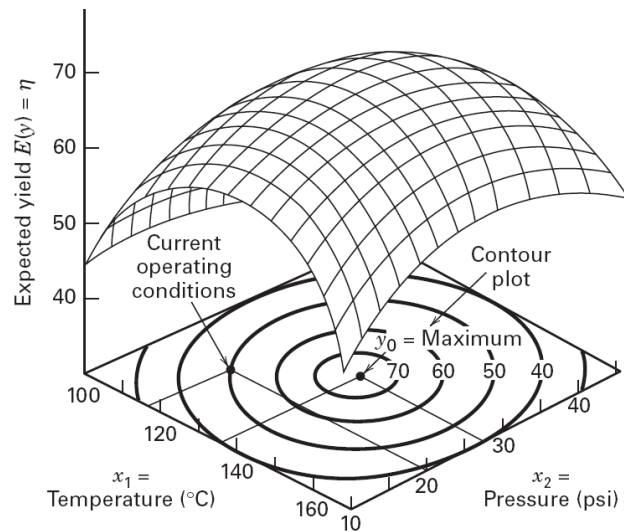


Figure 2.15. A contour plot of a response surface

$$y = \beta_0 + \beta_1 x_1 + \beta_2 x_2 + \dots + \beta_k x_k + \epsilon \quad \text{Eq. 2.40}$$

$$y = \beta_0 + \sum_{i=1}^k \beta_i x_i + \sum_{i=1}^k \beta_{ii} x_i^2 + \sum_{i < j} \beta_{ij} x_i x_j + \epsilon \quad \text{Eq. 2.41}$$

But if it is in curvature, higher degree of polynomial is applied as equation 2.41 in the form of second-order model. It is almost all RSM problems are followed first-order or/and second-order model. Fitted surface is an analysis method for RSM, called response surface designs. This design is to determine the optimum operations conditions and satisfied region (Montgomery, 2008).

- Design for fitting central composite design

Central composite design (CCD) is generally used for fitting second-order model as well as for response surface design. The different of the simplex design and central composite design was illustrated in Figure 2.16 with $k = 3$ factors. Two parameters including the distance of axial runs from design center (α) and amount of center points (n_c). The rotatability of CCD is conducted by distance α in optional and its value is functioned to the number of factorial portion points (n_f) as $\alpha = (n_f)^{1/4}$. Rotatability is important for second-order model for better predictions in interested zone.

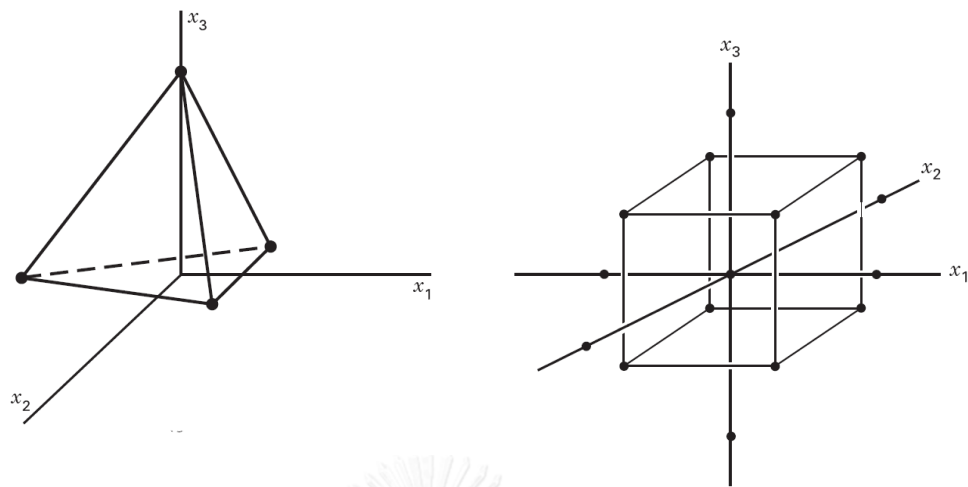


Figure 2.16. Simplex design (left) and central composite design (right) for $k = 3$

2.8 Literature Review

2.8.1 Reactor Development

Krichnavaruk et al. from Chemical Engineering Department of Chulalongkorn University (Thailand) (Krichnavaruk *et al.*, 2002) tried to develop the airlift contactor (ALC) in terms of gas liquid mass transfer ($K_L a$) by providing the perforated plate in the riser as show in Figure 2.17. The result shown that $K_L a$ with perforated plate provides twice value compared to the conventional system due to the increasing specific interfacial area between bubbles and liquid principally. Mass transfer coefficient (K_L) obtained from the system with perforated plate provides smaller value compared to conventional system. Optimal configuration of perforated plated including amount of the holes, hole size, and amount of the plates in ALC provides were investigated for highest $K_L a$ coefficient. In one case, one perforated plate (Plate # B-1: 13 holes with a hole size of 4 mm) with superficial gas velocity (U_{sg}) of 1.89 cm/s provides $K_L a$ coefficient 82.8% more than the conventional ALC.

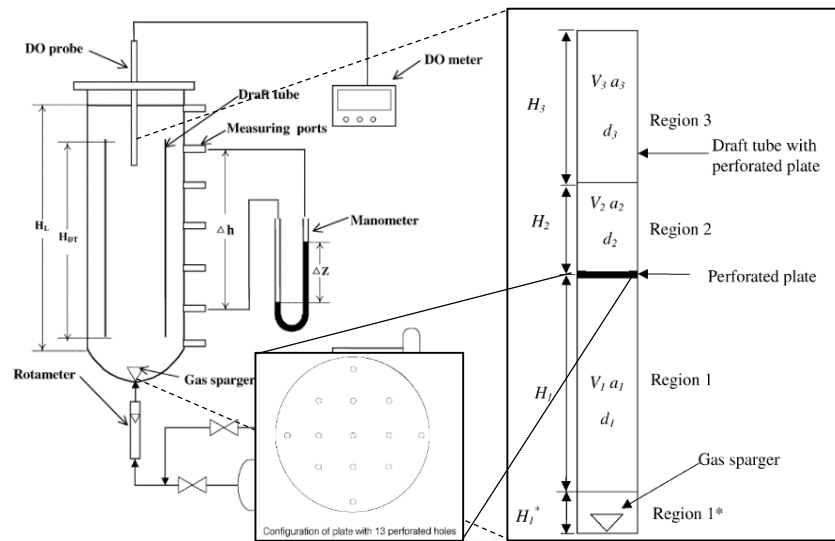


Figure 2.17. Airlift contactor (ALC) development with perforated plate in riser

Chen et al. from Chemical Engineering Department of National Tsing Hua University (Taiwan) (Chen *et al.*, 1997) tried to develop novel rectangular airlift reactor by installing the mesh baffle-plates to enhance gas holdup, $K_L a$ coefficient, and mixing time compared to conventional airlift and bubble column reactor as shown in Figure 2.18. The novel reactor with mesh baffle-plates can improve the reactor performance in terms of $K_L a$ coefficient up to 12% compared to a conventional airlift reactor with a simple operation condition.

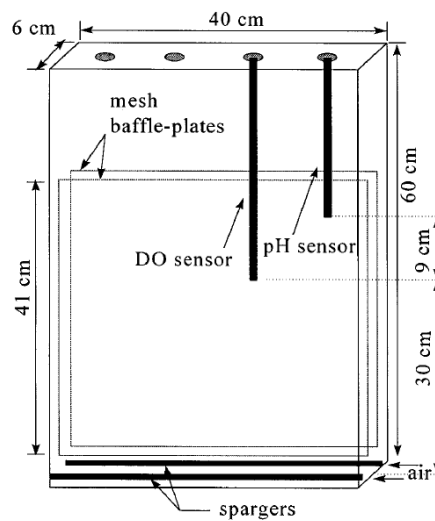


Figure 2.18. Airlift reactor (ALR) development with mesh baffle-plates

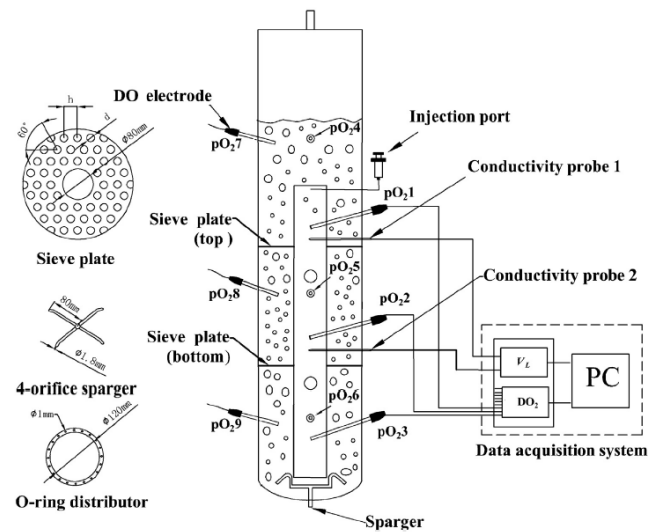


Figure 2.19. Airlift reactor (ALR) development with sieve plate in riser

Luo et al. from Mechanical Engineering College of Zhejiang University of Technology (China) (Luo *et al.*, 2013) try to develop the airlift reactor by installing the sieve plate in the riser in terms of hydrodynamics and mass transfer as shown in Figure 2.19. From the experimental result, it can be concluded that the sieve plate is significantly enhance gas holdup and $K_L a$ coefficient. Bubbles breaking is the main mechanism in a sieve pore after installing the sieve plate. O-ring gas distributor provides better $K_L a$ coefficient compare to 4-orifice nozzle. Optimal configuration of sieve plates including diameter of sieve port, free area ratio, and amount of sieve plates provides better yield hydrodynamic. Other more important from this sieve plate installation, it is recommended not only for two-phase reactor but three-phase reactor with low solid density or/and small solid particles as well. The higher diameter of sieve pore and free area ratio are important for preventing or reduce the biomass sedimentation and adhesion on sieve plates.

2.8.2 Iron Removal by BCR or ALR

El Azher et al. studied the iron (II) oxidation of the synthetic waters in a 63 L split-rectangular airlift reactor (El Azher *et al.*, 2008). High level of iron such as groundwater, typically from 5 to 20 mg/L was examined for this work. The operation parameters including gas flow rate, initial concentration of iron (II) was investigated in a batch condition. From the experimental results, the airlift reactor provides a good mixing, high mass transfer and pH control despite the strong sensitivity of the oxidation kinetics to the pH.

Kaksonen et al. was successfully with their work of the continuous iron oxidation and jarosite precipitates removal from low pH solution, ambient temperature and pressure after conducted in two-stage airlift bioreactor (ALBR) (Kaksonen *et al.*, 2014). From the experimental result, it can be concluded that the two-stage of ALBR provide efficient iron oxidation and enables precipitation of ferric iron in the form of well selling jarosite with only minor loss of Cu and Ni. This reactor process presented the promising a variety of hydrometallurgical process flow sheets. It provided better iron removal from ferrous without any chemical requirement.

Ebrahimi et al. studied on the ferrous iron oxidation in continuous biofilm airlift reactor mixed with the culture of *Acidithiobacillus ferrooxidans* and *Leptospirillum ferrooxidans* bacteria (Ebrahimi *et al.*, 2005). The parameters including ferrous iron oxidation rate, gas liquid mass transfer, biofilm formation, both types of bacteria were investigated. The highest oxidation rate of ferrous iron was obtained about 145 mol-Fe²⁺/m³.h while 0.25 h of hydraulic residence time was performed. The optimal conversion efficiency is 98% was obtained at loading rate of 100 mol/m³.h.

2.9 Summary and Research Focuses

In physically movement of groundwater, the flow is generally much slower than the surface water flow. That is one of the reasons suitability for chemical and biological processes, exist slowly enough to careless of surface water but should be problem in subsurface environment. Therefore, some chemicals from natural and human-induced activities can be found in groundwater. The chemical and contaminants in groundwater are classified into three groups including inorganic, organic, and microbiology contaminants.

- *Inorganic contaminants (IC)*: aluminum, antimony, arsenic, barium, beryllium, cadmium, chloride, chromium, copper, cyanide, dissolved solids, fluoride, hardness, iron, lead, manganese, mercury, nickel, nitrate (nitrogen), nitrite (nitrate and nitrite), selenium, silver, sodium, sulfate, thallium, and zinc
- *Organic contaminants (OC)*: volatile organic compounds, pesticides, plasticizer, chlorinated solvents, benzo(a)pyrene, and dioxin
- Microbiological contaminants (MC): coliform bacteria

Not only chemicals contaminant, there is also a physical characteristics of the groundwater such as turbidity, color, pH, odor, and taste which need to be treated before supplying for a user (USGS, 2015).

During the mention about groundwater contaminants, iron is generally focused due to the high existed frequency and amount. Several methods of the existed work for iron removal are summarized Table 2.10 with the operations.

Table 2.10. Summary of exited works for iron removal technology

Method	Removal efficiency	Operation condition	Uses
Electro-coagulation (EC)	95 to 99%	<ul style="list-style-type: none"> - Density 0.01 to 0.04 A/m² - pH basic approx. 7.5 - Very face and effective for water containing iron from low to high concentration 	Household use
Oxidation / filtration	80 to 90%	<ul style="list-style-type: none"> - pH ranges 7.5 to 8.5 	In rural area
Ion exchange (IE)	≈ 90%	<ul style="list-style-type: none"> - Effective of water contain Fe/Mn concentration less than 25mg/L 	Use for ground and surface water Minimum water use
Adsorption	84 to 92%	<ul style="list-style-type: none"> - Operate with anoxic suppressing oxidation of ferrous iron, iron removal by adsorptive filtration 	Good operation for surface water like well
Activated carbon and other filtration materials	75 to 90%	<ul style="list-style-type: none"> - Associate with chemical nature of the carbon source, or the amount of O₂ and H₂ - Chemical composition and concentration of the contaminant 	Municipal region
Subsurface iron removal	> 50%	<ul style="list-style-type: none"> - Periodically injection of aerated water is required 	Safe drinking water in rural areas
Aerated granular filter	70%	<ul style="list-style-type: none"> - pH 7.5 to 8 - Water temp. 15 to 30 °C 	Laboratory scale
Ultrafiltration / Microfiltration membrane process (UF/MF)	80 to 90%	<ul style="list-style-type: none"> - Low pressure or vacuum membrane filtration processes 	Household use

Modify from (Chaturvedi et al., 2012)

Table 2.11. BCR applications in air-water study and investigated parameter

System condition	Column-gas distributor	Investigated parameter
Air-water	Column with 0.3 m diameter, ring distributor with 1 mm holes	Gas holdup, bubble characteristics
Water-air, helium, argon and sulfur hexafluoride	Columns with 5 and 10 cm diameters, sintered plate distributor	Transition gas velocity and holdup, bubble rise velocities and bubble holdup
Air-water-glass beads, 35 μ m glass beads of concentration up to 40%	Column with 0.28 m diameter, 6-arm sparger with 1.5 mm of the hole diameter	Gas holdup, bubble characteristics, heat transfer
Air-water	Column with 20 cm in diameter, perforated plate sparger with diameter hole 69.1 mm	Liquid velocity profiles, bubble velocity distributions
Air-water	Studied column 14-19 and 44 cm, perforated plate spargers with 0.33, 0.4, 0.7 and 1 mm hole diameters and bubble cap distributor with diameter holes 5 mm	Fluid dynamics, liquid velocity profiles, gas holdup
Air-water	Column 10-40 and 100 cm	Liquid velocity and mixing measurement, gas holdup
Air-water	Column 20-40 and 80 cm, perforated plate spargers with diameter holes 0.5 mm	Local heat transfer measurements
Air-water	Column 10-38 and 100cm	CFD simulations, bubble properties, mass transfer

Modified from (Kantarci et al., 2005)

Aeration is the common process for oxidizing ferrous iron in water with high concentration, specifically higher than 5 mg/L (Michalakos *et al.*, 1997), as well as it is not required any chemicals. From a frequently applied technology of the aeration process, the contaminated water can be saturated with oxygen by operating different methods such as conventional tray aerator, gas-liquid contactor (bubble column reactor, airlift reactor). Table 2.11 is summarized the application of bubble column reactor (BCR) for air-water only as a literature review. One of the best multiphase contactors, Airlift Reactor (ALR) is considered as the promising type of gas-liquid reactor that provides many advantages such as well mixing performance, low shear rate, low energy consumption, low reaction time, and high gas-liquid mass transfer (Bekassy-Molnar *et al.*, 1997).

ALR is a special design and modification from bubble column or conventional bubble column reactor (BCR) and this reactor class have been studied to apply for oxidizing ferrous iron for drinking water production purpose as well (El Azher *et al.*, 2008).

❖ Research focuses

Even though Bubble Column or Airlift Reactor provide many advantages as aforesaid, several disadvantage of these reactor classes are required to improve such as the limitation of the bubble retention time in the reactor and the gas bubble integration, which assemble the bubble to be larger due to this system was not provided any blades or baffles. Moreover, high-level oxygen transfer efficiency is very necessary for oxidizing ferrous ion at high initial concentration. Therefore, the development of the reactor is still required in order to improve the oxygen transfer efficiency (OTE) as well as to improve oxidation yield of the ferrous iron. In this work, the author tries to develop from bubble column reactor or conventional airlift reactor by adding the vertical baffle to create a liquid recirculation from a riser to downcomer compartment and install the horizontal baffles in a riser to increasing the bubble retention time and bubble distribution. Its performance was evaluated in terms of overall volumetric

oxygen transfer coefficient (K_La) which is calculated from variation of the dissolved oxygen along the time in the system operation.

In this work, terminology of baffle is referred to horizontal baffle. The study was investigated both geometry modification and important aeration parameters including downcomer-to-riser ratio (A_d/A_r), baffle angle (α), baffle length (L_b), baffle quantity (N_b), recirculation area (A_r), the position of recirculation area (Y_r), baffle settling area (A_s), gas diffuser quantity (N_d), and gas flow rate (Q_g). Design of experiment (DOE) method was applied in this study for different purposes such as experimental condition design, screening influent factors, study respond of main factors, and construct prediction equation.

The best reactor performance was selected to study the oxidation of ferrous iron. In this part, the parameters including gas flow rate (Q_g) and initial concentration of ferrous iron ($[Fe^{2+}]_0$) were investigated. The synthetic groundwater was prepared by dissolving iron (II) sulphite ($FeSO_4 \cdot 7H_2O$) in de-aerated tap water. Ferrous iron concentration were noted and analyzed along the time by Phenanthroline Method (APHA *et al.*, 1915).

CHAPTER 3

METHODOLOGY

3.1 Study Overview

This work aimed to develop the reactor in order to improve the oxygen transfer for application of removal ferrous iron in groundwater. General overview of this work is classified into two main parts. First part is the development of reactor by adding the vertical baffle and installing horizontal baffles in a riser. The Novel BCR was applied for the second part, study ferrous iron oxidation process. The framework of this work is shown in Figure 3.1 and will be presented specifically in detail below.

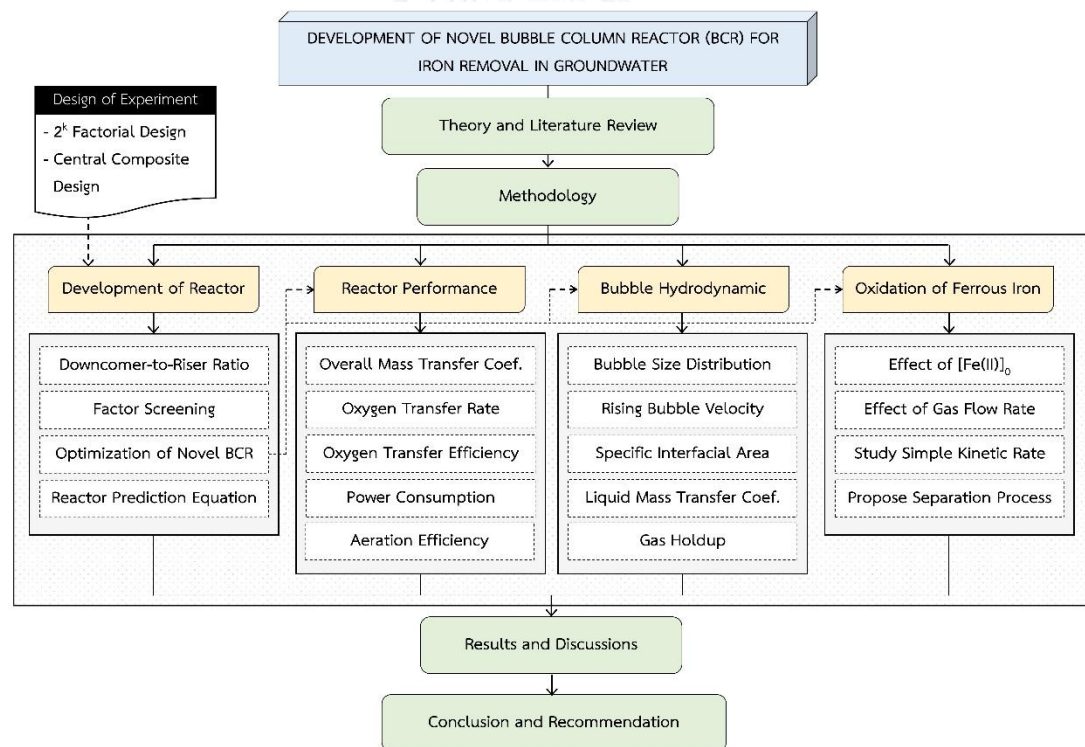


Figure 3.1. Overview of the framework

In this study, the series of work was described as the following points:

- It was investigated all influent factors for Design of Experiment (DOE) in terms of geometry modification and important aeration parameters including

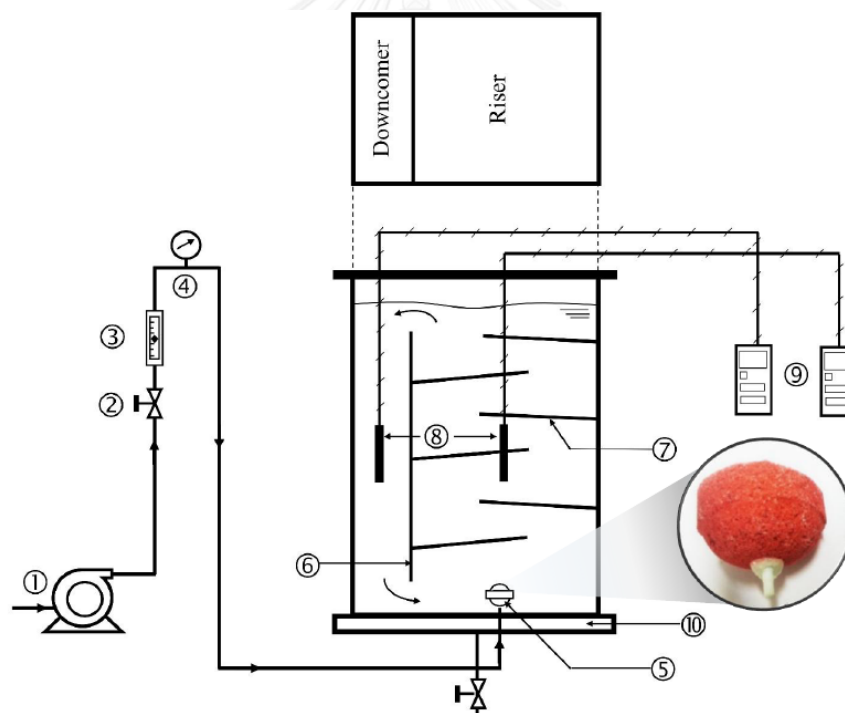
downcomer-to-riser ratio (A_d/A_r), baffle angle (α), baffle length (L_b), baffle quantity (N_b), recirculation area (A_r), the position of recirculation area (Y_r), baffle settling area (A_s), gas diffuser quantity (N_d), and gas flow rate (Q_g). In this study, terminology of baffle is referred to horizontal baffle.

- DOE method was used for design experimental condition in different steps including apply in screening main influent factors, study respond of main factors for the optimization. It was evaluated aeration performance in Novel BCR in different conditions in order to compare each performance base on K_La coefficient by using de-aerated tap water as liquid phase and oxygen from air bubble generation as gas phase.
- The experimental result was analyzed for different part including screening main influent factor part, optimizing the respond of design criteria and operating condition part, and construct the prediction equation part by DOE method of computer software, Minitab 17.
- Several Bubble Hydrodynamics parameters was studied in optimum reactor configuration including bubble size distribution, terminal rising bubble velocity, and specific interfacial area. Moreover, the gas holdup and liquid film mass transfer coefficient was studied in this section as well.
- The optimal design and operating condition of this Novel BCR was selected for studying oxidation of ferrous iron in the second part.
- The study of ferrous iron in the best optimum novel BCR was conducted by using a single ferrous iron pollutant as a synthetic groundwater. It was conducted as the batch reactor.
- In ferrous iron oxidation, it was investigated the experimental parameters including Gas Flow Rate (Q_g) and Initial Ferrous Iron Concentration ($[Fe^{2+}]_0$) with high concentration as in groundwater.

- The samples were sampled and analyzed different contacted time by using Phenanthroline method and the simple kinetic rate for this aeration process of ferrous iron was constructed.
- Separation process of ferric iron was studied for proposed methods including settling process, coagulation of alum dose, and filtration in terms of removal efficiency.

3.2 Experimental Set-up

The rectangular reactor was constructed by acrylic material with dimension of 0.50 m x 0.40 m and 0.80 m in high for containing 140 liters of water sample with the allowed 10 cm freeboard as shown in Figure 3.2.



- (1) Air pump (2) Air valve (3) Rotameter (4) Manometer
 (5) Rigid stone diffuser (6) Vertical baffle (7) Horizontal baffles (8) DO probes
 (9) DO meter (10) Rectangular airlift internal-loop reactor

Figure 3.2. Experimental set-up of Novel BCR

The rigid stone diffusers with the sphere shape of 6.1 cm in diameter were installed at the bottom of the tank (Figure 3.7) in order to provide an air to contact a water sample. Air was compressed by air pump model Atman HP-12000, then regulate the gas to the reactor by installing a rotameter (DWYER® Model) with air valve for ranging the gas flow rates supplied to the system. Manometer (pressure gauge) was connected in series to maintain the performance of air pump in system as well as to estimate the power consumption for air generating of the air pump. The water drainage pipe was made to drain the water after the experiment.

3.3 Materials and Chemicals

3.3.1 Novel Bubble Column Reactor

As mentioned, this rectangular airlift internal-loop reactor was constructed with a clear acrylic material with the thinness of 10 mm. The reactor cross section area is 0.2 m² with 0.8 m of the reactor high. The reactor was designed in the way that a conventional bubble column or internal airlift reactor can be adjusted to a novel bubble column reactor, as shown in Figure 3.3. The vertical baffle was comprised at the desire position of downcomer-to-riser ratio (A_d/A_r) and the bottom recirculation area (A_r) for the conversion to internal airlift reactor. The top view of the fitted vertical baffle and baffle flat was shown in Figure 3.4.

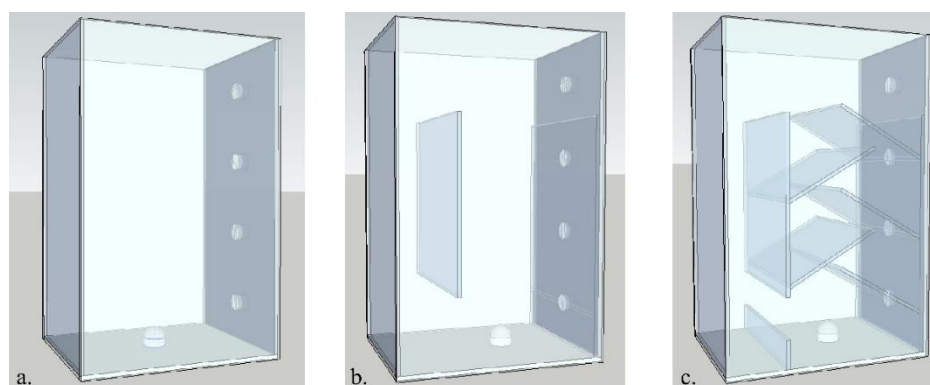


Figure 3.3. Three gas-liquid contactors: (a) BCR, (b) Internal ALR, (c) Novel BCR



Figure 3.4. Fitted vertical baffle in the reactor top view (a) and vertical baffle flat (b) for changing from BCR to ALR

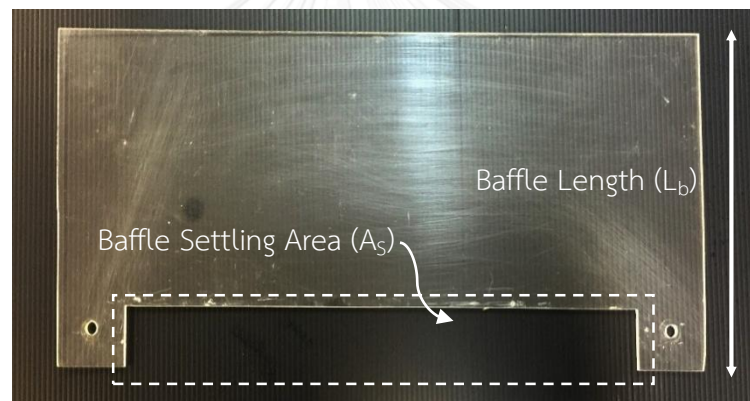


Figure 3.5. Horizontal baffles with free area for settleable particle

The vertical baffle flat was constructed with double supports at the bottom for better stable during installing into the reactor, about 5 cm of each at the end-side as showed in Figure 3.4-b. Novel BCR was installed more horizontal baffles in a riser compartment. The horizontal baffles is not actually present in the horizontal direction, but it is turned aside to this form and for simple note. However, it was varied depending on the study baffle angle ranges (α) of this work as shown in Table 3.1. Variables with factor levels for primary factor screening. The horizontal baffles were designed with the allowable settling area on the baffle (A_s) for solid particles separation.

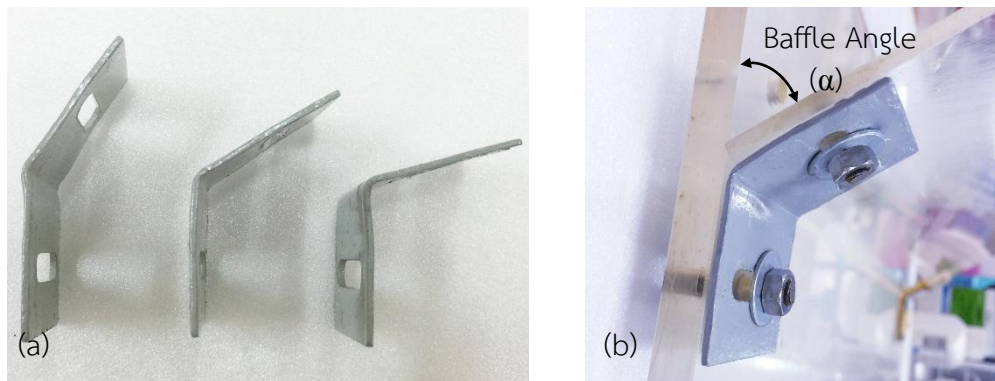


Figure 3.6. Baffle connecting: (a) L-supporter in different angles, and (b) baffles installation

The same as the vertical baffle, the supporter was designed for support it to the vertical baffle as shown in Figure 3.5 with different dimension, depend on the studied ranges (Table 3.1). The horizontal baffle length (L_b) was varied based on the studied ranges of this work (Table 3.1) as well. These vertical and horizontal baffle(s) were constructed by clear acrylic material with the thinness of 10 mm and 5 mm, respectively. As mentioned that the horizontal baffles was designed with the supported for connecting with vertical baffle, therefore, there was a supporter in the shape of letter “L” was designed for this requirement. For L-supporter was made by the steel bar due to it is bendable and high resistance material. However it was recovered by coating with spray acrylic paint. On the vertical and horizontal baffles, there were several holes for connecting each other easily (as shown in Figure 3.6) by using stainless screws. The bended angle was made based on the studied ranges of this work as shown in Table 3.1.

3.3.2 Reactor Comprised Devices

Some devices were required to complete the experiment set-up with the reactor and they were described as the following:

- *Air pump*: Because the rigid stone diffusers were selected in this experiment, the pump performance pressure should not be concerned strictly. The type of

air pump used in this work is Atman aquarium air pump model Atman HP-12000 with the maximum capacity: 0.032 MPa and 110 LPM.

- *Rotameter or air flow meter*: to varies and control an air flow rate for the experiments, air flow meter was used with the studied ranges. Air flow meter model DWYER® 0 to 23 LPM was used.
- *Manometer or pressure gauge*: pressure gauge model IMARI (0 to 1 kg/cm²) was used in this work to estimate the energy consumption.
- *Rigid stone diffuser*: it was installed at the bottom of the tank in order to provide an air to contact water sample. Even though these used stone diffusers are not actually presented as sphere, sphere shape diffuser was referred for these diffusers due to they are very looked like a sphere and for easy note to represent its shape. Stone diffusers with diameter of 6.1 cm (Figure 3.7), which determine from the actual volume of the diffuser, were used in this work. This diffuser class is the local product that can be purchased easily.
- *Other accessories*: beside these mentioned devices, other accessories were used including, flexible pipe, stainless steel valve, L-Y-X connector, etc.



Figure 3.7. Rigid stone diffuser for air distribution

3.3.3 Analysis Equipment

- *DO probe meters:* two different types of DO probe meter were used for measuring dissolved oxygen in water sample of this study including DO probe meter model DO-5512SD (installed in downcomer) and SDL150 (installed in riser) with measurement range 0 to 20 mg/L (accuracy ± 0.4 mg/L) or oxygen in air from 0 to 100% (accuracy $\pm 0.7\%$ O₂) at temperature 23 ± 5 °C and 0 to 50°C, respectively. Both of them were installed at the middle level of the water depth.
- *pH meter:* during ferrous iron oxidation process, pH need to be measured by pH meter as well as to determine the reaction kinetic. The pH meter model METTLER-TOLEDO was used in this study.
- *Thermometer:* not only a pressure, temperature is also another parameter to control DO saturation level. Both pressure and temperature are effect DO saturation as well as a Henry's law. In this study, the water temperature was measured by DO meters for aeration process and by pH meter for ferrous oxidation process.
- *Total iron and ferrous analysis set:* Phenanthroline Analysis method (APHA *et al.*, 1915) was performed for analysis ferrous concentration. Several important materials were used in this work are chemical substance, spectrophotometer (Model GENESYS 10S UV-VIS), glass cuvette 10 mm light path, nessler tubes, pipette, electric balance (Model OHAUS®), magnetic stirrer, laboratory hood, etc. Briefly describe of the analysis procedure was described in the followed section, Analytical Parameters.
- *Turbidity meter:* it was used to measure the turbidity to study the batch settling test, study alum dose for ferric separation, and measure the effluent sample after filtration. The turbidity meter model Lovibond-TB210IR was used in this work.

- *Bubble characteristic analysis, ImageJ application:* ImageJ is a public domain Java image processing program that can display, edit, analyze, process, save, and calculate area and pixel value statistics of user-defined selections (Rasband, 2008). In this study, it was used for studied the bubble characteristic of hydrodynamic parameter including bubble size, and bubble velocity. The capture process was briefly described in the followed section, Analytical Parameter.
- *Jar test set:* this experiment was performed in the section of separation process study in order to obtain the optimum level of alum addition. Alum was examined for improving the separation process of ferric iron sludge.
- *Alkalinity analysis set:* this test was analyzed in the alum addition to study the alum dosage for ferric iron separation process. Several materials was used in this section including chemical substance ($\text{Na}_2\text{S}_2\text{O}_3$, H_2SO_4), pH meter, magnetic starrier, Erlenmeyer flash, pipette, etc.

3.3.4 Chemical Reagents

All chemical substances were used up for different sections such as de-oxygenation in tab water, produce a synthesis groundwater, ferrous and total iron analysis, alum addition, and alkalinity analysis. Several chemical reagents are used in this work, listed as the following.

- Sodium Sulfitte (Na_2SO_3)
- Iron (II) Sulphite ($\text{FeSO}_4 \cdot 7\text{H}_2\text{O}$)
- Acetic Acid (Glacial) (CH_3COOH)
- Ammonium Acetate ($\text{CH}_3\text{COONH}_4$)
- Sodium Thiosulfate ($\text{Na}_2\text{S}_2\text{O}_3$)
- Cobalt (III) Chloride (CoCl_3)
- Sulfuric Acid (H_2SO_4)
- Potassium Permanganate (KMnO_4)
- Hydrochloric Acid (HCl)
- Sodium Bicarbonate (NaHCO_3)

- Hydroxylamine Hydrochloride ($\text{NH}_2\text{OH}\cdot\text{HCl}$)
- 1,10-Phenanthroline Monohydrate ($\text{C}_{12}\text{H}_8\text{N}_2\cdot\text{H}_2\text{O}$)
- Ammonium Iron (II) Sulfate ($(\text{NH}_4)_2\text{SO}_4\text{FeSO}_4\cdot 6\text{H}_2\text{O}$)

3.4 Design of Experiment (DOE)

One of the objectives in this work was to improve the oxygen transfer performance in terms of the overall mass transfer coefficient by finding out the best configuration of the reactor and other important operation parameters. Therefore, Design of Experiment (DOE) method was selected and applied in this study for (i) identifying the condition of the experiments, (ii) analyzing the influence of each parameter on K_La coefficient, and (iii) optimizing the design criteria and operating condition. This method can be used to estimate the effect of the factor and the response in the same time.

The 2^k factorial design and central composite response surface design (CCD-RSD) were sorted out for experimental design and analysis in the processes of screening factors and optimization the influent of investigated factors, respectively. In general, the 2^k design is very popular for application in factor screening experiments (Montgomery, 2008) and it is very useful in the early stages of experimental work when many factors are likely to be investigated. The most popular response surface design (RSD) is central composite design (CCD) which is usually used for modeling and analysis in order to optimize their responses. It was used for analyzing the experimental results including screening main influent factor part, optimizing the respond of design criteria and operating condition part, and construct the prediction equation. DOE method applied for this work was run by the computer software, Minitab 17.

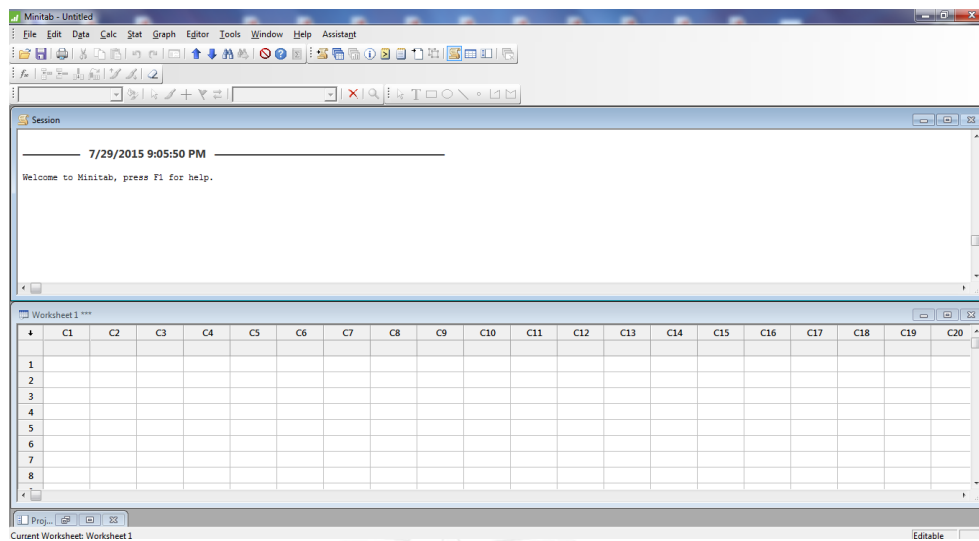


Figure 3.8. An interface of an application Minitab 17

Minitab is an application of statistic developed by several researchers in 1972 include Barbara F. Ryan, Thomas A. Ryan, Jr., and Brian L. Joiner at Pennsylvania State University and distributed by Minitab Inc in State College Pennsylvania (NIST, 2012). Minitab 17 is the latest version (2015) of the application software as shown interface in Figure 3.8.

3.5 Analytical Parameters

3.5.1 Oxygen Concentration

The dissolved oxygen concentration in the water samples was measured by DO probe meters. DO meter was installed at the middle level of the water depth in the reactor. Two DO meters were used to measure DO in riser and downcomer compartment.

3.5.2 Mass Transfer Parameters

- Overall mass transfer coefficient ($K_L a$)

The condition of the gas in the liquid, the solubility of the oxygen is very low such as the oxygen in the water. It is a controlled liquid phase process, thus, $K_L a$ is very important to study or/and analyze the absorption process of a system. Base on the non-stationary or dynamic method (Wolf-Dieter Deckwer *et al.*, 1992), $K_L a$ coefficient

was determined from the variation of the DO in liquid phase as showed in equation 3.1 and derive as equation 3.2:

$$\frac{dc}{dt} = K_L a(C^* - C) \quad \text{Eq. 3.1}$$

$$\ln(C^* - C) = -K_L a(t) + \ln C^* \quad \text{Eq. 3.2}$$

where C and C* are the dissolved oxygen concentration and level saturated dissolved concentration in a liquid phase, respectively. The dissolved oxygen in a liquid phase of this research is measured by DO probe meters. The slope of the equation provides a value of (-K_La).

- Liquid film mass transfer coefficient (K_L)

To understand the effects of surfactants molecules, a study of liquid film mass transfer coefficient (K_L) need to be studied to obtain from the overall mass transfer coefficient (K_La) and interfacial area (a) of the experiment. The K_L value can be determined (Sardeing *et al.*, 2006) as equation 3.3.

$$K_L = \frac{K_L a}{a} \quad \text{Eq. 3.3}$$

3.5.3 Power Consumption

As mentioned, the objective of this work is to evaluate the oxygen transfer of Novel BCR in terms of overall mass transfer coefficient (K_La) and power consumption. Then the power consumption in the reactor was determined by utilizing the equation 3.4 and 3.5 (Painmanakul *et al.*, 2004) where the total gas pressure drop is mainly related to the liquid height (ρ_Lg.H_L) and specific diffuser pressure drop (ΔP). ΔP_{Total} is the total pressure from both liquid height and diffuser. V_{Total} is the total volume of the liquid phase.

$$P_G = Q \times \Delta P_{\text{Total}} \quad \text{Eq. 3.4}$$

$$\frac{P_G}{V_{\text{Total}}} = Q \times \frac{\Delta P_{\text{Total}}}{V_{\text{Total}}} = Q \times \frac{\rho_L g H_L + \Delta P}{V_{\text{Total}}} \quad \text{Eq. 3.5}$$

3.5.4 Aeration Performance (OTR, OTE, AE)

Several aeration performance including oxygen transfer rate (OTR), oxygen transfer efficiency (OTE), and aeration efficiency (AE). Standard oxygen transfer rate (SOTR), standard oxygen transfer efficiency (SOTE), and AE can be calculated by equation 3.6, 3.7, and 3.8, respectively:

$$\text{SOTR} = K_L a_{(20^\circ\text{C})} C_{20}^* V \quad \text{Eq. 3.6}$$

$$\text{SOTE} = \frac{\text{Effective Oxygen}}{\text{Supplied Oxygen}} = \frac{\text{SOTR}}{Qg \times \rho_g \times O_w} \quad \text{Eq. 3.7}$$

$$\text{AE} = \frac{\text{SOTR}}{P_G} \quad \text{Eq. 3.8}$$

$$K_L a_{(T)} = K_L a_{(20^\circ\text{C})} \theta^{T-20} \quad \text{Eq. 3.9}$$

Where C_{20}^* is saturated dissolved concentration in a liquid phase at temperature 20°C [mg/L]. $K_L a_{(20^\circ\text{C})}$ is an oxygen mass transfer coefficient at 20°C and V is the liquid volume. Qg is gas flow rate, ρ_g is an air density, and O_w is an oxygen content in air by weight. P_G is the power consumption that can be determined from previous section 3.5.3.

The same as an establishment of BOD rate coefficient, the temperature effects are treated by applying a van't Hoff-Arrhenius expression by equation 3.9 and the θ value varies base on the test condition and typical range from 1.015 to 1.040. Both diffused and mechanical aeration devices typically used 1.024 (He *et al.*, 2003).

3.5.5 Bubble Hydrodynamic Parameters

The determination of the bubble hydrodynamic parameters is very important in order to understand the bubble characteristic effect on the treatment efficiency. Several

parameters require to study bubble hydrodynamics are bubble diameter (D_B), bubble rising velocity (U_B), bubble formation frequency (f_B), and determined interfacial area (a).

Photographic was captured by slow motion function of camera, iPhone 6 Plus device of Apple Inc. that can record slow motion video with 720p HD at 240 frames per second. It was used to analyze D_B with a computer software, ImageJ after choose in random of 100 moved bubbles in the operation. The average D_B is calculated by the equation 3.10 (Kracht *et al.*, 2008). Bubble rising velocity (U_B) is calculated of the distance two frames with its time require as the following equation 3.11 (Painmanakul *et al.*, 2008). Where ΔD is the distance from one frame to other [m], and t_{frame} is the time frame (s).

$$D_B = d_{32} = \frac{\sum_{i=1}^N d_i^3}{\sum_{i=1}^N d_i^2} \quad \text{Eq. 3.10}$$

$$U_B = \frac{\Delta D}{t_{\text{frame}}} \quad \text{Eq. 3.11}$$

$$f_B = \frac{Q_G}{V_B} \quad \text{Eq. 3.12}$$

Bubble formation frequency (f_B) refers to an amount of bubbles generated from the diffuser per period of time that can be calculated from the equation 3.12 (Painmanakul *et al.*, 2004). Where Q_G is a gas flow rate [m^3/s] and V_B is a bubble volume [m^3]. The interfacial area (a) were calculated from the ratio of the bubble surface (S_B) and reactor volume (V_{total}) by equation 3.13 and 3.14, respectively. Given that N_B is the amount of bubbles, H_L is a high of liquid [m], thus, the equation can be written as equation 3.15 where A is a cross-section area of the reactor [m^2] (Painmanakul *et al.*, 2005).

$$a = N_B \times \frac{S_B}{V_{\text{total}}} \quad \text{Eq. 3.13} \quad N_B = f_B \times \frac{H_L}{U_B} \quad \text{Eq. 3.14}$$

$$a = f_B \times \frac{H_L}{U_B} \times \frac{S_B}{V_{\text{total}}} = f_B \times \frac{H_L}{U_B} \times \frac{\pi D_B^2}{A H_L + N_B V_B} \quad \text{Eq. 3.15}$$

3.5.6 Ferrous and Total Iron Concentration

As mentioned already, there are several analytical methods to determine ferrous and total iron in the water including Atomic Absorption Spectrophotometry (AAS), Inductive Coupled Plasma (ICP), colorimetric (phenanthroline), etc. During the oxidation of ferrous iron in this work, the concentration of ferrous iron was sampled and analyzed by Phenanthroline method, followed standard method (APHA *et al.*, 1915). For detail of Phenanthroline method was attached in Appendix 10. Effluent iron concentration of sample in filtrated water was analyzed by Phenanthroline method as well.

3.5.7 Removal Efficiency (%R)

Ferrous ion removal efficiency (%R) value provided a performance of the absorption process as well as the oxidation process in the reactor. Removal efficiency was defined by the ratio between initial and final concentration of ferrous ion in the synthetic groundwater. The ferrous iron removal efficiency (%R) can be determined by the equation 3.16. Where C_i and C_f is the initial and along the time or final concentration of ferrous iron concentration (mg/L), respectively.

$$\% R = \frac{C_i - C_f}{C_i} \times 100 \quad \text{Eq. 3.16}$$

3.6 Experimental Procedures

The experiment was conducted in series of work as shown in Figure 3.9 which was divided into seven main parts including:

- Design and Installation of the Novel BCR,
- Experimental Design and Optimization of Novel BCR,
- Aeration Experimental Perform for $K_L a$ Coefficient Calculation,
- Novel BCR Performance and Prediction Equation,
- Study of Internal Parameter: Bubble Hydrodynamic Parameters
- Oxidation of Ferrous Iron with Novel BCR, and
- Study of Ferric Iron Separation Process

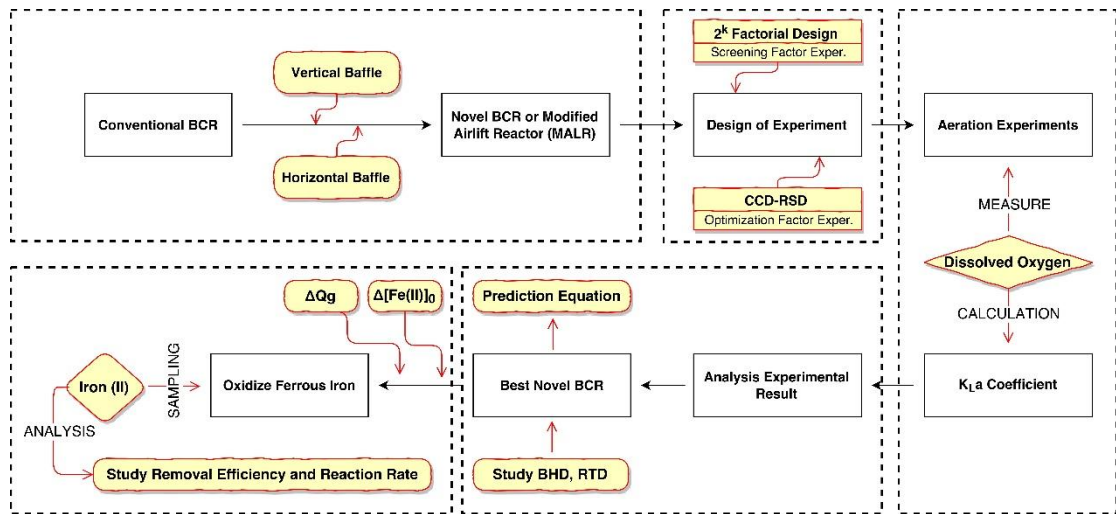


Figure 3.9. Experimental procedure

3.6.1 Design and Installation

Novel BCR of this study was developed from the conventional BCR and ALR as showed in Figure 3.10 that was supplemented by comprise the vertical baffle to create a liquid recirculation from the riser to downcomer compartment, and install horizontal baffles in the riser compartment to extend bubble retention time and improve air bubble distribution. This reactor design was studied in terms of geometry modification and important aeration parameters including downcomer-to-riser ratio (A_d/A_r), baffle angle (α), baffle length (L_b), baffle quantity (N_b), recirculation area (A_r), position of recirculation area (Y_r), baffle settling area (A_s), gas diffuser quantity (N_d), and gas flow rate (Q_g).

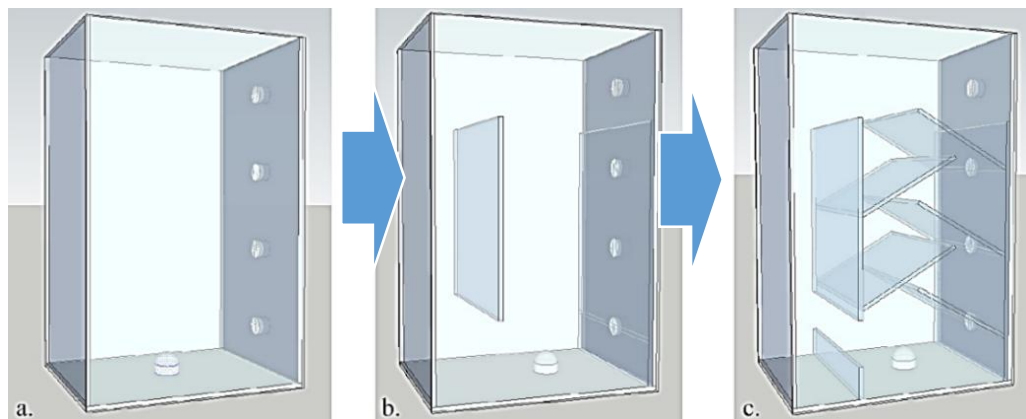


Figure 3.10. The reactor development concept

All of the investigated factors were studied in order to find out the optimum point in terms of $K_L a$ coefficient as the response value by vary the factor levels.

- Downcomer-to-Riser Ratio (A_d/A_r): this parameter is referred to the downcomer area (non-aerated cross section area) compared to the riser area (aerated cross section area) as showed in Figure 3.11. When the rectangular reactor was used, it can be represented by width length of the downcomer (W_d) compared to width length of the riser (W_r). $A_d/A_r = W_d/W_r$ for rectangular split-vessel and $A_d/A_r = (((W_d+W_r)^2)/(W_r^2)) - 1$ for concentric draught tube.

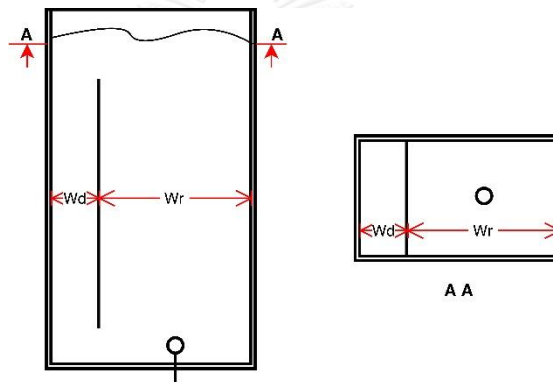


Figure 3.11. The variation of downcomer and riser compartment

- Gas diffuser quantity (N_d): amount of diffusers installed in the bottom of the reactor for gas distribution. The installation was arranged for appropriate space from one diffuser to other diffusers in riser compartment.
- Gas flow rate (Q_g): the gas supply to the system was varied for this work as well.
- Baffle angle (α): this parameter is referred to the horizontal baffles installed in the riser compartment. The angle value (α) is the angle of the modified baffles refereed to the vertical line where follow the clockwise for left hand side baffle(s) and opposite for the right hand side baffle(s) in the riser, presented in the unit of degree as showed in Figure 3.12.

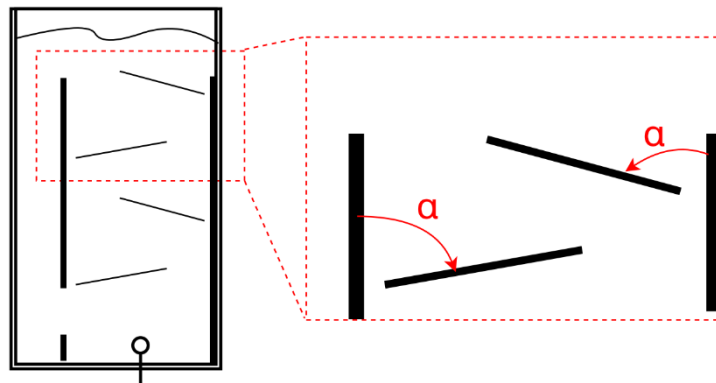


Figure 3.12. Installation of modified baffles (angle) in the riser compartment

- Baffle length (L_b): the length of the modified baffle in the riser compartment was defined the optimum from the varied length as well. It was installed at the both end-side in the riser as shown in Figure 3.13.

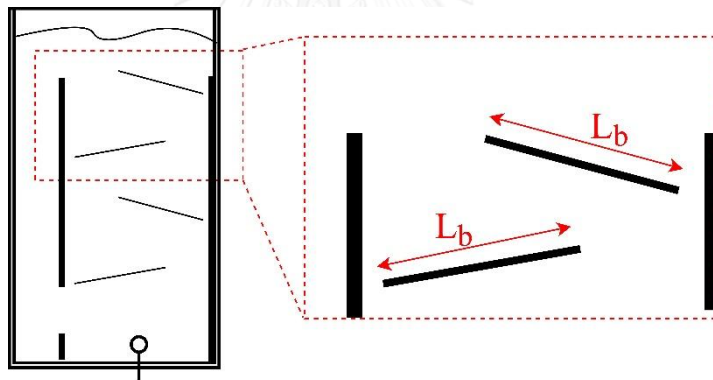


Figure 3.13. Modified baffles length installed in the riser compartment

- Recirculation area (A_r): this parameter is referred to the bottom recirculation space provided as shown in Figure 3.14-a. Recirculation area of this work was designed as a rectangular area that can be determined by width and length of recirculation area ($A_r = R_w \times R_L$).
- Baffle quantity (N_b): amount of modified baffles in the riser compartment was studied.

- Position of recirculation area (Y_r): the bottom recirculation area was studied different position, called position of recirculation area. It was varied by installing rectangular flat at the bottom with different high as shown in Figure 3.14-b.

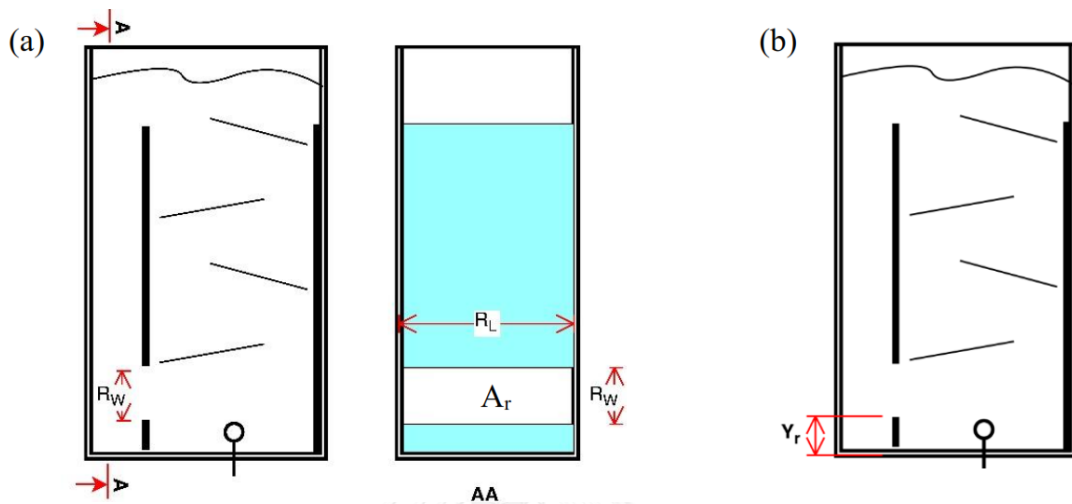


Figure 3.14. Design of the bottom recirculation area (a) and its position (b)

- Baffle settling area (A_s): on the modified baffles, there is a free space next to the vertical baffle for (i) allowing the solid particles in the reactor settle down, and (ii) to minimize the dead zone after install horizontal baffles. Settling area can be determined by the width and length of the settling space ($A_s = S_w \times S_L$) as shown in Figure 3.15.

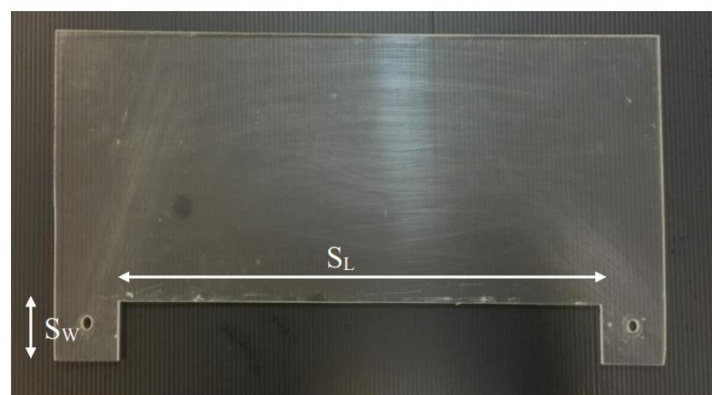


Figure 3.15. Designed baffle flat for installing the riser compartment

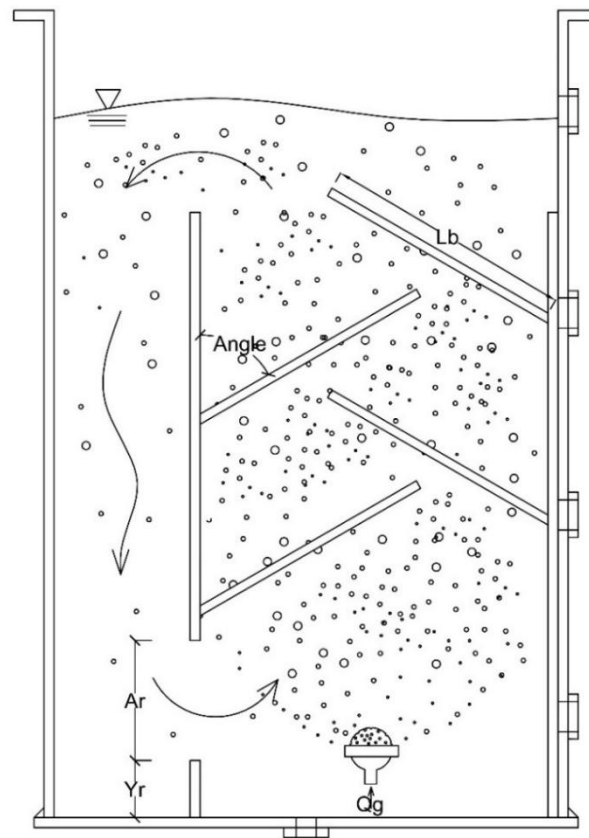


Figure 3.16. Novel BCR after comprised all baffles

The design of the reactor with all comprised baffles was illustrated in Figure 3.16 with the length from the bottom of the reactor to the center of the diffuser is approximated 5 cm. The reactor design compartments was attached in Appendix 2 for more detail.

3.6.2 Optimization of Novel BCR

The objective of this work is to evaluate the oxygen transfer in the Novel BCR after the development. The reactor development was investigated all influent factors with final outcome is the optimum reactor configuration and operation condition. The processes to supplement the reactor was presented in Figure 3.17.

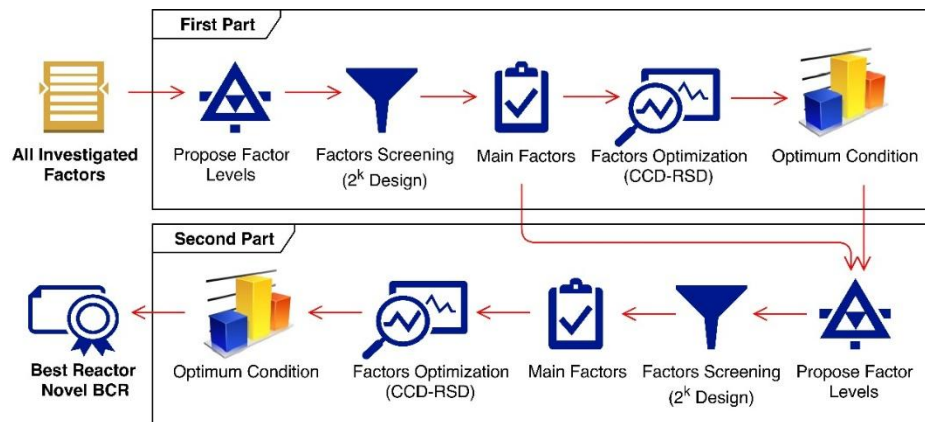


Figure 3.17. The development processes to obtain best reactor

The study of reactor development was divided into two parts. First part and second part were named as the early stage of the processes and the following process, respectively. Experimental design, perform, and analysis were done within two continued parts (first and second part) in order to obtain an accurate response due to the error of proposed factor levels in factor screening experiments. It is seemed like the double replications. However these replications are different from the normal due to the proposed variables and its levels are not the same for some cases.

Figure 3.18 represents about the problems which happened from the bad proposed factor levels for factor screening experiments. If the truth response graphic follows the linear form, the factor levels will affect only how low or high were selected as Figure 3.18-a. In opposition, if the truth response values provide the optimum curve, the proposed factor levels are more complicate as Figure 3.18-b. For example, two-level of (X_1 and X_4) or (X_2 and X_3) were proposed, the response values are very similar which is not represent the truth respond levels. These are the reasons for some factors which are the main factors on the response item in the truth response become less or no significant factor in the screening part.

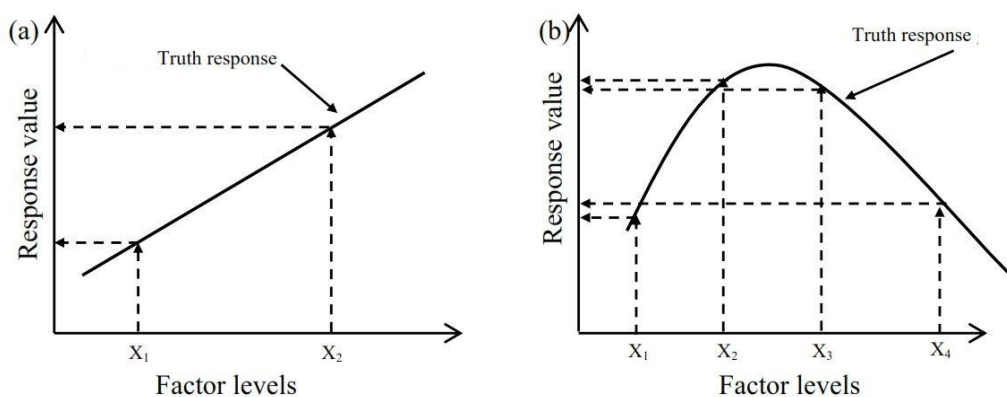


Figure 3.18. The effective plot between factor levels and response values

In this section, two main methodologies were used as shown in Figure 3.17 including factor screening experiments, and optimization of novel reactor. DOE method was selected and applied in this section for (i) identifying the condition of the experiments, (ii) analyzing the influence of each parameter on $K_L a$ coefficient, and (iii) optimizing the design criteria and operating condition.

- Factor Screening Experiments

The objective of this part is to find the main factors that have a significant effect on the response value, $K_L a$ coefficient. The 2^k factorial design of DOE was used to complete this target. This two-level factorial design is commonly used in the early stages of the experimental work when many factors are likely to be investigated. It is widely performed in factor screening experiments as this part referring (Montgomery, 2008).

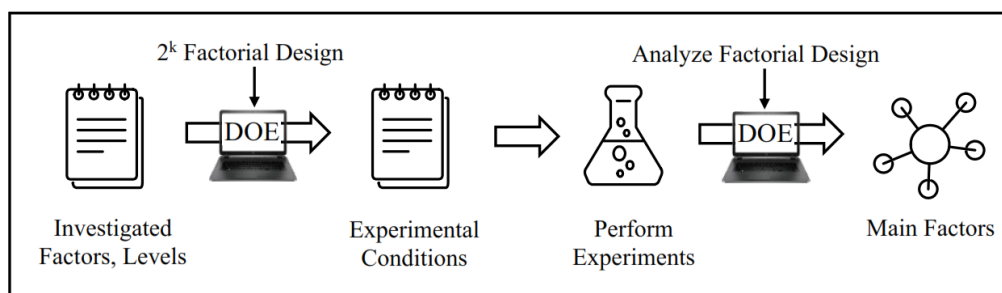


Figure 3.19. Factor screening process by 2^k factorial design

Table 3.1. Variables with factor levels for primary factor screening

Factors	Unit	Factor Levels	
		-	+
Baffle angle (α)	degree	50	90
Baffle length (L_b)	cm	17	23
Amount of baffle (N_b)	#	4	6
Amount of diffuser (N_d)	#	2	4
Settling area on baffle (A_s)	cm ²	30	90
Recirculation area (A_r)	cm ²	150	450
Position of recirculation area (Y_r)	cm	0	10

Table 3.2. The parameter measurement for factor screening experimental process

Variable	Parameter
<ul style="list-style-type: none"> ▪ Fixed variable 	
- Gas phase (absorbate)	Oxygen
- Liquid phase (absorbent)	De-aerated tap water
- Liquid volume	140 liters
- Temperature / Pressure	27 ± 2°C / 1 atm
<ul style="list-style-type: none"> ▪ Independent variable 	
- First part: all investigated factors and its level	Experimental condition generated from 2 ^k factorial design of DOE by Minitab 17
- Second part: studied factors and levels from first part	
<ul style="list-style-type: none"> ▪ Dependent variable 	
- Water saturation	Dissolved oxygen (DO)
- Response value	K _L a coefficient
- Analysis result	Main factors

The investigated factors and the levels value of the primary factor screening were shown in Table 3.1 where (-) and (+) are referred to low level and high level, respectively. Figure 3.19 presented the experimental processes for factor screening to obtain main factors and Table 3.2 presents the summary variable concerning in this section.

- Optimization and Predicted Equation

This section aimed to determine the optimum point of the main factors and construct the predicted equation in terms of main factors. Central composite design of response surface design (CCD-RSD) were sorted out for this section. CCD is the most popular design of the response surface methodology (RSM) which is usually used for modeling and analysis the problems. The response of the interest is influenced by several factors and the objective is to optimize this response (Montgomery, 2008). Three main influent factors which two of them was selected from factor screening experimental result, combine with gas flow rate parameter were used for CCD. Response surface design (RSD) was used to analyze experimental results for optimizing the response of design criteria and operating condition, and for constructing the prediction equation. The experimental process of the optimization part was presented in Figure 3.20 and the measured parameter was shown in Table 3.3 containing variable and parameter.

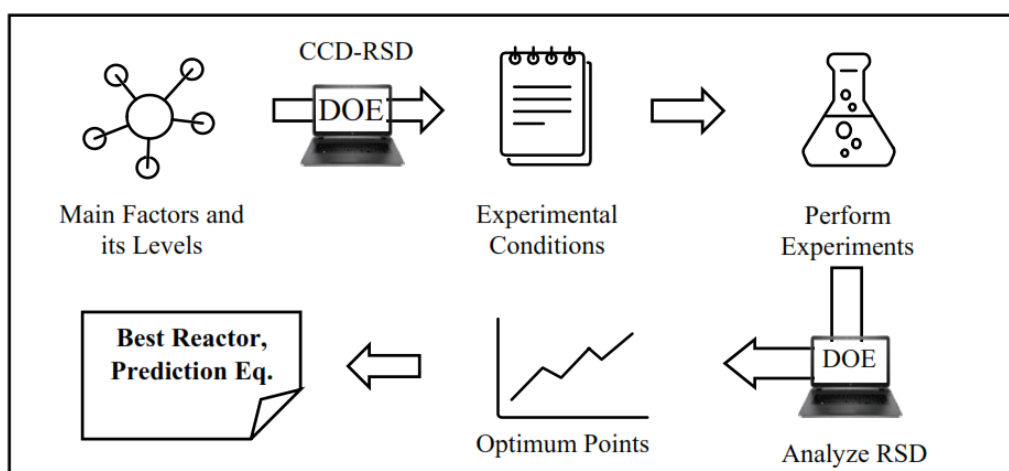


Figure 3.20. Experimental process of optimization part and prediction equation

Table 3.3. Parameter measurement for optimization process

Variable	Parameter
<ul style="list-style-type: none"> ▪ Fixed variable 	
- Gas phase (absorbate)	Oxygen
- Liquid phase (absorbent)	De-aerated tap water
- Liquid volume	140 liters
- Temperature / Pressure	27 ± 2°C / 1 atm
<ul style="list-style-type: none"> ▪ Independent variable 	
- First part: 3 main factors from first part of factor screening experiments	Experimental condition generated from Central
- Second part: 3 main factor from second part of factor screening experiments	Composite Design of DOE by Minitab 17
<ul style="list-style-type: none"> ▪ Dependent variable 	
- Water saturation	Dissolved oxygen (DO)
- Response value	K _L a coefficient
- Analysis result	Optimum conditions Prediction equation

3.6.3 Deoxygenation Process

To study the oxygen transfer in both aeration process and ferrous iron oxidation, it has to be examined from a variation of the dissolved oxygen (He *et al.*, 2003). Therefore, it should be started from the lower DO concentration by using the chemicals or stripping a nitrogen gas to reduce initial DO in tap water. In this work, sodium sulfite (Na₂SO₃) was used to reduce DO concentration in tap water, reaction of this oxygen reduction was expressed by equation 3.17.



From the equation 3.17, to remove 1 kg of DO, 8 kg of sodium sulphite is required. However, the amount of sodium sulphite should be added more than the calculated value by 10 to 15% due to the lag time for admixture. To expedite the reaction, a catalyst cobalt (III) chloride should be added once to the reactor with the concentration of 0.5 mg/L. After DO reached the concentration less than 10% of the saturation point for aeration process (He *et al.*, 2003) and less than 1mg/L for ferrous oxidation (El Azher *et al.*, 2008), the experiments were started.

3.6.4 Aeration Process

After DO concentration reached to the desired level, the air stripping system was started for providing the oxygen to the system (Figure 3.21). Air pump was connected to the diffusers with a rotameter and manometer to control airflow rate and measure the air pump pressure. The DO in the reactor was measured along the time by using two different DO probe meters for riser and downcomer compartment. The aeration process was performed until the DO reached at least 98% of saturated level (Stenstrom *et al.*, 2006). The saturated point can be determined from Appendix 1. After the variation of DO in the reactor was examined from DO probe meters, $K_L a$ coefficient was calculated then where presents as the slope of port between $\ln(C^*-C)$ and aeration time (Figure 3.21).

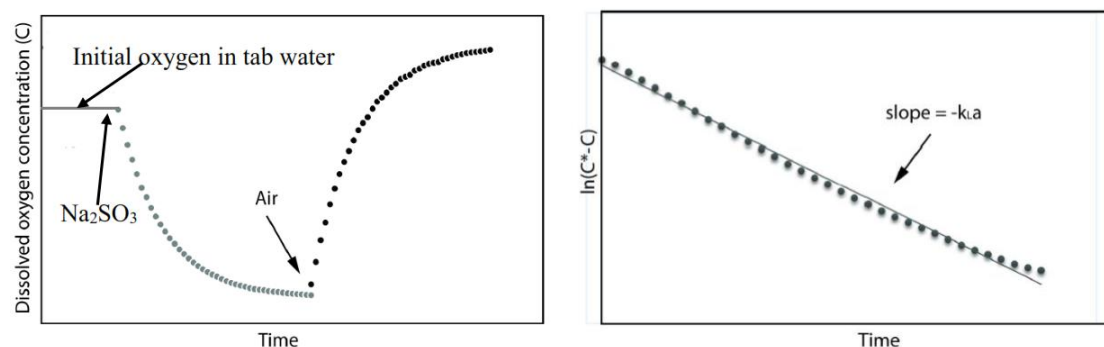


Figure 3.21. Process of oxygenation and $K_L a$ coefficient obtaining

3.6.5 Oxidation of Ferrous Iron

The objective of this section is to examine the removal efficiency of ferrous iron along the time of oxidation process in the reactor. The optimum level of a reactor configuration and operation parameter was used for this part. The parameters including gas flow rate (Q_g) and initial concentration of ferrous iron ($[Fe^{2+}]_0$) were investigated. The synthetic groundwater was prepared by dissolving iron (II) sulphite ($FeSO_4 \cdot 7H_2O$) with de-aerated tap water. Sodium sulphite (Na_2SO_3) was used to reduce the initial DO of tap water until less than 1mg/L at the initial step (El Azher *et al.*, 2008). During conducting the experiment, the concentration of ferrous iron was sampled and analyzed by Phenanthroline method.

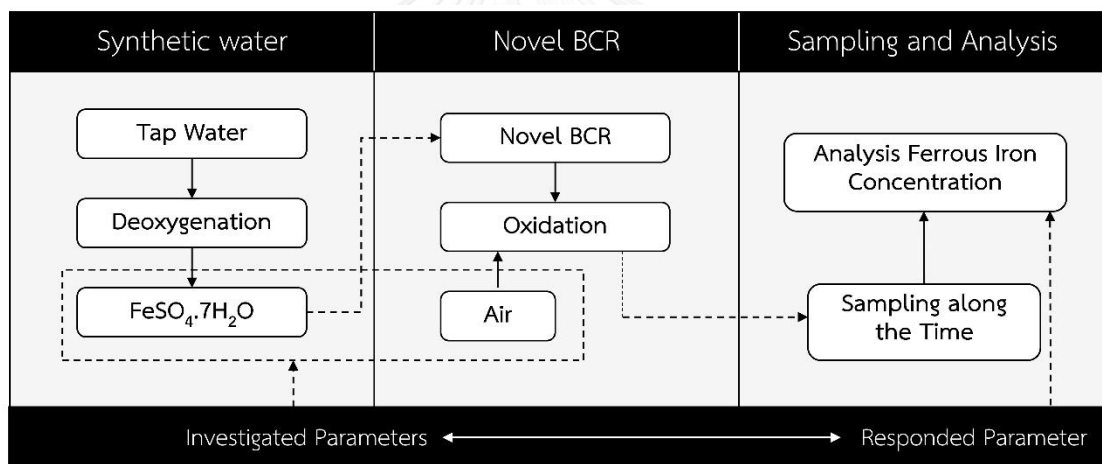
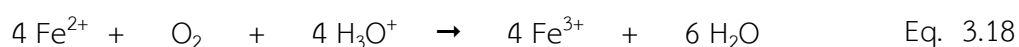


Figure 3.22. Experimental process of ferrous iron oxidation

Table 3.4. Parameter measurement for ferrous iron oxidation

Variable	Parameter
<ul style="list-style-type: none"> ▪ Fixed variable 	
- Reactor class	Best Novel BCR (optimum)
- Gas phase (absorbate)	Oxygen
- Liquid phase (absorbent)	Synthetic groundwater
- Liquid volume	140 liters
- Temperature / Pressure	27 ± 2°C / 1 atm
<ul style="list-style-type: none"> ▪ Independent variable 	
- Gas flow rate	2 to 10 LPM
- Initial concentration of ferrous iron	5 to 50 mg/L
<ul style="list-style-type: none"> ▪ Dependent variable 	
- Removal efficiency	Ferrous concentration

The physico-chemical oxidation of ferrous in water can be written as the stoichiometric equation 3.18. It shows that 1 mg of oxygen can oxidize 7 mg of ferrous iron. The experimental process of ferrous iron oxidation was presented in Figure 3.22 and the measured parameter was shown in Table 3.4 containing variable and parameter.



3.6.6 Ferric Iron Separation Process

As mentioned that the iron in groundwater will be removed by oxidizing the ferrous iron in a soluble form to an insoluble form, ferric iron and the ferric particles will be removed by future separation process such as sedimentation process, followed by filtration. Even though the ferric iron separation process is not the main object and there is not the novel technology, it will studied the batch settling test, alum dosage addition for improving the settling process, and the filtration test representative the depth filtration.

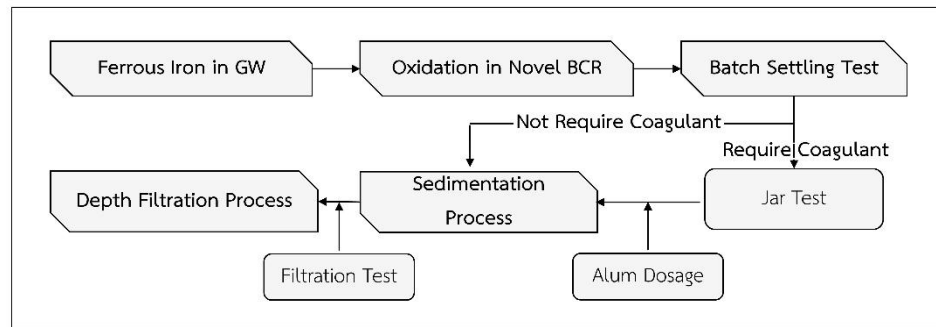


Figure 3.23. Serried processes for separation of ferric iron after oxidation

The objective of this section is to study the fraction removal in the Novel BCR as batch settling column test, jar test for studying the optimum concentration of alum to improve the settling process of ferric particle, and filtration test for studying the depth filtration test for removal the ferric particle. Batch settling test is aimed to identify the settling process by gravity after aeration process as well as to study the solid removal with overflow rate. If settling velocity is so low due to the small particle or colloid, therefore, alum coagulant is required in order to improve the settling process. In opposite, there is not required any coagulant after it is well settle down. Jar test is used for studying the optimum alum dose for addition as a coagulant.

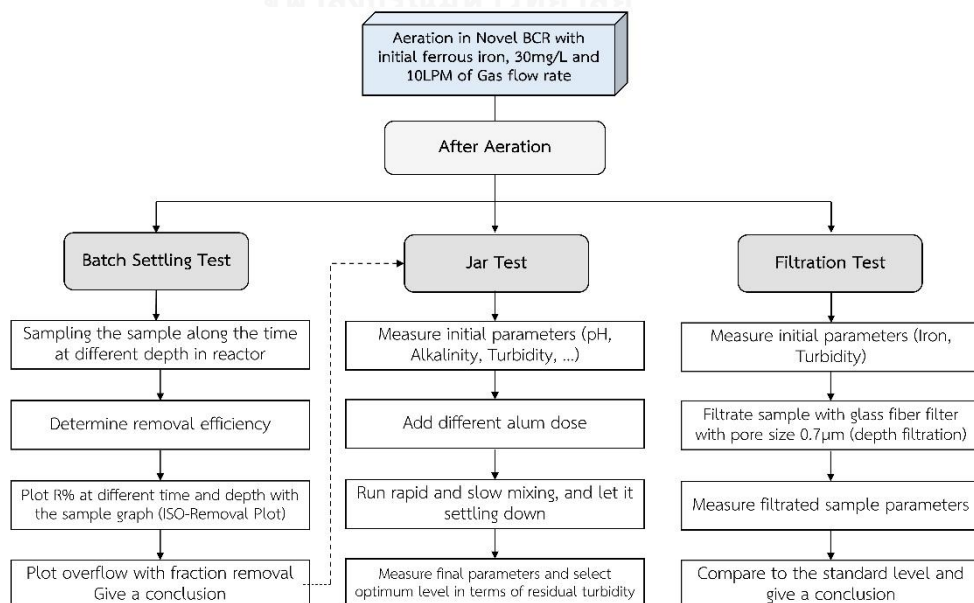


Figure 3.24. Flow diagram for studying ferric iron separation process

Table 3.5. Parameter measurement for ferric iron separation

Variable		Parameter
<ul style="list-style-type: none"> ▪ Fixed variable 		
- Reactor class		Novel BCR (Optimum)
- Pre-oxidized parameter		$[\text{Fe}^{2+}]_0 = 30 \text{ mg/L}$ $Q_g = 10 \text{ LPM}$
- Aerated water sample		Ferric iron, Ferrous iron, Turbidity, Alkalinity, pH
- Temperature / Pressure		$27 \pm 2^\circ\text{C} / 1 \text{ atm}$
<u>Batch Settling Test</u>		
<ul style="list-style-type: none"> ▪ Independent variable 	- Time	0 to 300 min
	- Depth (from water surface)	22 cm, 42 cm, 62 cm
<ul style="list-style-type: none"> ▪ Dependent variable 	- Fraction Removal ($R_T\%$)	Turbidity
<u>Jar Test</u>		
<ul style="list-style-type: none"> ▪ Independent variable 	- Alum concentration	5 to 80 mg/L
<ul style="list-style-type: none"> ▪ Dependent variable 	- Optimum alum	Residual turbidity
<u>Filtration Test</u>		
<ul style="list-style-type: none"> ▪ Independent variable 	- Filter type	Glass fiber filter with $0.7 \mu\text{m}$ of pore size
<ul style="list-style-type: none"> ▪ Dependent variable 	- Filtrated water quality	Total iron, turbidity

Moreover, the effluent of sedimentation process is continued to study for filtration process. To study depth filtration process, the water sample was sampled and filtrated with the glass fiber filter 0.7 μm of pore size which representative the depth filtration pore size as well. This experiment was conducted to confirm that depth filtration process can be used for this water sample or not by compared to the standard level in terms of iron concentration and turbidity (iron < 0.3 mg/L, turbidity < 5 NTU). The serried process of this separation process was shown in Figure 3.23. Flow diagram and summary variable table is shown in Figure 3.24 and Table 3.5, respectively.



CHAPTER 4

RESULTS AND DISCUSSIONS

This chapter presents the experimental and analysis results covering on two main objectives including the novel reactor development and the application of novel reactor optimum condition for ferrous iron oxidation. The results was divided into four main parts such as:

- **Development of Novel BCR**
 - Study downcomer-to-riser ratio
 - Factor screening for main factor
 - Optimization of Novel BCR for optimum level
 - Prediction equation for Novel BCR
- **Comparison of Novel BCR performance in terms of:**
 - Overall mass transfer coefficient
 - Oxygen transfer rate
 - Oxygen transfer efficiency
 - Power consumption
 - Aeration efficiency
- **Study of bubble hydrodynamic parameters**
 - Bubble size distribution (D_B)
 - Terminal rising bubble velocity (U_B)
 - Specific interfacial area (a)
 - Liquid film mass transfer coefficient (K_L)
 - Gas holdup (ϵ)
- **Oxidation of ferrous iron**
 - Effect of initial concentration of ferrous
 - Effect of gas flow rate
 - Study the simple kinetic rate
 - Proposed separation process for ferric iron

4.1 Development of Novel BCR

The result from this section, development of novel bubble column reactor (Novel BCR) was divided into three different parts including the effect of downcomer-to-riser ratio (A_d/A_r) on K_La coefficient, screening factors that provide main responses, and optimization of the main factors followed with prediction equation. The study of A_d/A_r should be included into the geometry parameter in screening process. However, it is not possible due to the limitation of the experiment such as the study of baffle length. That is why it was separated to study as presented in Figure 4.1. This section, reactor development is the main part of this work.

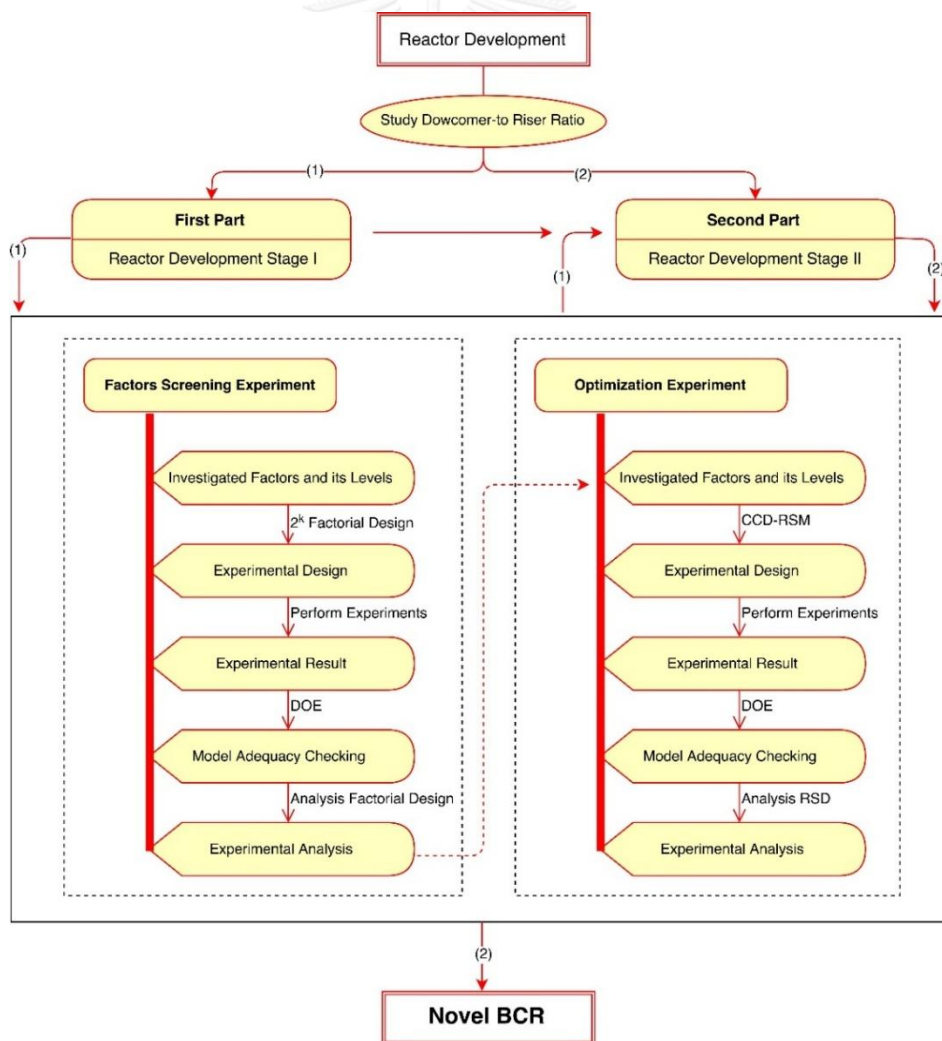


Figure 4.1. Reactor development process involve design, perform, and analysis

4.1.1 Downcomer-to-Riser Ratio

The influence of A_d/A_r ratio on $K_L a$ coefficient was studied with a gradual change of the cross-sectional area of non-aerated to aerated compartment of airlift reactor. It was ranged in six levels: 0.18, 0.30, 0.45, 0.64, 1.44, and 2.03. The experiment was conducted as simple airlift reactor (ALR) with its configuration presents in Table 4.1. The result was obtained from average dissolved oxygen in the reactor between downcomer and riser compartment where were assumed as minimum and maximum zone, respectively.

From the experimental result of Figure 4.2, the optimum value of A_d/A_r was obtained during it equals 0.45. Thus, width of downcomer and riser of this reactor work are 15.5 cm and 34.5 cm, respectively. The error bar is referred to the maximum and minimum values while maximum and minimum was obtained from riser and downcomer compartment, respectively. The result is very slightly similar (approximate $5.4 \pm 0.5 \text{ hr}^{-1}$) for every A_d/A_r values that is following the studied result of (Tobajas *et al.*, 1999). It was reported that the variation of A_d/A_r did not significantly change behavior of reactor as well as the gas holdup and liquid circulation velocity. Maximum $K_L a$ value whereas A_d/A_r equal 0.45 is quite the same to result of recent study, (Drandev, 2015), A_d/A_r equal 0.5 out of the varied value of 0.2 to 1.0 for every superficial gas velocities in riser ($U_G = 0.021$ to 0.004 m.s^{-1}).

Table 4.1. Experimental condition for study downcomer-to-riser ratio

Reactor	Gas flow rate (Q_g)	Amount of diffuser (N_d)	Recirculation area (A_r)	Position of Ar (Y_r)
Airlift Reactor	12 LPM	2 diffusers	300 cm^2	0 cm

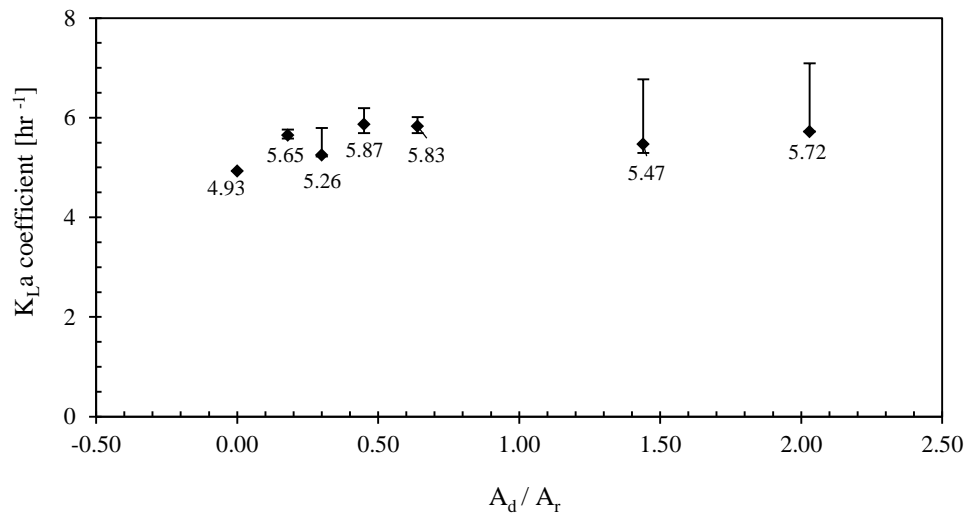


Figure 4.2. Variation of average $K_{L,a}$ coefficient value with different A_d/A_r ratio

4.1.2 Reactor Development Stage I

- Factor Screening

The section, reactor development stage I was mentioned as first part of the reactor development. Factors screening experiment was proposed for screen out the factors or variables that less significant response. The 2^{k-1} design, half running of 2^k factorial design was selected for screening factors process. The responded parameter, average $K_{L,a}$ coefficient was obtained from riser and downcomer compartment. This section, 64 experimental conditions were generated by 2-level factorial design with 95% confidence level of a single replication. The investigated factors and its levels was shown in Table 3.1. Experimental conditions were designed by Minitab 17 statistic application. It is shown in Table 4.2 where the (-) and (+) represents the low level and high level, respectively.

The experiments were performed based on the designed condition with 12 LPM of gas flow rate. This first part of the reactor development stage I, the experimental results was shown in Table 4.3 as the average value of $K_{L,a}$ coefficient. Full experimental result of this factor screening experiments part was attached in the Appendix 4, which was included the $K_{L,a}$ coefficient in riser and downcomer compartment.

Table 4.2. Experimental design by 2^{k-1} factorial for 1st factors screening

Run	A _S	A _R	Y _r	α	L _b	N _b	N _d	Run	A _S	A _R	Y _r	α	L _b	N _b	N _d
1	-	-	-	-	-	+	-	33	-	-	+	+	-	-	+
2	+	+	-	-	+	-	-	34	-	+	+	+	-	+	+
3	-	-	+	+	+	+	+	35	+	-	-	+	-	-	+
4	-	-	-	-	+	+	+	36	+	-	+	+	-	-	-
5	+	-	+	-	-	-	+	37	-	+	+	-	+	+	+
6	-	-	+	-	+	+	-	38	-	-	+	-	-	+	+
7	-	+	-	+	+	-	-	39	+	+	-	+	-	+	+
8	-	+	+	-	+	-	-	40	-	-	+	-	-	-	-
9	+	-	+	+	-	+	+	41	-	+	+	-	-	-	+
10	-	-	-	-	+	-	-	42	+	+	+	+	+	+	+
11	-	+	+	+	+	-	+	43	-	-	+	+	-	+	-
12	+	+	-	-	-	+	-	44	-	-	-	+	+	+	-
13	+	+	+	-	+	-	+	45	+	+	+	+	-	-	+
14	+	+	-	+	-	-	-	46	+	+	-	+	+	-	+
15	-	-	+	-	+	-	+	47	-	+	-	-	-	-	-
16	+	-	-	-	-	-	-	48	+	-	+	-	-	+	-
17	+	-	+	-	+	+	+	49	-	-	-	+	-	-	-
18	+	+	+	-	+	+	-	50	+	-	+	+	+	-	+
19	-	+	-	-	-	+	+	51	+	+	-	-	+	+	+
20	+	-	-	-	-	+	+	52	+	+	+	+	+	-	-
21	+	+	-	-	-	-	+	53	-	-	-	+	+	-	+
22	-	+	+	+	-	-	-	54	+	+	-	+	+	+	-
23	-	-	-	-	-	-	+	55	+	+	+	+	-	+	-
24	-	+	-	+	-	-	+	56	+	-	-	+	+	+	+
25	+	-	+	+	+	+	-	57	+	-	-	+	+	-	-
26	-	+	-	-	+	+	-	58	-	+	-	-	+	-	+
27	-	+	+	+	+	+	-	59	+	+	+	-	-	+	+
28	-	+	-	+	-	+	-	60	+	-	-	+	-	+	-
29	+	-	-	-	+	-	+	61	+	-	+	-	+	-	-
30	-	-	-	+	-	+	+	62	-	-	+	+	+	-	-
31	-	+	-	+	+	+	+	63	+	-	-	-	+	+	-
32	-	+	+	-	-	+	-	64	+	+	+	-	-	-	-

Table 4.3. Experimental result designed by 2^{k-1} factorial for 1st factors screening

Run	K_La [hr^{-1}]	Run	K_La [hr^{-1}]	Run	K_La [hr^{-1}]	Run	K_La [hr^{-1}]
1	5.35	17	7.44	33	4.74	49	4.51
2	4.41	18	7.55	34	5.50	50	9.26
3	5.36	19	6.35	35	8.55	51	4.31
4	5.22	20	6.02	36	7.86	52	8.64
5	8.21	21	8.22	37	5.57	53	6.26
6	5.61	22	6.32	38	6.07	54	3.66
7	5.93	23	5.63	39	6.59	55	6.39
8	6.85	24	5.30	40	5.51	56	3.19
9	7.29	25	5.95	41	6.89	57	3.11
10	6.84	26	5.52	42	7.40	58	7.30
11	6.17	27	4.89	43	4.52	59	5.78
12	5.24	28	4.44	44	3.72	60	5.94
13	9.24	29	4.03	45	8.99	61	8.90
14	8.15	30	4.96	46	5.39	62	5.03
15	7.01	31	4.19	47	5.53	63	4.17
16	6.54	32	6.62	48	5.76	64	7.41

The highest and lowest K_La coefficient was obtained in the Run 50 ($K_La \sim 9.26 \text{ hr}^{-1}$) and the Run 57 ($K_La \sim 3.11 \text{ hr}^{-1}$), respectively. The results of riser and downcomer are usually obtained as divergent values where the obtained from the riser compartment were better than the downcomer compartment as shown in Figure 4.3. Moreover, the K_La coefficient obtained in downcomer of external loop airlift reactor is usually neglected (Ghosh *et al.*, 2010).

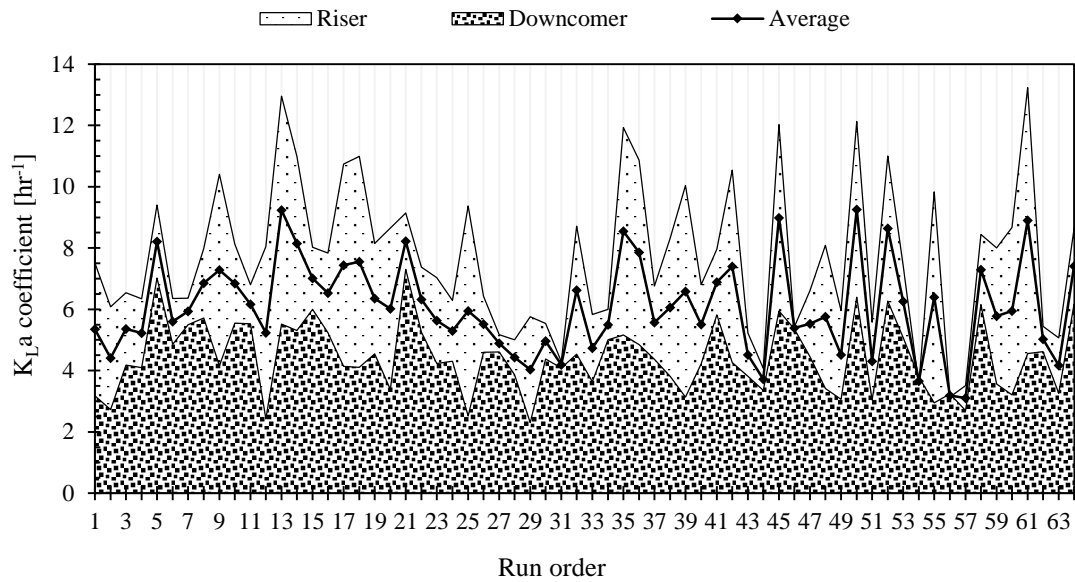


Figure 4.3. Experimental results, K_{La} coefficient of first factors screening

The results were analyzed by statistical analysis with a confidence level of 95%. Before start the analysis, model adequacy checking was applied to the results in order to check and verify the data quality (Gomez *et al.*, 2014; Montgomery, 2008). The model adequacy checking including residual plots for K_{La} coefficient of normal probability plot, versus fits, and versus order were determined by Minitab 17 and the results is shown in respective Figure 4.4, Figure 4.5, and Figure 4.6.

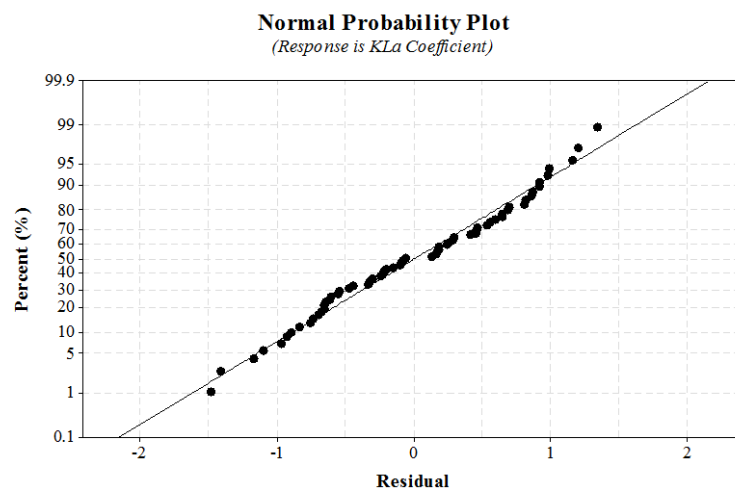


Figure 4.4. Normal probability plot for 1st factors screening

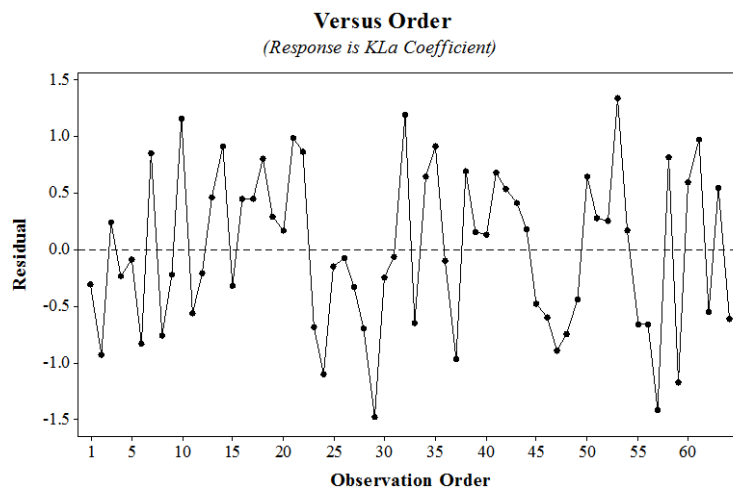


Figure 4.5. The versus order plot for 1st factors screening

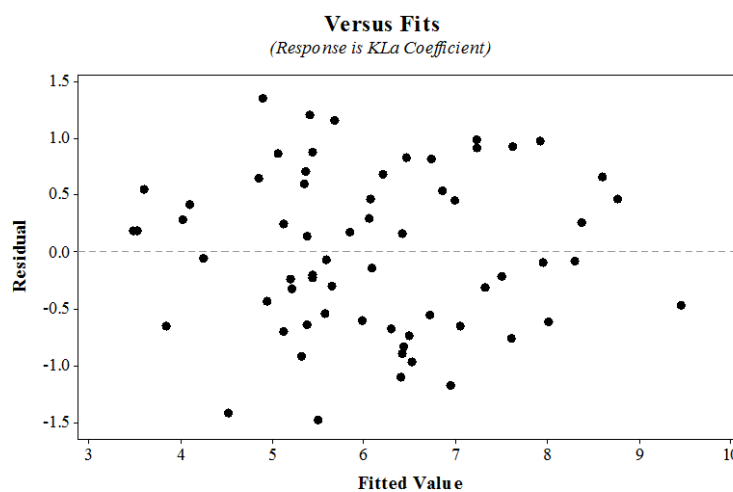


Figure 4.6. The versus fits plot for 1st factors screening

Base on the residual plot, these data can be concluded as an accurate and reliable data for analyzing due to the normal probability plot roughly followed a straight line, the versus fits scattered randomly about zero, and versus order fluctuate in a random pattern around the center line (Minitab, 2000; Yotto, 2015).

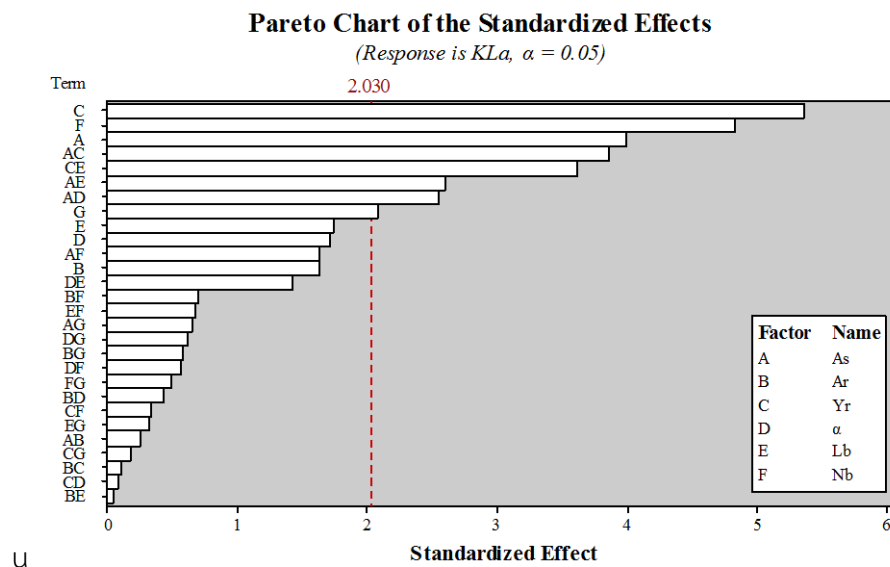


Figure 4.7. Pareto chart of standardized effect by single and interaction terms

Analysis of variance (ANOVA) was conducted in the model up through confidence level of 95% in two-sided interval ($\alpha = 0.05$) by Minitab 17 and the result was shown in Figure 4.7 for linear and Figure 4.8 for two-way interaction. The y-axis title, term is referred to the factor at a single or interaction (e.g. Term C is baffle angle (α), Term AF is interaction between baffle angle (α) and amount of baffle (N_b)). The full analysis of variance of this first factors screening was attached in Appendix 5. The main effect was ranked as order from the analysis of variance was shown in Table 4.4 with several values including effect, T, and P value.

Figure 4.7 is a Pareto chart which was used to present the effect comparing between the relative magnitude and statistical significance of single term effect and interaction term effect. The absolute value was used for this illustration. The reference line indicate which effects are significant. From Figure 4.7, three main effects that are the single significant factors are the position of recirculation area (Y_r), amount of baffle (N_b), and settling area on baffle (A_s). For the way of the single term effect and interaction term effect, this chart cannot present of responses characteristic but the main effective

plot and two-way interaction plot of respective Figure 4.8 and Figure 4.9 can be used for this purpose.

Main effects plot is very useful while several types of factor are likely to compare for find out which one are influences the response the most. The connected line of each variable determine whether or not a main effect is present for a variable. If the variable line is horizontal as parallel to the x-axis, there is no main effect present. In opposite, if the line is not horizontal, there is a main effect present. The greater different in the vertical position of the connected line, the greater the magnitude of the main effect. Comparing the slopes of line, the relative magnitude of the effect. For Figure 4.8 of three main effect, increasing values of A_s , Y_r , and N_b , better results was obtained from A_s and Y_r , except N_b .

The interaction plots for two-way interactions was constructed for evaluation the line for well understand how interactions affect the response. In this two-way interactions, if the two lines are parallel, no interaction takes place. Dissimilar, the greater lines depart from being parallel, there is greater interaction strength. From the experimental results of Figure 4.9, all most of the interaction plots in two-way are parallel each other. The several interactions were found in very low strength which is representative very low two-way interaction as well.

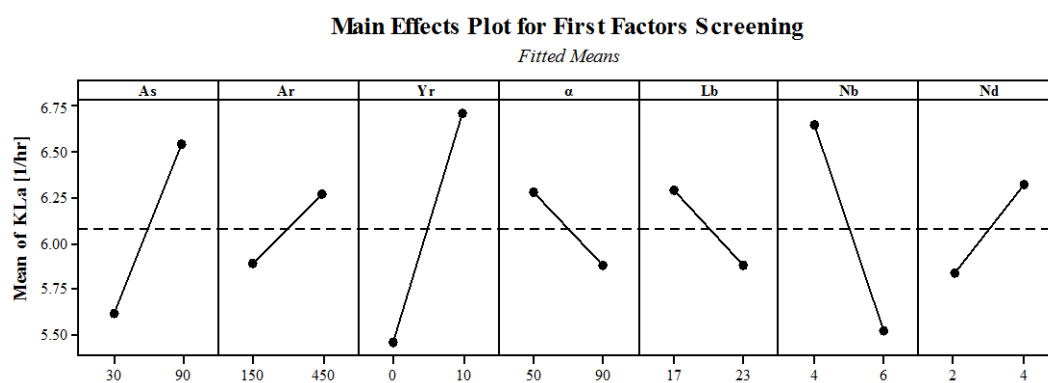


Figure 4.8. Main effective plot for single interaction (linear response)

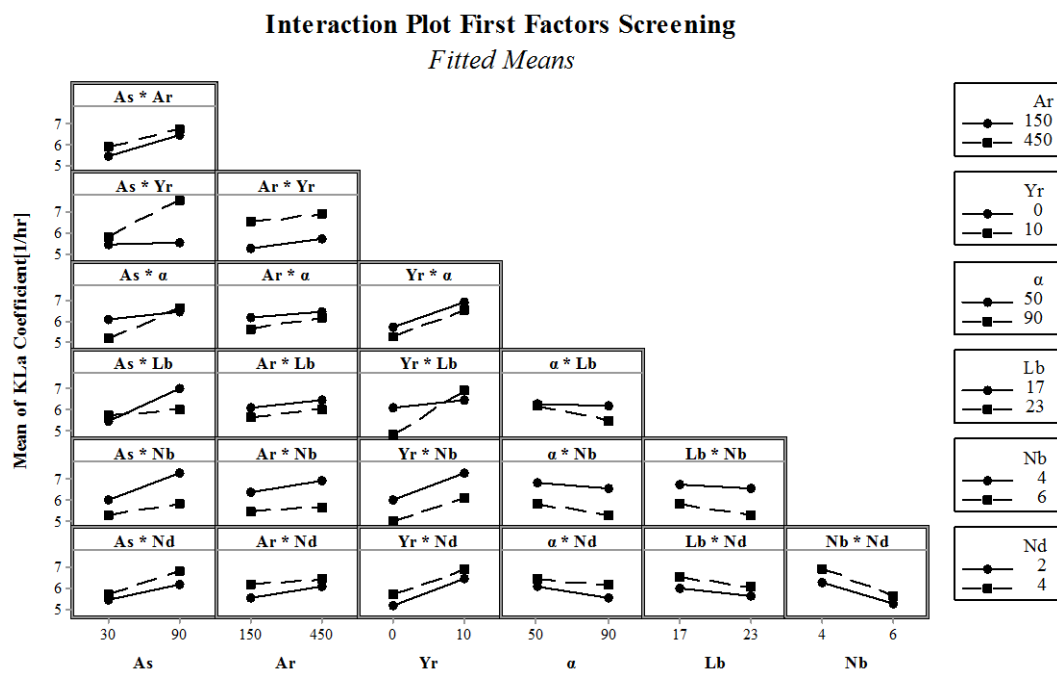


Figure 4.9. Interaction plot for two-way interaction

Table 4.4. Single response of effective value, T-value, and P-value

Main significant factors				Less significant factors			
Factor	Effect	T-Value	P-Value	Factor	Effect	T-Value	P-Value
Y_r	1.255	5.36	0.000	L_b	-0.408	-1.74	0.090
N_b	-1.130	-4.83	0.000	α	-0.403	-1.72	0.094
A_s	0.933	3.99	0.000	A_r	0.381	1.63	0.112
N_d	0.487	2.08	0.045				

To determine if a difference is statistically significant, check the P-value of each factor in the analysis of variance (Table 4.4). This table presents the same purpose as Figure 4.8 but it can show for specific statistical number better than the figure. Even though the P-value of N_d (0.045) is passed to be a significant factor as shown in Table 4.4 and Pareto chart (Figure 4.7), the level of its signification is still low compared to other three factors (0.000) and it is the limitation of the experiment in optimization part.

▪ Summary result of first factor screening

From the experimental and analysis results, three main factors including position of recirculation area (Y_r), amount of baffle (N_b), and settling area on baffle (A_s) will be obtained for optimization part. Even though there are only three factors that was selected to study in the next optimization, it does not mean that other four factors are not affect the performance of the K_{La} coefficient as well as the oxygen transfer in this reactor. It refers to the level of the influent to the response, means that other four factors is less affect than two selected factors. However the better factor value (one of two levels that provide higher K_{La} coefficient) of the less significant factors will be used in the optimization part such as baffle angle ($\alpha \sim 50^\circ$), baffle length ($L_b \sim 17$ cm), amount of diffuser ($N_d \sim 4$ diffusers), and bottom recirculation area ($A_r \sim 450$ cm²).

- Factor Optimization

The three main factors from the screening process were used in this section. However one factor, settling area on the baffle was excluded from the optimization section and instead by the gas flow rate variable due to the limitation of the experiment in optimization part (CCD-RSD) and A_s factor will affect the precipitated particle as settling process. Therefore three main factor for studying in this factor optimization are Y_r , N_b , and Q_g . The factor levels for this section was used 3-level factor, the code designs are -1, 0, +1 as shown in Table 4.5.

Table 4.5. Variables with factor levels for CCD-RSD

Main factors	Unit	Factor Levels		
		-1	0	+1
Gas flow rate (Q_g)	LPM	5	10	15
Amount of Baffle (N_b)	#	2	3	4
Position of recirculation area (Y_r)	cm	0	10	20

Table 4.6. Experimental condition designed by CCD for 1st factors optimization

Run	Qg [LPM]	Y _r [cm]	N _b [#]	Run	Qg [LPM]	Y _r [cm]	N _b [#]
1	0	0	0	11	0	0	0
2	0	0	0	12	0	0	0
3	0	0	0	13	-1	1	1
4	1	-1	1	14	1	-1	-1
5	-1	1	-1	15	1.68	0	0
6	1	1	1	16	0	1.68	0
7	0	0	-1.68	17	0	0	1.68
8	-1	-1	-1	18	0	-1.68	0
9	1	1	-1	19	-1.68	0	0
10	0	0	0	20	-1	-1	1

As mentioned, central composite of response surface designs (CCD-RSD) was selected to study in this section. After design the experiment by central composite full factorial design, the experimental conditions were generated as a single replicate. The code design of the experiment was shown in Table 4.6 with 20 experiments. From the experimental condition design of Table 4.6, there are the margin experiments that are generated by the software requirement for the design boundary.

The experiments were performed base on the designed condition. Average K_La coefficient that was obtained from riser and downcomer compartment are the response variable in this study. The experimental results were shown in Table 4.7. The highest and the lowest K_La coefficient was obtained in the respective Run 15 ($K_La \sim 13.43 \text{ hr}^{-1}$) and the Run 19 ($K_La \sim 1.40 \text{ hr}^{-1}$), where are the maximum and minimum gas flow rate provided. The results were analyzed by statistical analysis with a confidence level of 95%. Before starting the analysis, model adequacy checking was applied to

the results in order to check and verify the data quality (Gomez *et al.*, 2014; Montgomery, 2008).

Table 4.7. Experimental result for first factor optimization

Run	Qg [LPM]	Y _r [cm]	N _b [#]	K _L a [hr ⁻¹]	Run	Qg [LPM]	Y _r [cm]	N _b [#]	K _L a [hr ⁻¹]
1	10	10	3	8.140	11	10	10	3	7.885
2	10	10	3	8.295	12	10	10	3	7.865
3	10	10	3	8.410	13	5	20	4	3.580
4	15	0	4	9.110	14	15	0	2	11.070
5	5	20	2	3.690	15	18	10	3	13.425
6	15	20	4	10.405	16	10	27	3	6.640
7	10	10	1	7.290	17	10	10	5	6.050
8	5	0	2	3.560	18	10	-7	3	5.615
9	15	20	2	11.575	19	2	10	3	1.400
10	10	10	3	7.740	20	5	0	4	3.365

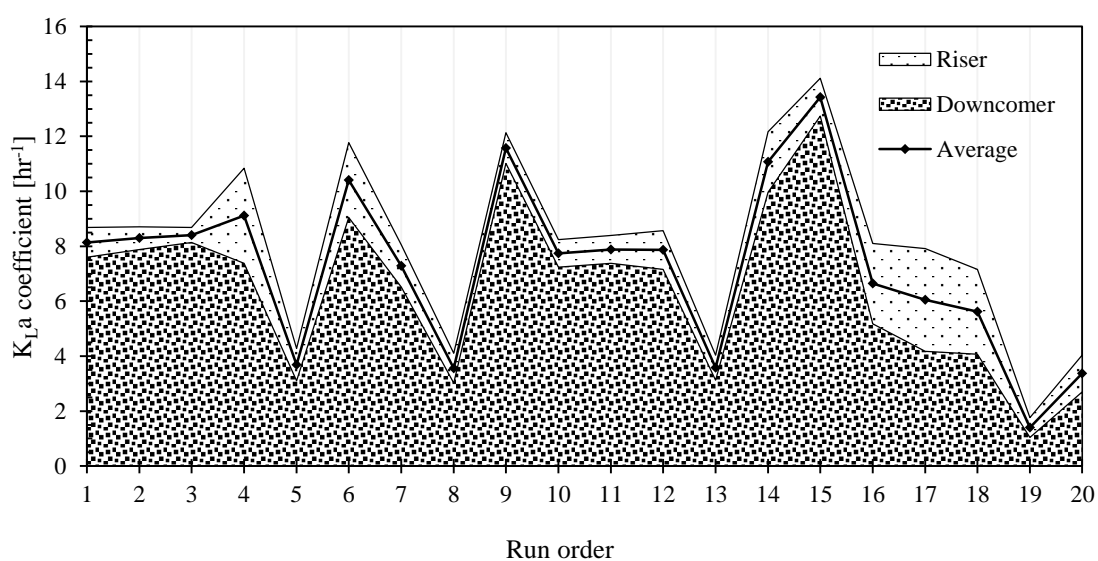


Figure 4.10. Experimental results, $K_{L,a}$ coefficient of first factors optimization

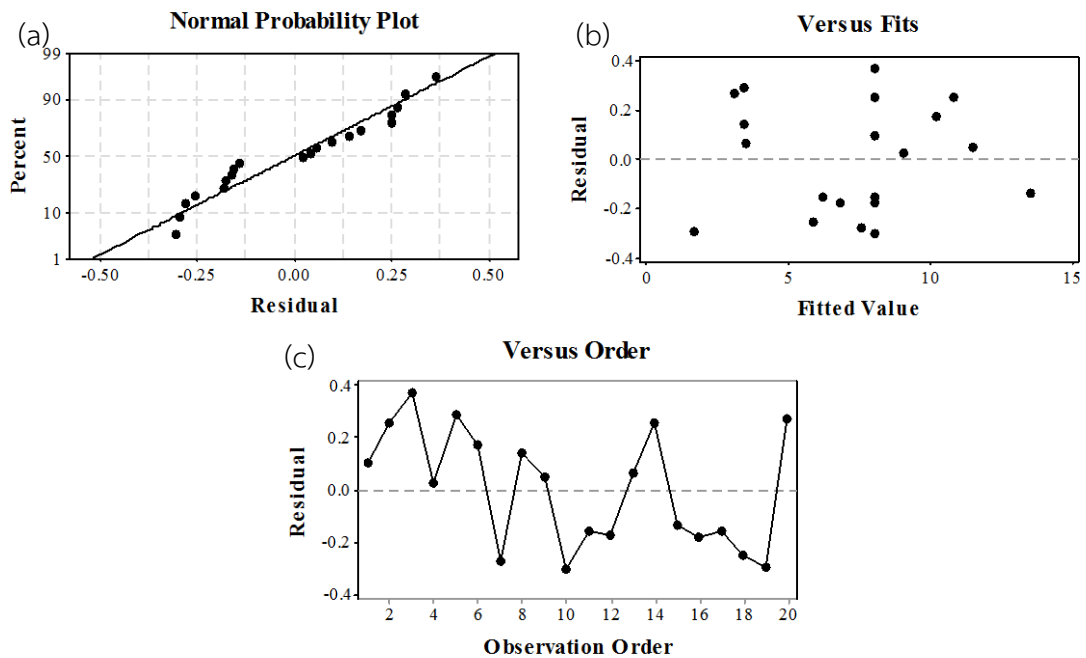


Figure 4.11. Residual plot of experimental result including (a) normal probability plot, (b) versus fits, and (c) versus order

Full experimental result of this factor optimization part was attached in Appendix 6. $K_L a$ coefficient which was examined from the riser and downcomer is shown in Figure 4.10. The model adequacy checking including residual plots for $K_L a$ coefficient of normal probability plot, versus fits, and versus order were examined by Minitab 17 and the results is shown in Figure 4.11. Base on the residual plots (Figure 4.11), these data can be concluded as an accurate and reliable data for analyzing due to the normal probability plot roughly followed a straight line, the versus fits scatted randomly about zero, and versus order fluctuate in a random pattern around the center line (Minitab, 2000; Yotto, 2015).

Analysis of variance (ANOVA) was conducted in the model up thought confidence level of 95% in two-sided interval ($\alpha = 0.05$) by Minitab 17. The experimental result statistical analysis of this section is presented in the Table 4.8 which included three different items: analysis of variance, model summary, and coded coefficient. This analysis is

covered the linear, square, and two-way interaction form for analysis of variance and coded coefficient.

As aforesaid, P-value is used to determine in the model for the statistically significant. Before take a look on the individual effects in the coded coefficients table, the P-values of F-test in analysis of variance table should be firstly observed. After the significant set of effects including linear or interaction effects were identified, check the coefficients table for individual effects evaluation. Using P-value, if it is less than or equal to α (in this study, $\alpha \sim 0.05$), it can conclude that the effect is significant. In opposite, if it is greater than α , the effect is not significant. S, R, adjusted R, and predicted R are used for examination the level of the model fits the data. Its values were used for selection the best fit model.

From Table 4.8, the value of the linear effect provides high F-test value (618.12), followed by the square effect (24.96), and the poorest one is two-way interaction effect (4.84). Comparing these main effect factor, gas flow rate variable is the highest significant effect and the lowest significant effect is the position of the bottom recirculation area. The main effects plot and interaction plot is shown in Figure 4.12 and Figure 4.13, respectively.

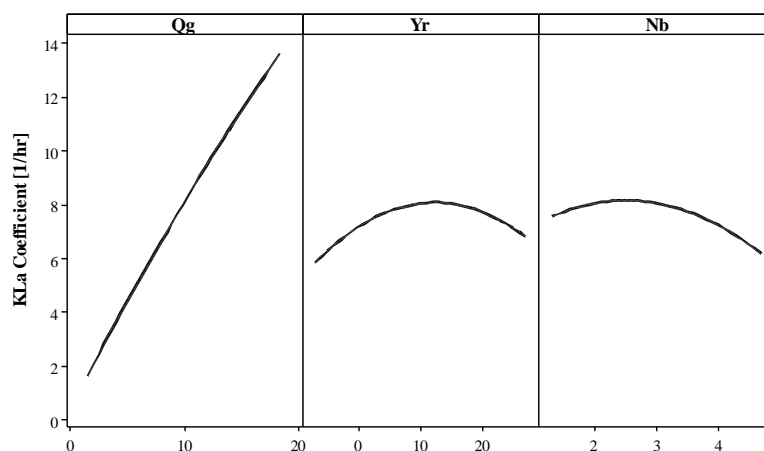


Figure 4.12. Main effects plot of the fitted mean value of K_{La} coefficient

Table 4.8. Experimental result statistical analysis of first factor optimization

Analysis of Variance					
Source	DF	Adj SS	Adj MS	F-Value	P-Value
Model	9	181.719	20.191	215.97	0
Linear	3	173.362	57.787	618.12	0
Qg	1	170.035	170.035	1818.77	0
Y _r	1	1.096	1.096	11.72	0.007
N _b	1	2.231	2.231	23.87	0.001
Square	3	6.999	2.333	24.96	0
Qg ²	1	0.306	0.306	3.27	0.101
Y _r ²	1	5.187	5.187	55.48	0
N _b ²	1	2.401	2.401	25.68	0
2-Way Interaction	3	1.358	0.453	4.84	0.025
Qg*Y _r	1	0.265	0.265	2.83	0.123
Qg*N _b	1	0.998	0.998	10.67	0.008
Y _r *N _b	1	0.096	0.096	1.02	0.336
Error	10	0.935	0.093		
Lack-of-Fit	5	0.58	0.116	1.63	0.302
Pure Error	5	0.355	0.071		
Total	19	182.654			
Model Summary					
S	R-sq	R-sq(adj)	R-sq(pred)		
0.30576	99.49%	99.03%	97.27%		
Coded Coefficients					
Term	Effect	Coef	SE Coef	T-Value	P-Value
Constant		8.043	0.125	64.5	0
Qg	7.057	3.529	0.083	42.65	0
Y _r	0.567	0.283	0.083	3.42	0.007
N _b	-0.808	-0.404	0.083	-4.89	0.001
Qg ²	-0.291	-0.146	0.081	-1.81	0.101
Y _r ²	-1.200	-0.600	0.081	-7.45	0
N _b ²	-0.816	-0.408	0.081	-5.07	0
Qg*Y _r	0.364	0.182	0.108	1.68	0.123
Qg*N _b	-0.706	-0.353	0.108	-3.27	0.008
Y _r *N _b	0.219	0.109	0.108	1.01	0.336

From the Figure 4.12 and Figure 4.13, the air flow rate increasing parallel along the response, $K_{L,a}$ coefficient which is different from other two factors. The optimum position of the recirculation point (Y_r) value that can provide a best $K_{L,a}$ coefficient value was found at 10 cm height from the bottom of the reactor. Optimum baffle quantity, there are 3 baffles installed that can improve the oxygen transfer in this reactor type.

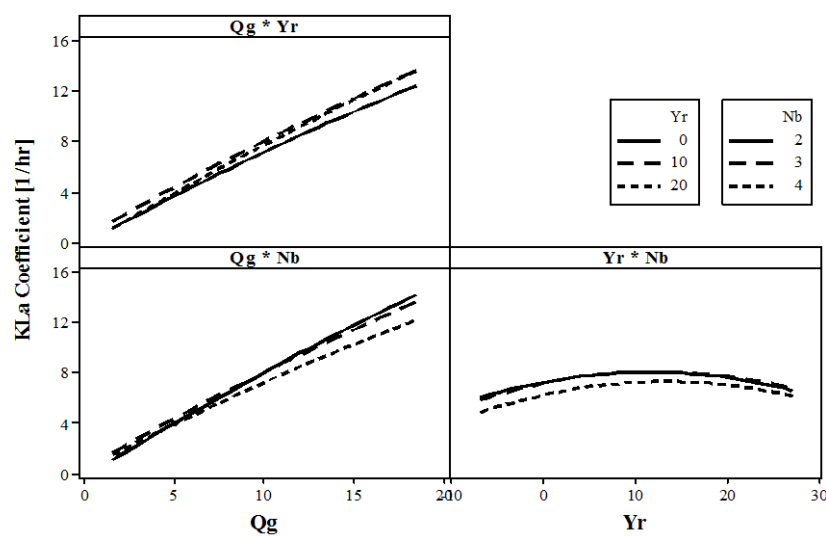


Figure 4.13. Interaction effects plot of fitted mean value of $K_{L,a}$ coefficient

The interaction plot is not different from the single effect, followed as the statistical analysis (Table 4.8). It shows that the interaction effects is not provide significant effect (P-value). For better understanding the factor optimization level, Minitab 17 provided the surface and contour plot of two interaction effect a time (other one variable was held its value) as shown in Figure 4.14 and Figure 4.15.

Not different from the interaction plot, the factors that were plotted with gas flow rate (Q_g), the optimum point cannot be found due to the response value ($K_{L,a}$ coefficient) is increasing parallel along the gas flow rate. Other more, gas flow rate factor is the most effective variable for diffused aeration system and it is for sure during increasing gas flow rate, mean increasing amount of the gas in the system.

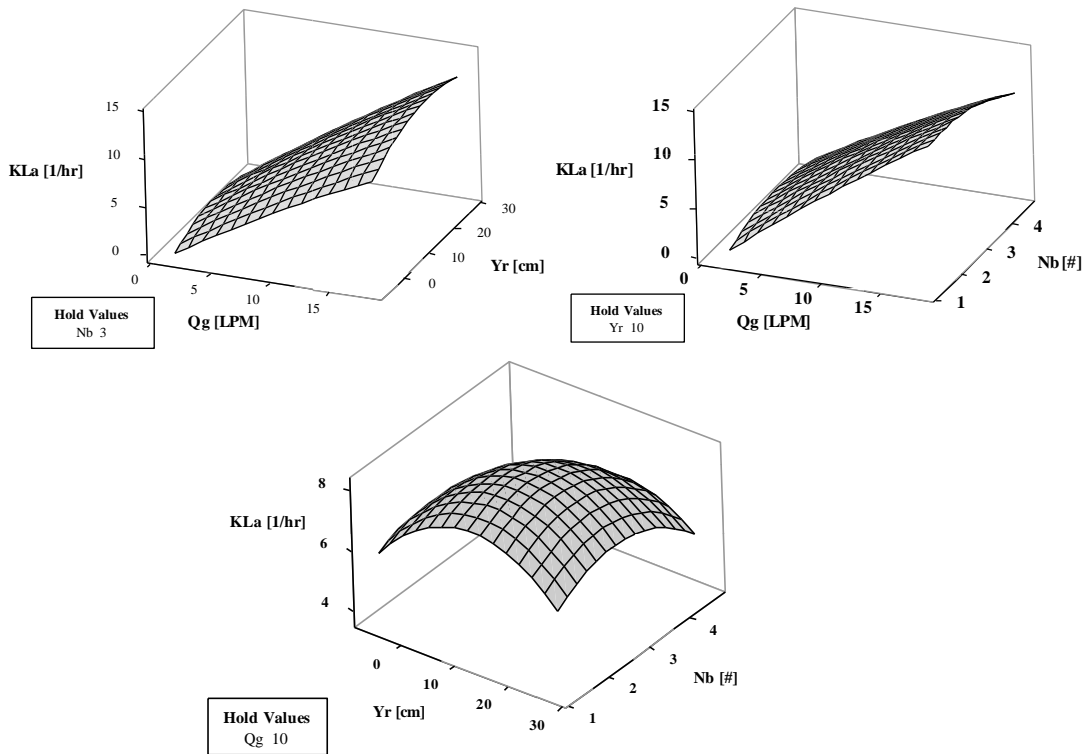


Figure 4.14. Surface plot of two factors a time for first factor optimization

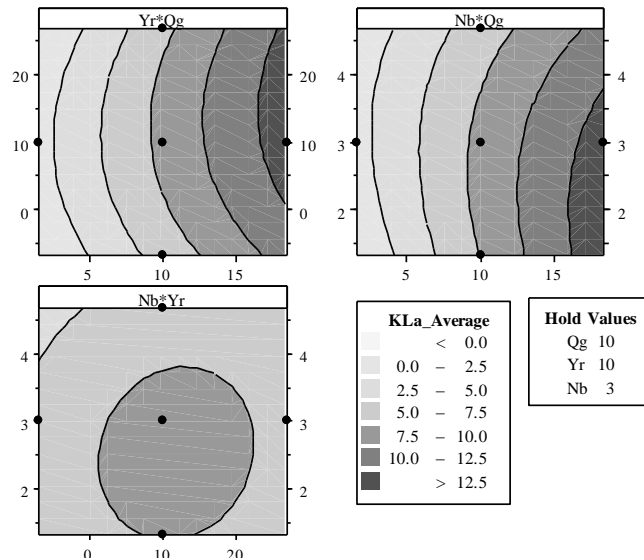


Figure 4.15. Contour plot of two factors a time for first factor optimization

▪ **Summary result of first factor optimization**

From the experimental and analysis results, the optimum level of the main factors including position of recirculation area (Y_r), and amount of baffle (N_b) are 10 cm and 3 horizontal baffles. However, gas flow rate cannot be found the optimum level due to it provided better response after increasing its levels. Moreover, better factor value (the level that provide highest K_La coefficient) of the other significant factors will be used for the novel reactor design criteria such as settling area on baffle ($A_s \sim 90 \text{ cm}^2$), baffle angle ($\alpha \sim 50^\circ$), baffle length ($L_b \sim 17 \text{ cm}$), amount of diffuser ($N_d \sim 4$ diffusers), and bottom recirculation area ($A_r \sim 450 \text{ cm}^2$).

4.1.3 Reactor Development Stage II

- Factor Screening

The section, reactor development stage II was mentioned as the second part of the reactor development. This second stage was not much described due to most of it were already mentioned in the first stage. The 2^{k-1} design, half running of 2^k factorial design was selected for factors screening process. Recirculation area factor is the lowest effected factor (Figure 4.8) and it was already applied the limited levels. For amount of diffuser, it were also applied the limited levels as well and it is response as the simple airlift reactor too. From the simple airlift and this study reactor, it was found that increasing effective surface of gas sparger or diffuser, better result was obtained.

Table 4.9. Variables with factor levels for 2^{k-1} factorial design

Factors	Unit	Factor Levels	
		-	+
Baffle angle (α)	degree	50	130
Baffle length (L_b)	cm	17	20
Amount of baffle (N_b)	#	2	4
Settling area on baffle (A_s)	cm^2	30	90
Position of recirculation area (Y_r)	cm	0	10

Therefore, these two factors was not investigated in this part. The investigated factors and the levels value were shown in *Table 4.9* where (-) and (+) are referred to low level and high level, respectively. This section, 16 experimental conditions were generated by 2-level factorial design with 95% confidence level of a single replication. Experimental conditions were designed by Minitab 17 statistic application. The experimental condition is shown in *Table 4.10*. The experiments were performed based on the designed condition.

The experimental results was shown in *Table 4.10*. The highest and the lowest K_La coefficient was obtained in the Run 1 ($K_La \sim 9.82 \text{ hr}^{-1}$) and the Run 2 ($K_La \sim 5.81 \text{ hr}^{-1}$), respectively. Full experimental result of this factor screening experiments part was attached in the Appendix 7. After complete the reactor development stage I, the factors and its levels were closed to the optimum level. Then the different response value, K_La coefficient between riser and downcomer compartment was minimized. The optimum point is the level that provides best condition for gas and liquid distribution. Therefore, the experimental results between riser and downcomer are slightly different only.

Analysis of variance (ANOVA) was conducted with confidence level of 95% in two-sided interval ($\alpha = 0.05$) by Minitab 17 and the result was shown in *Figure 4.16* for main effects and *Figure 4.17* for two-way interaction effects. Main effects plot is very useful while several types of factor are likely to compare for find out which one are influences the response the most. The connected line of each variable determine whether or not a main effect is present for a variable. If the variable line is horizontal as parallel to the x-axis, there is no main effect present. On the other hand, if the line is not horizontal, there is a main effect present. The greater different in the vertical position of the connected line, the greater the magnitude of the main effect. Comparing the slopes of line, it presents the relative magnitude of the effect. The interaction plots for two-way interactions was constructed for evaluation the line for well understand how interactions affect the response. In this two-way interactions, if the two lines are

parallel, no interaction takes place. Dissimilar, the greater lines depart from being parallel, there is greater interaction strength.

Table 4.10. Experimental design and results for second factor screening

Run	Y_r [cm]	N_b [#]	A_s [cm ²]	α [degree]	L_b [cm]	$K_L a$ [hr ⁻¹]
1	10	2	90	50	20	9.82
2	10	4	30	130	17	5.81
3	10	4	90	50	17	8.80
4	0	2	90	130	20	9.05
5	0	2	90	50	17	8.78
6	10	4	90	130	20	7.12
7	0	4	90	130	17	8.24
8	10	2	30	50	17	8.38
9	0	4	90	50	20	6.82
10	10	2	30	130	20	8.55
11	0	4	30	130	20	7.41
12	0	4	30	50	17	7.17
13	10	4	30	50	20	7.51
14	0	2	30	130	17	6.55
15	10	2	90	130	17	8.65
16	0	2	30	50	20	8.60

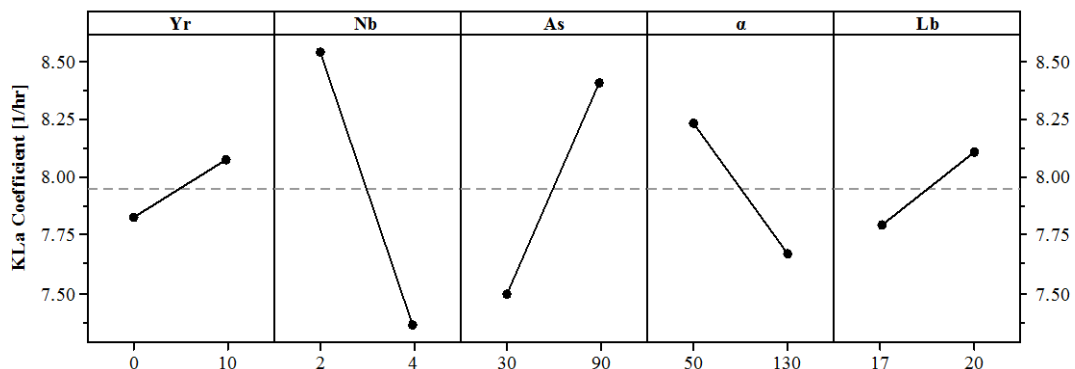


Figure 4.16. Main effective plot for 2nd factors screening

From Figure 4.16, three main effects which are the single significant factors are amount of baffle (N_b), settling area on baffle (A_s), and baffle angle (α). And experimental results of Figure 4.17, all most of the interaction plots in two-way are parallel each other. The several interactions were found in very low strength which is representative very low two-way interaction as well.

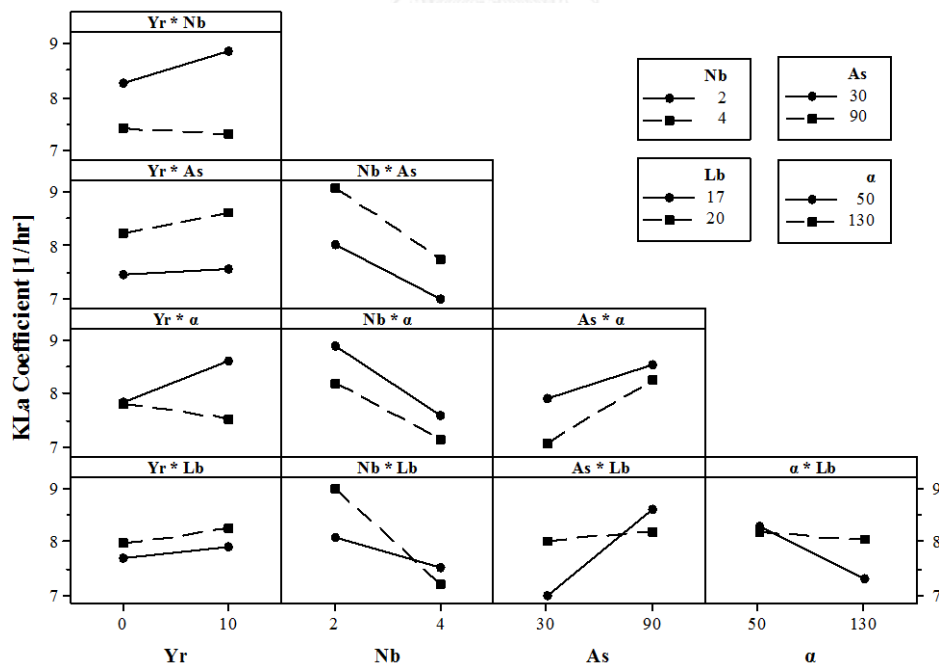


Figure 4.17. Interaction plot for 2nd factors screening

▪ **Summary result of second factor screening**

From the experimental and analysis results, three main factors including amount of baffle (N_b), settling area on baffle (A_s), and baffle angle (α) will be obtained for optimization part. However, less significant factors level that provide the highest $K_L a$ coefficient will be used its level in optimization part such as such as position of recirculation area ($Y_r \sim 10$ cm), and baffle length ($L_b \sim 20$ cm).

- **Factor Optimization**

The three main factors from the screening process were used in this section. Because of the limitation of the experiment in optimization part (CCD-RSD) and settling area on the baffle factor will affect the precipitated particle as settling process, it was excluded from the optimization section and instead by the gas flow rate variable. Therefore three main factor for studying in this factor optimization are Y_r , N_b , and Q_g . The factor levels for this section was used 3-level factor, the code designs are -1, 0, +1 as shown in Table 4.11.

After input the investigated factors and its level for central composite full factorial design, the experimental conditions were generated with double replications. In this work, the first factors optimization was conducted with single replicate due to it is not the final optimization. But it was double replications for the second or final factors optimization part.

Table 4.11. Variables with factor levels for CCD-RSD

Main factors	Unit	Factor Levels		
		-1	0	+1
Gas flow rate (Q_g)	LPM	5	10	15
Baffle angle (α)	degree	30	50	70
Amount of Baffle (N_b)	#	2	3	4

The conditional design of the experiment was shown in Table 4.12 with 40 experiments. From the experimental condition design of Table 4.12, there are the margin experiments which are generated by the software requirement for the design boundary. The experiments were performed base on the designed condition. Average K_La coefficient which was obtained from riser and downcomer compartment are the response variable in this study. The experimental results were shown with experimental condition design in Table 4.12. The highest and the lowest K_La coefficient was obtained in the respective Run 19 ($K_La \sim 10.80 \text{ hr}^{-1}$) and the Run 36 ($K_La \sim 1.59 \text{ hr}^{-1}$), where are the maximum and minimum gas flow rate provided.

Full experimental result of this factor optimization part was attached in Appendix 8. K_La coefficient that was examined from the riser and downcomer is shown in Figure 4.18. The results were analyzed by statistics analysis with a confidence level of 95%. Before start the analysis, model adequacy checking was applied to the results in order to check and verify the data quality (Gomez *et al.*, 2014; Montgomery, 2008). The model adequacy checking including residual plots for K_La coefficient of normal probability plot, versus fits, and versus order were examined by Minitab 17 and the results is shown in Figure 4.19. Base on the residual plots (Figure 4.19), these data can be concluded as an accurate and reliable data for analyzing due to the histograms showed the look as bell shape, the normal probability plot roughly followed a straight line, the versus fits scatted randomly about zero, and versus order fluctuate in a random pattern around the center line (Minitab, 2000; Yotto, 2015).

Table 4.12. Experimental condition designed by CCD for 1st factors optimization

Run	Qg [LPM]	α [°]	N _b [#]	K _L a [hr ⁻¹]	Run	Qg [LPM]	α [°]	N _b [#]	K _L a [hr ⁻¹]
1	10	50	3	6.67	21	10	50	3	6.99
2	5	70	4	2.38	22	5	70	4	2.14
3	10	50	1	4.23	23	5	30	4	3.48
4	10	16	3	5.13	24	15	70	4	8.54
5	10	16	3	5.13	25	15	30	4	9.07
6	10	50	3	6.41	26	10	50	3	6.28
7	15	30	4	9.73	27	15	30	2	8.94
8	10	50	3	6.41	28	5	30	2	3.27
9	10	50	3	6.15	29	15	30	2	10.34
10	5	30	2	3.05	30	2	50	3	1.65
11	15	70	2	10.34	31	10	50	3	5.98
12	10	50	3	6.13	32	5	70	2	3.72
13	10	50	3	6.23	33	5	30	4	3.34
14	10	50	3	6.32	34	18	50	3	10.78
15	10	50	1	4.63	35	15	70	4	7.56
16	10	50	3	5.95	36	2	50	3	1.59
17	10	50	5	5.02	37	10	50	3	5.99
18	10	50	5	5.13	38	5	70	2	3.36
19	18	50	3	10.80	39	15	70	2	9.41
20	10	84	3	5.72	40	10	84	3	5.17

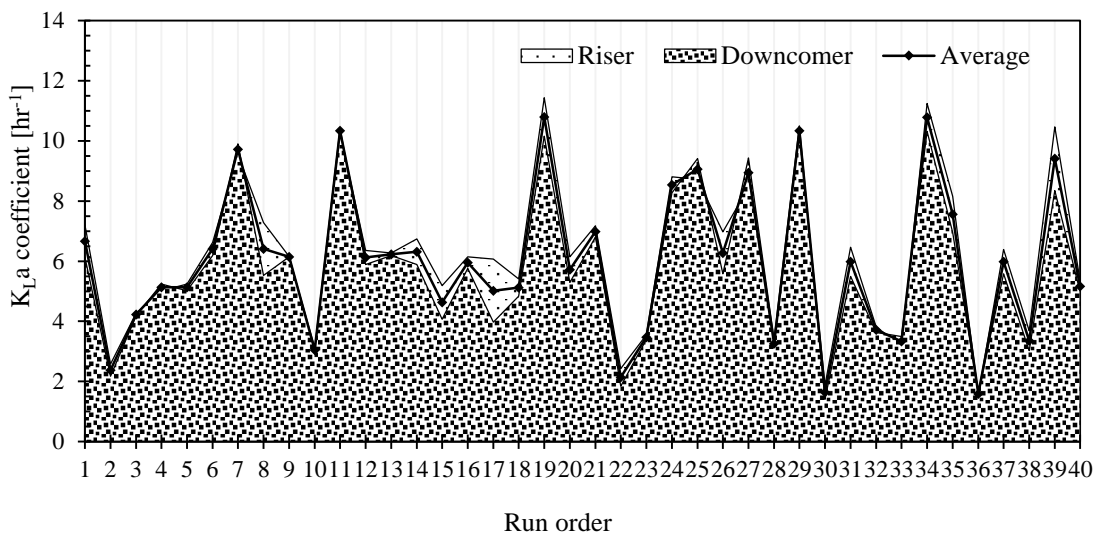


Figure 4.18. Experimental results, K_{La} coefficient of second factors optimization

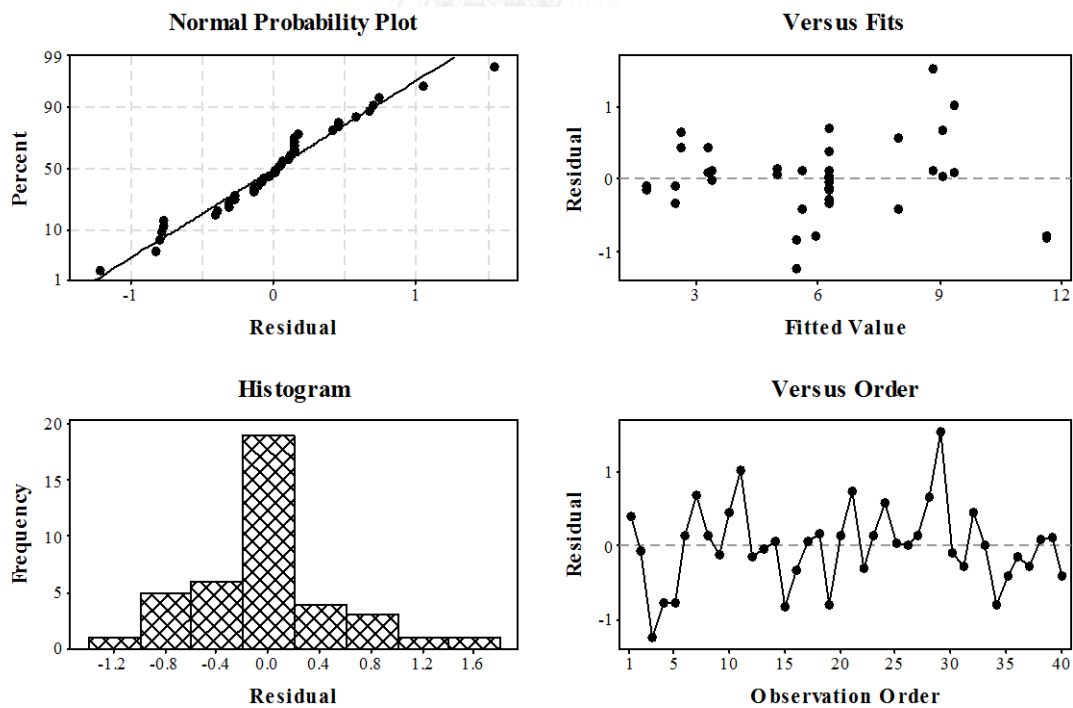


Figure 4.19. Residual plot for model adequacy checking of experimental results

Table 4.13. Experimental result statistical analysis of second factor optimization

Analysis of Variance					
Source	DF	Adj SS	Adj MS	F-Value	P-Value
Model	9	243.777	27.086	71.6	0
Linear	3	235.322	78.441	207.35	0
Qg	1	234.456	234.456	619.75	0
α	1	0.269	0.269	0.71	0.406
Nb	1	0.597	0.597	1.58	0.219
Square	3	5.725	1.908	5.04	0.006
Qg ²	1	0.556	0.556	1.47	0.235
α^2	1	0.987	0.987	2.61	0.117
Nb ²	1	4.035	4.035	10.67	0.003
2-Way Interaction	3	2.73	0.91	2.41	0.087
Qg* α	1	0.032	0.032	0.08	0.775
Qg*Nb	1	0.273	0.273	0.72	0.402
α *Nb	1	2.426	2.426	6.41	0.017
Error	30	11.349	0.378		
Lack-of-Fit	5	7.863	1.573	11.28	0
Pure Error	25	3.487	0.139		
Total	39	255.126			
Model Summary					
S	R-sq	R-sq(adj)	R-sq(pred)		
0.615066	95.55%	94.22%	90.76%		
Coded Coefficients					
Term	Effect	Coef	SE Coef	T-Value	P-Value
Constant		6.264	0.177	35.31	0
Qg	5.86	2.93	0.118	24.89	0
α	-0.198	-0.099	0.118	-0.84	0.406
Nb	-0.296	-0.148	0.118	-1.26	0.219
Qg ²	0.278	0.139	0.115	1.21	0.235
α^2	-0.37	-0.185	0.115	-1.62	0.117
Nb ²	-0.748	-0.374	0.115	-3.27	0.003
Qg* α	-0.089	-0.044	0.154	-0.29	0.775
Qg*Nb	-0.261	-0.131	0.154	-0.85	0.402
α *Nb	-0.779	-0.389	0.154	-2.53	0.017

Analysis of variance (ANOVA) was conducted with confidence level of 95% in two-sided interval ($\alpha = 0.05$) by Minitab 17. The experimental result statistical analysis of this section is presented in the Table 4.13, which included three different items: analysis of variance, model summary, and coded coefficient. As aforesaid, P-value is used to determine in the model for the statistically significant. Before take a look on the individual effects in the coded coefficients table, the P-values for F-test in analysis of variance table should be firstly observed. After the significant set of effects including linear or interaction effects were identified, check the coefficients table for individual effects evaluation. Using P-value, if it is less than or equal to α (in this study, $\alpha \sim 0.05$), it can conclude that the effect is significant. In opposite, if it is greater than α ($P > 0.05$), the effect is not significant. S, R, adjusted R, and predicted R are used for examination the level of the model fits the data. Its values were used for selection the best fit model.

From Table 4.13, the value of the linear effect provides high F-test value (207.35), followed by the square effect (5.04), and the poorest one is two-way interaction effect (2.41). Comparing these main effect factor, gas flow rate variable is the highest significant effect and the lowest significant effect is the baffle angle. The main effects plot and interaction plot is shown in Figure 4.20 and Figure 4.21, respectively.

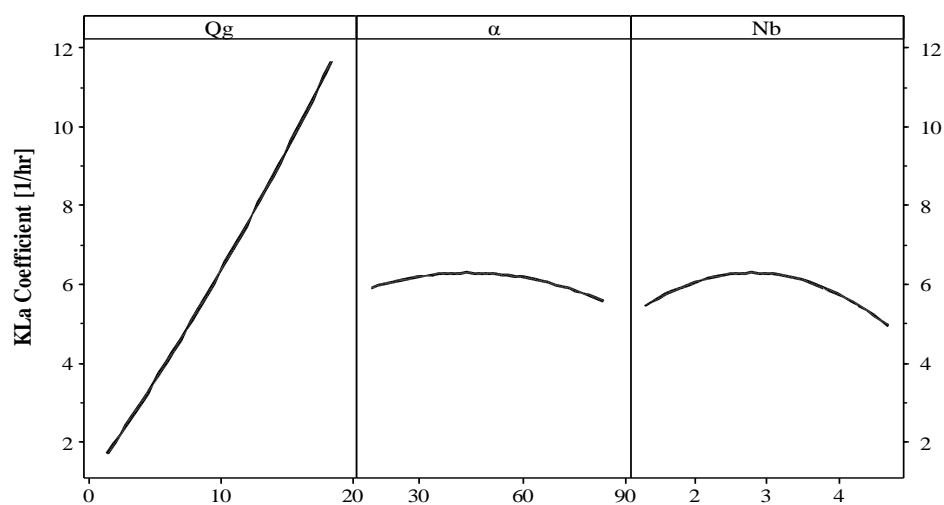


Figure 4.20. Main effects plot of the fitted mean value of K_La coefficient

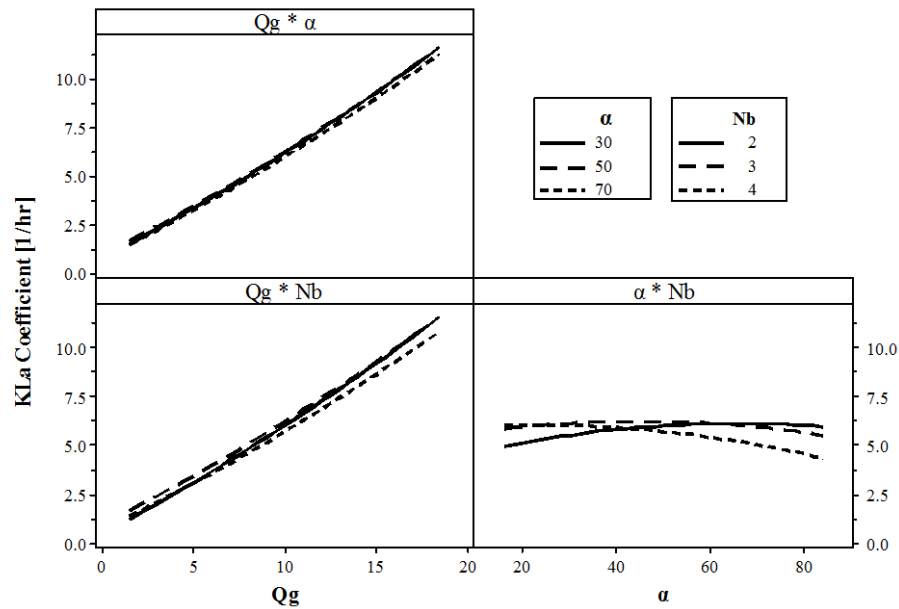


Figure 4.21. Interaction effects plot of the fitted mean value of K_{La} coefficient

From the Figure 4.20 and Figure 4.21, the air flow rate always increases parallel along the response, K_{La} coefficient which is different from other two factors. The optimum level of baffle angle (α) value that can provide a best K_{La} coefficient value was found at 50 degree. Optimum baffle quantity, there are still 3 baffles that can improve the oxygen transfer in this reactor type.

The interaction plot is not different from the single effect, followed as the statistical analysis (Table 4.13). It shows that the interaction effects do not provide significant effect (P-value). For better understanding the factor optimization level, Minitab 17 provided the surface and contour plot of two interaction effect a time (other one variable was held its value) as shown in Figure 4.22 and Figure 4.23. Not different from the interaction plot, the factors that were plotted with gas flow rate (Qg), the optimum point cannot be found due to the response value (K_{La} coefficient) is increasing parallel along the gas flow rate. Other more, gas flow rate factor is the most effective variable for diffused aeration system and it is for sure during increasing gas flow rate, mean increasing amount of the gas in the system.

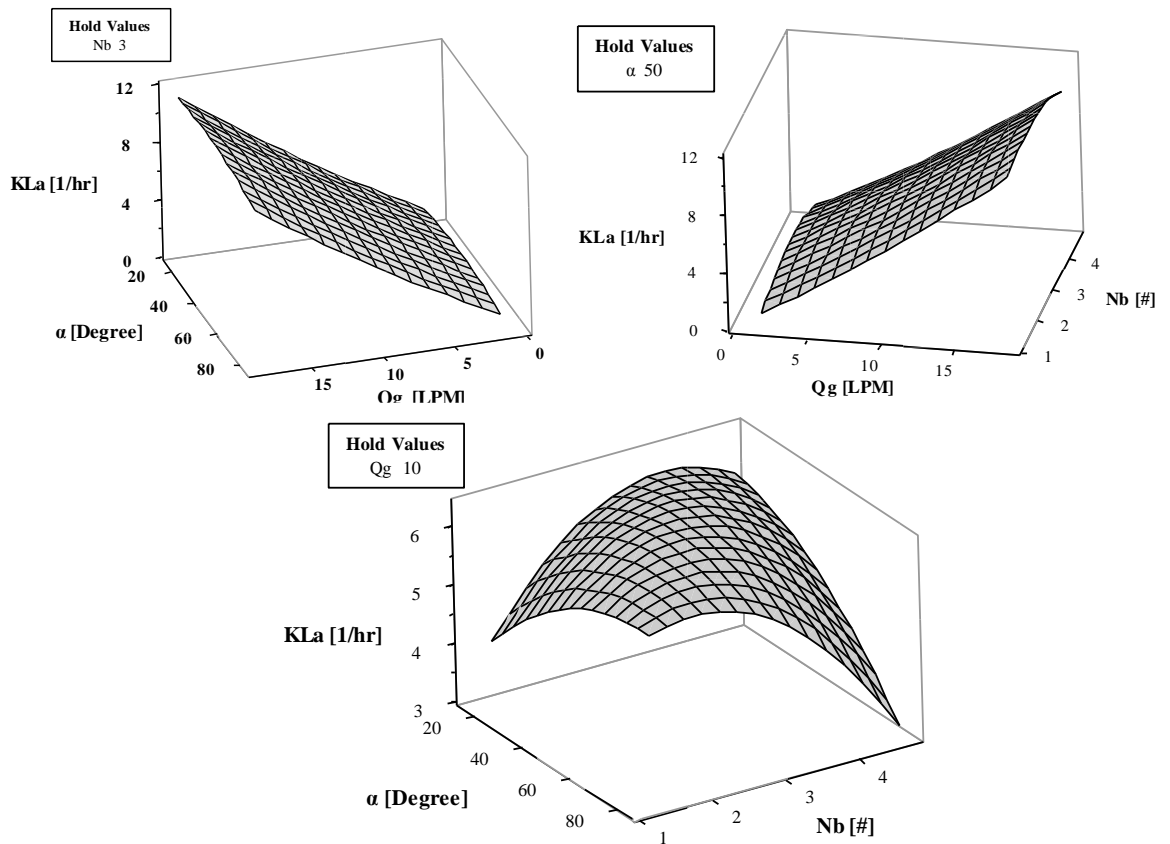


Figure 4.22. Surface plot of two factors a time for second factor optimization

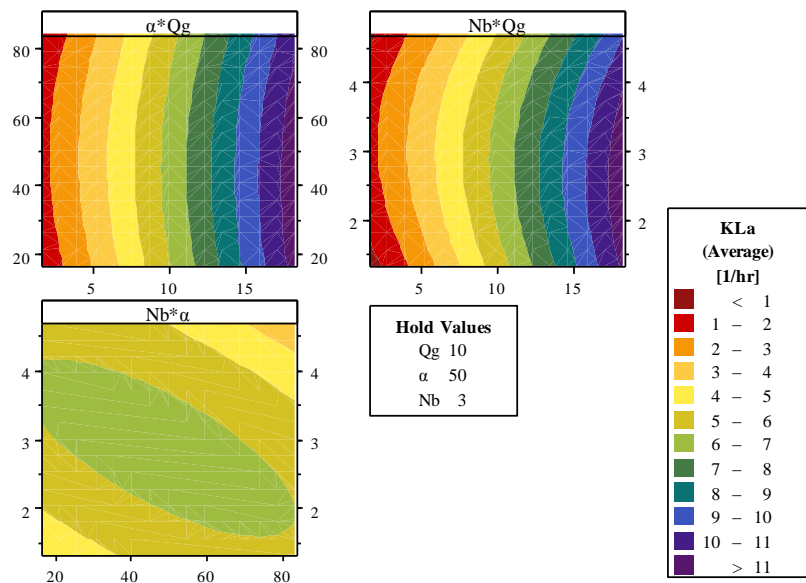


Figure 4.23. Contour plot of two factors a time for second factor optimization

▪ **Summary result of second factor optimization**

From the experimental and analysis results, the optimum level of the main factors including amount of baffle (N_b), and baffle angle (α) are 3 horizontal baffles and 50 degree, respectively. However, the optimum level of the gas flow rate cannot be identified due to it is provide better response after increasing its levels. Moreover, better factor level value that provide highest K_La coefficient of the other significant factors will be used for the novel reactor design criteria such as settling area on baffle ($A_s \sim 90 \text{ cm}^2$), position of recirculation area ($Y_r \sim 10 \text{ cm}$), and baffle length ($L_b \sim 20 \text{ cm}$).

4.1.4 Final Optimization and Prediction Equation

The second optimization is the final optimization of the reactor development stage II (second part) as well as the final optimization of this work. Table 4.14 and Figure 4.24 consist the summary of the optimization levels from stage I and II. This final optimum level is used for the reactor design criteria and operation condition.

Table 4.14. Final optimization for this novel reactor, Novel BCR

Investigated Factors		Factors Optimization Result	
		Stage I	Stage II or Final
	Downcomer-to-riser ratio (A_d/A_r) [-]	0.45	0.45
Main	Amount of baffle (N_b) [#]	3	3
	Settling area on baffle (A_s) [cm^2]	90	90
	Position of recirculation area (Y_r) [cm]	10	10
	Baffle angle (α) [degree]	50	50
Normal	Baffle length (L_b) [cm]	17	20
	Amount of diffuser (N_d) [#]	4	4
	Recirculation area (A_r) [cm^2]	450	450

From these results, amount of baffle (N_b), baffle angle (α), settling area on baffle (A_S), and position of recirculation area (Y_r) are mainly affect while:

- Amount of baffle (N_b) and baffle angle (α) is related to bubble hydrodynamic parameters as well as the bubble retention time and bubble distribution.
- Settling area on baffle (A_S) is related to the minimization of the death zone and improve the liquid movement in the reactor.
- Position of recirculation area (Y_r) is related to liquid recirculation from riser to downcomer. When it is at the optimum level such as at 10 cm from the bottom, it provide the short liquid recirculation stream line compared to 0 cm from the bottom. Therefore, it provides better result.

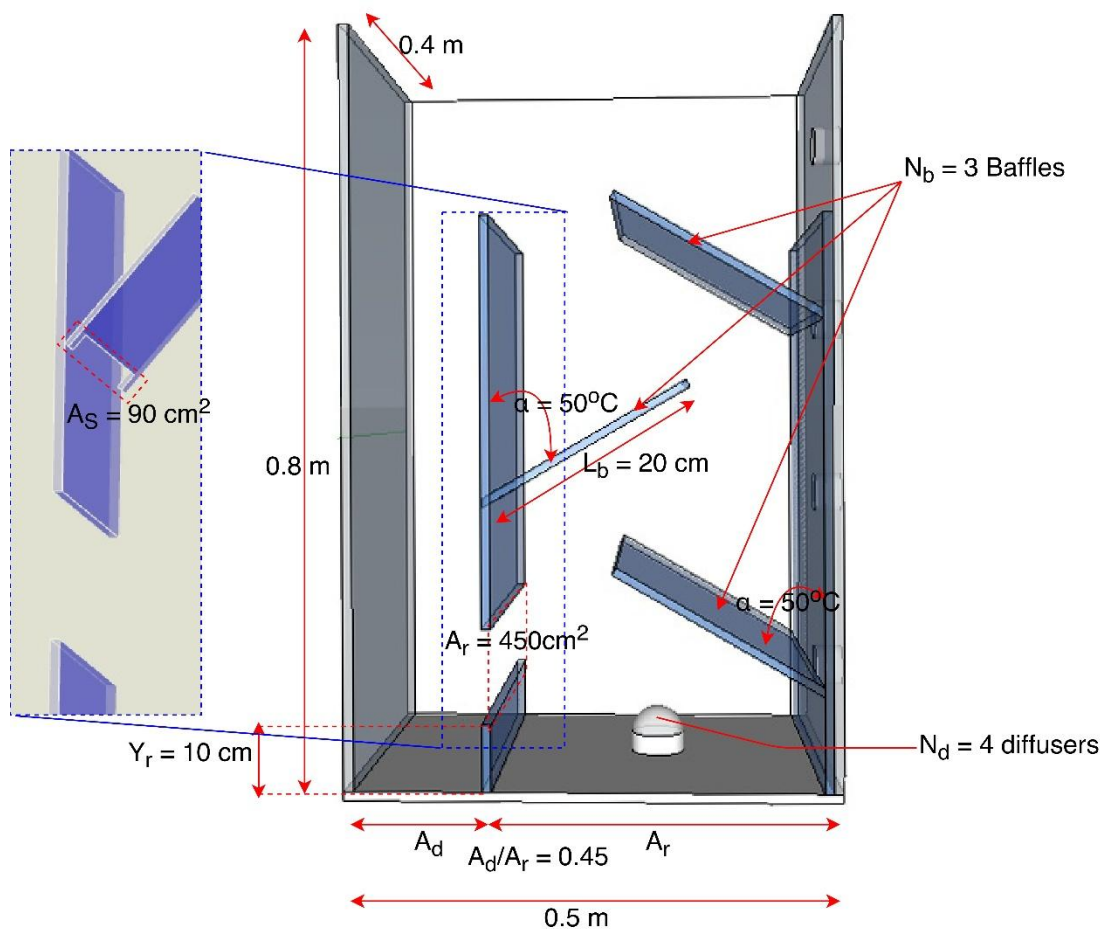


Figure 4.24. Optimum level for all investigated parameters of Novel BCR

$$\begin{aligned}
 K_{La} \text{ Coefficient} = & 0.00556Qg^2 - 0.000463\alpha^2 - 0.374N_b^2 - 0.00044(Qg \times \alpha) \\
 & - 0.0261(Qg \times N_b) - 0.01947(\alpha \times N_b) + 0.575Qg + 0.1041\alpha \\
 & + 3.332N_b - 6.80
 \end{aligned}
 \tag{Eq. 4.1}$$

The prediction regression equation of K_{La} coefficient as a function of main factors: Qg , α , and N_b was constructed in equation 4.1 by full quadratic (square, interaction, linear, and constant) of DOE from Minitab 17. Whereas K_{La} coefficient [hr^{-1}], Qg is the gas flow rate supply to the system [LPM], α is the angle of the modified baffles referred to the vertical line where follow the clockwise for left hand side baffle(s) and opposite for the right hand side baffle(s) in the riser [degree], and N_b is amount of baffles installed in riser compartment. The experimental and prediction equation result was plotted in Figure 4.25 where R square is 0.96 with $\pm 15\%$. Because of the mentioned correlation (equation 4.1) is constructed by full quadratic, then it consists full terms (10 terms where 3 are square terms, 3 are interaction terms, 3 are linear terms, and other one is constant value). However this correlation may over fitting, therefore, it was compared to other correlation as showed in Table 4.15.

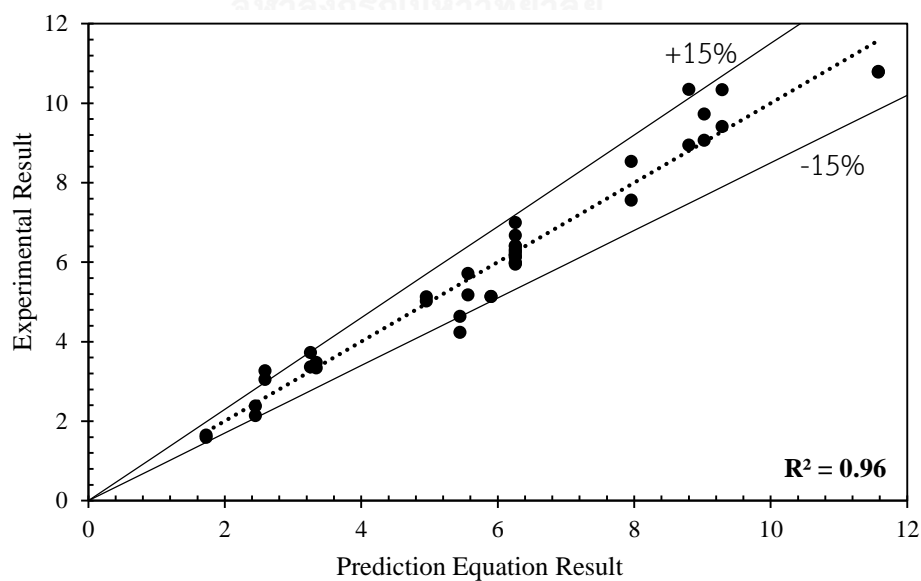


Figure 4.25. Scatter plot between prediction equation and experimental result

Table 4.15. Constructed correlation of K_La coefficient in Novel BCR

N°	Constructed Method	Full Correlation	Regression, R^2
1	Full Quadratic	$K_La = 0.00556Qg^2 - 0.000463\alpha^2 - 0.374N_b^2 - 0.00044(Qg \times \alpha) - 0.0261(Qg \times N_b) - 0.01947(\alpha \times N_b) + 0.575Qg + 0.1041\alpha + 3.332N_b - 6.80$	0.96
2	Deckwer et al.	$K_La = 0.0269 U_G^{0.82}$	0.85
3	Linear (DOE)	$K_La = 0.586Qg - 0.00496\alpha - 0.148N_b + 0.809$	0.92
4	Linear and Interaction (DOE)	$K_La = 0.687Qg + 0.0579\alpha + 1.087N_b - 0.00044(Qg \times \alpha) - 0.0261(Qg \times N_b) - 0.01947(\alpha \times N_b) - 3.12$	0.93
5	Linear and Squares (DOE)	$K_La = 0.00556Qg^2 - 0.000463\alpha^2 - 0.374N_b^2 - 0.475Qg + 0.0413\alpha + 2.097N_b - 2.87$	0.94
6	Reduce term(s) by trial-and-error from full quadratic (N° 1)	$K_La = -0.000463\alpha^2 - 0.374N_b^2 - 0.01947(\alpha \times N_b) + 0.575Qg + 0.1041\alpha + 3.332N_b - 6.80$	0.93
7	Derive coefficient of correlation N° 6 by DOE	$K_La = -0.000497\alpha^2 - 0.388N_b^2 - 0.01947(\alpha \times N_b) + 0.586Qg + 0.1032\alpha + 3.153N_b - 6.45$	0.95

The correlation N° 1 is the full quadratic as shown in equation 4.1. The correlation N° 2 was constructed by the exited work (W-D Deckwer *et al.*, 1974). Correlation N° 3, 4, and 5 were generated only linear, linear and interaction, and linear and squares function by DOE, respectively. N° 6 was tried to reduce the term(s) from the full correlation (N° 1) by using tried-all-and error method. However, the coefficient of the correlation N° 6 was changed due to the modified terms. Therefore, the coefficient of the terms was derived by using DOE. Finally, the most appropriate correlation that

provide less terms compared to the full correlation is the correlation N° 7 with fitted regression, R^2 equal 0.95. In conclusion, correlation N° 7 can be used for less terms (compared to full correlation) with most accuracy.

The full correlation (equation 4.1) was checked the sensitivity analysis to understand the limitation of this model. It was analyzed by one-at-a-time (OAT) technique in ranges of -30% to +30% of the input factors. The three input factors studied are gas flow rate (Q_g), baffle angle (α), and amount of baffles (N_b) in terms of the output change (%) from predicted model or correlation. The results from the change of the input ($\pm 30\%$) and the effect on output (%) are shown in Figure 4.26, Figure 4.27, and Figure 4.28. From these figures, it can be concluded that gas flow rate (Q_g) is the most sensitive parameter in the constructed model while other two parameters, baffle angle (α) and amount of baffles (N_b) are less sensitive parameters to the model output. From the Figure 4.26 of the input change factor is gas flow rate (Q_g), the input change in percent is almost the same as the output change in percent while other two input change factors (α , and N_b) are less output change compared to the input change in percent as shown Figure 4.27 and Figure 4.28.

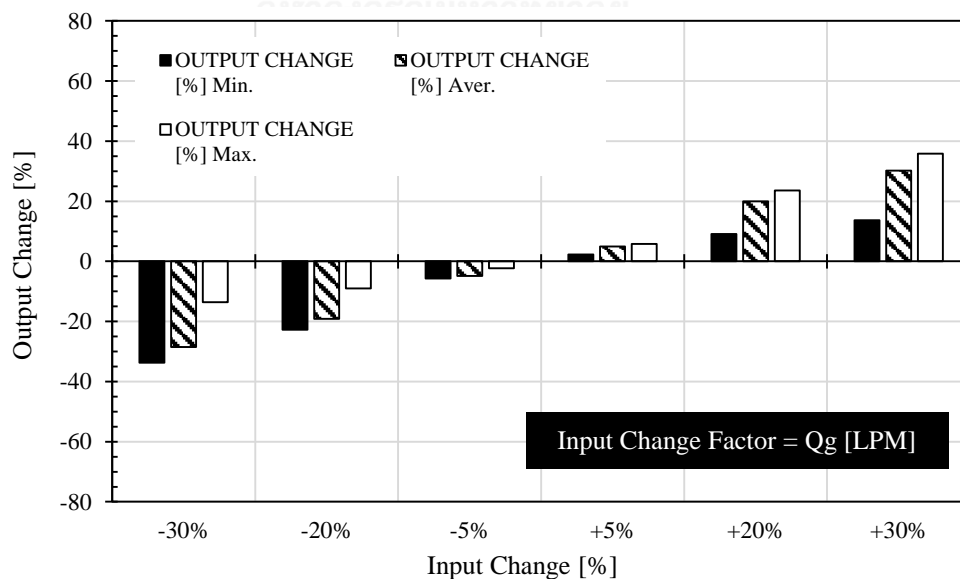


Figure 4.26. Output change (%) vs. input change (%) of gas flow rate factor

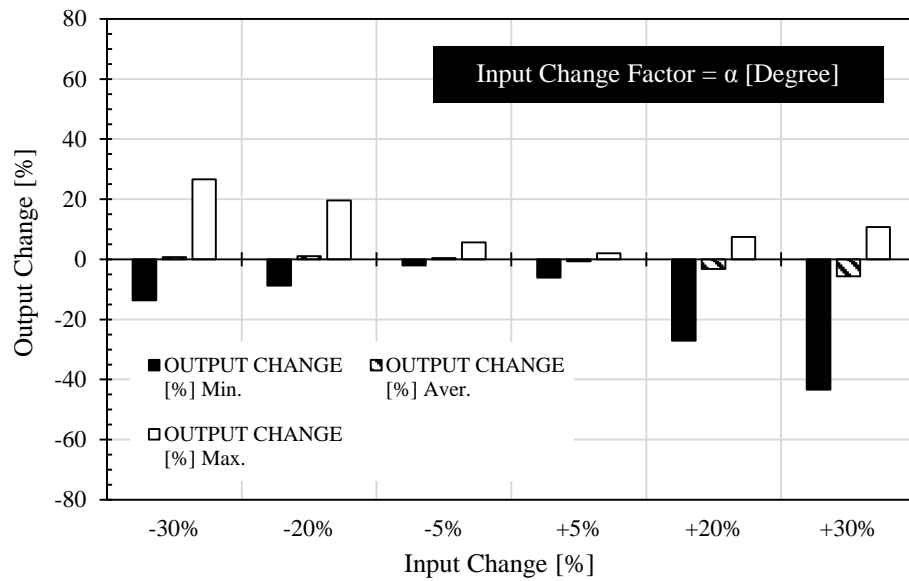


Figure 4.27. Output change (%) vs. input change (%) of baffle angle factor

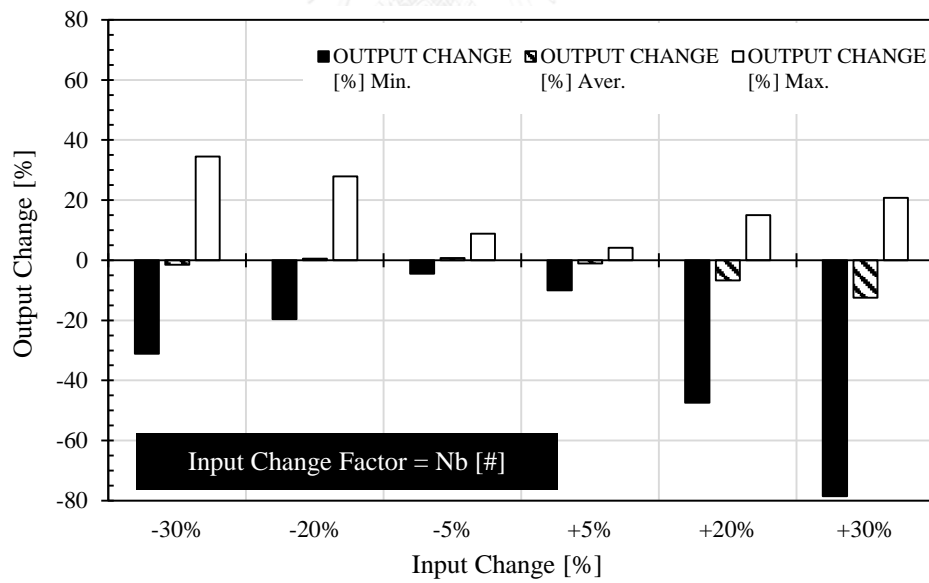


Figure 4.28. Output change (%) vs. input change (%) of amount of baffle factor

4.2 Comparison of Reactor Performance

In this comparison part, three various gas-liquid contactors performance including conventional Bubble Column Reactor (BCR), Airlift Reactor (ALR), and Novel BCR or Modified Airlift Reactor (MALR) as shown in Figure 3.3 were used to compare the reactor performances. Two rigid stone diffusers were used with the gas flow rates ranging from 4 to 16 LPM for this compared section.

The BCR experiment was conducted as a simple reactor without any modification while ALR was applied the vertical baffle plate to create an internal downcomer with 450cm² of the bottom recirculation area. Novel BCR is the novel design of this work with the optimum conditions as described in the final optimization from previous part (Table 4.14).

In this part, the comparison was concentrated in terms of K_La coefficient, oxygen transfer rate (OTR), oxygen transfer efficiency (OTE), aeration efficiency (AE), and power consumption. The experimental results are performed in the temperature operation at 27 ± 2°C and can be converted for a standard condition (20°C) by equation 3.9.

4.2.1 Overall Mass Transfer Coefficient

The response value is the average K_La coefficient, the average between K_La coefficient where were obtained from riser and downcomer compartment. From this results, increasing the gas flow can provide better result of K_La performance. The percentage of the improvement can be determined from the equation 4.2 (Imai *et al.*, 2011). The experimental results and improved values from the calculation is shown in Table 4.16. Their performance results in terms of K_La coefficient for three reactor types were plotted in Figure 4.29.

$$\% \text{ Improvement} = \frac{K_{L}a_{(\text{NovelBCR})} - K_{L}a_{(\text{BCR or ALR})}}{K_{L}a_{(\text{BCR or ALR})}} \times 100 \quad \text{Eq. 4.2}$$

Table 4.16. Experimental results and improvements in terms of K_La coefficient

Qg [LPM]	K_La Coefficient [hr^{-1}]			Novel BCR Improvement [%] compared to	
	BCR	ALR	Novel BCR	BCR	ALR
4	1.38	2.11	2.71	97.09	28.44
6	2.11	3.09	3.71	75.59	19.90
8	3.18	4.04	5.16	62.11	27.60
10	4.29	5.13	6.43	49.77	25.24
12	4.74	6.66	7.35	55.23	10.36
14	5.49	7.58	8.64	57.29	13.99
16	6.06	9.06	9.60	58.42	6.02

Concerning to the improvement performance, Novel BCR can be improved its performance in terms of K_La coefficient from 50 to 97% compared to BCR and 6 to 28% compared to ALR at the gas flow rates range from 4 to 16 LPM as shown in Table 4.16 and Figure 4.29. The percent of improvement is higher at the lower gas flow rate due to the better bubble distribution at lower compared to the higher gas flow rate and limitation of the oxygen transfer after it is close to the saturation level of the oxygen in water. Gas flow rate is the significant factor as higher K_La coefficient can be obtained after increasing its values. It is not only in Novel BCR, in conventional BCR or ALR as well. From this result, it was concluded that this new design reactor can improve oxygen transfer performance very well for aeration process without any extra energy.

From this improvement, it can be concluded that installing the horizontal baffles in the riser significantly enhanced the volumetric mass transfer coefficient and it is expected that it is significantly enhance the gas holdup as well. Because based on the review the existed works related to reactor development (Krichnavaruk *et al.*, 2002; Luo *et al.*, 2013; Zhao *et al.*, 1994), they tried to development the airlift reactor for improving the performance by installing the sieve plate or perforate plate in the riser of reactor. All of the developed reactors provide better performance comparing to the

conventional bubble column with different percentage improvements in terms of $K_{L,a}$ coefficient.

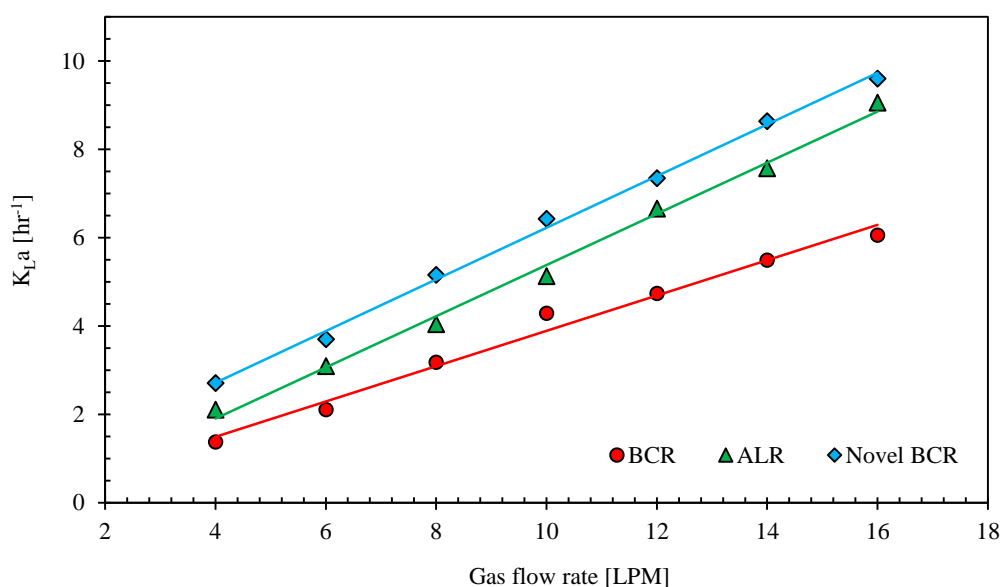


Figure 4.29. Comparison of three various gas-liquid contactors (BCR, ALR, Novel BCR) in terms of $K_{L,a}$ coefficient

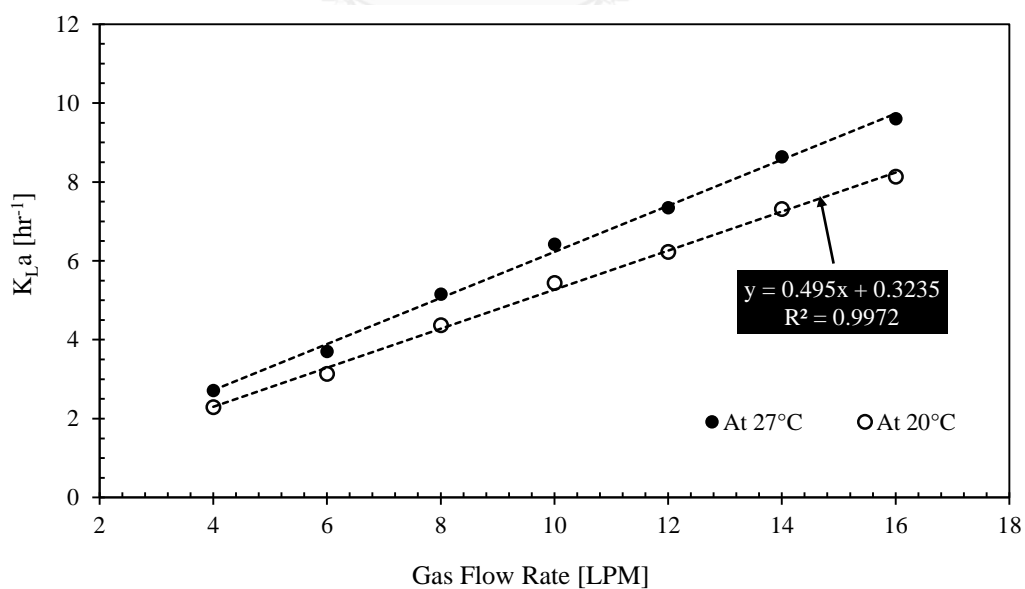


Figure 4.30. The $K_{L,a}$ coefficient conversation from 27°C to a standard temperature (20°C) of Novel BCR performance

To study the oxygen transfer rate at a standard condition, the K_La coefficient need to be converted from normal temperature to a standard temperature (20°C) by using equation 3.9. The K_La value obtained in Novel BCR at standard temperature was plotted in Figure 4.30. K_La value is decreasing due to the different temperature, 7°C. The treaded linear line of the standard K_La coefficient can be expressed in normal function of gas flow rate (Q_g) as written in equation 4.3. The treat line equation was implemented in function of gas flow rate and comparing with the experimental results as shown in Figure 4.31. The R square can be obtained up to 0.997.

$$K_La \text{ [hr}^{-1}\text{]} = 0.495 Q_g + 0.3235 \quad \text{Eq. 4.3}$$

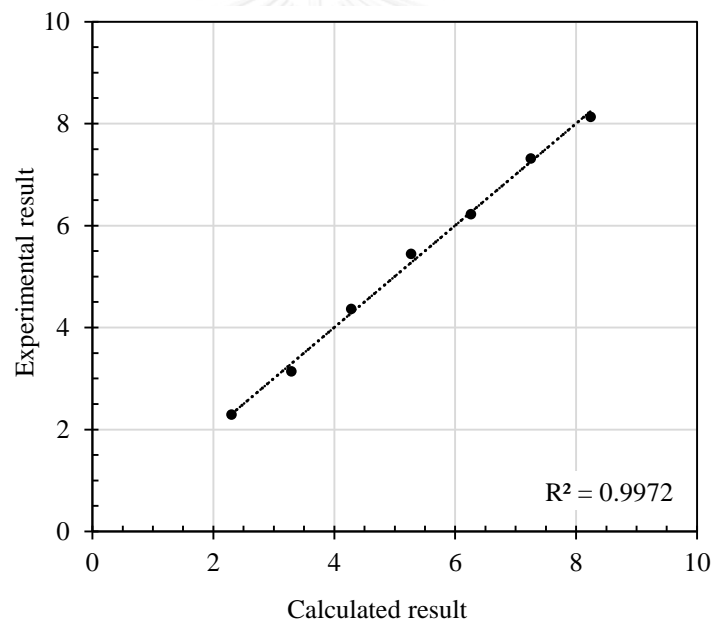


Figure 4.31. Experimental result vs. calculated result in terms of K_La coefficient

4.2.2 Oxygen Transfer Rate

The standard oxygen transfer rate (SOTR) is referred to the mass amount of oxygen that can be transferred to the liquid phase in a unit of time and it can be determined in terms of K_La coefficient, dissolved oxygen concentration at saturation level, and volume of liquid phase as equation 3.6. Therefore, the result behavior of SOTR is not different from overall mass transfer coefficient as shown in Figure 4.32.

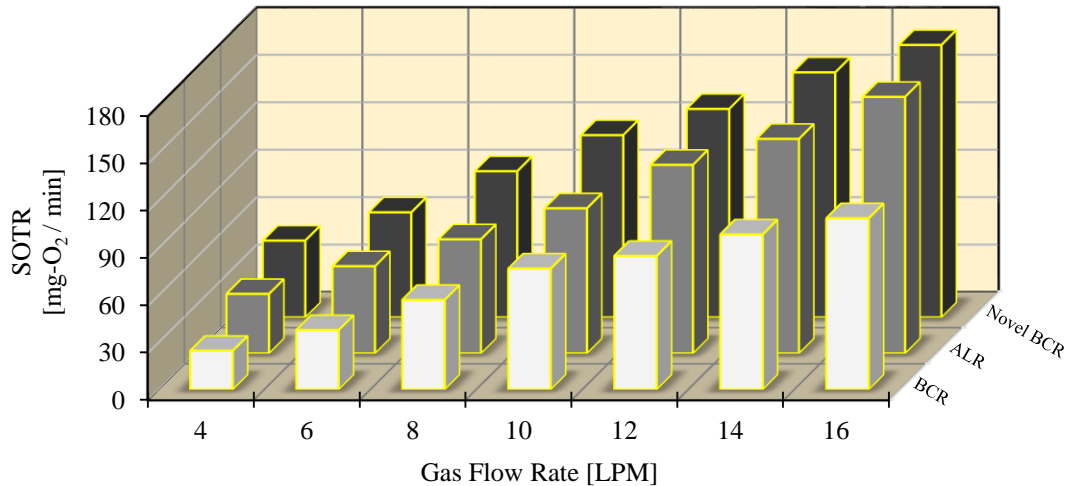


Figure 4.32. The SOTR vs. gas flow rate in BCR, ALR, and Novel BCR

The SOTR in BCR is ranged from about 25 to 109 mg-O₂/min while the Novel BCR can transfer the oxygen up to 49 to 172 mg-O₂/min for the ranged gas flow rate of 4 to 16 LPM. In this term, the Novel BCR performance can provide better SOTR about 24 to 64 mg-O₂/min compared to BCR and 11 to 10 mg-O₂/min compared to ALR in the studied ranges of gas flow rate. For example, if 10 LPM of gas flow rate was supplied to the system, there is only 77 mg of oxygen was transferred to the water in 1 minute for BCR operation. But if ALR was used for the sample gas flow rate (10 LPM), there is 92 mg of oxygen was transferred in 1 minute to the water. Moreover if it is in the Novel BCR operation, there is up to 115 mg of oxygen was transferred in 1 minute to the water. Then 38 mg of oxygen was more transferred for every minute by using Novel BCR instead of conventional BCR.

4.2.3 Oxygen Transfer Efficiency

The standard oxygen transfer efficiency (SOTE) is referred to the ratio between effective oxygen and supplied oxygen. The effective oxygen is the oxygen that was transferred to the liquid phase and it is oxygen transfer rate (OTR). Moreover, the supplied oxygen is the oxygen that was supplied from the air pump to the system through air sparger and it can be determined from the gas flow rate as shown in equation 3.7.

The result of this work, the standard oxygen transfer efficiency (SOTE) was plotted in Figure 4.33. SOTE are almost presented as the straight line along with the gas flow rate for all reactor configurations due to the varied constants of the supplied oxygen and effective oxygen are similar. SOTE are approximate 2.46, 3.40, and 4.03% of respective BCR, ALR, and Novel BCR. However the reactor performance in terms of standard oxygen transfer oxygen is improved during operation in Novel BCR compared to BCR and ALR.

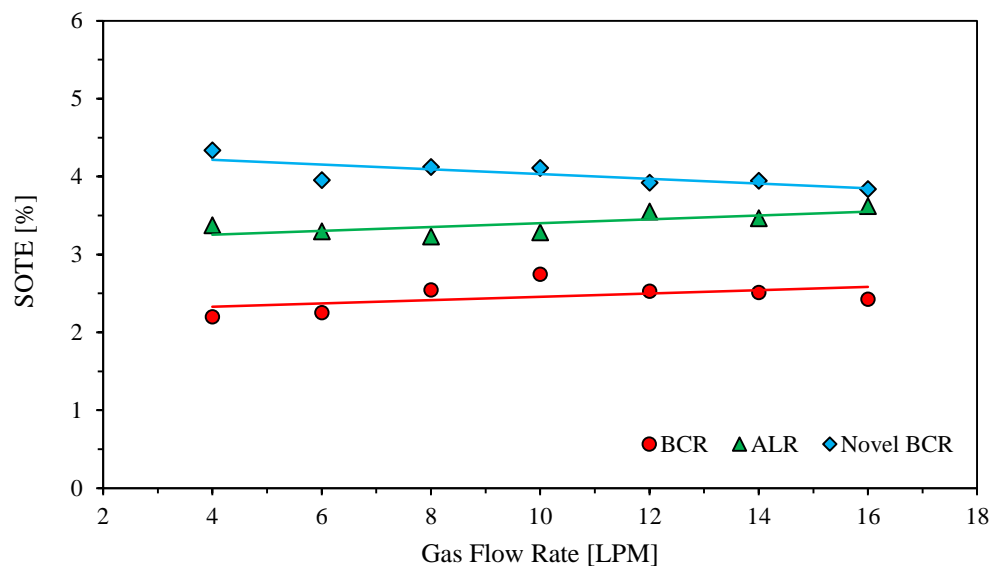


Figure 4.33. The SOTE vs. gas flow rate in BCR, ALR, and Novel BCR

4.2.4 Power Consumption

As mentioned that the reactor performance was compared in terms of power consumption and it can be determine by equation 3.4 where P is a net power consumption which can be determined in terms of gas flow rate and total pressure drop (ΔP). Therefore, the total pressure drop is mainly related with the gas flow rate as presented in Figure 4.34. The pressure drop values are the same for BCR, ALR, and Novel BCR. However it is increasing parallel with the gas flow rate ranging from 2.5 to 14.2 kPa at 4 to 16 LPM, respectively.

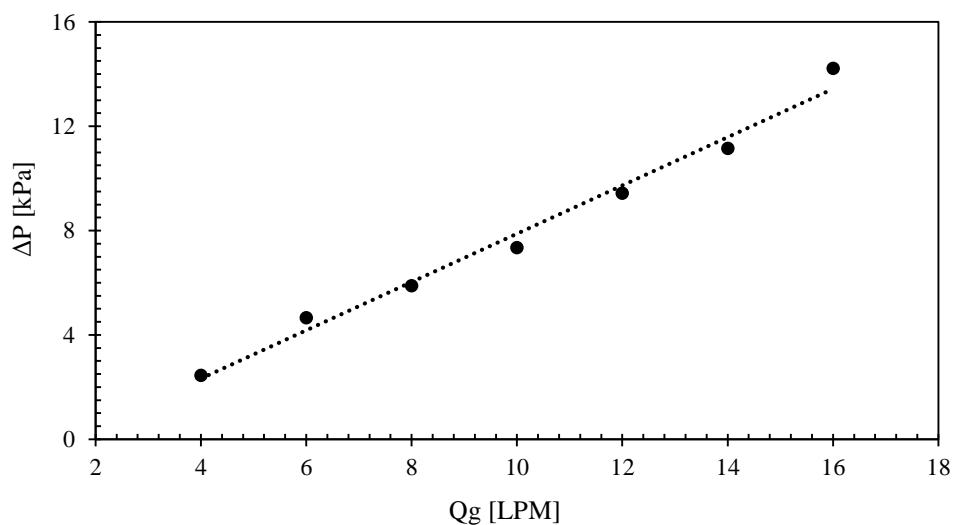


Figure 4.34. The pressure drop vs. gas flow rate

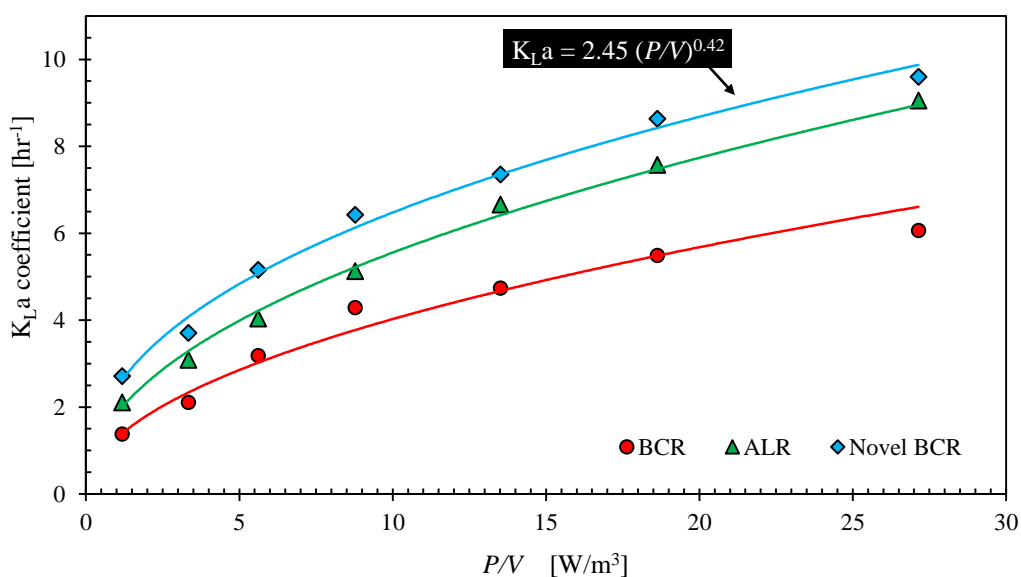


Figure 4.35. Unit volume power consumption (P/V) vs. $K_{L,a}$ in different reactors

The power consumption in terms of the unit volume power consumption (P/V) was plotted as a function of $K_{L,a}$ coefficient as shown in Figure 4.35. From this result, higher $K_{L,a}$ coefficient required high power consumption per unit of volume due to it was corresponding to amount of gas flow rate. Moreover, the correlation between unit volume power consumption and $K_{L,a}$ coefficient of Novel BCR was investigated and the

slope in logarithmic graph was 0.42. It means that $K_L a$ coefficient increase in power law relationship with P/V by $K_L a \sim 2.45(P/V)^{0.42}$.

Base on the result, if the same power was provided to all reactors, better oxygen transfer in terms of $K_L a$ coefficient was obtained from Novel BCR. For example, if 5.5 hr^{-1} of $K_L a$ coefficient was preferred, there is 18.5 W for 1 m^3 of water was required in BCR operation. But if Novel BCR was operated, it requires only 7.0 W.

4.2.5 Aeration Efficiency

Aeration efficiency in this study is referred to the ratio of the effective oxygen (STOR) compared to the power consumption used in the system. The result was plotted with gas flow rate as shown in Figure 4.36.

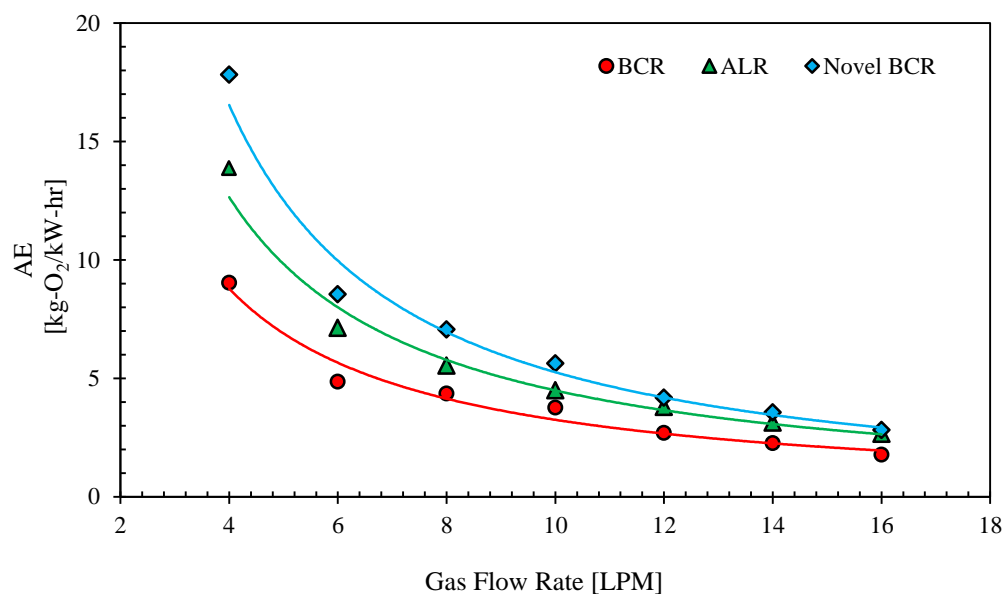


Figure 4.36. Aeration efficiency (at 20°C) vs. gas flow rate in BCR, ALR, and Novel BCR

The aeration efficiency of all reactors decreased along the gas flow rate in trend line of power with similar of slope, about 1.17 ± 0.08 . It should be noticed that AE in the operation with Novel BCR are the highest values compared to ALR and BCR. The highest AE of all reactors were obtained at the lowest gas flow rate and decreasing lower and

lower after increasing the gas flow rate. In novel reactor, the AE is decreasing from 17.82 kg-O₂/kW-hr at 4 LPM until 2.82 kg-O₂/kW-hr at 16 LPM in power form.

4.2.6 Summary Reactor Performance

Base one the experimental results and calculated results of this comparison part, it can be concluded that the novel reactor (Novel BCR) of this present work can provide better results compared to the conventional bubble column reactor and airlift reactor. The improvement of this reactor performance can be summarized as the following:

- K_La coefficient: Novel BCR can be improved from 50 to 97% compared to BCR and 6 to 28% compared to ALR at the gas flow rates range from 4 to 16 LPM.
- Oxygen Transfer Rate: Novel BCR performance can provide better SOTR, about 24 to 64 mg-O₂/min compared to BCR and 11 to 10 mg-O₂/min compared to ALR in the studied ranges of gas flow rate (4-16 LPM).
- Oxygen Transfer Efficiency: SOTE are approximate 2.46, 3.40, and 4.03% of respective BCR, ALR, and Novel BCR.
- Power Consumption: If the same power was provided to all reactors, better oxygen transfer was obtained from Novel BCR. Correlation between unit volume power consumption and K_La coefficient was examined.
- Aeration Efficiency: AE in the operation with Novel BCR is the highest values compared to ALR and BCR.

4.3 Study Bubble Hydrodynamic Parameters

4.3.1 Bubble Size Distribution

The bubble size distribution was measured at the middle level of the water depth where it was considered as the effective bubble size on the oxygen transfer performance in three various reactors including BCR, ALR, and Novel BCR. It was studied in different gas flow rate, ranged from 4 to 16 LPM. The experiments were conducted with 2 rigid stone diffusers at the center cross sectional area of the riser.

- Bubble Column Reactor

The bubble size distribution of BCR was plotted as histogram in Figure 4.37 where the X axis is the bubble diameter in unit of mm. From this results, the most frequency of the bubble size is around 30 of the total sample size is 100. It can be concluded that the bubble is mixed many sizes including small bubble, medium bubble, and big bubble. For the mean value of the bubble size is ranged from 3.93 to 4.03 mm while the bubble size determined from d_{32} formula (equation 3.10) is ranged from 4.11 to 4.24 mm from the studied ranges of gas flow rate from 4 to 16 LPM. The d_{32} is the average bubble size was used to present the bubble in gas-liquid contactor.

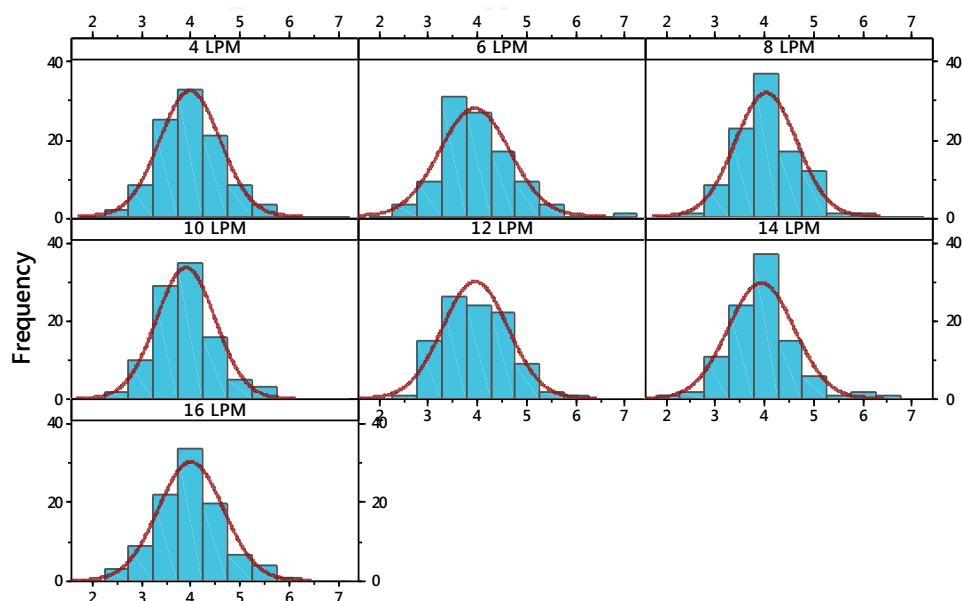


Figure 4.37. Bubble size distribution in BCR with different gas flow rates

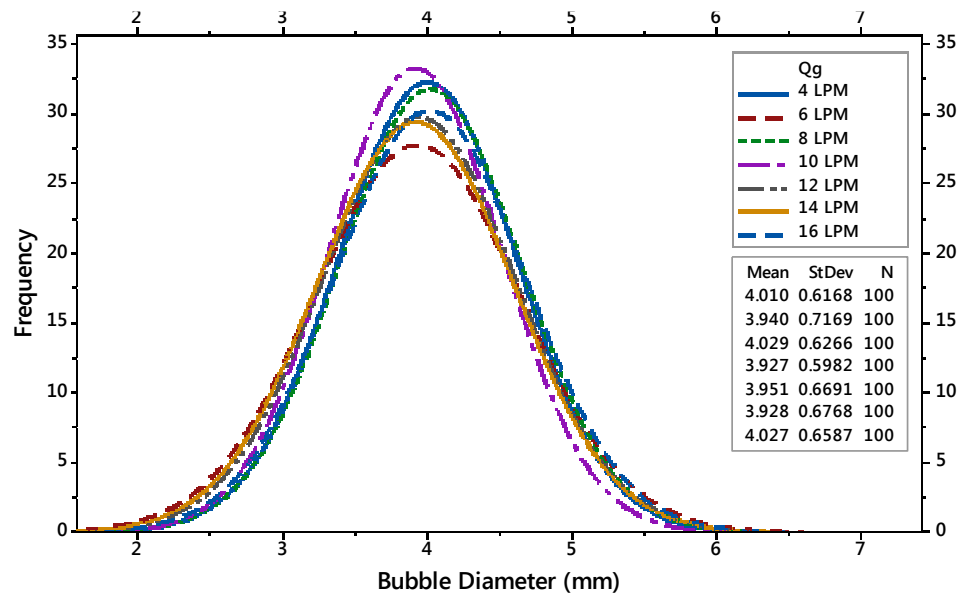


Figure 4.38. All-in-one bubble size distribution in BCR

For this reactor (Novel BCR), the gas flow rate does not significantly effect to the bubble size. Mean bubble size is 3.98 ± 0.05 mm as presented in Figure 4.38. From Figure 4.38, the most frequency of the bubble sizes are presented next to the bubble diameter of 4 mm. However the bubble size determined from d_{32} is 4.18 ± 0.07 mm.

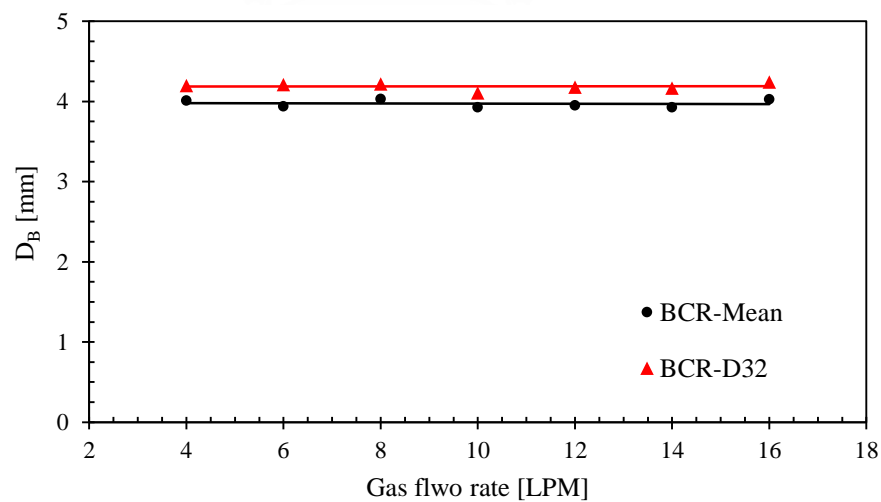


Figure 4.39. Bubble size in BCR from mean value and d_{32} calculation value

The bubble size distribution as the mean value and d_{32} calculation was plotted in Figure 4.39. From this result, the bubble diameter as d_{32} is a little bit higher than mean bubble size. Moreover, bubble size representative by d_{32} is more appropriate for this work case (Kracht *et al.*, 2008).

- Airlift Reactor

The bubble size distribution in conventional airlift reactor was studied the same gas flow rate as in conventional bubble column reactor as well. The result of the experimental was plotted in histogram with fitted line as shown in Figure 4.40 and Figure 4.41 where the X axis presents bubble diameter (mm).

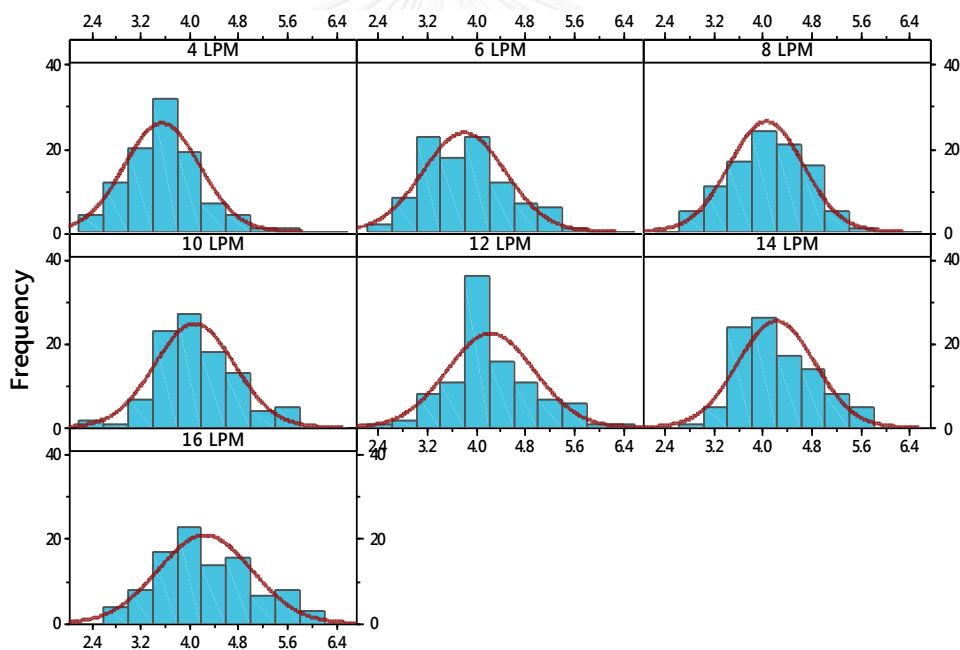


Figure 4.40. Bubble size distribution in ALR with different gas flow rates

From this results, the most frequency of the bubble size is around 20 to 30 of the total sample size is 100. It can be concluded that the bubble is mixed many sized. For the mean value of the bubble size is ranged from 3.57 to 4.27 mm while the bubble size determined from d_{32} formula is ranged from 3.78 to 4.54 mm from the studied ranges of gas flow rate from 4 to 16 LPM.

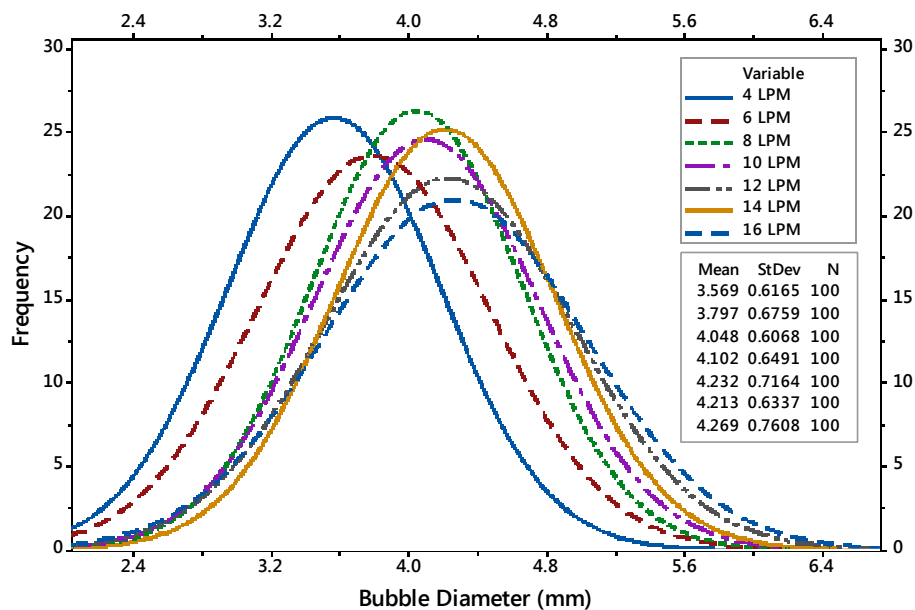


Figure 4.41. All-in-one bubble size distribution in ALR

For this reactor, the gas flow rate is slightly significantly effect to the bubble size. Mean bubble size is 3.92 ± 0.35 mm as presented in Figure 4.41. From Figure 4.41, the most frequency of the bubble sizes are presented randomly along the gas flow rate. However the bubble size determined from d_{32} is 4.16 ± 0.38 mm. The bubble size distribution as the mean value and d_{32} calculation was plotted in Figure 4.42. From this result, the bubble diameter as d_{32} is a little bit higher than mean bubble size.

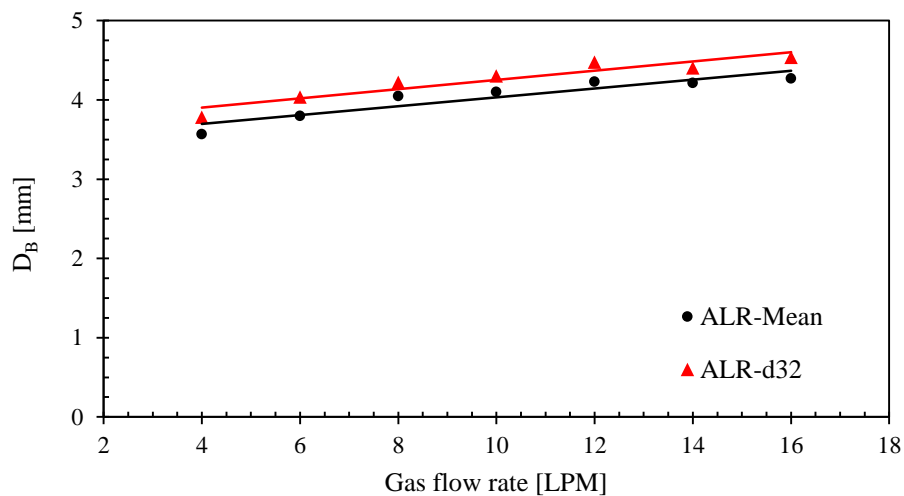


Figure 4.42. Bubble size in ALR from mean value and d_{32} calculation value

- Novel Bubble Column Reactor

In this section, the study of the bubble size distribution in novel reactor was investigated the same gas flow rate in the best condition. It was studied the same gas flow rate as in BCR and ALR. The experimental results were plotted in histogram with fitted line as shown in Figure 4.43 and Figure 4.44, which X axis presents the bubble diameter in the unit of millimeter.

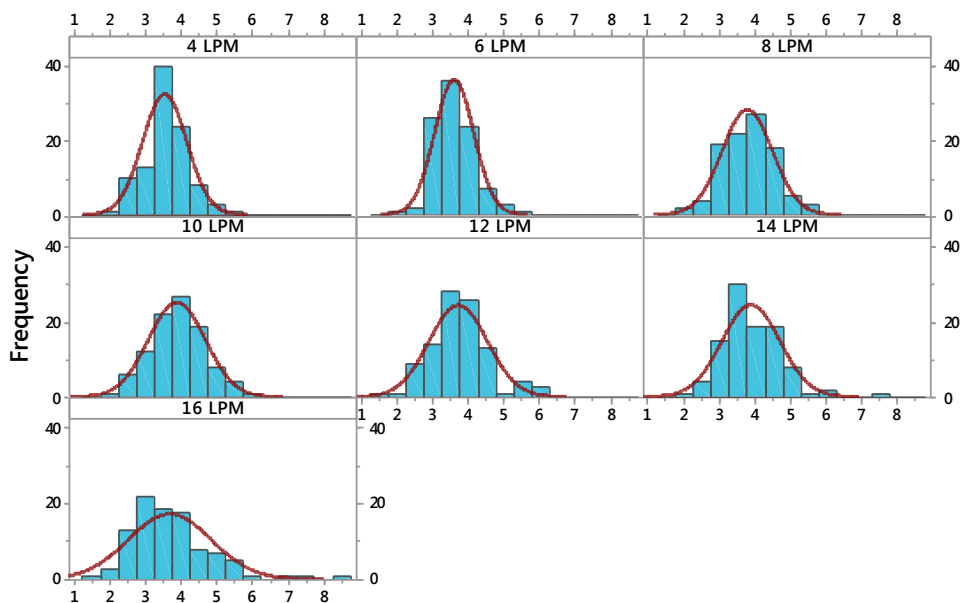


Figure 4.43. Bubble size distribution in Novel BCR with different gas flow rate

From these results, the most frequency of bubble size is around 15 to 35 of total sample size (100 samples). It can be concluded that air bubble in reactor is mixed with different sizes. For the mean value of the bubble size is ranged from 3.57 to 3.91 mm while the bubble size determined from d_{32} formula is ranged from 3.78 to 4.49 mm from the studied ranges of gas flow rate from 4 to 16 LPM. For this reactor class, the gas flow rate is slightly significant effect to the bubble size. Mean bubble size is approximately 3.74 ± 0.17 mm as presented in Figure 4.44.

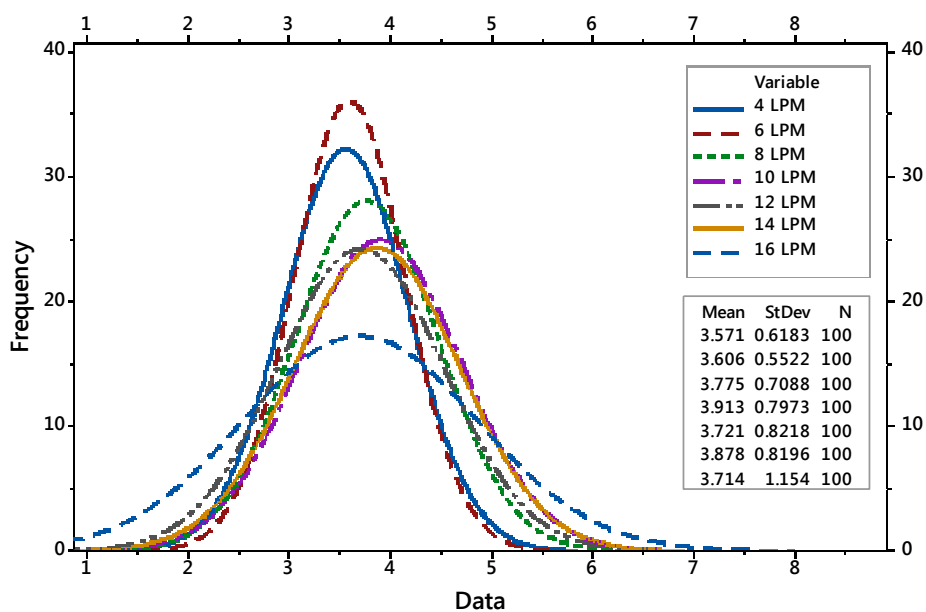


Figure 4.44. All-in-one bubble size distribution in Novel BCR

From Figure 4.44, the most frequency of the bubble sizes are presented randomly along the gas flow rate. The bubble size distribution as the mean value and d_{32} calculation was plotted in Figure 4.45. From this result, the bubble diameter as d_{32} is a little bit higher than mean bubble size. It is about 4.13 ± 0.36 mm.

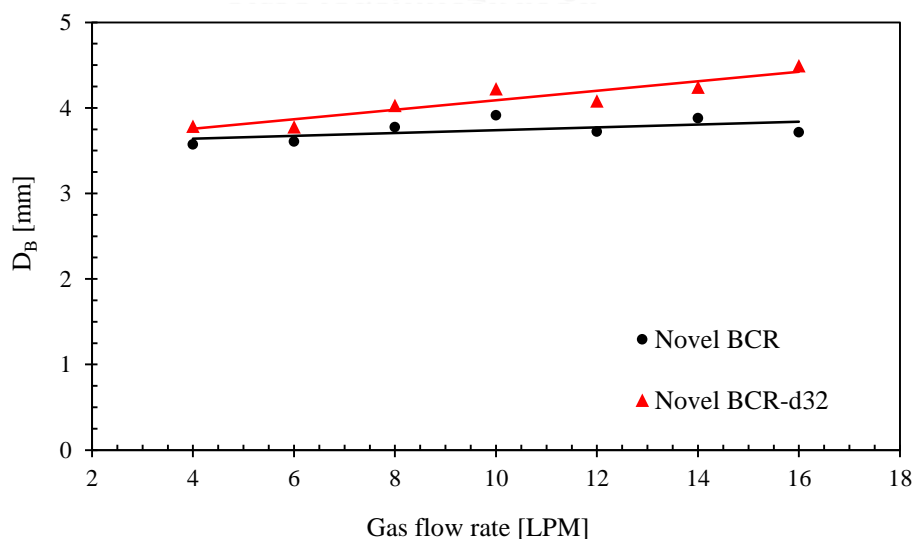


Figure 4.45. Bubble size in Novel BCR from mean value and d_{32} calculation value

- Discussion of Bubble Size

The bubble size distribution in three various gas-liquid contactors including BCR, ALR, and Novel BCR was illustrated together with different gas flow rates in Figure 4.46. From the result, the bubble size in BCR is almost constant along the gas flow rate (approximate 4.18 mm). Moreover, the bubble size in ALR and Novel BCR are increasing along the gas flow rate.

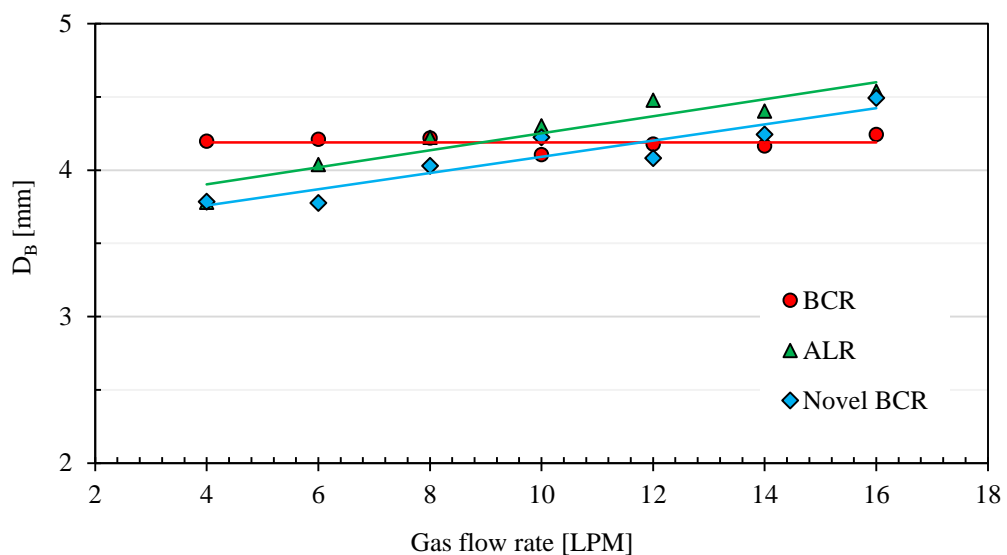


Figure 4.46. The bubble size (d_{23}) in different reactors

It can be concluded that cross sectional area of the BCR (0.2 m^2) is big enough for the bubble rising in the reactor without effect each other, therefore, the bubble size is not significant affected by the gas flow rate. However, after the cross sectional area was reduced by dividing for riser (0.138 m^2) and downcomer (0.062 m^2) to create the internal loop for liquid recirculation, the gas flow rate is slightly significant effect on the bubble size in ALR and Novel BCR operation as the exited work (Chuenchaem, 2013; Thaphet, 2013). Specific observation on the bubble size, it was found that the bubble sizes in Novel BCR are the smallest for every gas flow rate. From this result, it can be concluded that installing horizontal baffles in riser can improve the air bubble distribution to avoid the bubble integration between the generated air bubbles in the

reactor. That is why the bubble sizes are still maintained in the small size as well as provide better effect surfaces of the air bubble compared to the bubble in BCR and ALR. As the theory, larger effective surface of air bubble, better oxygen transfer was obtained. In this section, effective surface is referred to the surface of the air bubble that can be used for oxygen transfer from gas to liquid phase. In overview, it is one main reason of the internal parameter that this reactor (Novel BCR) provides better performance in terms of oxygen transfer as well as $K_L a$ coefficient.

4.3.2 Terminal Rising Bubble Velocity

In this section, the terminal rising bubble velocity (U_B) was studied in different reactors including BCR, ALR, and Novel BCR with ranging the gas flow rate from 4 to 16 LPM. The terminal rising bubble velocity was measured by frame-stepping forwards of the captured slow motion video as mentioned. The sampled point was located at the middle level of the reactor. Five random rising bubbles were measured (Thaphet, 2013) and calculated by equation 3.11.

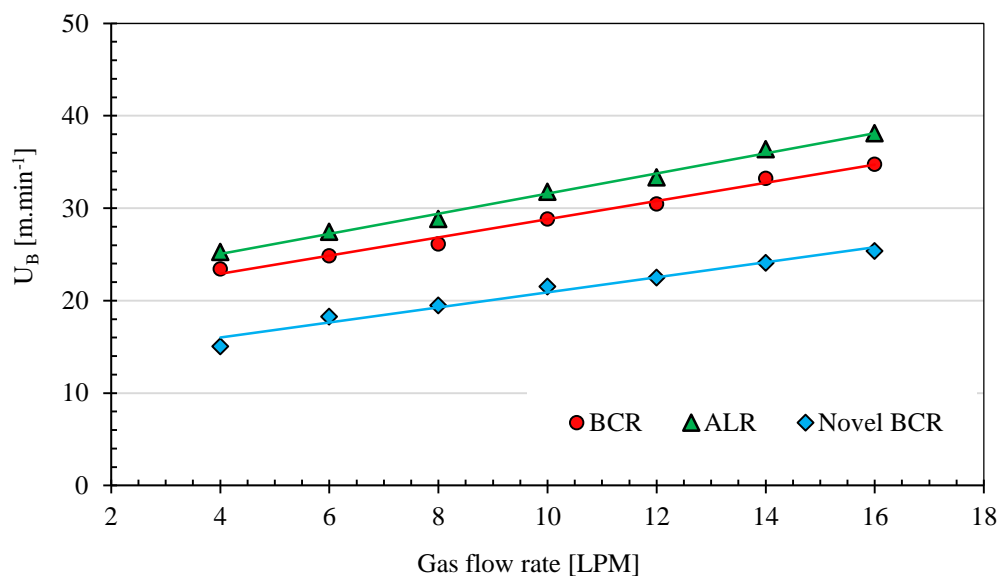


Figure 4.47. Terminal rising bubble velocity in different reactors

The experimental and calculated results of the terminal rising bubble velocity were plotted in Figure 4.47. The rising bubble velocity in bubble column is increasing along parallel with the gas flow rate, specifically from 23.4 to 34.7 m.min⁻¹ at 4 to 16 LPM. In airlift reactor, the rising bubble velocity increasing from 25.3 to 38.1 m.min⁻¹ along the studied gas flow rate. Moreover, the rising bubble velocity in novel reactor (Novel BCR) ranges from 15.0 to 25.4 m.min⁻¹ of the ranged gas flow rate.

In terms of the comparison in different reactors, the rising bubble velocity in ALR is higher than operation in BCR for every gas flow rates because of the effect of the bubble size and liquid recirculation in the reactor. The larger bubble size and the liquid recirculation in ALR are the main significantly influent to this results. However it was found that the rising bubble velocity in Novel BCR provides the lowest values compared to BCR and ALR operation for every gas flow rate. It can be concluded that the installation the horizontal baffles in the riser compartment causes the decreasing rising bubble velocity as well as reduce the liquid recirculation velocity. Moreover, low rising bubble velocity can improve the gas holdup in the reactor. In conclusion, this terminal rising bubble velocity is another internal parameter that can improve the oxygen transfer in Novel BCR.

4.3.3 Specific Interfacial Area

The specific interfacial area (a) was defined by the ratio between the total air bubble surface and total volume (liquid and gas) in the reactor as shown in equation 3.15. However, the parameter H_L (m) is the length that the bubble transport in the liquid. Then it is represented the water depth in conventional BCR or ALR that do not have an air bubble recirculation in downcomer only. For this Novel BCR, H_L is referred the air bubble stream line along the horizontal baffles from the air sparger until exit. The specific interfacial area (a) was plotted with different gas flow rate in BCR, ALR, and Novel BCR as shown in Figure 4.48. The interfacial area is increasing as the gas flow rate increases for every reactors class. The interfacial area in BCR is enlarged from 1.22 to 3.25 m⁻¹ for the respective gas flow rate from 4 to 16 LPM, which is slightly different

with the operation in the ALR, from 1.27 to 2.79 m^{-1} . Moreover, the interfacial area in Novel BCR is ranged from 2.63 to 5.25 m^{-1} , which is higher than BCR and ALR.

Take a look the results and discussion on the performance comparison between BCR and ALR, the interfacial area from the operation in BCR is a little bit higher than in ALR because of the higher rising bubble velocity and larger bubble size in ALR compared to those in BCR. However the mass transfer coefficient in ALR was found that it is better than the operation in BCR due to the mixing level from the liquid recirculation in ALR.

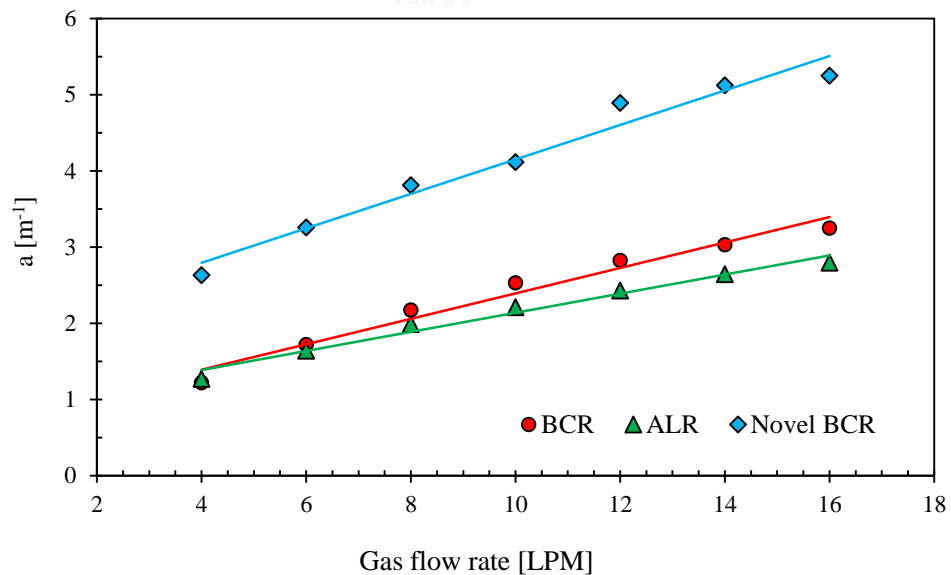


Figure 4.48. Specific interfacial area vs. gas flow rate in different reactors

Therefore, even though the specific interfacial area of the bubble in ALR is worth than BCR, the oxygen transfer performance in ALR is still better than BCR due to the liquid mixing (higher liquid turbulence) in the reactor. By the way, the interfacial area in Novel BCR is widely higher compared to other two reactors due to the maintained bubble in the small size and the slow rising bubble velocity. In conclusion, these interfacial area results represent why the Novel BCR was improved its performance compared to other two reactors.

4.3.4 Liquid Film Mass Transfer Coefficient (K_L)

The result of the liquid film mass transfer coefficient (K_L) should be included with the overall mass transfer coefficient ($K_L a$) but because it is required the result of the specific interfacial area (a), therefore, it was examined in this section. The K_L coefficient is defined by the $K_L a$ coefficient and interfacial area. The resulting K_L coefficient at temperature 20 °C was plotted together with the gas flow rate in different reactors as shown in Figure 4.49.

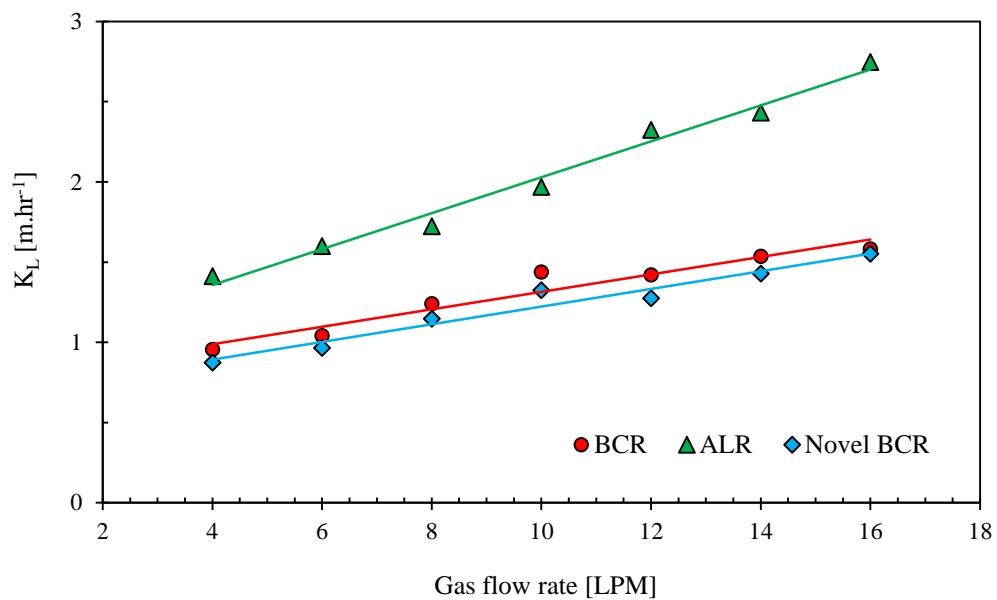


Figure 4.49. K_L coefficient at 20°C vs. gas flow rate in different reactors

From this result, it can be concluded that the K_L coefficient obtained from ALR provided the highest value, from 1.41 to 2.75 m.hr⁻¹ for the studied ranges of the gas flow rate (4 to 16 LPM) while BCR and Novel BCR are ranged from 0.95 to 1.58 m.hr⁻¹ and 0.87 to 1.55 m.hr⁻¹, respectively. These results can be discussed with the K_L coefficient prediction of Higbie (Higbie, 1935) while this Higbie's theory (Penetration Theory) is valid applying for the mobile spherical bubbles ($D_B > 2.5$ mm) (Painmanakul *et al.*, 2009) as this work. The correlations between the bubble hydrodynamic parameters (U_B and D_B) and K_L coefficient was presented by equation 4.4 where D is

the mass diffusivity coefficient of the solute in solvent phase and for this work, it is the diffusivity coefficient of the oxygen in water.

Based on equation 4.4 of Higbie's theory, it can be said that higher rising bubble velocity, increased K_L coefficient was obtained. In opposite, higher bubble diameter decreased K_L coefficient value. Therefore, K_L coefficient of ALR is the highest one compared to other reactors (BCR, and Novel BCR) due to its rising velocity and bubble size performance. Moreover, because of the lowest rising bubble velocity and bubble size of Novel BCR, the small values of K_L coefficient were obtained.

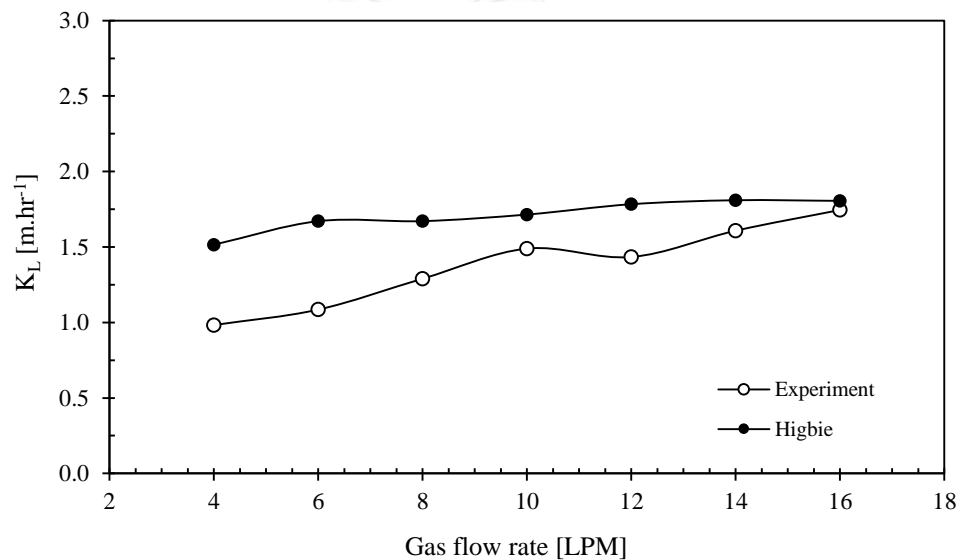


Figure 4.50. Comparison of experimental K_L values in Novel BCR with values obtained by Higbie's model

$$K_L = 2 \sqrt{\frac{D \cdot U_B}{\pi \cdot D_B}} \quad \text{Eq. 4.4}$$

The comparison of the K_L coefficient from the experiment of this work and the correlation of Higbie's theory in Novel BCR was plotted in Figure 4.50. However, the result was converted to 25 °C of temperature due to the diffusivity coefficient (D) usually provided at this temperature. From Figure 4.50, K_L value obtained from Higbie is slightly increased from 1.52 to 1.81 m.hr⁻¹ while those from the experiments

increased from 0.98 to 1.75 m.hr⁻¹. The K_L coefficient value obtained with Higbie's equation are closed to those obtained experimentally at higher gas flow rate. However it is not much significant differences for all overall values, the average and maximum difference of these values are 20% and 35%, respectively. This is probably due to the modification of the reactor of this study and the error of the experiment.

4.3.5 Gas Holdup

Gas holdup (ϵ) is the volumetric fraction between the gas volume and the total volume of the mixed gas and liquid. It is usually examined from the different water levels before and after the operation but it cannot be noted the this difference for this work due to the large reactor volume as well as cross sectional area with a little bit low superficial gas velocity. In this section, although gas holdup is usually studied in a separation part from bubble hydrodynamic parameter, it was presented from the bubble hydrodynamic parameter for this work. The gas holdup in BCR varied from 0.85×10^{-3} to 2.30×10^{-3} for the ranges of gas flow rate from 4 to 16 LPM and 0.80×10^{-3} to 2.11×10^{-3} for ALR operation. Moreover, the gas holdup in Novel BCR provides highest values ranging from 1.37×10^{-3} to 3.23×10^{-3} compared to BCR and ALR. Other more, the gas holdup in Novel BCR is the highest due to the bubble rising velocity and the bubble size. This result is represent only the bubble hydrodynamic parameter, however the improvement of ALR compared to BCR can be caused by the liquid mixing level as mentioned in the previous section as well.

4.4 Ferrous Iron Oxidation

Ferrous iron oxidation process in this work is such as one of the application that can perform with this novel reactor (Novel BCR) for treatment of iron contaminant in groundwater, which requires oxygen transfer of aeration process. In this part, the experiment was examined the effect of gas flow rate (Q_g) and initial concentration of ferrous iron ($[Fe^{2+}]_0$) on oxidation process. It was obtained in semi-batch experiments. The pH in the reactor was not maintained as the fixed value, it changed naturally base

on the reaction in the reactor. The gas flow rate was conducted in the range from 2 to 10 LPM with the same initial concentration of $[\text{Fe}^{2+}]_0$, 15 mg/L. Other more, 10 LPM of gas flow rate was maintained during the study of initial ferrous concentration of 5, 15, 30, and 50 mg/L were varied.

4.4.1 Effect of Initial Concentration of Ferrous

The reduction ratio of ferrous concentration was plotted in Figure 4.51. From this result, the oxidation of ferrous is faster at lower initial concentration of ferrous. Furthermore, the oxidation of ferrous iron operated in the Novel BCR is better than conventional BCR. For instance at aerated time 100 min and $[\text{Fe}^{2+}]_0$ equal 50 mg/L, the ferrous concentration can be deduced in Novel BCR until 3% while in BCR is still at 6.4%.

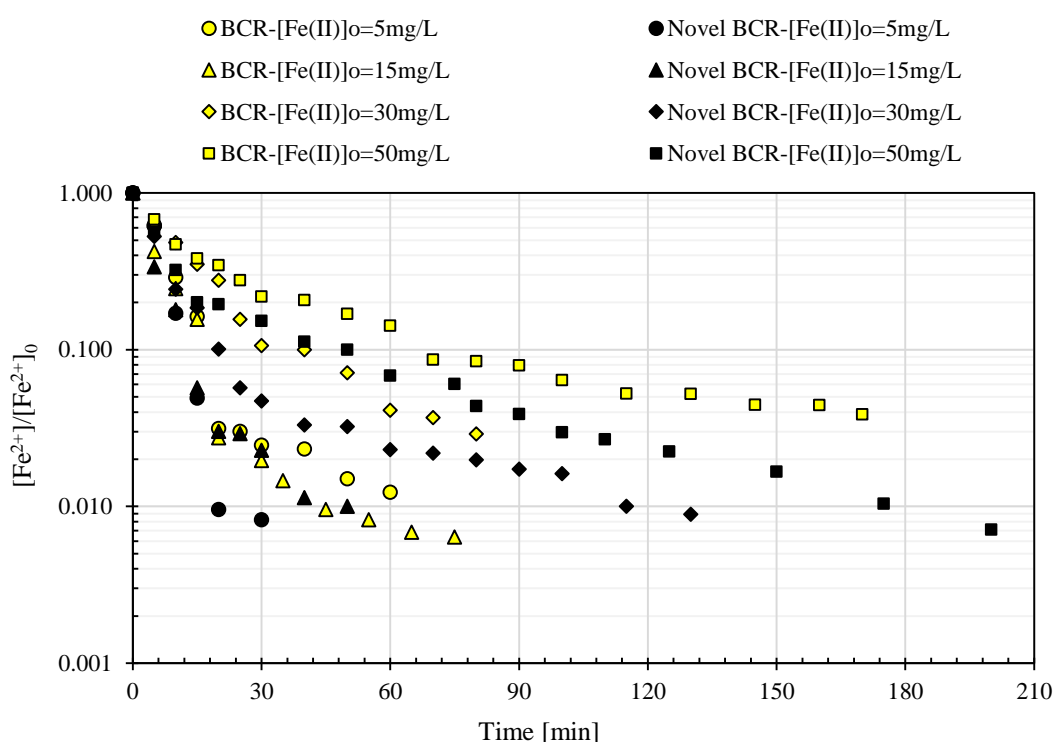


Figure 4.51. Semi-logarithmic scale plot of ferrous reduction ratio with different $[\text{Fe}^{2+}]_0$ in BCR and Novel BCR ($Q_g = 10$ LPM)

However, (El Azher *et al.*, 2008) presented that ferrous oxidation is much faster when $[Fe^{2+}]_0$ increase, which is opposite with the result of this work. It is incomparable of this works to Azher's work due to air supplied to the system. This work is mainly focused on the optimum aeration process which provided 10 LPM of air flow rate for 140 L of the synthetic groundwater volume while Azher's work provided up to 80 LPM for 63 L only. It is another reason of their work that increasing gas flow rate did not affect apparently on ferrous oxidation due to the extremely gas flow rate was supplied.

4.4.2 Effect of Gas Flow Rate

This section, the effect of the gas flow rate was studied only in Novel BCR which is this present work. The experimental results were plotted in Figure 4.52. This result showed that increasing a gas flow rate provided better conversion yield. From illustration, the ferrous concentration was oxidized better at 10 LPM of the gas flow rate compared to 5 and 2 LPM. In order to precipitate the ferrous iron to be lower than limited value for drinking water source (0.3 mg/L) with 15 mg/L as an initial concentration, there is required more than 27 min for operating with gas flow rate 2 LPM, 43 min for 5 LPM, and 64 min for 10 LPM.

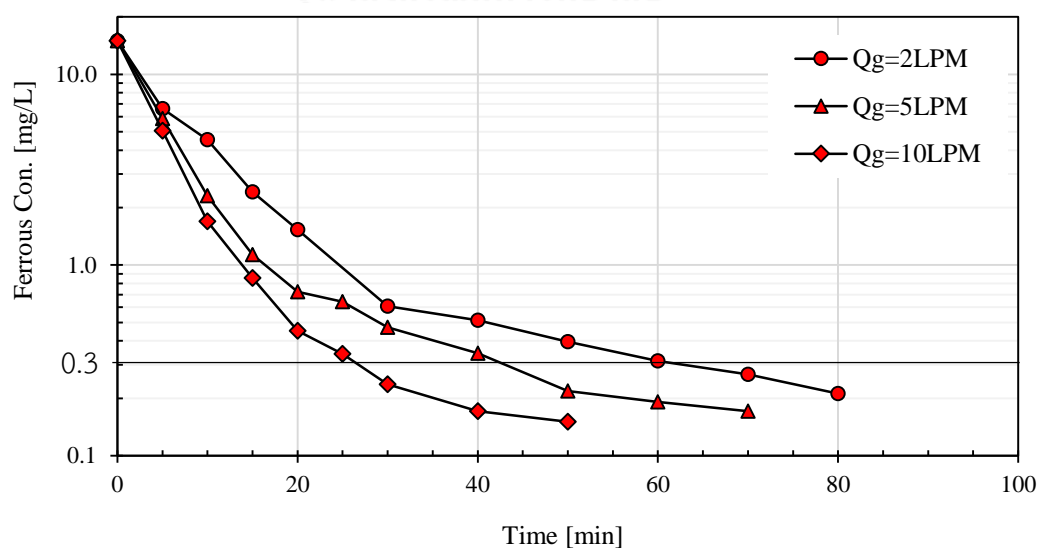


Figure 4.52. Ferrous concentration along aeration time with different gas flow rate (Q_g) in Novel BCR ($[Fe^{2+}]_0 = 15 \text{ mg/L}$)

4.4.3 Study Simple Kinetic Rate

Experimental results of previous section can now be reanalyzed for studying the simple kinetic rate. For this determination the kinetic of iron oxidation, it was studied only the simple kinetic including rate constant (k) in zero-order, first-order, and second-order. This reaction rate was studied in the novel reactor with the initial concentration of ferrous iron is 50 mg/L and the gas flow rate is 10 LPM. The zero-order, first-order, and second-order were obtained by plotting between $[\text{Fe}^{2+}]$, $\ln[\text{Fe}^{2+}]$, and $1/[\text{Fe}^{2+}]$, respectively with the operation time as shown in Figure 4.53. From the plotted result, the rate constant for zero-order is $0.13 \text{ mg}\cdot\text{L}^{-1}\cdot\text{min}^{-1}$ with the low R-square, 0.41 while the rate constant of first-order is 0.02 min^{-1} with 0.92 of R-square. For second-order, the rate constant is $0.01 (\text{mg}/\text{L}\cdot\text{min})^{-1}$ with 0.86 of the R squared.

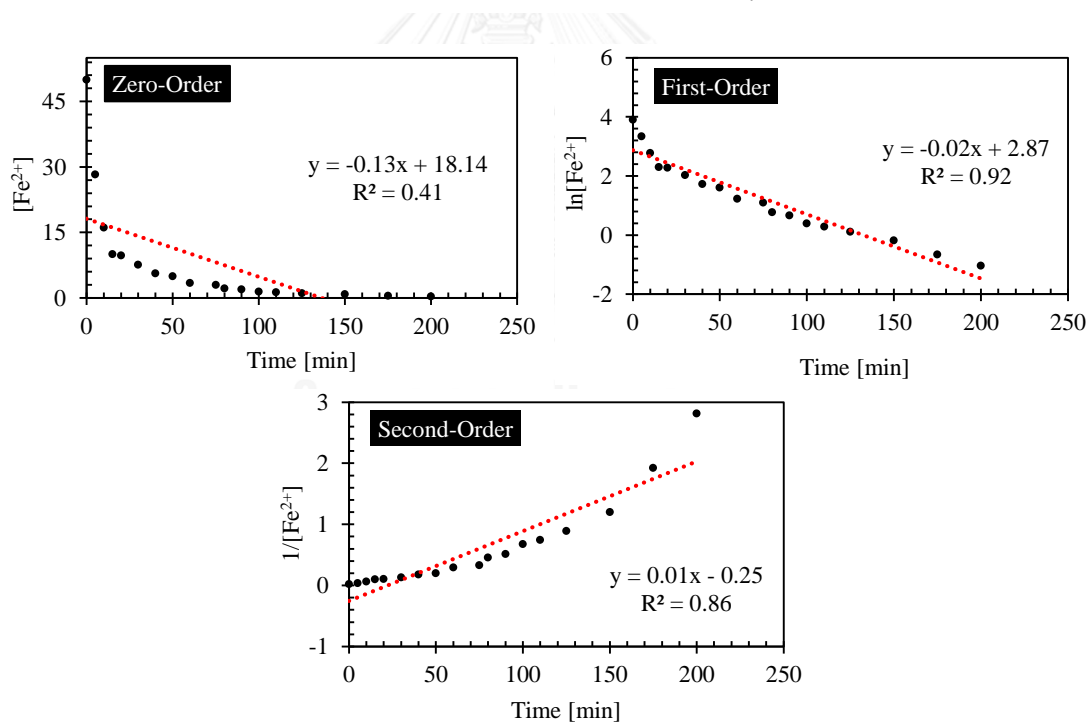


Figure 4.53. Scatter plot for the rate constant in zero, first, and second-order

$$r = \frac{dC}{dt} = -0.02[\text{Fe}^{2+}]$$

Eq. 4.5

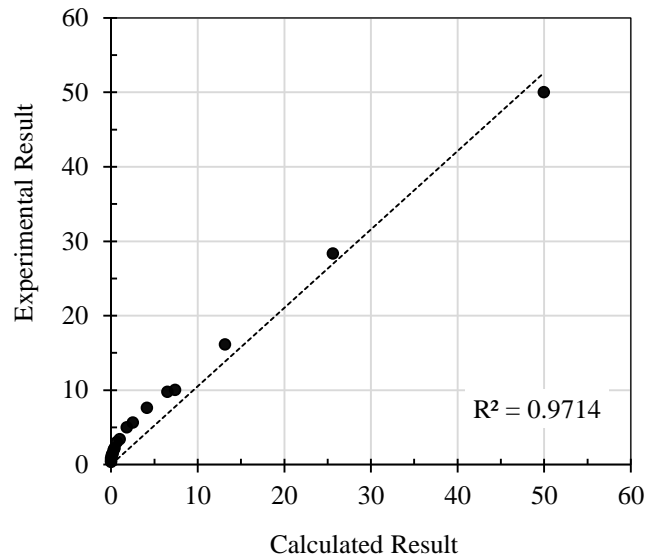


Figure 4.54. Ferrous concentration obtained from experiment and calculation of proposed kinetic rate

For the simple kinetic rate, first-order is the most appropriate kinetic order as well as the highest R-square compared to zero and second-order in terms of concentration of ferrous iron. The kinetic rate (r) of the ferrous oxidation in Novel BR was proposed in a simple form as expressed in equation 4.5. The values obtained from this proposed kinetic rate was plotted with the experimental value as shown in Figure 4.54 in terms of the concentration of ferrous. The R-square from this examine can be obtained up to 0.97.

4.4.4 Proposed Separation Process for Ferric Iron

In this section, the study the fraction removal in the Novel BCR by batch settling column test, study ferric particle removable of depth filtration by filtration test, and study the optimum concentration of alum to improve the settling process of ferric particle by jar test was conducted in different parts. After oxidizing the ferrous iron in Novel BCR 130 minutes by 10 LPM of gas flow rate and 30 mg/L of initial concentration, the aerated groundwater was sampling to study in this section.

- Batch Settling Test: Gravity Separation

The samples was sampling different port in the riser compartment along the time after the aeration was stopped as shown in Figure 4.55. Batch settling test was studied its performance in terms of turbidity, which was measured by turbidity meter. There are four sampling ports including Port I, Port II, Port III, and Port IV where are 2 cm, 22 cm, 42 cm, and 62 cm from the water surface, respectively. However, only three ports was used due to the top port (Port I) is too close to the water surface, which is hard to plot the iso-removal. The settling test was studied 5 hours and sampling time-step is 30 minutes.

After the experiment, the results were examined within several steps as detail described in (Reynolds, 1977). The result for batch settling test in Novel BCR of ferric iron was shown in Figure 4.56 with the average initial turbidity is 314 NTU. The raw results were attached in the Appendix 9. The water characteristic of this section was shown in Figure 4.58.

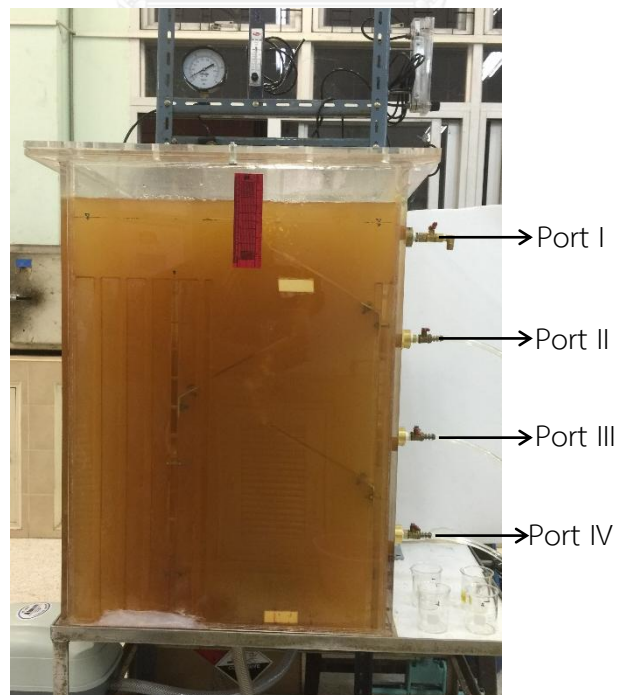


Figure 4.55. Sampling ports for batch settling test

Based on the result of Figure 4.56, the fraction removal (R_T) was decreased 80% until 25.8% while the overflow varied from 0.12 m.hr⁻¹ to 0.74 m.hr⁻¹. Higher overflow provided the lower fraction removal with the slop of 0.67. The correlation between fraction removal (R_T) and overflow (V_0) of this section was constructed in power function, $R_T \sim 20.55 V_0^{-0.67}$ as shown in Figure 4.56.

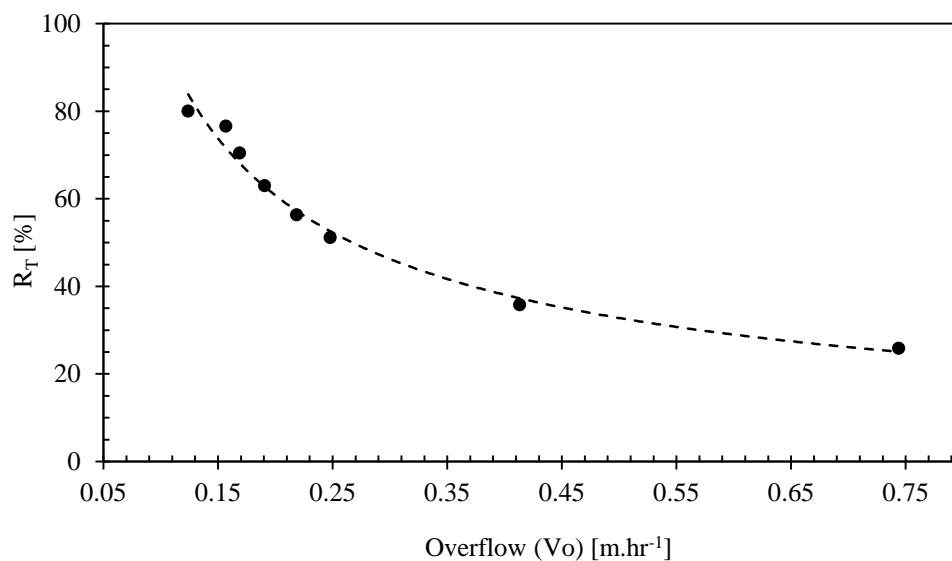


Figure 4.56. Settling result of fraction removal vs. overflow in Novel BCR

- Jar Test: Alum Dosage

The jar test was conducted in order to obtain the optimum concentration of Alum for improving the settling performance of ferric iron. The detail describe of the jar test procedure was presented in (Black *et al.*, 1957). Because of tap water was used up for synthetic groundwater, the alkalinity should be enough for consumption of coagulant. However, after oxidation with oxygen, the alkalinity was reduced as shown the literature review of ferrous iron oxidized by oxygen (Table 2.1). The sodium bicarbonate (NaHCO_3) was added in this study for the sufficient alkalinity to react with aluminum sulfate to produce the hydroxide floc. After add the sodium bicarbonate, it may affect the pH a little bit. However, the value of pH need to concern due to it can affect the

floc forming after add alum. The optimum pH range for alum is from about 4.5 to 8.0 (Reynolds, 1977).

The alum concentration was studied in the range from 5 to 30 mg/L. After finished the jar test, residual turbidity was measured and plotted as shown in Figure 4.57. From the experimental result, increasing alum concentration is significant effect the residual turbidity by reduction those amount. However, adding its concentration ≥ 15 mg/L, the efficiency is reduce a lot. It is meant that after providing the alum concentration ≥ 15 mg/L, the higher residual turbidities were obtained and some of them may cause by itself after exited adding.

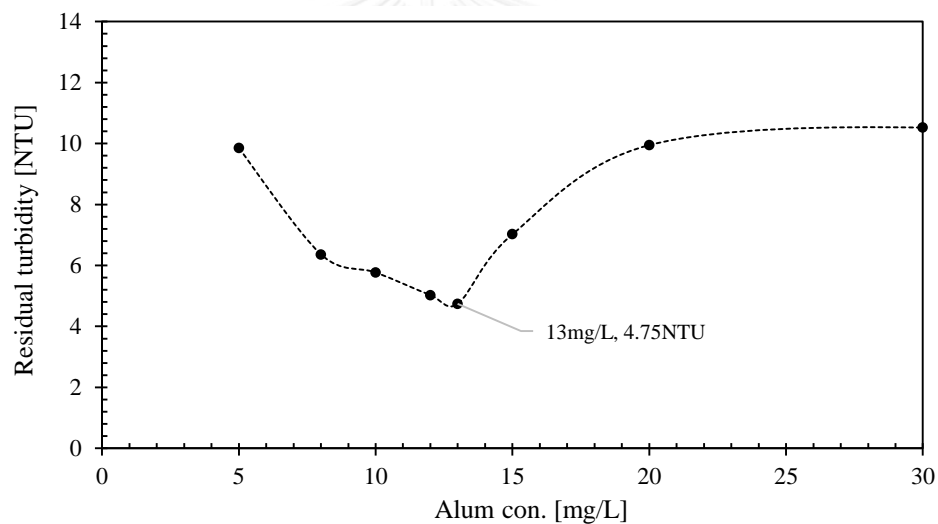


Figure 4.57. Residual turbidity after jar test from different alum concentrations

Future more, the turbidity can be reduced from more than 300 NTU until less than 5 NTU (4.75 NTU) after adding 13 mg/L of alum. It can be concluded that the alum concentration for improving the settling process, 13 mg/L was finalized as the optimum dosage for ferric particle in this work. The water characteristic of this section was shown in Figure 4.58.

- Filtration Test: Depth Filtration

The objective of this test is to confirm that depth filtration can be used for removal the ferric iron to less than the standard level or not. The pore size of the filter is representative the pore size of depth filtration can be determined by the preferred particle size to remove and uniformity coefficient of depth filtration, which is detail described in (Reynolds, 1977). Therefore, glass fiber filter with 0.7 μm of pore size was used in this section. This section, the samples were sampled after aerated 130 minutes with 10 LPM in Novel BCR and initial concentration of ferrous iron is 30 mg/L. The influent and effluent water characteristic was shown in Table 4.17 and Figure 4.58.

From the experimental result, the turbidity can be removed from 315 NTU until 0.25 NTU, which is less than the water standard level for drinking water source (< 5 NTU). Before aeration, the ferrous or total iron is about 30 mg/L and after aeration, the ferrous iron was reduced to 0.27 mg/L. After filtration test, the total iron can be removed until the concentration equals 0.06 mg/L, which is less than the water standard level for drinking water source (< 0.3 mg/L for WHO or USEPA, < 0.5 mg/L for PCD-Thailand). In conclusion, the depth filtration can remove ferric iron very well in terms of turbidity and iron concentration of this work.

Table 4.17. Water characteristic before and after filtration test

Test	Turbidity [NTU]	Ferrous / Total Iron [mg/L]
Before filtration	315	0.27 (ferrous iron)
After filtration	0.25	0.06 (total iron)

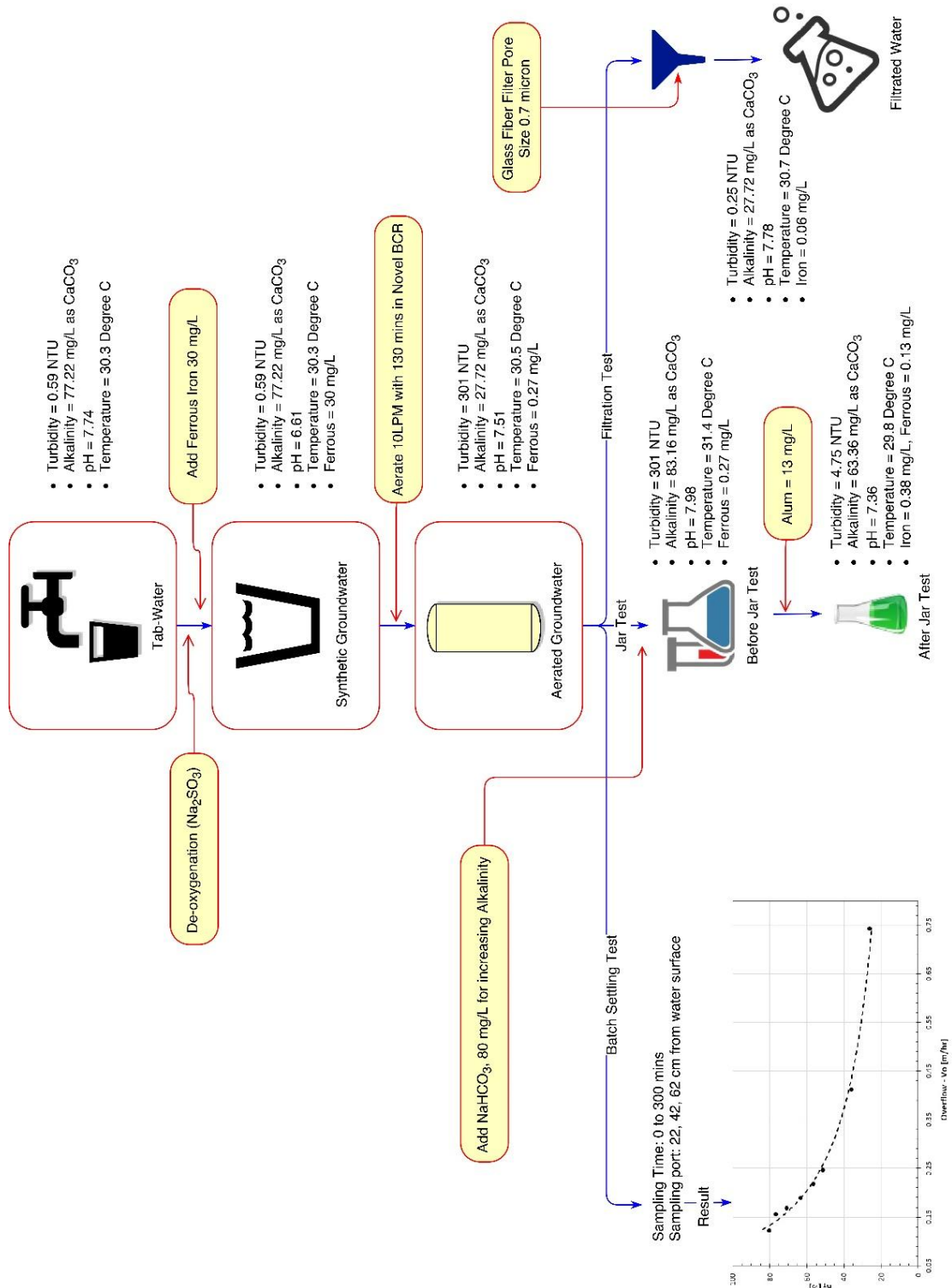


Figure 4.58. Summary the separation process for ferric iron in this work

CHAPTER 5

CONCLUSION AND RECOMMENDATION

5.1 Conclusion

The objectives of this work is to develop the Novel Bubble Column Reactor (Novel BCR) after comprised the vertical baffle and install horizontal baffles in a riser compartment, and to study the removal of ferrous iron with high level concentration such as in groundwater by oxidation process. The optimal Novel BCR configuration and operation condition was analyzed and applied for ferrous iron removal part. The results of this work can be concluded as the following:

- **Reactor Development:**

- The main influent factor are Amount of Baffle (N_b), Baffle Angle (α), Position of Bottom Recirculation Area (Y_r), and Settling Area on Baffle (A_s).
- The optimum configuration of Novel BCR are Downcomer-to-Riser Ratio ($A_d/A_r \sim 0.45$), Amount of Baffle ($N_b \sim 3$ baffles), Baffle Angle ($\alpha \sim 50^\circ$), Position of Recirculation Area ($Y_r \sim 10$ cm), Settling Area on Baffle ($A_s \sim 90$ cm²), Amount of Diffuser ($N_d \sim 4$ diffusers), Bottom Recirculation Area ($A_r \sim 450$ cm²), and baffle length ($L_b \sim 20$ cm).
- The prediction equation of the correlation between Gas flow rate, Baffle angle, Amount of baffle, and $K_L a$ coefficient as the response was constructed.

- **Reactor Performance:**

- The Novel BCR can improve its performance in terms of $K_L a$ coefficient approximate 50 to 97% compared to BCR and 6 to 28% compared to ALR at the gas flow rates range from 4 to 16 LPM.
- The Novel BCR performance provides better standard oxygen transfer rate about 24 to 64 mg-O₂.min⁻¹ compared to BCR and 11 to 10 mg-O₂.min⁻¹ compared to ALR (4-16 LPM).

- The standard oxygen transfer efficient are approximate 2.46%, 3.40%, and 4.03% of the respective BCR, ALR, and Novel BCR.
- Better oxygen transfer was obtained from Novel BCR after the same power was provided. Correlation between unit volume power consumption and K_La coefficient was examined.
- Aeration efficiency in the operation with Novel BCR provides the highest values compared to ALR and BCR.
 - **Bubble Hydrodynamic Parameters:**
 - Bubble size: the bubble sizes in Novel BCR are the smallest for every gas flow rate compared to BCR and ALR. It can be concluded that installing horizontal baffles in riser can improve the air bubble distribution to avoid the bubble integration between the generated air bubbles in the reactor.
 - Rising bubble velocity: Novel BCR provides the lowest values of the rising bubble velocity compared to BCR and ALR for every gas flow rate. It can be concluded that the installation the horizontal baffles in the riser compartment causes the decreasing rising bubble velocity, which can improve the gas holdup in the reactor.
 - **Ferrous Iron Oxidation:**
 - The oxidation of ferrous iron is faster at lower initial concentration of ferrous and the operation in the Novel BCR provides better oxidizing compared to the conventional BCR.
 - Higher gas flow rate provides better conversion yield for ranges of 2 to 10 LPM.
 - The low overflow of settling process of ferric iron was obtained, which probably caused by the low particle size, colloid ($d_p < 10 \mu\text{m}$). The coagulant, alum was

used 13 mg/L to improve the settling performance. Moreover, depth filtration can remove ferric iron very well in terms of turbidity and iron concentration.

5.2 Recommendation

Based on the whole experience and the experimental result of this work, several recommendations for future work was proposed as the following:

- For the reactor development, the method for reactor scale-up/-down should be studied and tested to confirm the reactor performance and for apply in the real application.
- For well understanding the gas holdup, very accuracy equipment such as the water level sensors should be used for accurate values besides using the bubble hydrodynamic parameter to determine gas holdup.
- For well understand the internal mechanism in the reactor, the study of the liquid movement or liquid mixing level should be studied such as residence time distribution (RTD) or/and computational fluid dynamics (CFD).
- The real contaminant of groundwater with high concentration of ferrous iron should be used to study the effect of the complex form on the oxidation process or removal efficiency.
- The Novel BCR should be applied to check its performance with other contaminates that require the saturated oxygen in the water such as Arsenic.

REFERENCES

- APHA, AWWA, WPCF, & WEF. (1915). *Standard methods for the examination of water and wastewater* (Vol. 2): American Public Health Association, American Water Works Association, Water Pollution Control Federation, Water Environment Federation.
- ASCE. (1992). *ASCE Standard-Measurement of Oxygen Transfer in Clean Water.*
- Bando, Y., Nishimura, M., Sota, H., Suzuki, S., & Kawase, N. (1992). Flow characteristics of countercurrent bubble column with perforated draft tube. Chemical Engineering Science, 47(13), 3371-3378.
- Bekassy-Molnar, E., Majeed, J., & Vatai, G. (1997). Overall volumetric oxygen transfer coefficient and optimal geometry of airlift tube reactor. Chemical Engineering Journal, 68(1), 29-33.
- Black, A., Buswell, A. M., Eidsness, F. A., & Black, A. (1957). Review of the jar test. Journal (American Water Works Association), 49(11), 1414-1424.
- Chaturvedi, S., & Dave, P. N. (2012). Removal of iron for safe drinking water. Desalination, 303, 1-11.
- Chen, C.-P., Yang, S.-J., & Wu, W.-T. (1997). A novel rectangular airlift reactor with mesh baffle-plates. Biotechnology techniques, 11(6), 439-441.
- Choi, K., Chisti, Y., & Moo-Young, M. (1995). Split-channel rectangular airlift reactors: Enhancement of performance by geometric modifications. Chemical Engineering Communications, 138(1), 171-181.
- Chuenchaem, C. (2013). *Effect of Bubble Hydrodynamic and Liquid Phase on Mass Transfer Mechanism in Bubble Column.* (Master Degree), Chulalongkorn University.
- Clifford, D. A. (1999). Ion exchange and inorganic adsorption. Water quality and treatment, 4, 561-564.

- Couvert, A., Bastoul, D., Roustan, M., & Chatellier, P. (2004). Hydrodynamic and mass transfer study in a rectangular three-phase air-lift loop reactor. Chemical Engineering and Processing: Process Intensification, 43(11), 1381-1387.
- Crittenden, J. C., Trussell, R. R., Hand, D. W., Howe, K. J., & Tchobanoglous, G. (2012). *MWH's Water Treatment: Principles and Design*: John Wiley & Sons.
- Daniel, C. (1959). Use of half-normal plots in interpreting factorial two-level experiments. Technometrics, 1(4), 311-341.
- Deckwer, W.-D. (1980). On the mechanism of heat transfer in bubble column reactors. Chemical Engineering Science, 35(6), 1341-1346.
- Deckwer, W.-D., Burckhart, R., & Zoll, G. (1974). Mixing and mass transfer in tall bubble columns. Chemical Engineering Science, 29(11), 2177-2188.
- Deckwer, W.-D., & Field, R. W. (1992). *Bubble column reactors* (Vol. 200): Wiley New York.
- Degaleesan, S., Dudukovic, M., & Pan, Y. (2001). Experimental study of gas-induced liquid-flow structures in bubble columns. AIChE journal, 47(9), 1913-1931.
- Drandev, S. S. (2015). *Study of the Hydrodynamics, Mass Transfer and Energy Requirements of a Rectangular Air-lift Bioreactor for Electrical Power Generation*. The University of Western Ontario.
- Duranceau, S. (2001). Selection of a nitrate removal process for the City of Seymour, Texas. Membrane practices for water treatment. S. Duranceau (ed.). American Water Works Association, Denver, Colorado.
- Ebrahimi, S., Fernández Morales, F., Kleerebezem, R., Heijnen, J., & Van Loosdrecht, M. (2005). High-rate acidophilic ferrous iron oxidation in a biofilm airlift reactor and the role of the carrier material. Biotechnology and bioengineering, 90(4), 462-472.
- Edzwald, J. K. (2011). *Water Quality & Treatment: A Handbook on Drinking Water*. McGraw-Hill New York.

- El Azher, N., Gourich, B., Vial, C., Souлами, M. B., & Ziyad, M. (2008). Study of ferrous iron oxidation in Morocco drinking water in an airlift reactor. Chemical Engineering and Processing: Process Intensification, 47(9), 1877-1886.
- EPA. (1989). Fine pore aeration systems. Manual EPA Design-Center for Environmental, 1-89.
- Facon, T. (2001). From vision to action: a synthesis of experiences in Southeast Asia.
- Faust, S. D., & Aly, O. M. (1998). *Chemistry of water treatment*: CRC Press.
- Ghosh, T., Bhattacharyya, D., & Kim, T.-h. (2010). Effect of Fractional Gas hold-up (ϵ_G) on Volumetric Mass Transfer Co-efficient (KLa) in Modified Airlift Contactor. International Journal of Advanced Science and Technology, 16, 21-30.
- Gomez, F., & Sartaj, M. (2014). Optimization of field scale biopiles for bioremediation of petroleum hydrocarbon contaminated soil at low temperature conditions by response surface methodology (RSM). International Biodeterioration & Biodegradation, 89, 103-109.
- Hartung, H. (1951). Committee Report: Capacity and loadings of suspended solids contact units. Jour. AWWA, 43(4).
- Hazen, A. (1904). On sedimentation. Transactions of the American Society of Civil Engineers, 53(2), 45-71.
- He, Z., Petiraksakul, A., & Meesapya, W. (2003). Oxygen-transfer measurement in clean water. J. KMITNB, 13(1), 13-19.
- Higbie, R. (1935). *The rate of absorption of a pure gas into still liquid during short periods of exposure*.
- Hyndman, C. L., Larachi, F., & Guy, C. (1997). Understanding gas-phase hydrodynamics in bubble columns: a convective model based on kinetic theory. Chemical Engineering Science, 52(1), 63-77.
- Imai, T., & Zhu, H. (2011). *Improvement of Oxygen Transfer Efficiency in Diffused Aeration Systems Using Liquid-Film-Forming Apparatus*: INTECH Open Access Publisher.

- Kaksonen, A. H., Morris, C., Hilario, F., Rea, S. M., Li, J., Usher, K. M., . . . du Plessis, C. (2014). Iron oxidation and jarosite precipitation in a two-stage airlift bioreactor. Hydrometallurgy, *150*, 227-235.
- Kantarci, N., Borak, F., & Ulgen, K. O. (2005). Bubble column reactors. Process Biochemistry, *40*(7), 2263-2283.
- Kawagoe, K., Inoue, T., Nakao, K., & Otake, T. (1976). Flow-Pattern and Gas-Holdup Conditions in Gas-Sparged Contactors. International Chemical Engineering, *16*(1), 176-183.
- Kawamura, S. (2000). *Integrated design and operation of water treatment facilities: John Wiley & Sons.*
- Kilonzo, P. M., Margaritis, A., Bergougnou, M., Yu, J., & Ye, Q. (2007). Effects of geometrical design on hydrodynamic and mass transfer characteristics of a rectangular-column airlift bioreactor. Biochemical Engineering Journal, *34*(3), 279-288.
- Kracht, W., Gomez, C., & Finch, J. (2008). Controlling bubble size using a frit and sleeve sparger. Minerals Engineering, *21*(9), 660-663.
- Krichnavaruk, S., & Pavasant, P. (2002). Analysis of gas-liquid mass transfer in an airlift contactor with perforated plates. Chemical Engineering Journal, *89*(1), 203-211.
- Lenntech. (2015). Iron in groundwater. 2015, from <http://www.lenntech.com/groundwater/iron.htm>
- Lu, X., Ding, J., Wang, Y., & Shi, J. (2000). Comparison of the hydrodynamics and mass transfer characteristics of a modified square airlift reactor with common airlift reactors. Chemical Engineering Science, *55*(12), 2257-2263.
- Luo, L., Yuan, J., Xie, P., Sun, J., & Guo, W. (2013). Hydrodynamics and mass transfer characteristics in an internal loop airlift reactor with sieve plates. Chemical Engineering Research and Design, *91*(12), 2377-2388.
- Margat, J., & Van der Gun, J. (2013). *Groundwater around the world: a geographic synopsis: CRC Press.*

- Marianne, M. (2007). Testing Groundwater. 2015, from <http://www.wqpmag.com/testing-groundwater>
- McMurry, J., Fay, R. C., & Fantini, J. (2004). Chemistry: Prentice Hall.–2001.–1067 p.
- Metcalfe, E. (2003). Inc., Wastewater engineering treatment and reuse: McGraw-Hill, New York.
- Michalakos, G. D., Nieva, J. M., Vayenas, D., & Lyberatos, G. (1997). Removal of iron from potable water using a trickling filter. *Water Research*, 31(5), 991-996.
- Minitab, I. (2000). MINITAB statistical software. *Minitab Release*, 13.
- Montgomery, D. C. (2008). *Design and analysis of experiments*: John Wiley & Sons.
- NEIW. (2005). SEQUENCING BATCH REACTOR DESIGN AND OPERATIONAL CONSIDERATIONS. *New England Interstate Water*.
- NGA. (2013). Facts about global groundwater usage. *National Groundwater Association Factsheet*, 9-2013.
- NIST. (2012). OMNITAB 80. 2015, from <http://www.nist.gov/itl/sed/omnitab-80.cfm>
- NSE. (2008). The drop on water Iron and manganese [Press release]
- Painmanakul, P., & Hébrard, G. (2008). Effect of different contaminants on the α -factor: Local experimental method and modeling. *Chemical Engineering Research and Design*, 86(11), 1207-1215.
- Painmanakul, P., Loubiere, K., Hebrard, G., & Buffière, P. (2004). Study of different membrane spargers used in waste water treatment: characterisation and performance. *Chemical Engineering and Processing: Process Intensification*, 43(11), 1347-1359.
- Painmanakul, P., Loubière, K., Hébrard, G., Mietton-Peuchot, M., & Roustan, M. (2005). Effect of surfactants on liquid-side mass transfer coefficients. *Chemical Engineering Science*, 60(22), 6480-6491.
- Painmanakul, P., Wachirasak, J., Jamnongwong, M., & Hebrard, G. (2009). Theoretical Prediction of Volumetric Mass Transfer Coefficient ($k_L a$) for Designing an Aeration Tank. *Engineering Journal*, 13(3), 13-28.

- Pino, L., Solari, R., Siquier, S., Antonio Estevez, L., Yopez, M., & Saez, A. (1992). Effect of operating conditions on gas holdup in slurry bubble columns with a foaming liquid. Chemical Engineering Communications, 117(1), 367-382.
- Ranade, V. V. (2001). *Computational flow modeling for chemical reactor engineering* (Vol. 5): Academic press.
- Rasband, W. S. (2008). ImageJ. <http://rsbweb.nih.gov/ij/>.
- Reynolds, T. D. (1977). *Unit operations and processes in environmental engineering*: Brooks.
- Sardeing, R., Painmanakul, P., & Hébrard, G. (2006). Effect of surfactants on liquid-side mass transfer coefficients in gas-liquid systems: a first step to modeling. Chemical Engineering Science, 61(19), 6249-6260.
- Sarin, P., Snoeyink, V., Bebee, J., Jim, K., Beckett, M., Kriven, W., & Clement, J. (2004). Iron release from corroded iron pipes in drinking water distribution systems: effect of dissolved oxygen. Water Research, 38(5), 1259-1269.
- Siebert, S., Burke, J., Faures, J.-M., Frenken, K., Hoogeveen, J., Döll, P., & Portmann, F. T. (2010). Groundwater use for irrigation—a global inventory. Hydrology and Earth System Sciences, 14(10), 1863-1880.
- Snoeyink, V. L., & Jenkins, D. (1980). *Water chemistry*: John Wiley.
- Stenstrom, M. K., Leu, S.-Y. B., & Jiang, P. (2006). Theory to practice: oxygen transfer and the new ASCE standard. Proceedings of the Water Environment Federation, 2006(7), 4838-4852.
- Stumm, W., & Lee, G. F. (1961). Oxygenation of ferrous iron. Industrial & Engineering Chemistry, 53(2), 143-146.
- Sung, W., & Morgan, J. J. (1980). Kinetics and product of ferrous iron oxygenation in aqueous systems. Environmental Science & Technology, 14(5), 561-568.
- Thaphet, N. (2013). *Effect of Plastic Media on Mass Transfer and Bubble Hydrodynamic Parameters in Bubble Column and Airlift Reactor*. (Master Degree), Chulalongkorn University

- Thorat, B., & Joshi, J. (2004). Regime transition in bubble columns: experimental and predictions. Experimental Thermal and Fluid Science, 28(5), 423-430.
- Tobajas, M., Siegel, M. H., & Aplitz, S. E. (1999). Influence of geometry and solids concentration on the hydrodynamics and mass transfer of a rectangular airlift reactor for marine sediment and soil bioremediation. The Canadian journal of chemical engineering, 77(4), 660-669.
- USGS. (2015). Contaminants Found in Groundwater. 2015, from <http://water.usgs.gov/edu/groundwater-contaminants.html>
- Vrba, J., & van der Gun, J. (2004). The world's groundwater resources. International Groundwater Resources Assessment Centre, Utrecht.
- Wu, X., & Merchuk, J. C. (2003). Measurement of fluid flow in the downcomer of an internal loop airlift reactor using an optical trajectory-tracking system. Chemical Engineering Science, 58(8), 1599-1614.
- Wu, Y., Ong, B. C., & Al-Dahhan, M. (2001). Predictions of radial gas holdup profiles in bubble column reactors. Chemical Engineering Science, 56(3), 1207-1210.
- Yotto, A. (2015). *Petroleum Oil Contaminated Soil Washing by Ethylene Glycol Monobutyl Ether and Sodium Dodecyl Sulfate Surfactants*. (Master Degree), Chiang Mai University
- Zhang, T., Wang, J., Wang, T., Lin, J., & Jin, Y. (2005). Effect of internal on the hydrodynamics in external-loop airlift reactors. Chemical Engineering and Processing: Process Intensification, 44(1), 81-87.
- Zhao, M., Niranjana, K., & Davidson, J. (1994). Mass transfer to viscous liquids in bubble columns and air-lift reactors: influence of baffles. Chemical Engineering Science, 49(14), 2359-2369.
- Živorad, R. (2004). Design of experiments in chemical engineering. WILEY-VCH Verlag GmbH & Co. KGaA, Weinheim, 154-158.



APPENDIX

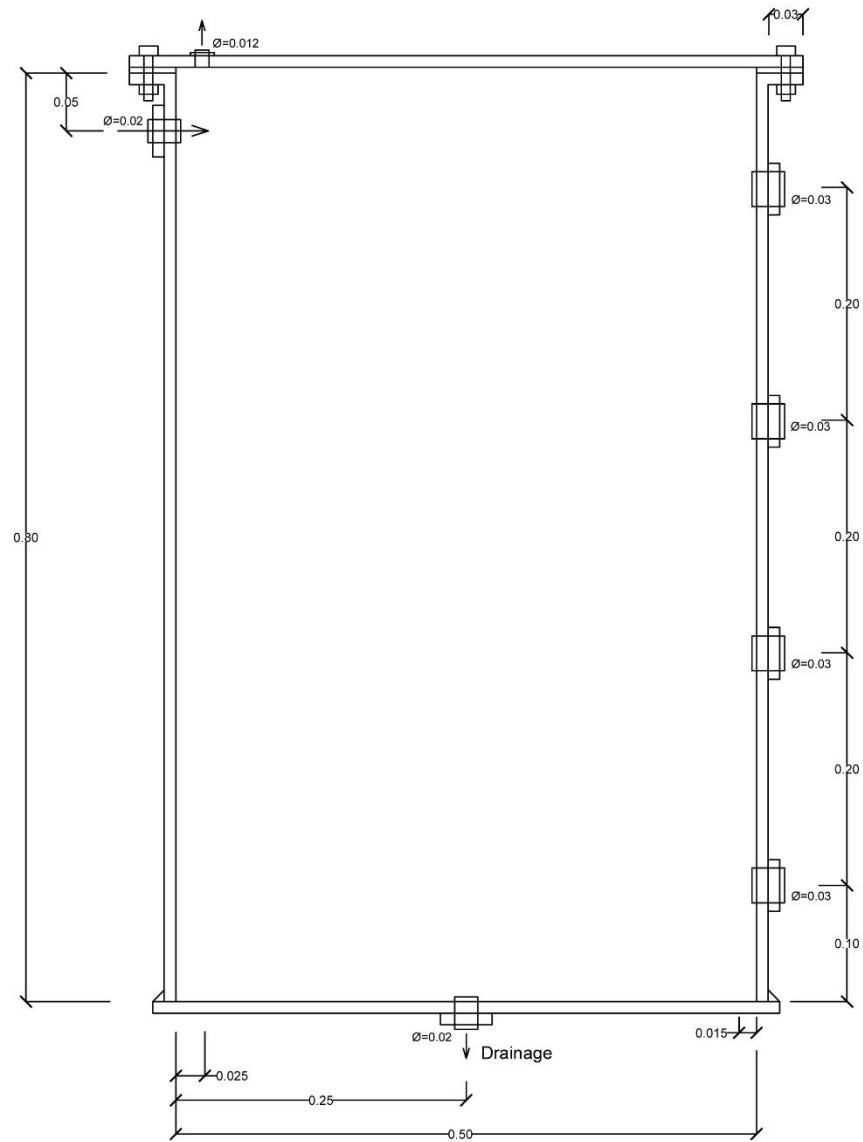
จุฬาลงกรณ์มหาวิทยาลัย
CHULALONGKORN UNIVERSITY

Appendix 1: Dissolved-oxygen concentration in water as a function of temperature and pressure (Salinity = 0)

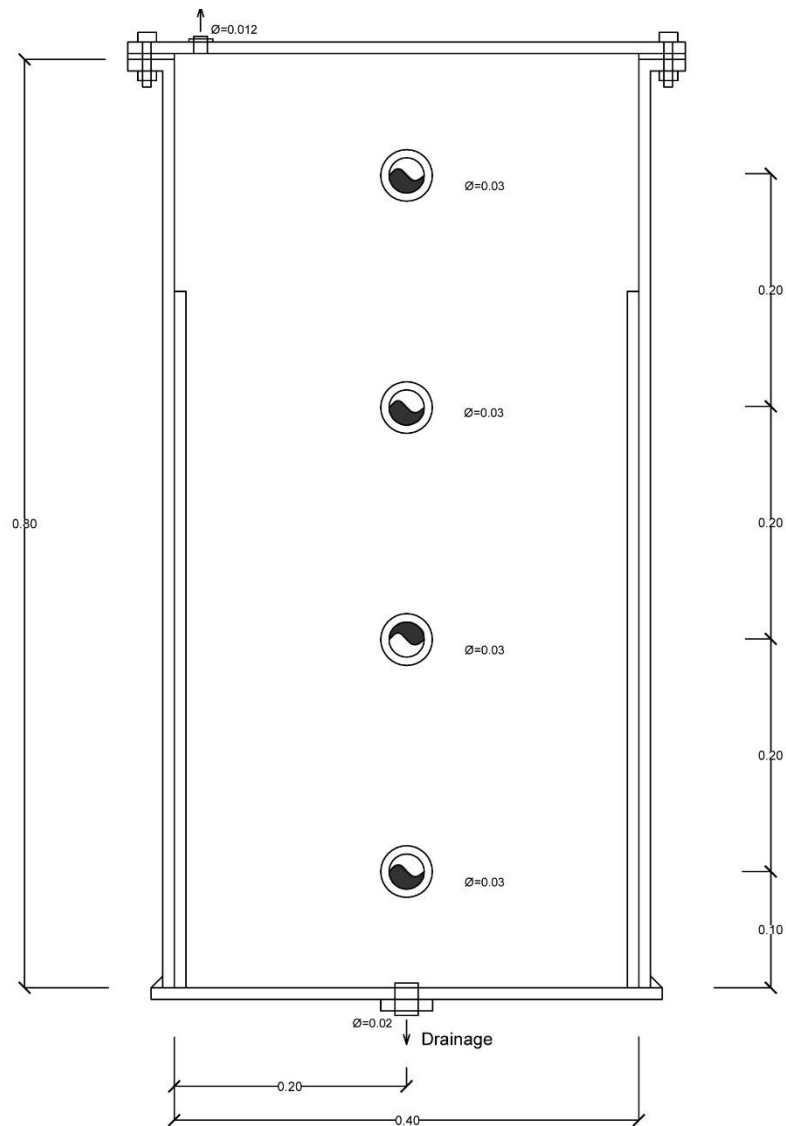
Temp. (°C)	Dissolved-oxygen concentration, mg/L									
	Barometric pressure, millimeters of mercury									
	735	740	745	750	755	760	765	770	775	780
10	10.90	10.98	11.05	11.13	11.20	11.28	11.35	11.43	11.50	11.58
11	10.65	10.72	10.80	10.87	10.94	11.02	11.09	11.16	11.24	11.31
12	10.41	10.48	10.55	10.62	10.69	10.77	10.84	10.91	10.98	11.05
13	10.17	10.24	10.31	10.38	10.46	10.53	10.60	10.67	10.74	10.81
14	9.95	10.02	10.09	10.16	10.23	10.29	10.36	10.43	10.50	10.57
15	9.73	9.80	9.87	9.94	10.00	10.07	10.14	10.21	10.27	10.34
16	9.53	9.59	9.66	9.73	9.79	9.86	9.92	9.99	10.06	10.12
17	9.33	9.39	9.46	9.52	9.59	9.65	9.72	9.78	9.85	9.91
18	9.14	9.20	9.26	9.33	9.39	9.45	9.52	9.58	9.64	9.71
19	8.95	9.01	9.07	9.14	9.20	9.26	9.32	9.39	9.45	9.51
20	8.77	8.83	8.89	8.95	9.02	9.08	9.14	9.20	9.26	9.32
21	8.60	8.66	8.72	8.78	8.84	8.90	8.89	9.02	9.08	9.14
22	8.63	8.49	8.55	8.61	8.67	8.73	8.79	8.84	8.90	8.96
23	8.27	8.33	8.39	8.44	8.50	8.56	8.62	8.68	8.73	8.79
24	8.11	8.17	8.23	8.29	8.34	8.40	8.46	8.51	8.57	8.63
25	7.96	8.02	8.08	8.13	8.19	8.24	8.30	8.36	8.41	8.47
26	7.82	7.87	7.93	7.98	8.04	8.09	8.15	8.20	8.26	8.31
27	7.68	7.73	7.79	7.84	7.89	7.95	8.00	8.06	8.11	8.17
28	7.54	7.59	7.65	7.70	7.75	7.81	7.86	7.91	7.97	8.02
29	7.41	7.46	7.51	7.57	7.62	7.67	7.72	7.78	7.83	7.88
30	7.28	7.33	7.38	7.44	7.49	7.54	7.59	7.64	7.69	7.75

Source: Metcalf, 1819

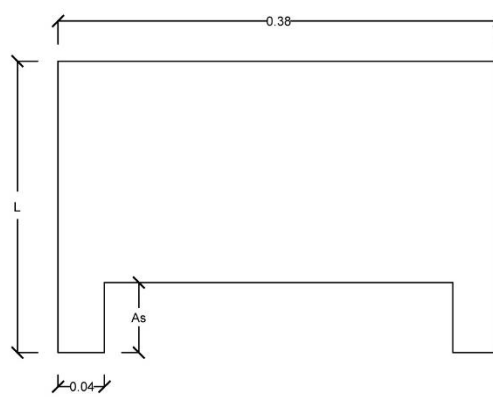
Appendix 2: Design of the Novel Bubble column Reactor



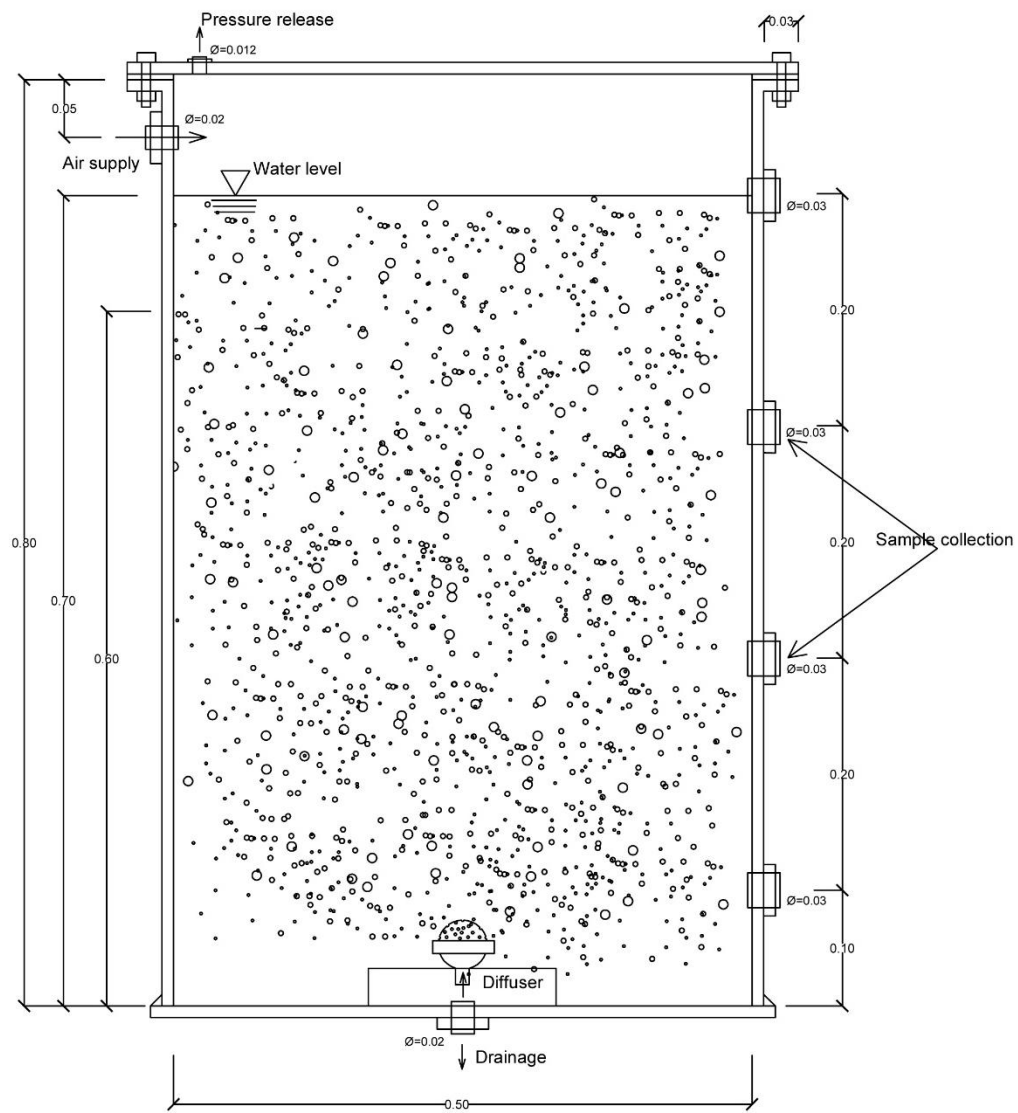
Front view of the bubble column reactor



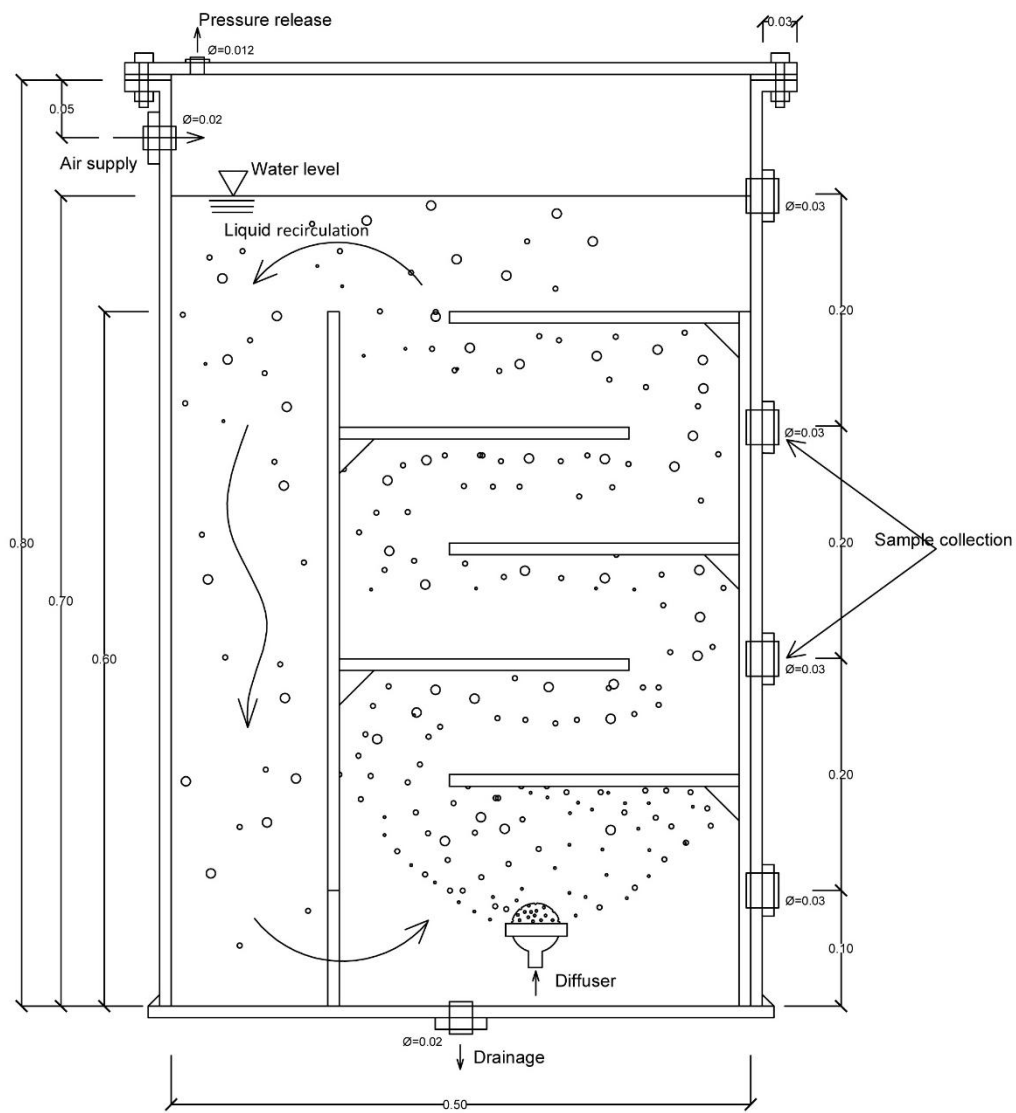
Side view of the bubble column reactor



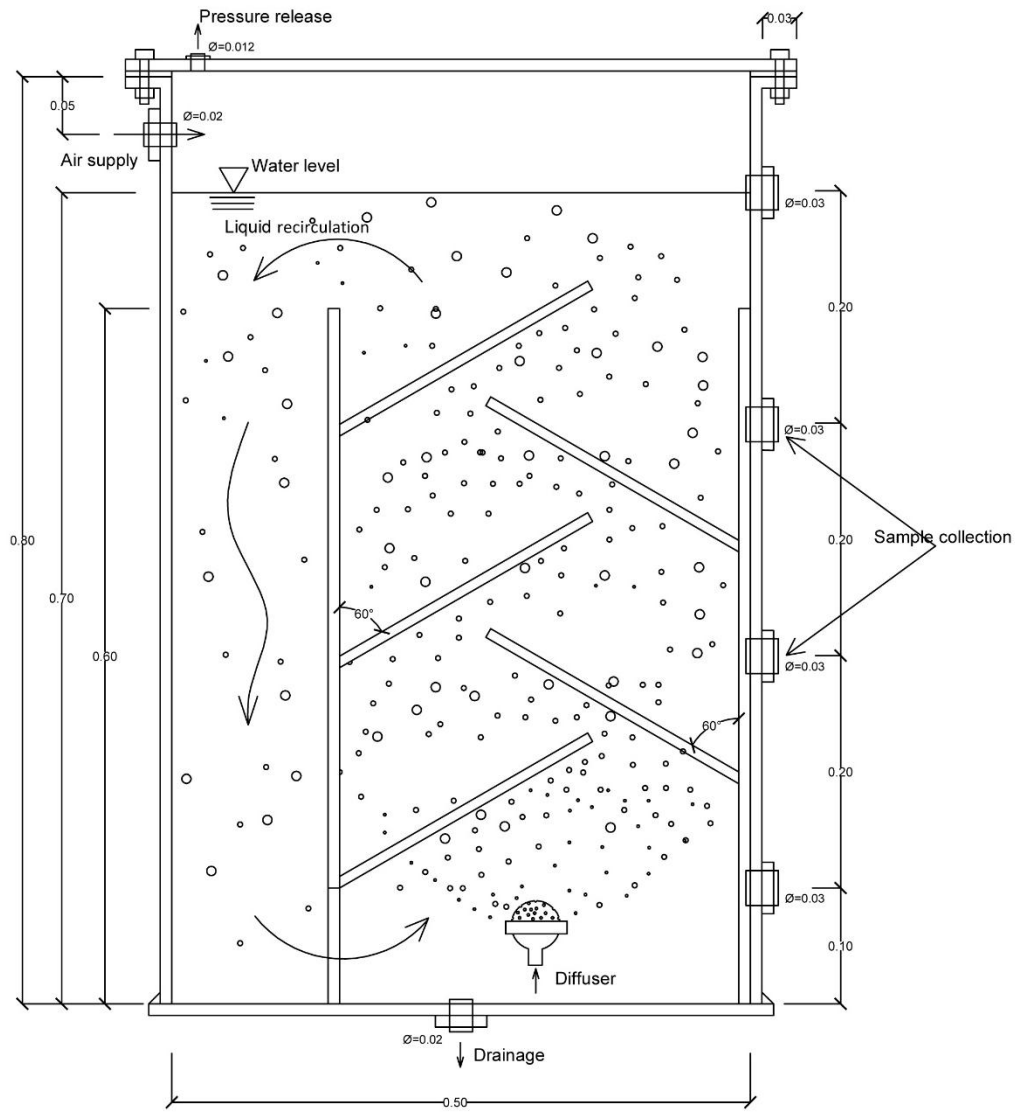
Horizontal baffles installed in riser compartment



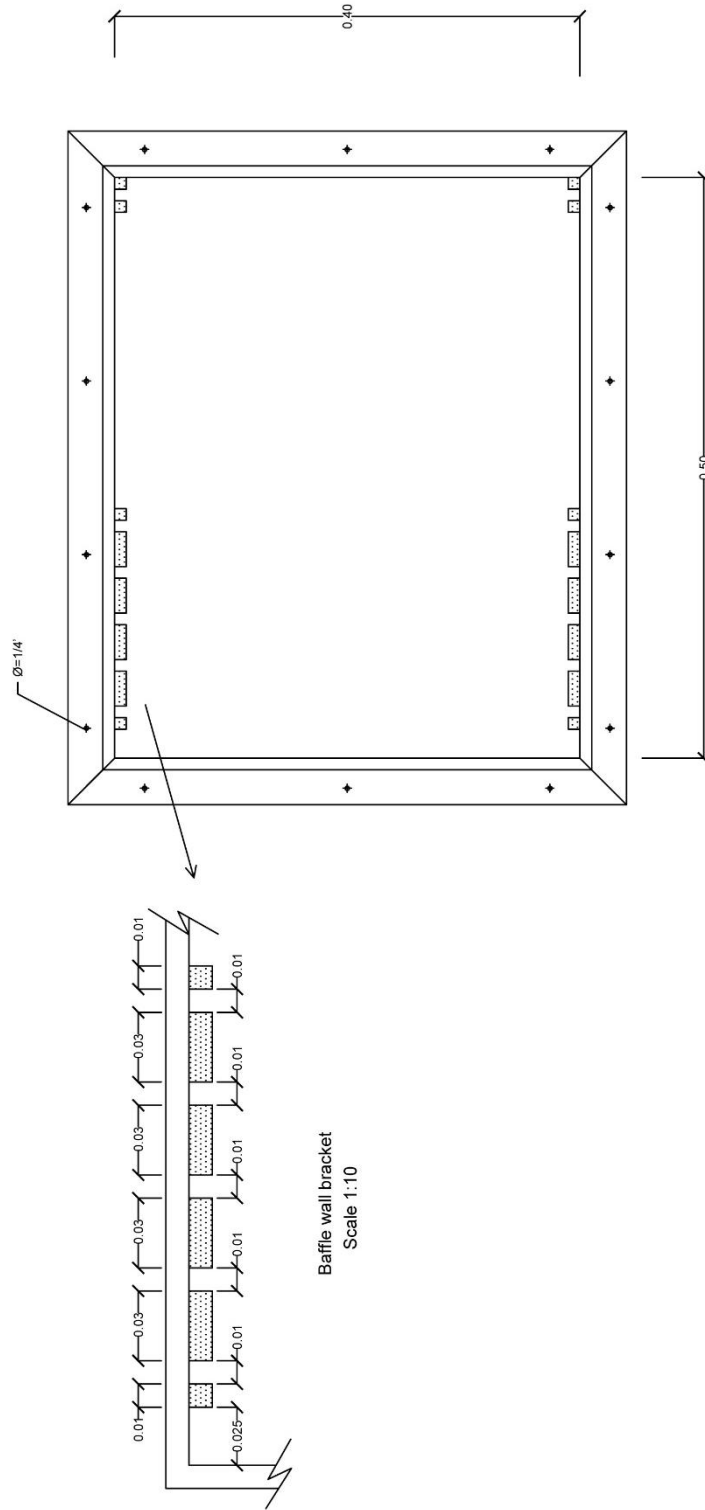
Conventional bubble column reactor operation



Novel BCR after install vertical and horizontal baffles (baffle angle = 90°)



Novel BCR after install vertical and horizontal baffles (baffle angle $< 90^\circ$)



Top view of Novel BCR and bracket to support and vary vertical baffle

Appendix 3: Experimental result: Downcomer-to-riser ratio

A_d/A_r	K_La Coefficient [sec^{-1}]			K_La Coefficient [hr^{-1}]		
	Downcomer	Riser	Average-DO	Downcomer	Riser	Average-DO
0.00	0.00137	0.00137	0.00137	4.93	4.93	4.93
0.18	0.00155	0.00160	0.00157	5.58	5.76	5.65
0.30	0.00145	0.00161	0.00146	5.22	5.80	5.26
0.45	0.00158	0.00172	0.00163	5.69	6.19	5.87
0.64	0.00158	0.00167	0.00162	5.69	6.01	5.83
1.44	0.00147	0.00188	0.00152	5.29	6.77	5.47
2.03	0.00159	0.00197	0.00159	5.72	7.09	5.72

Appendix 4: Experimental result: Factors screening in first part

Run	A_s	A_r	Y_r	α	L_b	N_b	N_d	$K_L a$ Coefficient [hr^{-1}]		
								Riser	Down.	Aver.
1	30	150	0	50	17	6	2	7.51	3.18	5.35
2	90	450	0	50	23	4	2	6.08	2.73	4.41
3	30	150	10	90	23	6	4	6.54	4.18	5.36
4	30	150	0	50	23	6	4	6.34	4.10	5.22
5	90	150	10	50	17	4	4	9.40	7.02	8.21
6	30	150	10	50	23	6	2	6.35	4.86	5.61
7	30	450	0	90	23	4	2	6.36	5.50	5.93
8	30	450	10	50	23	4	2	7.98	5.72	6.85
9	90	150	10	90	17	6	4	10.41	4.16	7.29
10	30	150	0	50	23	4	2	8.13	5.55	6.84
11	30	450	10	90	23	4	4	6.80	5.53	6.17
12	90	450	0	50	17	6	2	8.04	2.43	5.24
13	90	450	10	50	23	4	4	12.95	5.52	9.24
14	90	450	0	90	17	4	2	10.99	5.31	8.15
15	30	150	10	50	23	4	4	8.02	6.00	7.01
16	90	150	0	50	17	4	2	7.84	5.23	6.54
17	90	150	10	50	23	6	4	10.74	4.14	7.44
18	90	450	10	50	23	6	2	10.99	4.11	7.55
19	30	450	0	50	17	6	4	8.15	4.55	6.35
20	90	150	0	50	17	6	4	8.65	3.39	6.02
21	90	450	0	50	17	4	4	9.14	7.30	8.22
22	30	450	10	90	17	4	2	7.38	5.26	6.32
23	30	150	0	50	17	4	4	7.03	4.23	5.63
24	30	450	0	90	17	4	4	6.29	4.31	5.30
25	90	150	10	90	23	6	2	9.37	2.52	5.95

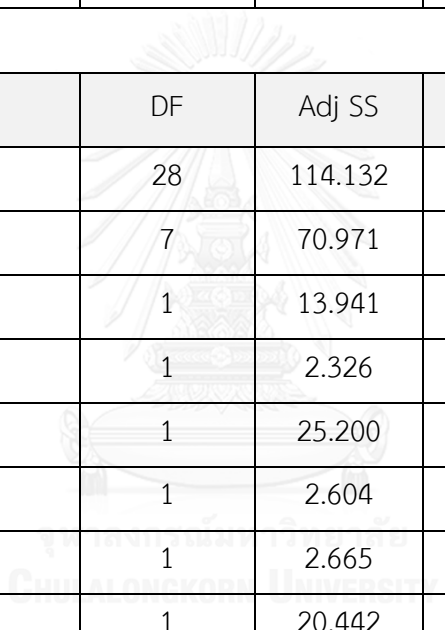
26	30	450	0	50	23	6	2	6.43	4.60	5.52
27	30	450	10	90	23	6	2	5.17	4.61	4.89
28	30	450	0	90	17	6	2	5.00	3.87	4.44
29	90	150	0	50	23	4	4	5.76	2.30	4.03
30	30	150	0	90	17	6	4	5.54	4.38	4.96
31	30	450	0	90	23	6	4	4.29	4.09	4.19
32	30	450	10	50	17	6	2	8.71	4.53	6.62
33	30	150	10	90	17	4	4	5.83	3.64	4.74
34	30	450	10	90	17	6	4	6.00	5.00	5.50
35	90	150	0	90	17	4	4	11.93	5.16	8.55
36	90	150	10	90	17	4	2	10.86	4.85	7.86
37	30	450	10	50	23	6	4	6.76	4.37	5.57
38	30	150	10	50	17	6	4	8.32	3.81	6.07
39	90	450	0	90	17	6	4	10.04	3.13	6.59
40	30	150	10	50	17	4	2	6.80	4.22	5.51
41	30	450	10	50	17	4	4	7.96	5.82	6.89
42	90	450	10	90	23	6	4	10.54	4.26	7.40
43	30	150	10	90	17	6	2	5.22	3.81	4.52
44	30	150	0	90	23	6	2	4.08	3.35	3.72
45	90	450	10	90	17	4	4	12.02	5.95	8.99
46	90	450	0	90	23	4	4	5.42	5.36	5.39
47	30	450	0	50	17	4	2	6.61	4.45	5.53
48	90	150	10	50	17	6	2	8.09	3.42	5.76
49	30	150	0	90	17	4	2	5.96	3.06	4.51
50	90	150	10	90	23	4	4	12.13	6.39	9.26
51	90	450	0	50	23	6	4	5.58	3.04	4.31
52	90	450	10	90	23	4	2	11.00	6.27	8.64
53	30	150	0	90	23	4	4	7.43	5.08	6.26

54	90	450	0	90	23	6	2	3.53	3.79	3.66
55	90	450	10	90	17	6	2	9.83	2.95	6.39
56	90	150	0	90	23	6	4	3.14	3.24	3.19
57	90	150	0	90	23	4	2	3.51	2.70	3.11
58	30	450	0	50	23	4	4	8.44	6.15	7.30
59	90	450	10	50	17	6	4	8.00	3.56	5.78
60	90	150	0	90	17	6	2	8.67	3.21	5.94
61	90	150	10	50	23	4	2	13.24	4.56	8.90
62	30	150	10	90	23	4	2	5.44	4.62	5.03
63	90	150	0	50	23	6	2	5.07	3.26	4.17
64	90	450	10	50	17	4	2	8.64	6.18	7.41



Appendix 5: Analysis of variance of experimental result in first factors screening

Coded Coefficients				
Term	Effect	Coef	T-Value	P-Value
Constant		6.081	51.93	0.000
A_S	0.933	0.467	3.99	0.000
A_r	0.381	0.191	1.63	0.112
Y_r	1.255	0.628	5.36	0.000
α	-0.403	-0.202	-1.72	0.094
L_b	-0.408	-0.204	-1.74	0.090
N_b	-1.130	-0.565	-4.83	0.000
N_d	0.487	0.243	2.08	0.045
$A_S * A_r$	-0.059	-0.029	-0.25	0.803
$A_S * Y_r$	0.904	0.452	3.86	0.000
$A_S * \alpha$	0.598	0.299	2.56	0.015
$A_S * L_b$	-0.609	-0.305	-2.60	0.013
$A_S * N_b$	-0.383	-0.192	-1.64	0.111
$A_S * N_d$	0.154	0.077	0.66	0.516
$A_r * Y_r$	-0.025	-0.012	-0.11	0.917
$A_r * \alpha$	0.101	0.051	0.43	0.668
$A_r * L_b$	-0.012	-0.006	-0.05	0.961
$A_r * N_b$	-0.166	-0.083	-0.71	0.484
$A_r * N_d$	-0.135	-0.067	-0.58	0.569
$Y_r * \alpha$	0.021	0.010	0.09	0.930
$Y_r * L_b$	0.847	0.423	3.62	0.001
$Y_r * N_b$	-0.078	-0.039	-0.33	0.741

$Y_r * N_d$	-0.043	-0.021	-0.18	0.856
$\alpha * L_b$	-0.335	-0.168	-1.43	0.161
$\alpha * N_b$	-0.133	-0.066	-0.57	0.574
$\alpha * N_d$	0.143	0.072	0.61	0.545
$L_b * N_b$	-0.158	-0.079	-0.68	0.504
$L_b * N_d$	-0.076	-0.038	-0.32	0.748
$N_b * N_d$	-0.116	-0.058	-0.49	0.625
				
Source	DF	Adj SS	Adj MS	F-Value
Model	28	114.132	4.0761	4.65
Linear	7	70.971	10.1387	11.55
A_S	1	13.941	13.9409	15.89
A_r	1	2.326	2.3256	2.65
Y_r	1	25.200	25.2004	28.72
α	1	2.604	2.6042	2.97
L_b	1	2.665	2.6651	3.04
N_b	1	20.442	20.4417	23.30
N_d	1	3.793	3.7928	4.32
2-Way Interactions	21	43.161	2.0553	2.34
$A_S * A_r$	1	0.055	0.0552	0.06
$A_S * Y_r$	1	13.086	13.0863	14.91
$A_S * \alpha$	1	5.730	5.7300	6.53
$A_S * L_b$	1	5.941	5.9414	6.77
$A_S * N_b$	1	2.352	2.3524	2.68
$A_S * N_d$	1	0.378	0.3782	0.43
$A_r * Y_r$	1	0.010	0.0098	0.01

$A_r * \alpha$	1	0.164	0.1640	0.19
$A_r * L_b$	1	0.002	0.0021	0.00
$A_r * N_b$	1	0.439	0.4389	0.50
$A_r * N_d$	1	0.290	0.2903	0.33
$Y_r * \alpha$	1	0.007	0.0068	0.01
$Y_r * L_b$	1	11.467	11.4667	13.07
$Y_r * N_b$	1	0.098	0.0977	0.11
$Y_r * N_d$	1	0.029	0.0293	0.03
$\alpha * L_b$	1	1.796	1.7956	2.05
$\alpha * N_b$	1	0.282	0.2822	0.32
$\alpha * N_d$	1	0.328	0.3278	0.37
$L_b * N_b$	1	0.400	0.4001	0.46
$L_b * N_d$	1	0.092	0.0923	0.11
$N_b * N_d$	1	0.214	0.2139	0.24
Error	35	30.710	0.8774	
Total	63	144.842		

Appendix 6: Experimental result: Factor Optimization in first part

Run Order	Qg	Y _r	N _b	K _L a Coefficient [hr ⁻¹]		
				Riser	Downcomer	Average
1	10	10	3	8.680	7.600	8.140
2	10	10	3	8.710	7.880	8.295
3	10	10	3	8.680	8.140	8.410
4	15	0	4	10.840	7.380	9.110
5	5	20	2	4.280	3.100	3.690
6	15	20	4	11.770	9.040	10.405
7	10	10	1	8.060	6.520	7.290
8	5	0	2	4.100	3.020	3.560
9	15	20	2	12.130	11.020	11.575
10	10	10	3	8.240	7.240	7.740
11	10	10	3	8.390	7.380	7.885
12	10	10	3	8.570	7.160	7.865
13	5	20	4	4.030	3.130	3.580
14	15	0	2	12.170	9.970	11.070
15	18	10	3	14.110	12.740	13.425
16	10	27	3	8.100	5.180	6.640
17	10	10	5	7.920	4.180	6.050
18	10	-7	3	7.160	4.070	5.615
19	2	10	3	1.760	1.040	1.400
20	5	0	4	4.030	2.700	3.365

Appendix 7: Experimental result: Factors screening in second part

Run Order	Y_r	N_b	A_s	α	L_b	$K_L a$ Coefficient [hr^{-1}]		
						Riser	Downc.	Average
1	10	2	90	50	20	9.79	9.84	9.82
2	10	4	30	130	17	5.76	5.86	5.81
3	10	4	90	50	17	9.07	8.52	8.80
4	0	2	90	130	20	9.25	8.84	9.05
5	0	2	90	50	17	8.64	8.91	8.78
6	10	4	90	130	20	6.99	7.24	7.12
7	0	4	90	130	17	7.76	8.72	8.24
8	10	2	30	50	17	8.08	8.67	8.38
9	0	4	90	50	20	7.75	5.89	6.82
10	10	2	30	130	20	8.36	8.73	8.55
11	0	4	30	130	20	7.42	7.4	7.41
12	0	4	30	50	17	7.2	7.14	7.17
13	10	4	30	50	20	8.21	6.81	7.51
14	0	2	30	130	17	6.76	6.33	6.55
15	10	2	90	130	17	8.63	8.67	8.65
16	0	2	30	50	20	8.44	8.75	8.60

Appendix 8: Experimental result: Factors optimization in second part

Run Order	Qg	α	N _b	K _L a Coefficient [hr ⁻¹]		
				Riser	Downcomer	Average
1	10	50	3	7.21	6.13	6.67
2	5	70	4	2.58	2.18	2.38
3	10	50	1	4.27	4.19	4.23
4	10	16	3	5.02	5.24	5.13
5	10	16	3	5.24	5.02	5.13
6	10	50	3	6.62	6.19	6.405
7	15	30	4	9.55	9.90	9.725
8	10	50	3	7.28	5.53	6.405
9	10	50	3	6.15	6.14	6.145
10	5	30	2	2.98	3.11	3.045
11	15	70	2	10.26	10.41	10.335
12	10	50	3	6.36	5.89	6.125
13	10	50	3	6.27	6.19	6.23
14	10	50	3	6.74	5.89	6.315
15	10	50	1	5.19	4.07	4.63
16	10	50	3	6.14	5.76	5.95
17	10	50	5	6.07	3.97	5.02
18	10	50	5	5.41	4.84	5.125
19	18	50	3	11.43	10.16	10.795
20	10	84	3	6.14	5.29	5.715
21	10	50	3	7.18	6.80	6.99
22	5	70	4	2.43	1.85	2.14
23	5	30	4	3.55	3.40	3.475
24	15	70	4	8.80	8.27	8.535
25	15	30	4	8.72	9.41	9.065

26	10	50	3	6.97	5.58	6.275
27	15	30	2	8.45	9.43	8.94
28	5	30	2	3.13	3.40	3.265
29	15	30	2	10.18	10.50	10.34
30	2	50	3	1.88	1.41	1.645
31	10	50	3	6.46	5.50	5.98
32	5	70	2	3.81	3.63	3.72
33	5	30	4	3.19	3.49	3.34
34	18	50	3	11.24	10.32	10.78
35	15	70	4	8.16	6.95	7.555
36	2	50	3	1.57	1.61	1.59
37	10	50	3	6.39	5.58	5.985
38	5	70	2	3.69	3.03	3.36
39	15	70	2	10.47	8.35	9.41
40	10	84	3	5.36	4.98	5.17

Appendix 9: Experimental result: Batch Settling Test

Port N°	Depth [cm]	Turbidity [NTU]									
		30	60	90	120	150	180	210	240	270	300
I	2	12	26	46	62	67	76	75	74	84	88
II	22	14	23	28	36	51	54	70	75	83	86
III	42	12	21	19	41	46	40	53	76	82	82
IV	62	6	12	19	26	30	45	54	73	78	80

Appendix 10: Phenanthroline method for ferrous and total iron

▪ Reagents

- Hydrochloric acid (HCl)
- Hydroxylamine solution, prepare by dissolve 10 g of hydroxylamine ($\text{NH}_2\text{OH}\cdot\text{HCl}$) in 100 ml of distilled water.
- Ammonium acetate buffer solution, prepare by dissolve 250 g of ammonium acetate ($\text{NH}_4\text{C}_2\text{H}_3\text{O}_2$) in 150 ml of distilled water. Add 700 ml of Acetic acid (glacial grade).
- Phenanthroline solution, prepare by dissolve 100 mg of 1,10-phenanthroline monohydrate ($\text{C}_{12}\text{H}_8\text{N}_2\cdot\text{H}_2\text{O}$) in 100 ml of distilled water. Then let stir and heat at 80°C . Let discard it while the solution appears in dark color. Otherwise, add 2 drops of HCl. (1 ml is enough for Fe concentration less than $100\ \mu\text{g}$).
- Stock iron solution, prepare by add 20 ml of H_2SO_4 to 50ml of distilled water slowly and dissolve 1.404 g of ferrous ammonium sulfate ($\text{Fe}(\text{NH}_4)_2(\text{SO}_4)_2\cdot 6\text{H}_2\text{O}$). Then let dilute it to 1000 ml by distilled water. 1 ml of this solution is equal to $200\ \mu\text{g}$ of Fe.
- Standard iron solutions, prepare in daily for use by one of these methods:
 - Method-1: Pipet 50 ml of stock iron solution into 1000 ml of volumetric flask. Then dilute to 1000 ml with distilled water, 1 ml of this solution is equal to $10\ \mu\text{g}$ -Fe. Or
 - Method-2: Pipet 5 ml of stock iron solution into 1000 ml of volumetric flask. Then dilute to 1000 ml with distilled water, 1 ml of this solution is equal to $1\ \mu\text{g}$ -Fe.

▪ **Procedure**

For Total Iron:

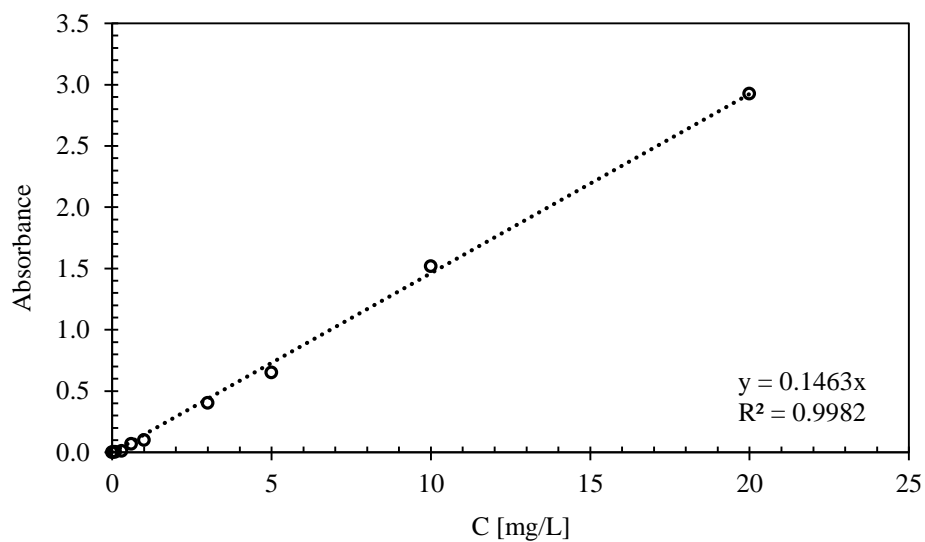
- First, let measure 50 ml of sample into 250 ml of beaker. Please use the small portion and dilute to 50 ml with distilled water while the sample contains more than 200 μg of iron.
- Then add 2 ml of HCl and 1 ml of hydroxylamine solution ($\text{NH}_2\text{OH}\cdot\text{HCl}$) in to the solution. Add few glass beads and heat to boiling for make sure that all of the iron is dissolved. Continue boiling until volume is reduced to 15 to 20 ml and let cool it to the room temperature.
- Measure the sample to nessler tube, then add 10 ml of acetate buffer solution ($\text{NH}_4\text{C}_2\text{H}_3\text{O}_2$), and add 4 ml of phenanthroline solution. Let dilute to 50 ml with distilled water and leave for about 10 to 15 minutes for maximum color.
- Measure absorbance by spectrophotometer at 510 nm of wavelength.
- Prepare a blank by using distilled water as the sample, then follow step 1 to 3.
- Prepare the standard curve by standard iron solution for concentration of 10, 20, 30, 40, 50 and 60 μg by:
 - Dilute the stock iron solution by 1 ml is 10 μg for 1, 2, 3, 4, 5, and 6 ml.
 - Measure to nessler tube (50 ml), then dilute with distilled water to 50 ml.
 - Follow the step 1 to 4.
 - Plot the standard curve between Fe concentration (X-axis) and absorbance (Y-axis).

Calculation; Fe (mg/l) = (μg Fe from graph) / (Volume of sample (ml.))

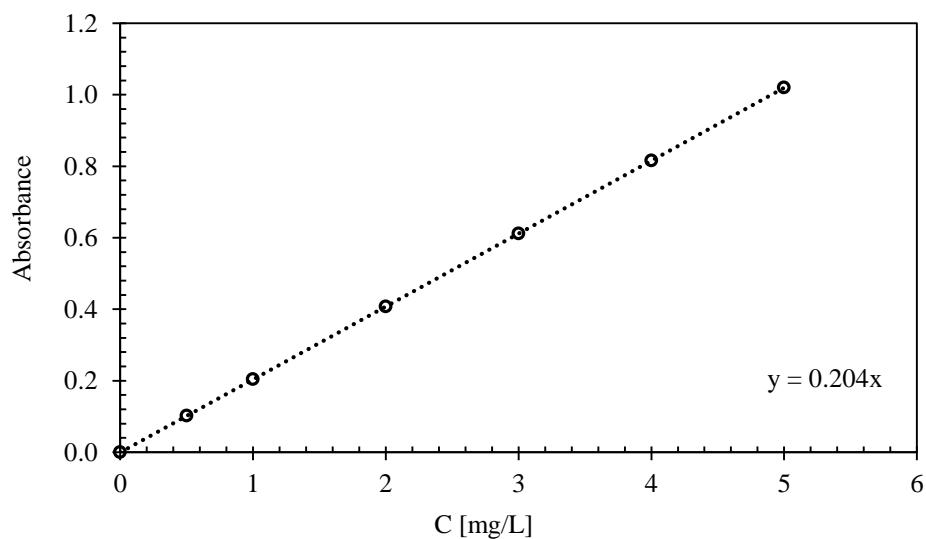
For Ferrous Iron:

- Add 2 ml of HCl into 100 ml bottle. Sampling the sample directly into bottle from the source.
- Measure 50 ml of sample from that bottle into nessler tube (100 ml), then add 20 ml of phenanthroline solution and 10 ml of acetate buffer solution ($\text{NH}_4\text{C}_2\text{H}_3\text{O}_2$). Let stir and dilute it to 100 ml.
- Leave it 5 to 10 minutes (not let the sample expose to the light) and then let measure the color intensity at wavelength of 510 nm.
- Prepare the blank solution by using distilled water and add 1 ml of HCl per 100 ml of sample. Last, let follows step 2 to 3.
- Prepare the standard curve by standard iron solution for desired concentration by:
 - Dilute the stock iron solution during 1 ml of this solution is 10 μg for 1, 2, 3, 4 and 5 ml.
 - Measure to 50 ml of nessler tube, then add 1 ml of HCl and dilute with distilled water to 50 ml.
 - Let following step 2 to 3.
 - Plot standard curve between Fe concentrations (X-axis) an absorbance (Y-axis).

For this work, the standard curve was constructed as the following figures.



The standard curve for ferrous iron analysis by Phenanthroline method



The standard curve for total iron analysis by Phenanthroline method

VITA

Mr. Saret Bun was born in 1992 in Kampong Speu Province, Cambodia. He earned a degree of Bachelor of Engineering in Water Resource Engineering and Rural Infrastructure from Institute of Technology of Cambodia (Cambodia) in July 2014.

He got a scholarship from ASEAN University Network Southeast Asia Engineering Education Development Network Program (AUN/SEED-Net) of Japan International Cooperation Agency (JICA) to continue Master degree of Engineering in Environmental Engineering at Faculty of Engineering, Chulalongkorn University (Thailand) in August 2014.

